

# Durham E-Theses

---

## *Polyester resin concrete: mix development and the structural behaviour of some components*

Shohada, Mohsen-Fadaee

### How to cite:

---

Shohada, Mohsen-Fadaee (1987) *Polyester resin concrete: mix development and the structural behaviour of some components*, Durham theses, Durham University. Available at Durham E-Theses Online: <http://etheses.dur.ac.uk/9299/>

### Use policy

---

The full-text may be used and/or reproduced, and given to third parties in any format or medium, without prior permission or charge, for personal research or study, educational, or not-for-profit purposes provided that:

- a full bibliographic reference is made to the original source
- a [link](#) is made to the metadata record in Durham E-Theses
- the full-text is not changed in any way

The full-text must not be sold in any format or medium without the formal permission of the copyright holders.

Please consult the [full Durham E-Theses policy](#) for further details.

# Polyester Resin Concrete

## Mix development and the structural behaviour of some components

By

MOHSEN-FADAEI SHOHADA

B.Sc Civil Engineering

The copyright of this thesis rests with the author.  
No quotation from it should be published without  
his prior written consent and information derived  
from it should be acknowledged.

A thesis submitted for the degree of  
Doctor of Philosophy

The Department Of Engineering

University Of Durham

December 1987



10 MAY 1988

## ACKNOWLEDGEMENTS

This research has been achieved with the participation of many people who extended their help, support, encouragement and friendship.

Firstly, I would like to express my deepest thanks to my supervisor, Dr.G.M.Parton of the Department Of Engineering Science, University Of Durham, for his most invaluable help, encouragement and concern throughout the course of this thesis.

Sincere thanks are extended to all the workshop staff and laboratory technicians, in particular to Mr.B.Rosscamp, Mr.B.Scurr and T.Brown.

Lastly, but not least, I am gratefull to my family, father, mother, wife Amanda, daughter Mina and son David, for their love and continous encouragement.

## SYNOPSIS

This research has been planned to develop, firstly a polymer concrete mix, using polyester resin with a high ratio of aggregate to resin together with a good workability for ease of flow and at the same time, having a high modulus and strength values. All the individual materials available for making the polymer concrete have been examined to find out the best available type and the best combination of these materials.

Secondly, using this mix to construct some prefabricated structural component, and to study the behaviour of this component, under the service loads. These structural components were sandwich beams, access floor panels, sandwich panels for a prefabrication housing system, Bridge-Deck and corrugated sheeting for roof and wall cladding.

Tests were carried out on these components and the results were compared with the conventional material such as <sup>Portland cement</sup> concrete and asbestos cement. The advantages of polymer concrete over these materials were demonstrated very clearly.

Finally a prefabricated polymer concrete bungalow was constructed and racking tests were carried out to demonstrate the stability of this house under the high wind pressures.

## STATEMENT OF COPYRIGHT

All rights reserved. No part of this thesis may be reproduced, stored in a retrieval system, or transmitted, in any form or by means, electronic, mechanical, photocopying, recording or otherwise, without the prior permission of the author.

## CONTENTS

ACKNOWLEDGEMENTS	i
SYNOPSIS	ii
STATEMENT OF COPYRIGHT	iii
CONTENTS	iv
LIST OF FIGURES & TABLES	xi
NOTATION	xx
<b>1. INTRODUCTION AND HISTORICAL BACKGROUND OF POLYESTER RESIN</b>	<b>1</b>
<b>2. MATERIAL USED FOR CONSTRUCTION OF POLYMER CONCRETE</b>	<b>5</b>
2.1 Aggregate (sand and micro filler)	5
2.1.1 Type of sand and filler	6
2.1.2 Determination of bulk densities and Selection of suitable filler	12
2.1.3 Sieve analyses	12
2.1.4 Chemical analysis	22
2.1.5 Determination of specific gravity, moisture content bulk density and pH value	22

2.2	Polyester resin	27
2.2.1	Resin preparation	28
2.2.2	Determination of viscosity	30
2.3	General aspects of monomers, inhibitors, catalysts, and accelerators	38
2.3.1	Introduction	38
2.3.2	Monomers	39
2.3.3	Inhibitors or stabilizers	39
2.3.4	Catalysts	40
2.3.5	Accelerators	40
2.4	Cured polyester resin	40
<b>3.</b>	<b>MIX DESIGN AND DETERMINATION OF THE PROPERTIES OF POLYMER CONCRETE</b>	<b>43</b>
3.1	Introduction	43
3.2	Determination of the grading of the aggregate	43
3.2.1	Fuller grading	45
3.2.2	Gap grading	46
3.3	Workability test	46
3.3.1	Method of test	49
3.3.2	Workability test results	54
3.4	Direct tensile test	54
3.4.1	Preparations of samples and testing	54

3.5	Modulus of rupture test	58
3.5.1	Preparations of samples and testing	58
3.6	Effect of catalyst level	65
3.6.1	Effect of catalyst level on get time	65
3.6.2	Effect of catalyst level on curing time	69
3.6.3	Effect of filler addition on curing time for 6% catalyst level in polyester resin	73
3.6.4	Effect of catalyst level on strength	73
3.7	Relationship between time and development of the strength	76
3.8	Water absorption test	76
3.9	Density measurement of the polymer concrete	79
3.10	Compressive strength	83
3.11	Conclusions	83
<b>4.</b>	<b>SANDWICH BEAMS</b>	<b>88</b>
4.1	Introduction	88
4.2	Dimensions, construction and schedule of the beams	89
4.3	Beams: Preparation for testing and testing procedure	91
4.4	Sandwich concrete beams	96
4.5	Theory of the sandwich beam	96
4.6	Results and discussions	99
4.7	Conclusions	110

<b>5.</b>	<b>ACCESS FLOOR PANEIS</b>	<b>112</b>
5.1	Introduction	112
5.2	Dimensions and schedule of the panels	116
5.3	Method of construction	116
5.3.1	Sandwich panels	116
5.3.2	Solid panels	117
5.4	Preparation for testing and testing procedure	122
5.5	Results and discussions	124
5.5.1	Sandwich panels	124
5.5.2	Solid panels	125
5.6	Theoretical calculations	131
5.7	Conclusions	139
<b>6.</b>	<b>SANDWICH PANELS</b>	<b>141</b>
6.1	Introduction	141
6.2	Schedule of the panels	141
6.2.1	Standard sandwich panel	144
6.2.2	Window panels	144
6.2.3	Single-skin panels	144
6.3	Manufacturing procedures	145
6.3.1	Moulds and dimensions	145
6.3.2	The casting process	145
6.3.3	Curing	149

6.4	Testing	150
6.5	Instrumentation and testing procedure	150
6.5.1	Loading rig	150
6.5.2	Method of testing	153
6.6	Results and calculations	160
6.7	Conclusions	185
<b>7.</b>	<b>POLYMER CONCRETE BRIDGE-DECK</b>	<b>191</b>
7.1	Introduction	191
7.2	Dimensions and schedule of polymer concrete Bridge-Deck	191
7.3	Method of construction	193
7.4	Test procedure	193
7.5	Results and calculations	195
7.6	Conclusions	202
<b>8.</b>	<b>POLYMER CONCRETE SHEETING</b>	<b>204</b>
8.1	Introduction	204
8.2	Dimensions and schedule of polymer concrete sheeting	205
8.3	Method of construction	209
8.4	Test configurations	211
8.4.1	Tests on small flat specimens	211
8.4.2	Bending tests on corrugated sheet	211
8.5	Results and calculations	212

8.6	Comments on the results	221
8.6.1	Small flat specimens	221
8.6.2	Corrugated specimens	224
8.7	Conclusions	226
<b>9.</b>	<b>RACKING TESTS ON A BUNGALOW</b>	<b>228</b>
9.1	Introduction (Prefabrication housing system)	228
9.2	The test structure	231
9.3	Test conditions	233
9.4	Test equipment	235
9.5	Test result	237
9.6	Conclusions	237
<b>10.</b>	<b>PHENOLIC RESIN</b>	<b>246</b>
10.1	Introduction	246
10.2	Chemical nature of phenolic resin systems	246
10.3	Test results and comments	247
<b>11.</b>	<b>CONCLUSIONS</b>	<b>249</b>
<b>APPENDICES</b>		
1.	Appendix One:	
	Grading curves	255
2.	Appendix Two:	

	Simply supported beams by Macaulay's method	279
3.	Appendix Three:	
	Sandwich beams theory	281
4.	Appendix Four:	
	Behaviour of sandwich panel under bending and buckling	290
5.	Appendix Five:	
	Design procedures of B-DECK programme	294
6.	Appendix six:	
	Wind loads	302
7.	Appendix seven:	
	Figures of slab loading accessories	311
8.	Appendix eight:	
	Finite element analysis for the corrugated sheets	316
	<b>REFERENCES</b>	<b>323</b>
	<b>OUTPUTS OF THE COMPUTER</b>	<b>329</b>

## LIST OF FIGURES AND TABLES

Table (2.1). Determination of bulk density and selection of suitable filler.

Table (2.2). Results of sieve analyses.

Figure (2.3). Grading curve (sand No: 1-4).

Figure (2.4). Grading curve (filler: pozzolan).

Figure (2.5). Grading curve ( filler: B.L.H).

Figure (2.6). Grading curve (filler: silica flour).

Figure (2.7). Grading curve (filler:Ballotini).

Figure (2.8). Grading curve (filler: fillite).

Figure (2.9). Grading curve (filler: china clay grade E & D).

Table (2.10A). Chemical analyses of the sands.

Table (2.10B). Chemical analyses of some filler.

Table (2.11). Results of specific gravity, moisture content, bulk density & PH value.

Figure (2.12). Flow diagram for production of a polyester resin.

Figure (2.13). Effect of temperature on viscosity of polyester resin.

Figure (2.14). Effect of temperature on viscosity of polyester resin.

Figure (2.15). Effect of time on viscosity at 60° C of polyester resin.

Figure (2.16). Effect of temperature on viscosity of polyester resin containing  
24% WT.filler.

Figure (2.17). Effect of filler addition on viscosity of polyester resin  
at 40° C

Figure (3.1). Workability test, using vibration.

Figure (3.2). Effect of aggregate/resin ratio on workability.

Figure (3.3). Effect of vibration on workability.

Table (3.4A). Results of the direct tensile test.

Table (3.4B). Results of the direct tensile test.

Table (3.5A). Results of the rupture test.

Table (3.5B). Results of the rupture test for different mixes.

Table (3.6A). Results of the rupture test for mix (T102).

Table (3.6B). Results of the rupture test for mix (T102).

Table (3.6C). Results of the rupture test for mix (S101).

Table (3.7). Results of the rupture test for mix (SS) and (TT).

Figure (3.8). Effect of catalyst level on gel time.

Figure (3.9). Time taken for the polymer concrete to be gelled with different  
% of catalyst.

Figure (3.10). Effect of catalyst level on curing time of polyester resin at  
room temperature.

Figure (3.11). Alteration of the temperature during the copolymerization.

Figure (3.12). Effect of filler addition on curing time for 6% catalyst level  
in polyester resin at room temperature.

Figure (3.13). Effect of catalyst level on elastic modulus and strength.

Figure (3.14). Relationship between time and development of strength (curing time).

Table (3.15). The results of the water absorption test.

Table (3.16A). The results of the compressive strength and density.

Table (3.16B). The results of the compressive strength and density.

Table (4.1). Beam specification's.

Figure (4.2A). Position of the dial gauges and points load.

Figure (4.2B). Arrangement of loading. (1 point loading).

Figure(4.2C). Cross section of the beam.

Figure (4.2D). Position of the strain gauges.

Table (4.3). Concrete beam specifications.

Table (4.4). Determination of deflection under various loads.

Table (4.5). Comparison between the theoretical and experimental values of the beams.

Figure (4.6). Set No. 1. Results of the sandwich beam.

Figure (4.6). Set No: 2 Results of the sandwich beam.

Figure (4.6). Set No: 3 Results of the sandwich beam.

Figure (4.6). Set No: 4 Results of the sandwich beam.

Figure (4.6). Set No: 5 Results of the sandwich beam.

Table (4.7). Comparison in deflection/unit load between the beams, assuming

no ribs and the beam with ribs.

Table (5.1A). Schedule of the sandwich floor panels.

Table (5.1B). Schedule of the solid floor panels.

Figure (5.3). Sandwich panel with no ribs.

Figure (5.4). Sandwich panel with ribs.

Figure (5.5). Solid panels with ribs.

Figure (5.6). Solid panels with no ribs.

Table (5.8A). Results of the floor panel test.

Table (5.8B). Results of the floor panel test.

Table (5.8C). Results of the floor panel test.

Table (5.8D). Results of the floor panel test.

Table (5.9A). Results of the ultimate load for the sandwich panels.

Table (5.9B). Results of the ultimate load for the solid panels.

Figure (6.1). Schedule of the panels according to the type of the panels.

Figure (6.2). Schedule of the panels according to the type of testing.

Figure (6.3). Details of the standard panel junction.

Figure (6.5). Test arrangement (Transverse loading- Two point loading).

Figure (6.6). Arrangement. (Transverse loading all sides supported).

Figure (6.7). General arrangement of the test rig for the panels in end load  
and transverse load. (simply supported at ends).

Figure (6.8). Deflection of the panel under the transverse load at position  
1,2 and 3.

Figure (6.9). Strain at the central cross section under the transverse load.

Table (6.10). Results of the panels under the transverse load. (simply  
supported at the ends).

Figure (6.11). Position of the dial gauges & strain gauges on the panel.

Figure (6.12). Variation of the deflection for different position on the panel  
under the transverse load.

Figure (6.13). Variation of the strain for different position on the panel  
under the transverse load.

Table (6.14). The results of the panel, under the transverse load, supported on all the sides.

Figure (6.15). Profile of the panel at X-X section, showing the deflection under the various loads.

Figure (6.16). Profile of the panel at Y-Y section, showing the deflection under the various loads.

Figure (6.17). Creep test for the panel, simply supported on all sides, under the transverse loading.

Figure (6.18). The relationship between the critical load for a pin-ended axially loaded compression member and  $(L/r)$ .

Table (6.19A). Results of the simply supported panels under the axial load and the transverse load.

Table (6.19B). Results of the simply supported panel under the axial load & the transverse load.

Figure (6.20). The relationship between the direct stress and the compressive stress for the panel, simply supported on its two ends.

- Figure (7.1). Typical section BRIDGE - DECK.
- Figure (7.2). Test configuration.
- Figure (7.3). Typical load/deformation graph.
- Figure (7.4). Modular ratio comparison.
- Table (7.5). Results of the test on BRIDGE - DECK specimens.
- Table (7.6). Calculation values for the BRIDGE - DECK.
- Figure (7.7). The comparison between the theoretical and the experimental value of the ultimate load.
- Table (8.1). The schedule of the test on sheeting.
- Table (8.2). The specification of the initial trial mixes.
- Figure (8.3). The profile of the corrugated sheets.
- Figure (8.4). The layout of a sheeting plant.
- Table (8.6A). Test results on the small, flat specimens.
- Table (8.6B). Test results on the small, flat specimens.
- Table (8.7A1). The results of the second moment of area & the position of the N.A for the corrugated sheet specimens.

Table (8.7A2). The results of the second moment of area & the position of the

N.A for the corrugated sheet specimens.

Table (8.7B). The results of the ultimate stress & the modulus for the

corrugated sheet specimens.

Figure (8.8). Comparison between the asbestos - cement & the polymer concrete sheets.

Figure (8.9A). Polymer concrete specimen (4.2).

Figure (8.9B). Asbestos-cement specimen.

Figure (9.1). Typical junction.

Figure (9.2). Plan of elevation of the bungalow.

Figure (9.3A). Gauge locations load in line with eaves.

Figure (9.3B). Gauge locations load in line with gable.

Figure (9.4). Diagram of loading frame.

Table (9.5A). Loads and displacement (load along the eaves).

Table (9.5B). Loads and displacement (load along the gable).

Figure (9.6). Racking tests (displacement for dial gauge No:1).

## NOTATIONS

The following notations are those generally used in this thesis

If other are used they will be mentioned following their appearance

$a$	Distance from support to the load
$b$	Width of the section
$L$	Span between the supports
$t$	Thickness of the faces
$d$	Depth of the section
$d_1$	Distance between the centre line of the upper and lower faces
$c$	Depth of the core
$\rho$	Density
$\phi$	Relative rotation
$F$	Factor of safety
$\nu$	Poisson's ratio
$\nu_f$	Poisson's ratio of the face
$\epsilon_u$	Ultimate displacement
$A$	Cross-section of area
$A_p$	Cross-section of area of the polymer concrete
$A_s$	Cross-section of area of the steel reinforcement normal to its length
$\Delta$	Deflection
$\Delta_{max}$	Maximum deflection

$y_b$	Deflection due to bending
$y_s$	Deflection due to the shear
$W$	Total applied load
$W_p$	Load at the end of elastic behaviour
$W_u$	Ultimate load
$q$	Uniformly applied load
$\bar{y}$	Vertical distance of centroid from origin
$\bar{y}_t$	Vertical distance of centroid from origin at the top of specimens section
$\bar{y}_b$	Vertical distance of centroid from origin at the bottom of specimens section
$I$	Second moment of area
$M$	Bending moment
$M_u$	Ultimate moment
$M_t$	Moment at the top of the specimens cross-section
$M_b$	Moment at the bottom of the specimens cross-section
$\sigma$	Stress
$\sigma_t$	Tensile stress
$\sigma_{t(d)}$	Direct tensile stress
$\sigma_{t(in)}$	Indirect tensile stress resulting from the rupture test
$\sigma_f$	Stress at the end of the elastic behaviour
$\sigma_u$	Stress at failure
$\sigma_c$	Compressive strength resulting from the cube test
$E$	Elastic modulus

$E_f$	Elastic modulus of the face
$E_r$	Elastic modulus of the rupture
$E_s$	Elastic modulus of the steel
$E_p$	Elastic modulus of the polymer concrete
$m$	Modular ratio ( $E_s/E_p$ )
$G$	Shear modulus of the core
$D$	Flexural rigidity ( $EI$ )
$D_1$	Flexural rigidity (associated with sandwich beam, neglecting the local bending of the stiffness of the face) ( $E_f b t d^2$ )/2
$D_2$	Flexural rigidity (associated with sandwich panel, with cylindrical bending and neglecting the local bending stiffness of the face) ( $E_f t d^2$ )/2( $1 - \nu_f^2$ )
$\epsilon$	Strain in general
$\epsilon_s$	Steel strain at yeild
$\epsilon_p$	Polymer concrete strain at tensile fracture

# CHAPTER (1)

## CHAPTER ONE

### 1. Introduction and historical background of polyester resin

The history of polyester resin can be traced back to as early as 1847, when a Swedish chemist, J.J Berzelius, obtained a white amorphous solid of a resinous nature by reacting *Tartaric acid* with *Glycerol*. The reaction was subsequently modified in England, by replacing the Tartaric acid with *Phthalic Anhydride acid*. This particular work was carried out by Watson Smith who, in 1902, obtained a wide range of resinous products from such reactions, which he named *Glyptal*.

In 1904, Blaise and Marcilly prepared polyesters from hydroxypivalic acid and assigned chain formulae to the products. The term *alkyd*, which is derived from a combination of the words Alcohol acid, arrived in 1927 when Kienle combined fatty acids with polyesters and improved the drying properties.

Carothers was the first person who prepared polyesters with clearly defined polymeric structures, which he later described as being 'produced by recurring condensation of monomers'. His work was so thorough that manufacturing techniques used to this day are still essentially based on the reactions used in his experiments. He prepared polyesters from phthalic anhydride and ethylene glycol, and from maleic anhydride and ethylene glycol. Condensation reactions were initially performed under ordinary pressure and, in the last phase, under vacuum. When he used maleic anhydride or fumaric acid, he polymerised the monomers in a stream of



nitrogen. It was this work that is the basis of the modern technology and chemistry of polyesters.

As can be seen, the term polyesters covers a variety of species of polymeric materials. There is a linear thermoplastic, an example of which is terylene, the man made fibre. Then there are the cross-linked resins which are generally referred to as the alkyd resins. Lastly there are the chemically unsaturated polyesters.

A great advance was considered to have been made in 1937 when Carlton Ellis, in USA, discovered that by adding unsaturated monomers to unsaturated polyesters the setting (curing) time was substantially reduced. In 1941 he obtained a patent which covered the technique of copolymerising polyesters, made from maleic anhydride, with styrene and then curing this with peroxide catalysts, thereby increasing the rate of cure of the polyester by about thirty times. This made the polyester resins attractive for use on a commercial basis and was the first time that the unsaturated polyesters were suggested as moulding materials.

The second world war increased the development rate of polyesters. In 1942 the reinforcement of polyester polymers by glass fibres was discovered by the United States rubber company.

In 1946 polyester resins were first offered to specialized industries such as the aircraft industry. Alkyd moulding materials were first produced in the USA in 1948 and then later in Great Britain (1952). The problems that existed at that time were mainly shrinkage and cracking during the cross-linking reaction. Fillers were evaluated in a search for a remedy to these problems. As a result numerous

fillers were offered on the market which claimed to reduce shrinkage and thereby reduce cracking, and also give better surface appearance, better hardness values, greater abrasion resistance and better electrical characteristics. The products were, however, still brittle and the need for better physical and mechanical properties accelerated the use of fibre reinforcement. Chopped animal fibres were used to produce dough moulding compounds which were subsequently moulded to make distributor caps for cars, and other similar small objects.

Major developments were taking place with regard to curing systems for different conditions. Up to 1946 cure had to be carried out at temperatures around  $100^{\circ}\text{C}$ . In 1949 a patent indicated that by mixing a peroxide and dimethylaniline into the resin, a cold curing system could be attained.

However, in the USA, glass fibre reinforced boat hulls were made in 1946, but the probable reasons for the delay in the acceptance of glass fibre as reinforcement was its high cost and also its scarcity. With the change in these two aspects during 1948 and 1949 the growth pattern also changed and the upsurge is recorded to have started in real earnest by 1952.

However, manufacturers of glass fibre still had numerous difficulties to overcome, an example being that the earliest fabrics had to be impregnated with resin in the loom. This led to the development of the various forms of glass for reinforcement.

By this time many other cold curing catalyst systems had followed including the ones which are widely used now as cobalt naphthenate and peroxides such as

methylethy ketone peroxide and cyclohexanone peroxide. These effective cold curing systems opened the way for the fabrication of larger structures and as a result wider areas of application.

Now there are over a hundred different applications where glass fibre reinforced polyester are employed due to their reasonable price and excellent properties.

The desirable properties of the polyesters are:

Excellent dimensional stability, high strength, high stiffness, low creep at elevated temperatures, excellent electrical properties, good chemical resistance and low mould shrinkage.

Disadvantages which place some limitations on their use are:

Limited stability at very high temperatures, costs high compared with conventional structural materials, stiffness low compared with, eg. structural metals.

# CHAPTER (2)

## CHAPTER TWO

### 2. Material used for construction of polymer concrete

#### 2.1 Aggregate (sands and micro filler)

Aggregate is much cheaper than resin and maximum economy is obtained by using as much aggregate as possible in the manufacture of polymer concrete. The commonly held view that aggregate is a completely inert filler is not true, its physical characteristics and its chemical composition may affect to a varying degree the properties of polymer concrete. The characteristics of the aggregate which may have significant effect on polymer concrete behaviour are its strength, deformation, durability, toughness, hardness, specific gravity, chemical composition, shape and surface texture and the most important one from the users point of view is particle size distribution or grading.

Micro fillers are also used to reduce crazing, shrinkage, the co-efficient of expansion, porosity, as well as improving moulding characteristics.

In finished products surface appearance, dimensional stability, abrasion, moisture and temperature resistance, fire retarding and creep, can be improved by the choice of appropriate aggregate and micro filler materials. However, care must be taken in the selection of these fillers, for instance using a filler with high pH

Alumina (*aluminium oxide*),  $Al_2O_3$ ; Silica (*silicon dioxide*),  $SiO_2$  ; Zirconia (*zirconium dioxide*)  $ZrO_2$ .

It can be used in small quantities as a pigment. It increases the workability of the mix but it is too expensive for using as a filler. It is not flammable and melting point is approximately about  $1800^{\circ}C$ . The specific gravity is between 3.7 to 4.2 and the primary particles will lie in the range 0.05 to  $0.40\ \mu m$  with a mean size of 0.15 to  $0.24\ \mu m$ .

## **2. Talc:**

The material referred to locally as talc, is pure white dolomite with a minimum 99% calcium, magnesium carbonate content, used in the paint and plastic industries. The particle size distribution lies between  $45\ \mu m$  to  $2\ \mu m$  and with pH value of 10 would not be suitable for the cold curing system.

## **3. Fillite:**

Fillite is a filler with a free flowing hollow microsphere with a composition of alumina ( $Al_2O_3$ , 27% – 33%) and silica ( $SiO_2$ , 55% – 65%) and iron ( $Fe_2O_3$ , 4% max.). With low density, it can reduce bulk density of the mix and therefore may be cost-effective, but at the same time it can reduce the strength of the end products, therefore the amount of fillite used in the mix is limited. The effect of fillite on strength has been investigated thoroughly and has been reported later in this thesis.

## **4. Pellite:**

Pellite is produced by passing selected molten slag direct from the blast furnace

down a vibrating chute through water jets onto a rapidly rotating drum. The molten slag expands rapidly to many times its original volume on contact with the water. The expanded slag is broken into small particles which are hurled by the drum through a water mist whilst they are still red hot, causing them to become fully or partially rounded with a smooth glassy surface. When cool, the pelletised particles are blended and screened onto coarse and fine grades. The composition is mainly of lime, silica and alumina, ( $CaCO_3$ ,  $SiO_2$  and  $Al_2O_3$ ). The particle sizes lie between 2.4mm to 300  $\mu m$  for fine grade.

#### **5. Silica Flours :**

As the name indicates, it is pure silica powder with a minimum content of 99% ( $SiO_2$ ). It is produced from indigenous deposits of sand. The particle sizes are between 50 to 2 $\mu m$ , with the mean particle size of 15  $\mu m$ .

#### **6. Omya (B.L.H):**

This is a high purity, surface treated calcium carbonate (limestone of organian origin). The surface treatment renders the particle completely hydrophobic, thus increasing its chemical inertness and its compatibility with organic media. Further advantages of the treatment; ease of dispersion and can not be affected by moisture. The omya manufacturing plants are based on very large deposits of pure clean calcite or amorphous chalk. It is produced in omyens plants in France and imported into the U.K. It has a mean particle size of 5 microns and a max particle size of 20 microns.

## **7. Pozzolan:**

The material referred to locally as pozzolan, is a material in the form of a fine powder which is a by-product produced during the burning of coal, generally for the generation of electricity. Most of the ash particles formed during the combustion fuse (approx 80%) and are fine enough to be carried with the combustion gases from the furnace. The material is also known as pulverized-fuel ash or pfa. To avoid the release of pfa into the atmosphere the combustion gases are channelled through a system of mechanical and electrostatic precipitators which progressively remove the finer particles. Pfa particles range in size from approximately 1mm to less than 0.5 microns.

The amount and the quality of the pfa produced from power stations is governed by several factors, which include:

1. The source of the coal
2. The efficiency of the pulverisation
3. The efficiency of the furnace and its operation
4. The method of precipitating the ash from the combustion gases
5. The demand for electricity.

These factors can effect the colour of the pfa, the residual fuel (carbon) content, the magnesium and sulphate contents and the overall particle size distribution. Therefore although some sources of pfa increase the workability and strength of the mix, care must be taken in the selection of these materials, to ensure that they undergo strict quality control checks.

#### 8. Ballotini:

These are perfectly spherical soda (A) glass particles with a minimum surface area and hence, a very much lower effect on resin viscosity. Since the amount of filler used has a direct effect on the viscosity of the resin, higher loading of ballotini can be used in a resin system while maintaining a viscosity equal to that of another filler with a lower loading. The incorporation of ballotini glass spheres into a resin system reduces its shrinkage, but of particular importance is the isotropic behaviour giving uniform shrinkage in all directions. This very useful property allows moulding of low shrinkage to be made to very high tolerance.

#### 9. Trihyde:

This grade is a pure alumina trihydrate,  $Al(OH)_3$ , *approx.* 99.6%. It is intended for use as a flame retardent filler in plastics materials. The pH value is about  $9 \pm 1$ .

#### 10. China clays (grade E and D ):

This is a white powder with the main composition of silica ( $SiO_2$ ) and alumina ( $Al_2O_3$ ). The pH value is around 5. The particle size distribution lies between  $20\mu m$ -  $2\mu m$ .

#### 11. Neosyl (ET):

Sodium silicate and sulphuric acid are the raw materials used in the production of this filler. They are reacted together under precisely controlled conditions to give a slurry of precipitated silica, and sodium sulphate in solution. The slurry is then filtered and washed with water to remove the sodium sulphate, and after that the

silica is dried and then milled to the required particle size distribution.

The main part of the composition is the silica ( $SiO_2$ ) with the minimum amount of 98% . Soda ( $Na_2O$ ) and sulphate ( $SO_4$ ) are the residual components.

The PH value is approximately 6, with the average size  $6.5\mu m$  and S.G of 2.

### 2.1.2 Determination of bulk densities and selection of suitable <sup>micro</sup> fillers

The bulk densities of all the fillers were determined, and with the constant volume ( $0.07 \times 10^{-3} m^3$ ), they were mixed with a standard amount of resin (200gr). The ease of workability and the colour were observed, and they are listed in table (2.1) in the order of the highest workability.

The following fillers were chosen as having suitable properties. (ie; cheapness, good workability, colour, lightness, natural PH value) for further investigations:- pozzolan, Tioxide, Ballotini, Omya(B.L.H), Silica flour, china clay and Fillite.

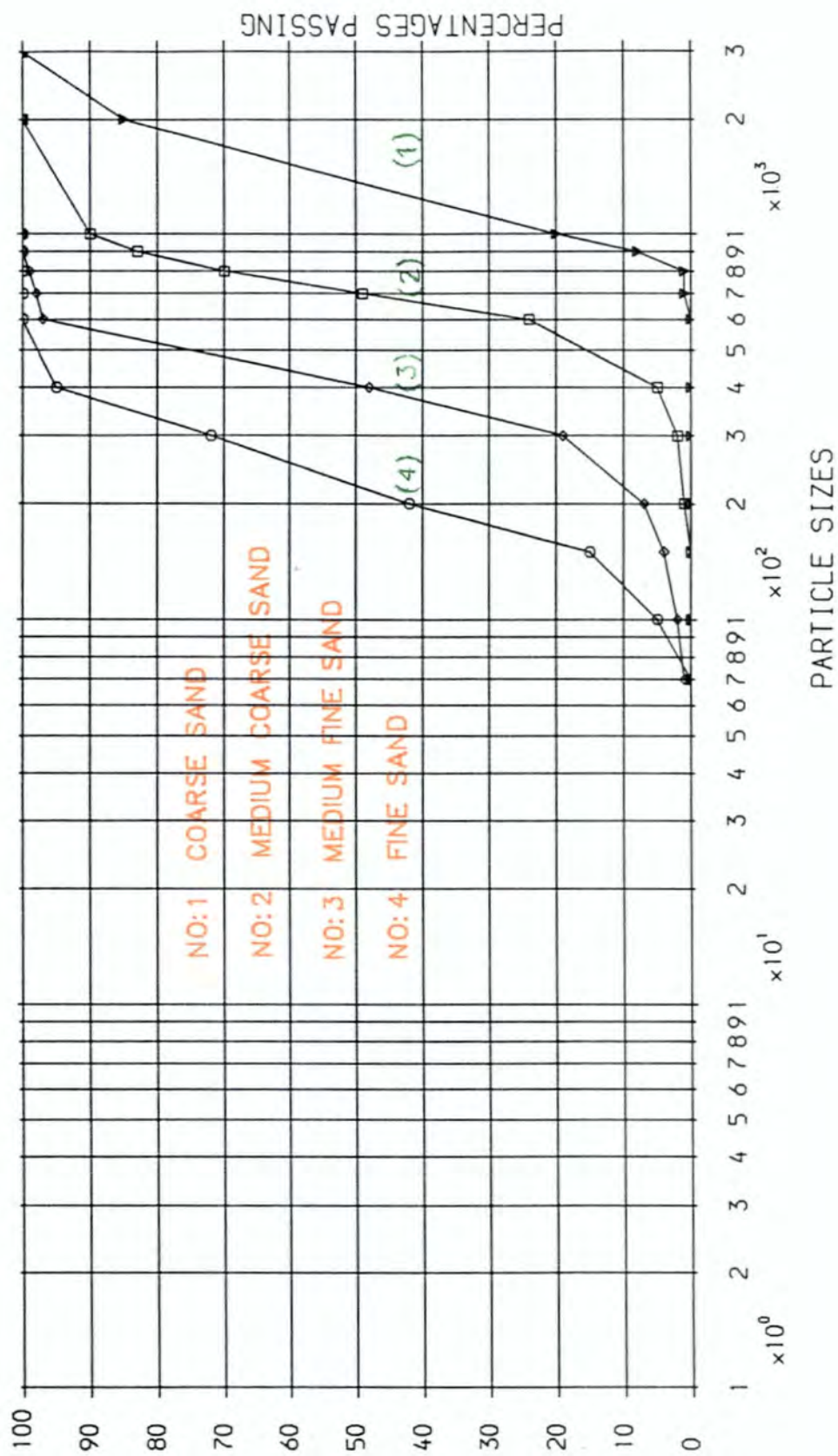
### 2.1.3 Sieve analyses

The grading of an aggregate has a great effect on all the properties of the product which will be important from the engineering point of view, such as density, water absorption, heat transmsion, and, above all, strength.

The sieve analyses carried out on the aggregates used in this research were done in the usual way, by separating the aggregate particles by passing the aggregate over a series of sieves of decreasing mesh size. The weights of aggregate retained on each sieve were recorded and from that the % of the weight passing the sieves were

## GRADING CURVE

SAND NO: 1, 2, 3 & 4



NO:1 COARSE SAND

NO:2 MEDIUM COARSE SAND

NO: 3 MEDIUM FINE SAND

NO: 4 FINE SAND

(1)

12

3

(4)

## PARTICLE SIZES

calculated and the grading data and curves were obtained: These can be seen in tables (2.2 and 2.3).

The sieve analyses for the micro filler were carried out by the pipette (sedimentation) method according to BS 1377. A small amount of the filler (approx 12g) was placed in a conical flask and 25ml of 2 % sodium hexametaphosphate was added. The flask was half filled with distilled water and then the flask was vigorously shaken until the sample was brought into suspension.

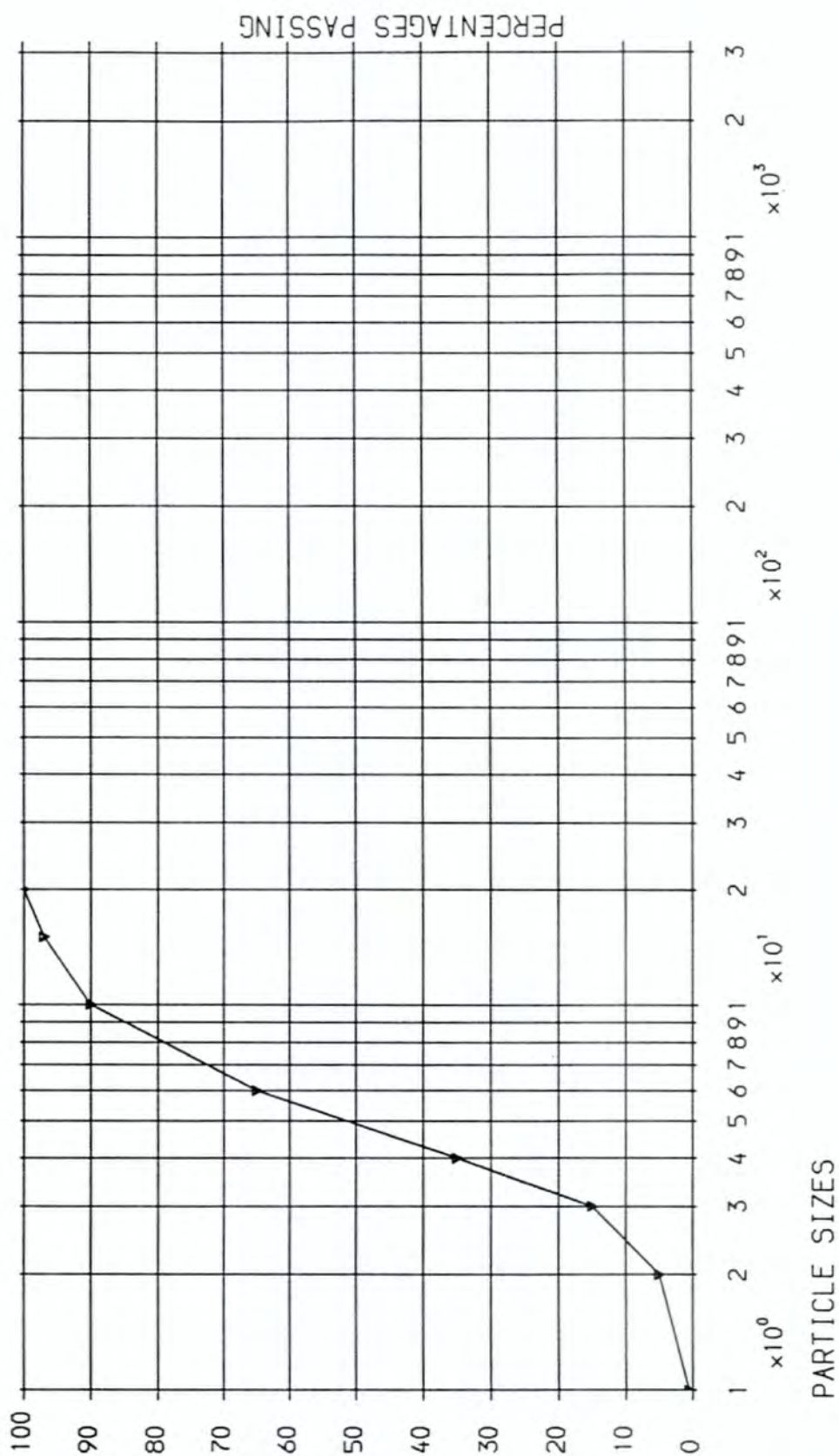
This was then transferred to a graduated 500ml sedimentation tube and topped up with distilled water to exactly 500ml. After 24 hours in a temperature bath (25°C), the tube was taken out and shaken thoroughly and then replaced in the bath. At the same instant as the tube containing the soil suspension was replaced in the bath, the stop watch was started.

The pipette samples were taken at 10cm depths at various time intervals. The samples were drawn up into the pipette. These were dried and the weight of residue was recorded for these time intervals and by using the following formula the particle size and % of particles passing were calculated.

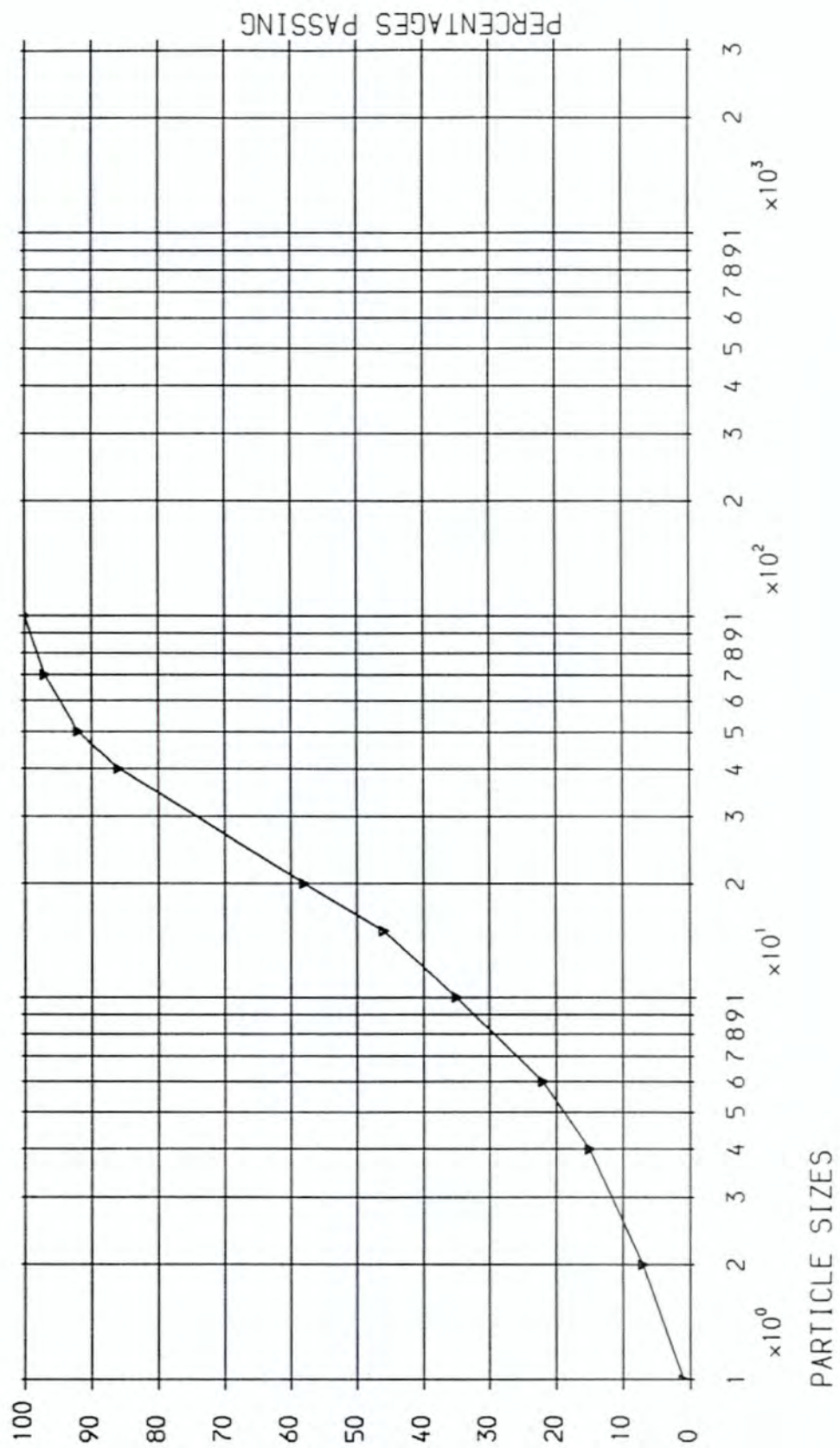
$$\% \text{ of particle passing} = \frac{100(W_d - W_c)}{V \times W_1} \quad 2.1$$

$$\text{particle size} = F \times \sqrt{\frac{10}{\text{time}(\text{min})}} \quad 2.2$$

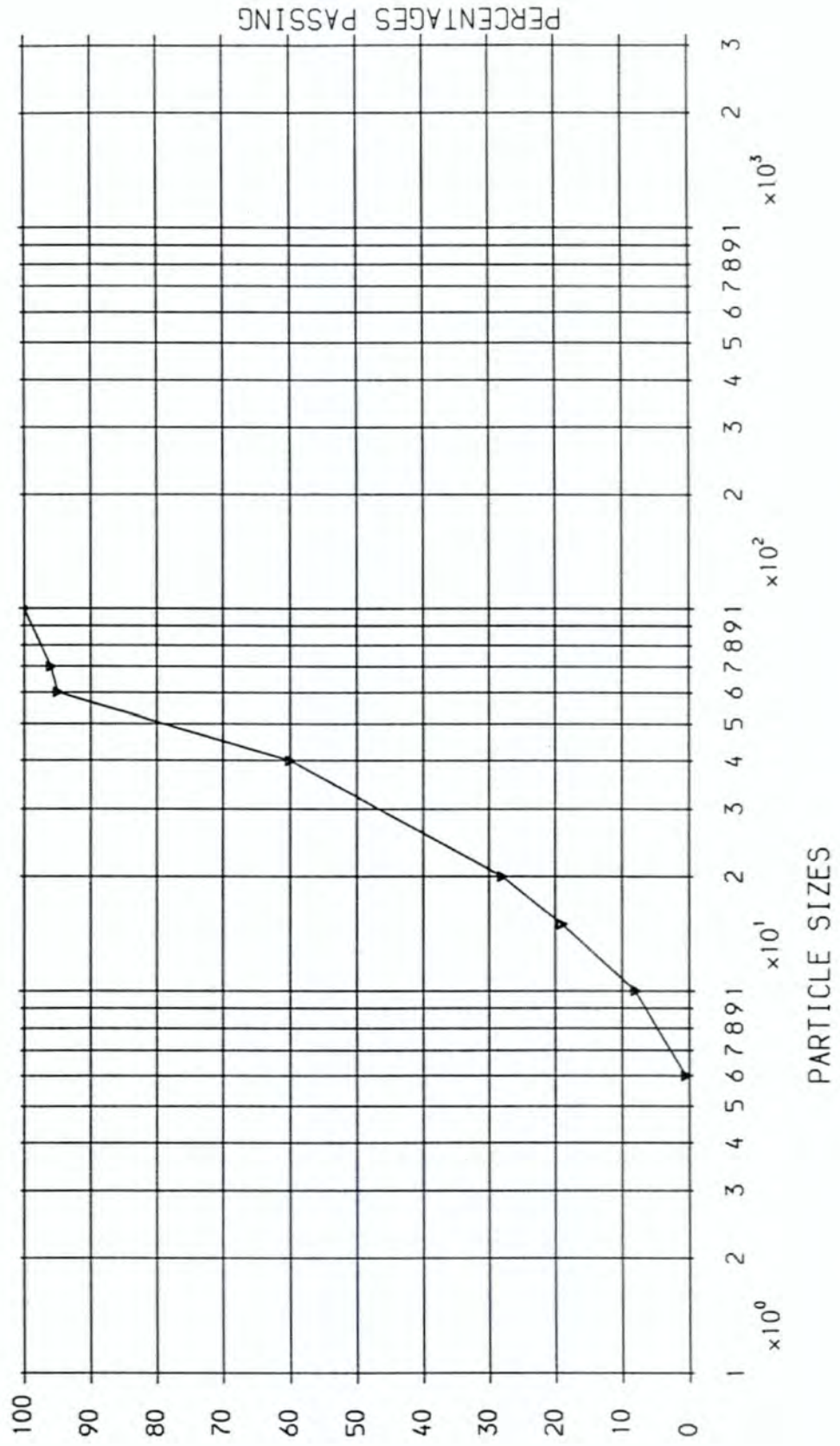
# GRADING CURVE FILLER: B.L.H



# GRADING CURVE FILLER: SILICA FLOURS

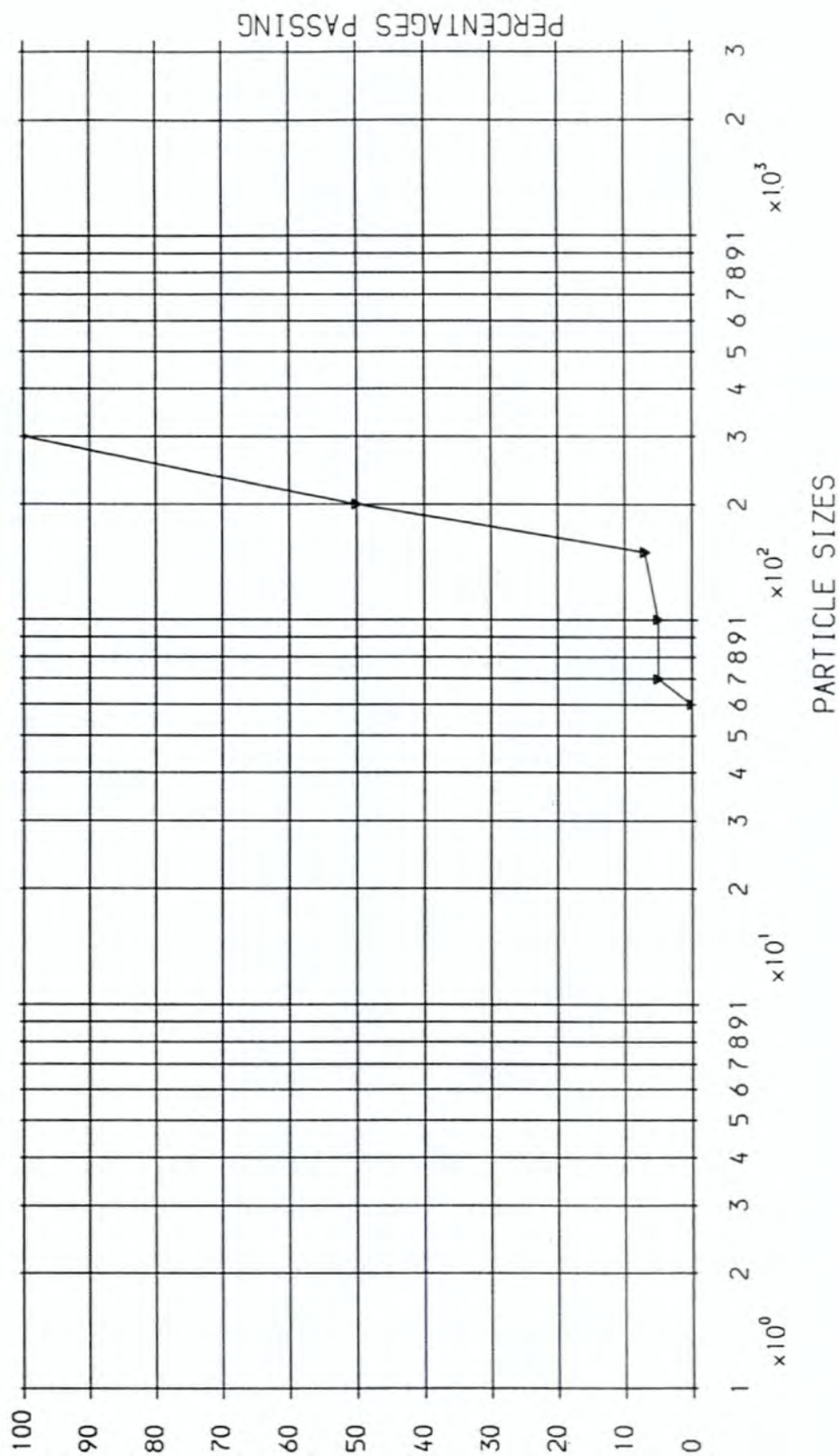


# GRADING CURVE FILLER: BALLOTINI

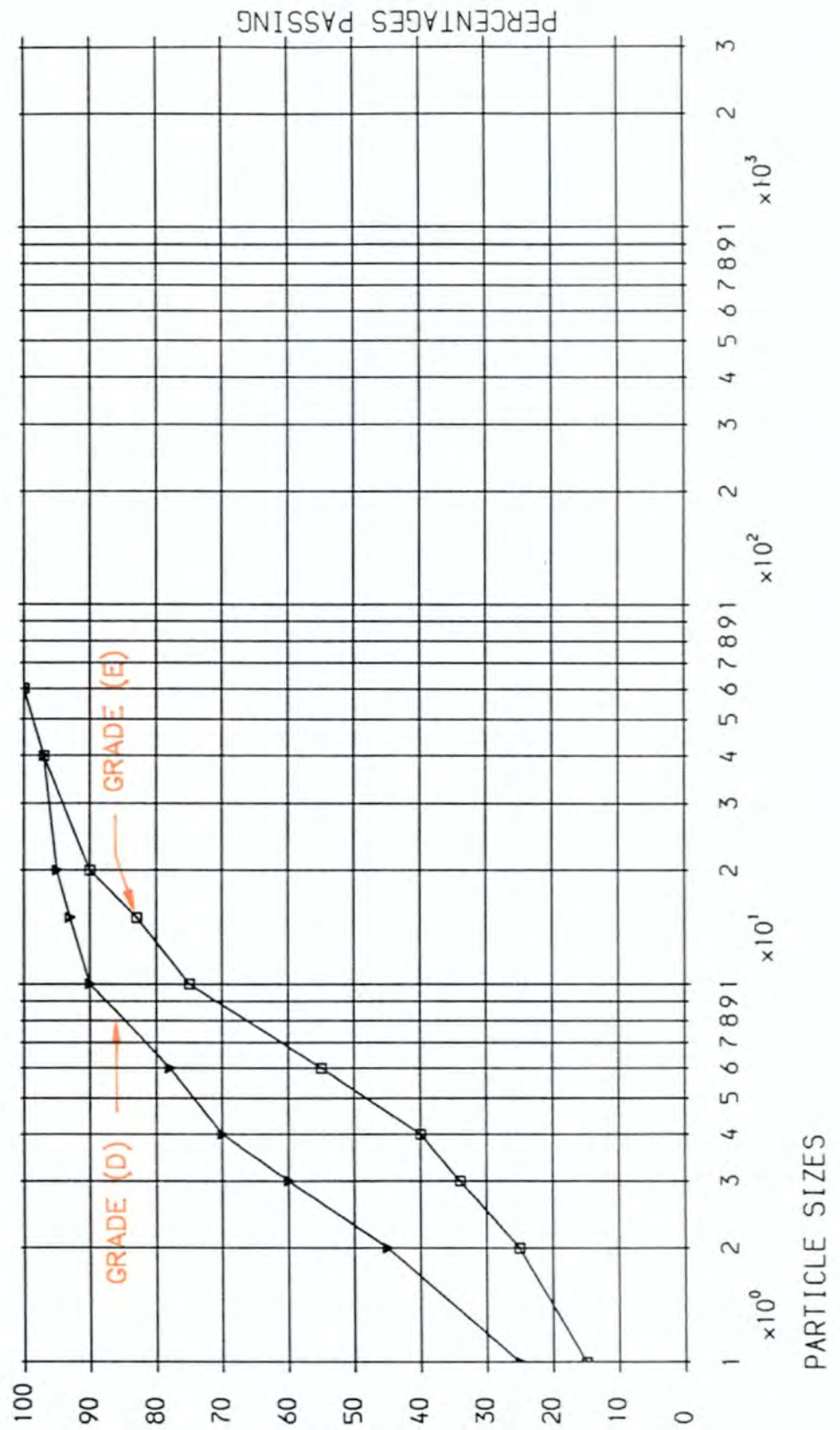


# GRADING CURVE

FILLER: FILLITE



# GRADING CURVE      FILLER: CHINA CLAY, GRADE E & D



Where:

$W_d$  = weight of container plus dry soil

$W_c$  = weight of container

$V$  = volume of pipette used (9.6752ml)

$W_1$  = gr. per ml of suspension

$F$  = coefficient factor depending on S.G and the bath temperature.

As a result the particle size distribution charts were drawn, and are shown in tables (2.4 - 2.9).

#### **2.1.4 Chemical analysis**

For each analysis approximately 50g of filler were ground to a fine powder and digested into 50ml of hydrochloric acid (HCl) and hydrofluoric acid (HF) until the solution was clear.

The % of all elements were obtained by atomic absorption. The test results are shown in table (2.10).

#### **2.1.5 Determination of specific gravity, moisture contents, bulk density and pH value**

##### **1. *Specific gravity and moisture content***

The specific gravity and the moisture content of all the aggregates and micro fillers were determined according to BS 1377.

## 2. Bulk density

The bulk density of the micro fillers were determined in Toluene according to (BS812). 10 g of oven dried sample was placed in a 50ml glass stoppered measuring cylinder. Toluene was then added up to the 40ml mark and the sample was shaken and left to settle for 6 hours. The bulk volume was read off in ml(V) and bulk density was calculated with the following formula:

$$\text{Bulk density} = \frac{10}{V}(\text{gr/ml}) \quad 2.3$$

## 3. pH value

A solution in which hydrogen and hydroxide ion concentrations are equal(eg. pure water) is termed an exactly neutral solution ie;  $[H]^+ = [OH]^- = 10^{-7} \text{mol dm}^{-3}$ . If  $[H]^+$  is greater than  $10^{-7}$ , the solution is acid and if less than  $10^{-7}$  the solution is alkaline.

The quantity pH is the logarithm (to the base 10) of the hydrogen - ion concentration with negative sign, ie;  $pH = -\log[H]^+ \text{ or } [H]^+ = 10^{-pH}$ . Thus a neutral solution with  $[H]^+ = 10^{-7}$  has a pH of 7, and a solution with a hydrogen-ion concentration of  $1 \text{mol dm}^{-3}$  has a pH of 0 ( $[H]^+ = 10^0$ ), and a solution with a hydroxide ion concentration of  $1 \text{mol dm}^{-3}$  has a pH of 14 as  $[H]^+ \times [OH]^- = K_w = 10^{-14} \text{mol dm}^{-3}$  where  $K_w$  is the ionic product of water at  $25^\circ\text{C}$ .

Determination of the pH value for the samples was carried out according with BS 1377. The samples were air dried, crushed and passed through a 3.35mm sieve.

30gr of a sample was weighed into a 100ml beaker. 75ml of distilled water was added and the suspension stirred and then left for several hours.

The pH meter was calibrated using standard buffer solutions and then the electrode was immersed in the sample. The pH value of the soil suspension was reported to the nearest 0.1 pH unit.

All the results from the above tests can be seen in table (2.11).

## 2.2 Polyester resins

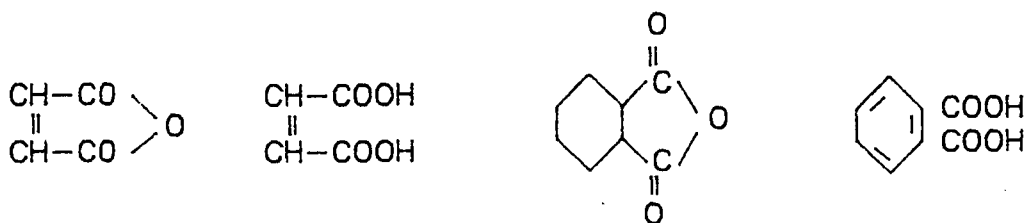
Three basic types of structural units make up the backbone of unsaturated polyesters. They are;

- i. the saturated acid units,
- ii. the unsaturated acid units,
- iii. the glycol unit.

The unsaturated acid provides the sites for cross-linking between chains to give the final infusible and insoluble product. The saturated acid molecules determine the spacing of the unsaturated acid units along the chain, and also the concentration. The glycol provides the means for esterification and joining up of the two acids to form the polymer chain.

The choice of acids and glycols for resin manufacture is of importance. Both the chemical nature of the components and the quantities employed play important roles. The most common acids (or anhydrides) employed are *maleic* or *fumaric*,

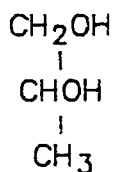
*phthalic, isophthalic, adipic acids*. The majority of resin used in this research was a combination of *maleic* and *phthalic acids* with the following structural formula:



Maleic anhydride    Maleic acid    Phthalic anhydride    Phthalic acid

The relative quantities of each influences the cross linking density and the water absorption of the resin.

Glycols are yet another of the resin constituents which can influence properties. By far the most common in use is propylene glycol with the following structural formula:



### 2.2.1 Resin preparation

Normally all polyester resins are prepared in a resin kettle where the condensation reaction is carried out.

The *alcoholic* and *acidic* constituents are first charged into the resin kettle and the temperature raised slowly to  $140^\circ\text{C}$ , with continuous stirring. The oxygen present in the vessel is then flushed out by an inert gas. The reactants are refluxed and an inert solvent such as xylene is added to distill off azeotropically the water of

reaction. The temperature is then slowly raised to  $190^{\circ}\text{C}$  until the acid value of the resin has reached 38-45 (the acid value is an indication of the amount of free unreacted acid remaining, and is expressed as the number of mg. of potassium hydroxide required to neutralize 1g. of sample).

On reaching the required acid value, the reactants are cooled to below  $150^{\circ}\text{C}$ , when the resin is ready for mixing with the reactive monomer. These resins, when dissolved in this monomer are highly reactive, and the cross-linking reaction can be started off by a free radical mechanism, and will gel. However, this can be stopped by adding chemicals known as *inhibitors* which prevent the free radicals from reacting. Such materials are quinone, hydroquinone and catechol.

Thus, before adding the resin from the kettle to another kettle containing the reactive monomer it is essential first to dissolve an inhibitor in the monomer. When the inhibitor has been well dispersed the polyester resin is added and stirred thoroughly. Finally the resin is ready for discharging into containers. A flow diagram of the process can be seen in Fig (2.12)

The following resins were used in the experimental work: Resin 401, 602, 247, 1077-6005, L.V, L.V.M. However, it has to be noted that these names are just a figure chosen by the manufacturers.

### **2.2.2 Determination of viscosity**

The viscosity is a property of a liquid which resists shear deformation increasingly, with increasing rate of deformation (BS 188).

Control of the viscosity of resin is achieved by the degree of condensation, the criteria being average molecular weight and molecular weight spread, and also the water content of the resin. A relatively small amount of residual water will reduce the viscosity substantially, but water also reduces reactivity. The more 'reactive' a resin is to an acid catalyst, the shorter will be the cure time.

The viscosity of the resin was measured by a **FERRANTI SHIRLEY VIS-COMETER MR3** which has the following units:

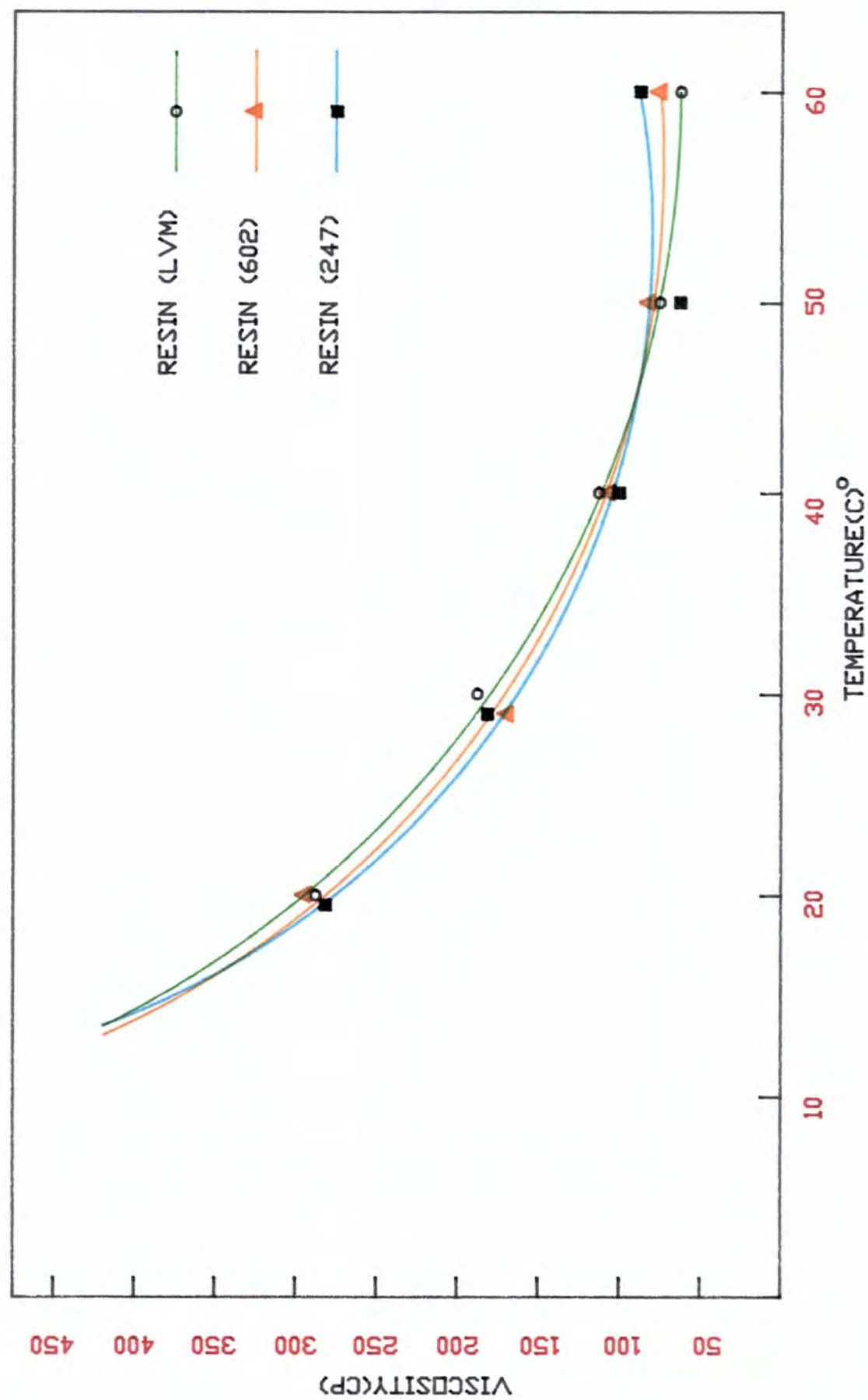
- a. measuring unit
- b. control unit
- c. set of cones

A small amount of resin was sheared on the narrow symmetrical gap between the cone and the plate with the apex of the cone just touching the surface of the plate.

The cone was driven by a variable speed motor through the Torque dynamometer consisting of the torque spring and a potentiometer. The dynamometer measured the viscous traction of the cone. The following tests were carried out on the polyester resin:

### **1. Effect of temperature on viscosity of polyester resin**

Five different types of resin were investigated in this exercise. For each test a small amount of resin was placed between the cone and the plate. After the resin reached the required temperature, twelve readings were taken at different ranges and speeds. Then, the plate was cleaned and the test repeated three times at each



Fig(2.13).Effect of temperature on viscosity of polyester resin

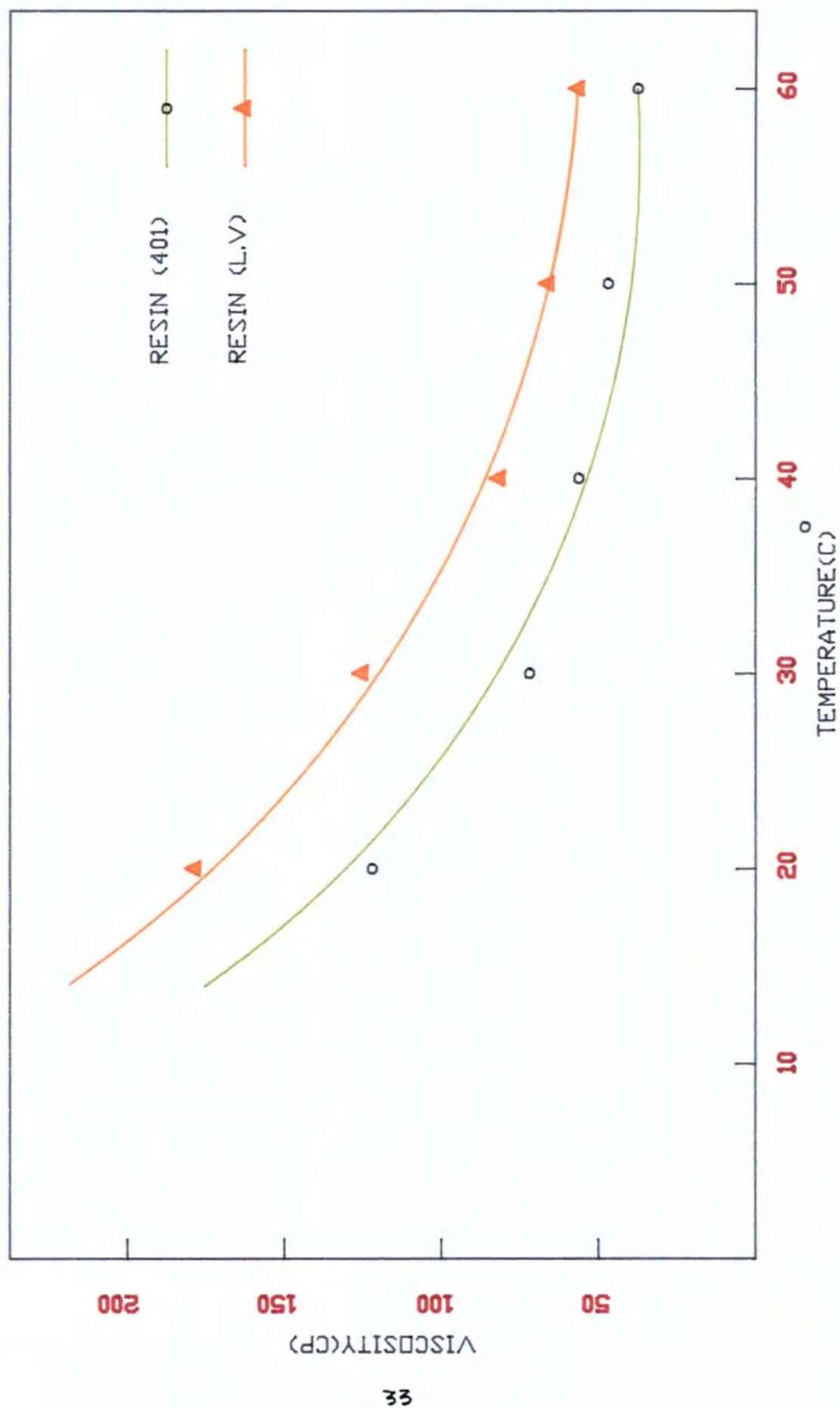


Fig.(2.14). Effect of temperature on viscosity of polyester resin.

specific temperature. The average of the 36 readings gave the viscosity of the resin at that temperature. The graphs were plotted (fig 2.13 and 2.14) and the following conclusions were drawn:

- i. as the temperature increases, the viscosity of the resin decreases.
- ii. below  $15^{\circ}\text{C}$  the viscosity of the resin was excessively high and it would not be recommended that the resin should be used for cold curing system moulding, if the room temperature is below  $15^{\circ}\text{C}$ .

## **2. Effect of time on viscosity at $60^{\circ}\text{C}$ of polyester resin**

Resin (401) and resin (L.V.M) were chosen for this particular test. Two small containers of resin (401) and (L.V.M) were placed in an oven at  $60^{\circ}\text{C}$ . The viscosity of the resins were measured as above, at 4 hour intervals (fig 2.15) and the following values were observed:

- i. As time passed by, the viscosity of the resin increased, and after 3 days the resin was totally solid.
- ii. Although the viscosity of the 401 was much lower than the L.V.M at the start of the test, after 36 hours the positions were reversed.

## **3 Effect of temperature on viscosity of polyester resin containing 24 % of filler, by weight**

Using the resin 401 and L.V.M, two types of filler were examined. (pozzolan and B.L.H). The same exercise as No 1 was repeated (fig 2.16) and the following conclusions were obtained.

- i. At any given temperature, viscosity of a resin containing pozzolan is much

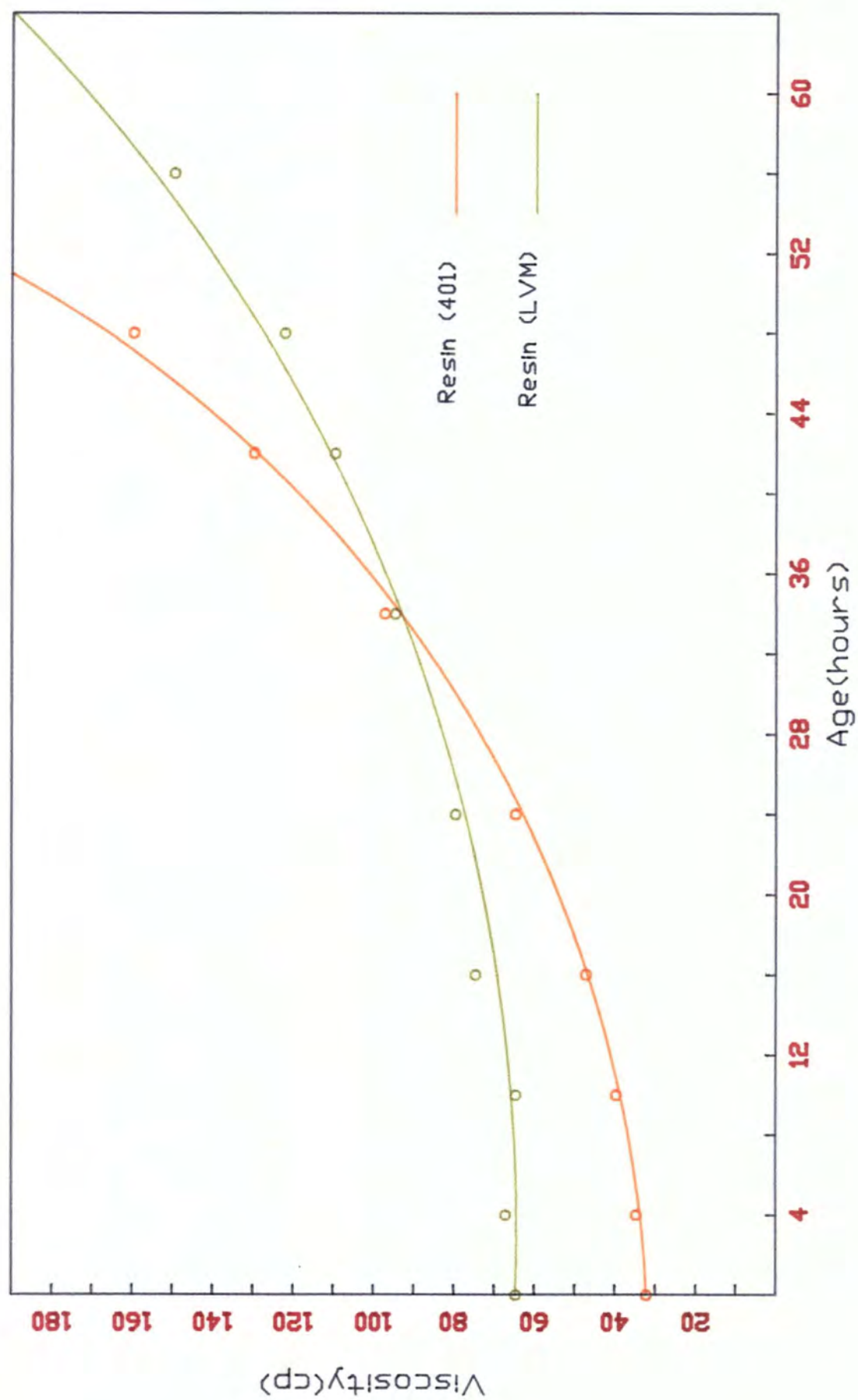


Fig.(2.15).Effect of time on viscosity at 60 °C of polyester resin.

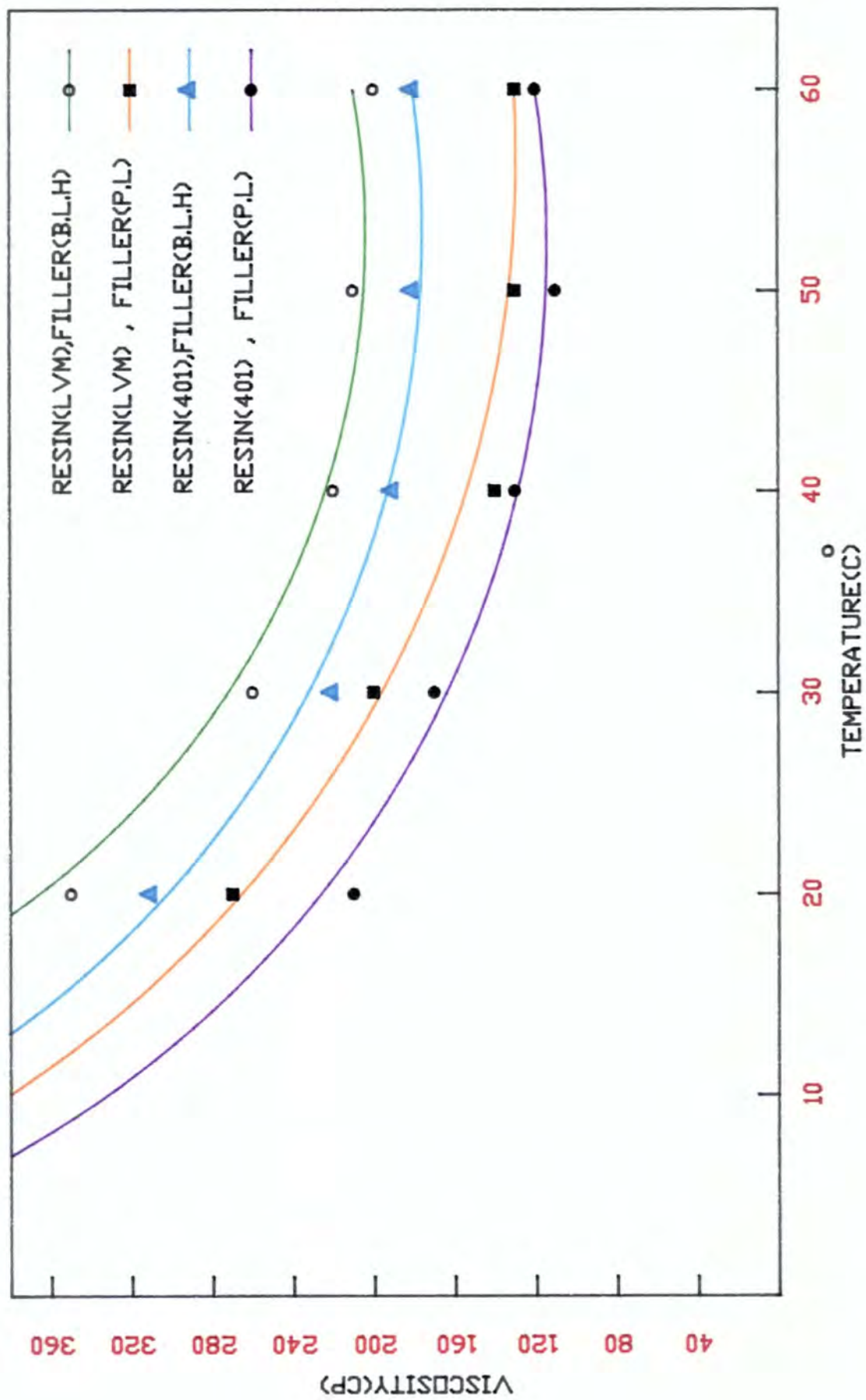


Fig.(2.16) Effect of temp. on viscosity of polyester resin containing 24% WT. filler

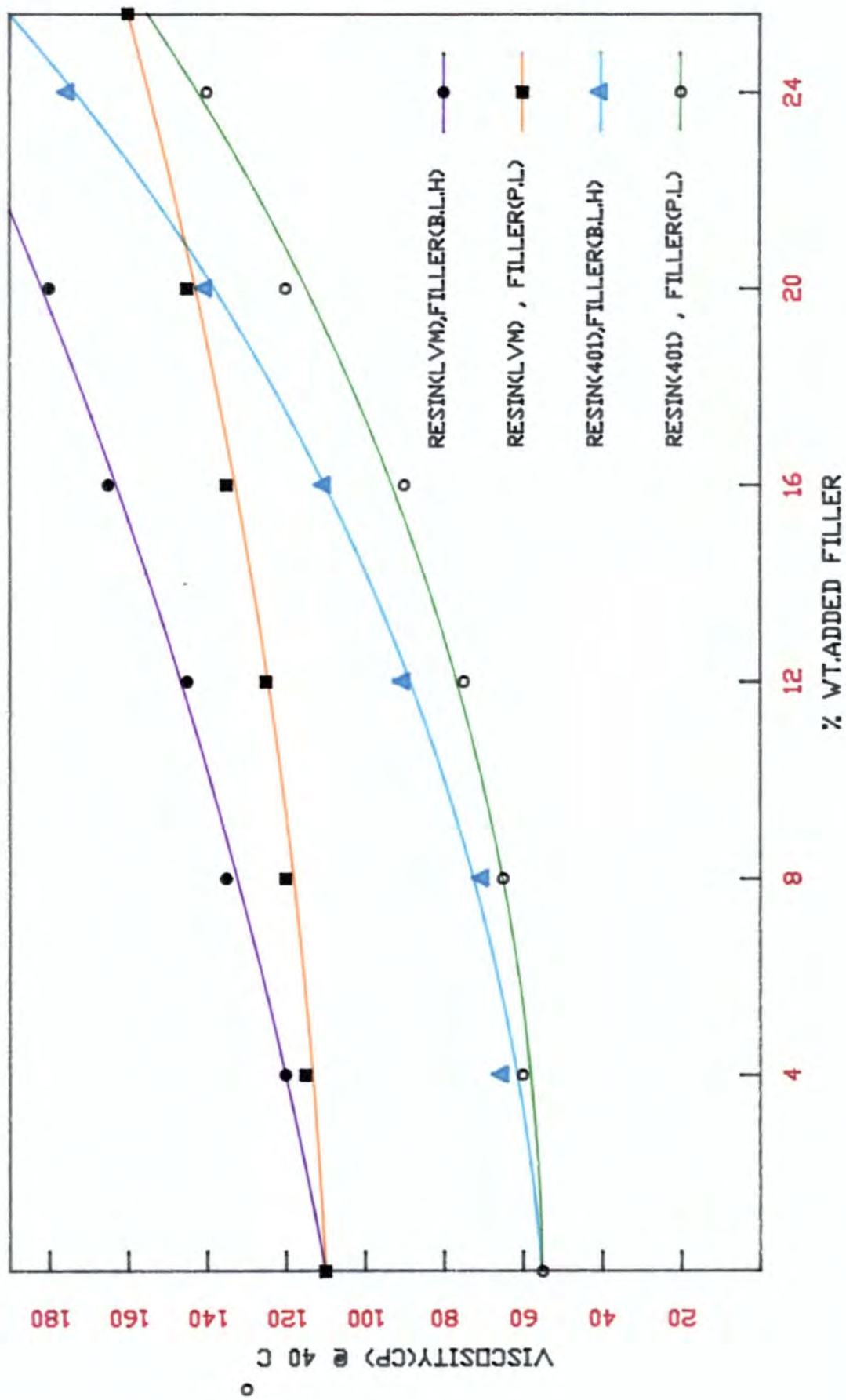


Fig.(2.17).Effect of filler addition on viscosity of polyester resin at 40 °C

lower than the one containing (B.L.H),ie; higher loading of pozzolan can be used in a resin while maintaining a viscosity equal to that of another filler with a lower loading.

- ii. The viscosity of the resin L.V.M containing 24% wt. of any filler is lower than the viscosity of the resin 401 containing the same filler. ie; The resin L.V.M is capable of much higher % of loading of filler.

#### **4. Effect of filler addition on viscosity of polyester resin at 40°C**

The viscosity of the resin(L.V.M) and (401) at a particular temperature (40°C with variable % of filler was measured. Fig (2.17) shows that any filler will increase the viscosity of the system and hence reduce ease of flow.

### **2.3 General aspects of monomers, inhibitors, catalysts and accelerators**

#### **2.3.1 Introduction**

Although unsaturated polyester resins will eventually gel without the use of additives, particularly under the influence of UV light, the rate of gelation and cure is too slow for practical purposes. Before going any further, there are some aspects that must be more fully understood, they are as follows:

1. **Pot life** is the time the resin may be stored before it gels.
2. **Gel time** is the time it takes the resin to change from a liquid to a soft flexible solid.

3. **Cure time** is the period required to develop the full properties of the composition, particularly maximum or near maximum hardness.

### 2.3.2 Monomers

The most commonly used reactive monomer for unsaturated polyesters is **styrene**. The composition of the polyester resin is designed so that the resin is soluble in styrene and gives a syrup of a consistency suitable for laminating. It is a mobile, colourless liquid boiling at  $146^{\circ}\text{C}$ . Styrene itself will polymerize readily under the action of light, heat or catalysts to give a thermoplastic polymer with good electrical insulating properties, chemical and water resistance. To some extent these properties are reflected in the polymer of styrene with an unsaturated polyester resin. The copolymer has the additional property of being a *cross - linked* product.

### 2.3.3 Inhibitors or stabilizers

The resin solutions in styrene are unstable, tending to gel on storage, even in the absence of catalysts, particularly at elevated temperature or in sunlight. In order to ensure a reasonable potlife in the uncatalysed state, inhibitors or stabilizers, such as *hydroquinone* or *tert-butyl catechol* are added to the resins by the manufacturers. In general, commercial polyester resins are stable for at least six months.

### 2.3.4 Catalysts

To speed up the cure it is necessary to add certain auxiliary materials. All formulations require the addition of a catalyst. Most organic peroxides will catalyse the resins such as **methyl ethyl ketone peroxide (MEKP)**

### 2.3.5 Accelerators

In the case of cold curing formulations, it is also necessary to employ accelerators. Accelerators are sometimes called promoters and they speed up the action of the catalyst. Normally they are **cobalt soaps** or **amines**. Catalysts and promoters must never be mixed directly with one another, since the mixture is likely to explode.

The effect of catalysts and accelerators on the mix has been investigated thoroughly and has been reported in chapter 3.

The accompanying table (2.18) provides a summary of the chemical formulas and general characteristics of all material used in conjunction with polyester resin.

## 2.4 Cured polyester resin

The liquid resin can be converted into the solid state by a chemical reaction termed **copolymerization**. Curing or cross linking of the polyester resin to form a tough solid is achieved by the use of small quantities of organic peroxides, conventionally called **catalysts**, dissolved in the resin. The peroxide releases free radicals which initiate curing of the polyester resin. Once started, the process is rapid and

# CHAPTER (3)

## **CHAPTER THREE**

### **3. Mix Design and determination of the properties of polymer concrete**

#### **3.1 Introduction**

Polymer concrete mix design can be defined as the procedure by which, for any given set of conditions, the proportions of the constituent materials are chosen so as to produce a polymer concrete with all the required properties for the minimum cost.

These requirements are considered at two stages. First of all, in the fluid state or the stage in which it is to be handled, placed and compacted in its final form, it should be sufficiently workable, with reasonable gel time (time taken for the mix to become soft flexible, solid). Secondly in its hardened state the polymer concrete should have adequate durability, the required strength and also the desired surface finish within the minimum curing time.

#### **3.2 Determination of the grading of the aggregate**

As mentioned earlier, the aggregate is much cheaper than the resin and from economic points of view, the aggregate must occupy as large a relative volume as possible. Also, there are some technical reasons, as the greater the amount of solid

particles that can be packed into a given volume of polymer concrete the higher will be its strength.

Therefore it is necessary to produce a mix that can be compacted to a maximum density with a reasonable amount of work. There is no doubt that the grading of aggregate is a major factor in the workability of the mix. However, it has to be pointed out that there is no one ideal grading curve, but a compromise should be aimed at. Apart from the physical requirements, the economic problem must not be forgotten.

The aggregate particles of a given size pack so as to form voids that can be penetrated only if the next smaller size of particles is sufficiently small.

This means that there must be a minimum difference between the sizes of any two adjacent particles fraction. This theory has led to the advocacy of grading curves parabolic in shape (Fuller grading), and gap grading.

Either of two mix design philosophies may be adopted. The grading curve attributed to Fuller, and widely accepted as a basis for mix design, is a largely empirical formulation which allocates proportionate volumes of all aggregate fractions as a simple function of particle size. The gap graded mix is designed on the principle that the largest aggregate size must be allowed to pack closely, so that the 'interference size' is omitted, and the small size is chosen to pass through the interstitial voids in the close packed matrix of the large particles.

### 3.2.1 Fuller Grading

The Fuller Grading is defined by Fullers expression:

$$P = 100 \times \sqrt{\frac{D}{D_{max}}} \quad (3.1)$$

Where:

$P$  is the percentage passing size  $D$  ,

$D_{max}$  is the maximum particle size.

Therefore, knowing the grading of the target mix (ie; the mix to be achieved when the components are mixed in the proportions) and the grading of individual components, the % of each material was found by calculating or graphically using the method of Road Note No. 4. However, this technique was slow and not necessarily giving the best solution, especially when more than three aggregates have to be combined. Later a computer programme was written to give the best possible combination of up to 14 different sizes of aggregate, (see Appendix 1).

It has to be noted that in Fullers Expression, the density of all the aggregates is assumed to be equal. However, if at any time a filler with a low density has to be used, compared with any other material in the mix, the % by weight of that filler has to be adjusted to give the same volume of filler if it had the same bulk density, ie; if a filler with a density of  $1000 \text{ kg/m}^3$  has to be mixed with the aggregates of density around  $1700 \text{ kg/m}^3$ , after calculating the % by weight of that filler, it has to be reduced by the factor of  $\frac{1000}{1700}$

### 3.2.2 Gap Grading

Gap grading can be defined as a grading in which one or more intermediate size fractions are omitted. On a grading curve, gap grading is represented by a horizontal line over the range of size omitted.

Geometrical analysis of close-nested spheres asserts that the small (filler) size must be no greater than one sixth of the large size, and that the large and small aggregates will be in volume ratio about 70% to 30%. Accepting this as a starting point, much experimental trial is required to achieve the best result with the aggregates available.

22 different mixes were designed using filler (B.L.H) or (pozzolan) with the maximum size of aggregate of  $2400\mu m$  or  $1200\mu m$ .

The temperature and type of resin were kept constant throughout the operations. Also it has to be noted that no catalyst or any type of additive were used in this exercise.

The combination of individual material for some mixes together with the grading curves can be seen in Appendix (1).

### 3.3 Workability Test

The term workability is used to describe the ease of placement of the polymer concrete and it depends on many factors such as :

### **1. Aggregate/resin ratio**

It is obvious that as the aggregate/resin ratio increases, the workability of the mix decreases. For a given mix there is a limit where, beyond this ratio, the workability drops excessively and it will be impossible to place the mix into the mould even with the aid of vibration.

### **2. size, grading shape and texture of the aggregate and micro filler.**

For given resin and aggregate contents, the workability of polymer concrete is mainly influenced by the total surface area of the aggregate. The surface area is governed by the maximum size, grading and shape of the aggregate.

Workability decreases as the specific surface increases, since this requires a greater proportion of resin to wet the aggregate particles thus leaving a smaller amount of resin for lubrication.

Also aggregate with a smooth texture results in higher workabilities than aggregates with a rough texture. Absorption characteristics of aggregate also effect workability. In such a case workability drops, the extent of the reduction being dependant on the aggregate content and its absorption capacity.

### **3. Type of resin.**

The critical factors are the viscosity, the type of additives used in the resin by the manufacturers and pot life of the resin, which all are somehow related to each other. The viscosity of the resin has a direct effect on the workability of the mix and itself depends on many factors such as the amount of *styrene* and water content in the resin. If the pot life of the resin is too short the viscosity of the resin increases

with time and at some stage the resin becomes solid.

#### **4. Temperature.**

This is one of the major factors which influence the workability of the mix and it has a direct effect on the viscosity of the resin. For a given mix it would be advisable to work at an ambient temperature not less than  $20^{\circ}\text{C}$  (see 2.2.2), with the materials to be 'preheated' before mixing, ie; by storage at this ambient temperature.

#### **5. Vibration.**

The process of compacting the polymer concrete consists essentially of the elimination of entrapped air and is achieved by means of vibration. The use of vibration as a means of compaction makes it possible to use drier mixes and therefore allows the use of a mix with higher aggregate/resin ratio. However, if a mix is too wet, it should not be vibrated as segregation may result.

#### **6. Time.**

When catalyst is added to the mix, there is a limit of time in which the mix can be poured and vibrated. As time passes, the workability of the mix reduces until the mix becomes totally unworkable. However, this time (gel time) can be controlled by choosing the right amount of catalyst accelerator and heat.

#### **7. Size, shape and surface roughness of mould.**

It is clear that when the section is narrow and complicated, or when there are numerous corners or inaccessible parts, the polymer concrete must have a high workability so that full compaction can be achieved with a reasonable amount of

effort. Also the smoother surface finish results in less friction between the mould and mix, thus higher workability.

The size and shape of the mould depends on the required application, but the surface roughness can be improved by polishing the surface before using. For small components, it is advisable to use moulds with polypropylene, ensuring a good surface finish and at the same time ensuring that the resin will not stick to the mould.

#### **8. Additive.**

There are some additives available that can be mixed with the resin to improve workability of the mix, but care must be taken to ensure that they do not effect any other properties of the polymer concrete, such as its strength. Some pigments proved to increase the workability of the mix without effecting the strength and at the same time giving a smooth surface finish with a good colour.

#### **9. Reinforcement.***(fibre glass)*

The fibre glass absorbs some of the free resin in the mix. Therefore whenever fibre glass reinforcement is used, a mix with a higher workability is required. However, it may be advisable to wet the fibre glass with resin before pouring the mix whenever possible.

### **3.3.1 Method of test**

As the majority of the products made in this research had very thin faces, a mix was required with very high workability to achieve these uniform thin faces.

Thus the methods of measuring workability for fresh concrete were not suitable for this purpose and a new method had to be designed to determine the workability of such rich mixes.

A computer programme was written to draw circular diagrams from the same centre but of different diameter starting from 100mm up to 300mm with different colours. Each circle was numbered according to its radius dimensions (eg the circle with radius 100mm was called no:10 ) the graph was placed on a table and covered with a sheet of glass. A 150mm metal cone with the top and bottom diameter of 50 and 100mm respectively was placed on the glass in such a way that it covered circle no:5, with the small opening at the top. It has to be noted that the cone was washed and polished thoroughly to minimize the friction between the mix and the metal before starting each test.

The cone was filled with polymer concrete and the top surface was levelled off with a knife. The mould was firmly held against its base during the entire operation, this was facilitated by handles brazed to the mould.

Immediately after filling, the cone was slowly lifted, and the unsupported polymer concrete collapsed in a circular pattern. At the same time a stop watch was started. The time taken for the mix to pass through each circle was noted until there was no more movement. The test was repeated with the same mix and the average of the two tests was taken. The results have been reported later in this chapter.

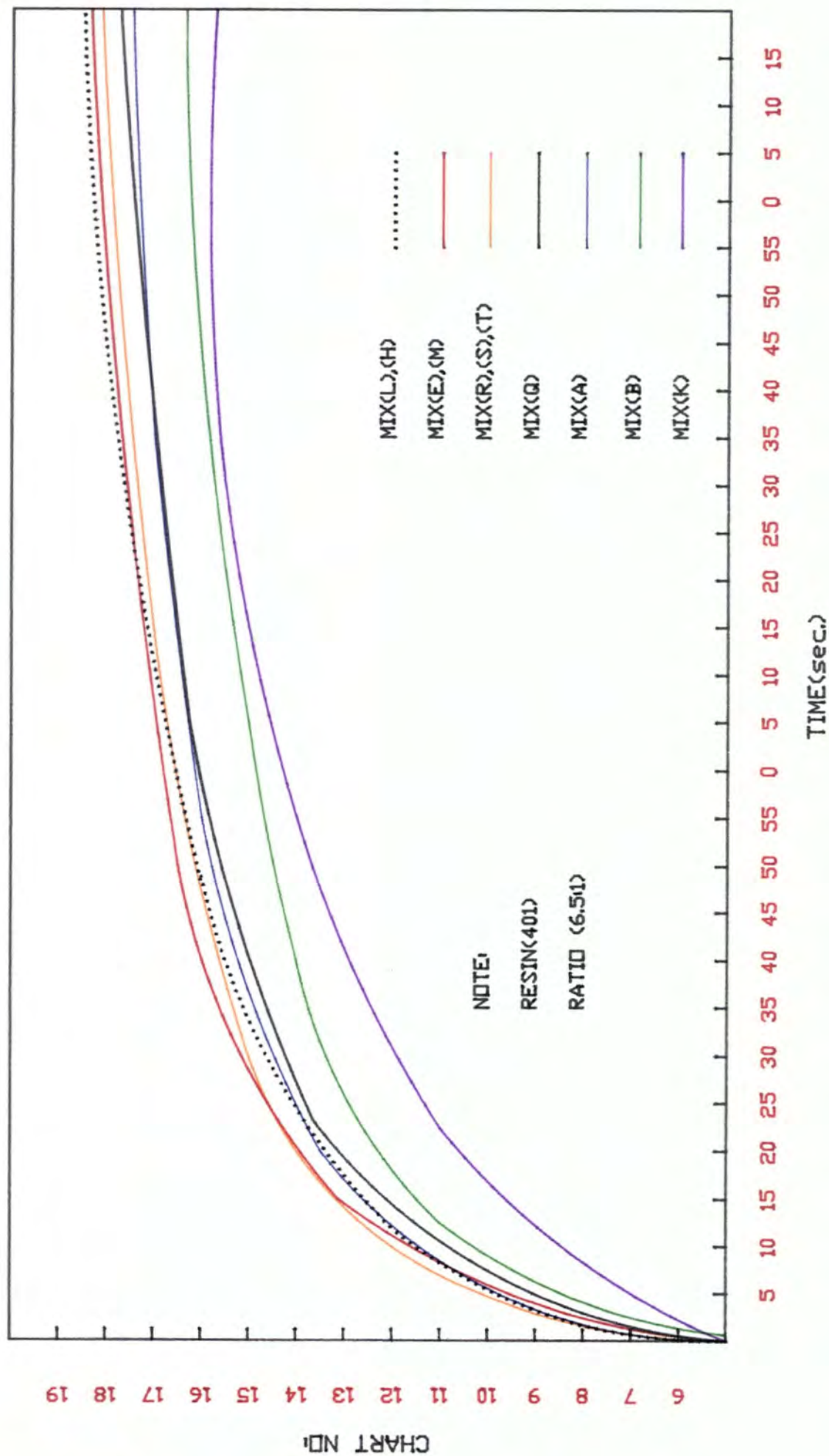


Fig.(3.1).Workability test,using vibration.

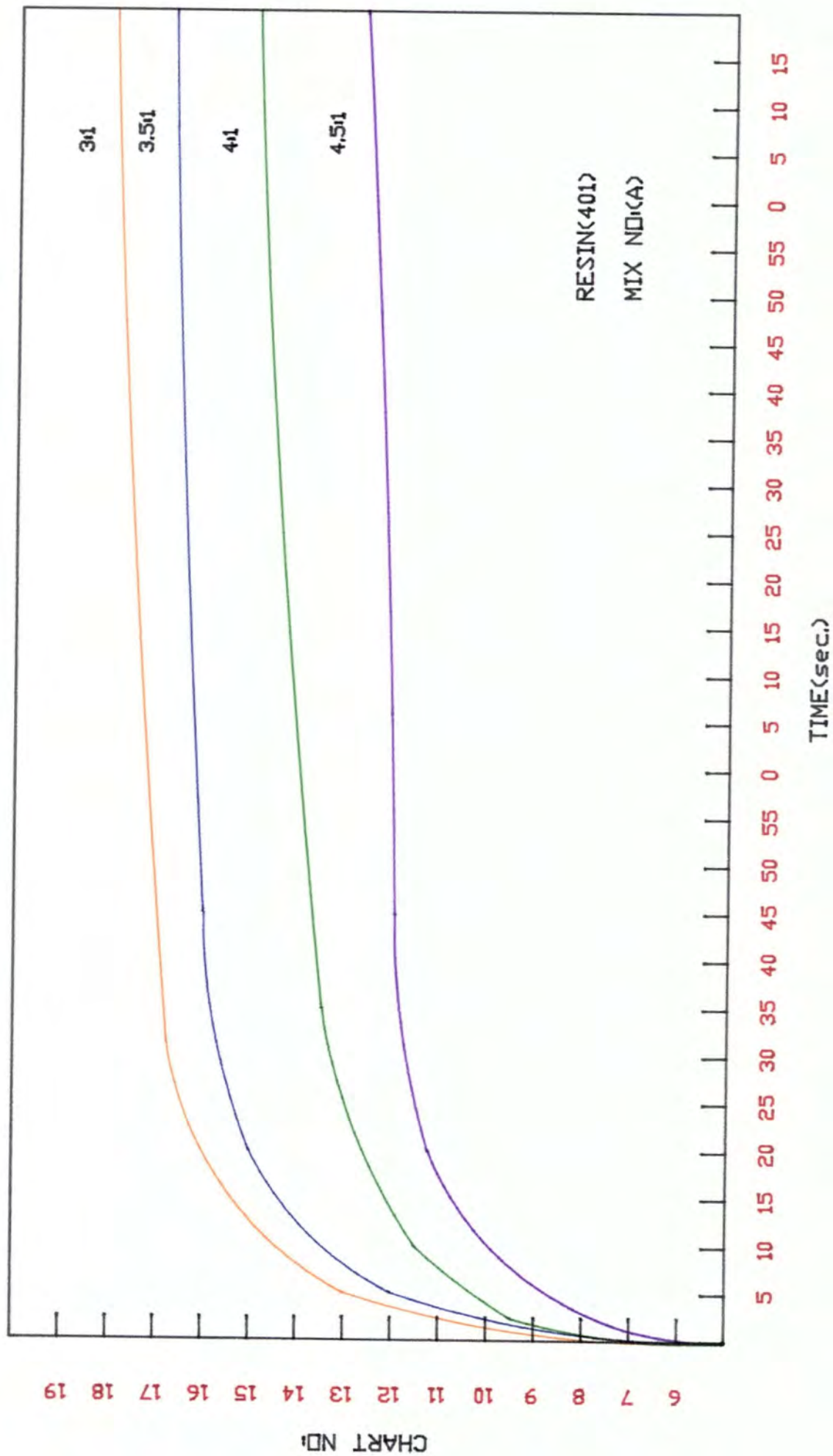


Fig.(3.2).Effect of aggregate/resin ratio on workability.

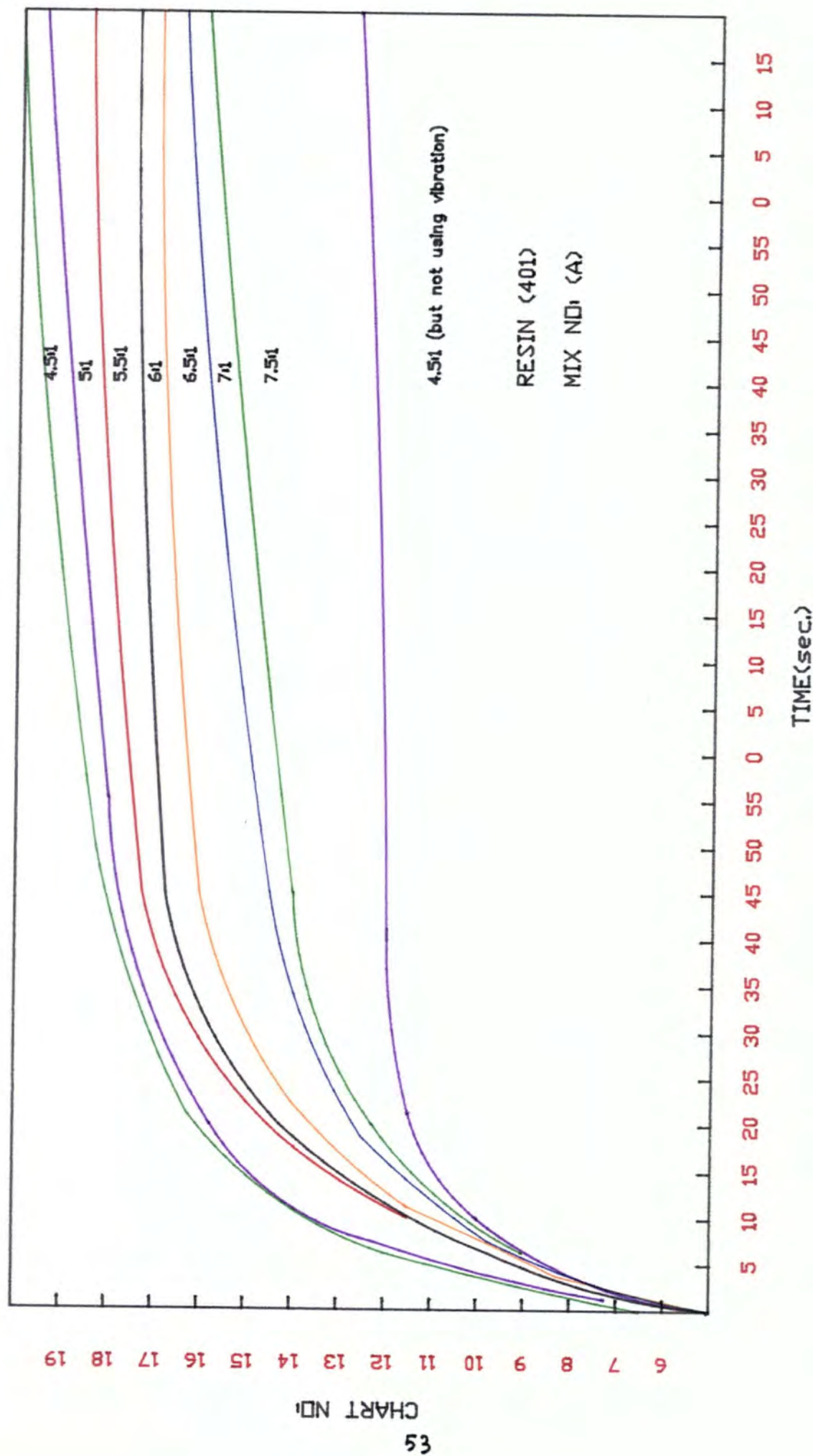


Fig.(3.3).Effect of vibration On workability.

### **3.3.2 Workability test results**

#### **1. Comparison between the mix's**

Workability tests were carried out on all the trial mixes using the resin (401) and micro filler (pozzolan). From the results mixes No. (A,Q,L,M,H,E,S,T) were chosen for further investigation. All the results are shown in fig (3.1).

#### **2. Effect of agg/resin ratio on workability**

Fig. (3.2) shows clearly that workability of any mix decreases as the agg/resin ratio increases. However above a certain ratio (in this case 4.1:5) the test is unable to measure the workability without the aid of vibration.

#### **3. Effect of vibration on workability**

Workability tests were carried out on mix No. (1) but this time a small vibrator (k 10) was fixed underneath the table at the centre. It can be seen from Fig (3.3) how vibration can help the ease of flowing of the mix. The technique was able to measure the workability of the mix up to agg/resin ratio of 7.5:1.

### **3.4 Direct tensile test**

#### **3.4.1 Preparations of samples and testing**

Polypropylene moulds were constructed for producing the tension samples. The moulds were prepared to provide each sample with three holes near each end. The positions of these holes were chosen to be symmetrical about the centre line of the sample. The C.S.A of the samples at each end were increased to avoid the

early appearance of cracks and/or the earlier failure which may happen due to the existence of the holes.

Several samples with different mixes were cast with cross sectional dimensions of  $100 \times 10\text{mm}$  at each end and  $60 \times 10\text{mm}$  along the centre section. All the tension samples were cured for 2 days at room temperature ( $20^\circ\text{C}$ ) and after removing them from the mould, two pairs of Demec gauge points together with a strain gauge size (PL-10) were fixed at each face of the sample using araldite adhesive.

The tension tests were carried out on all the samples in the Denison testing machine model T42 B4. Four steel plates with two round bars were used to transfer the tension load from the machine to the sample. Two plates were well tightened around the sample at each end by three bolts passing through the holes of the samples.

Round bars were joined to the plates by hinge joints; these were used for fixing the sample into the two jaws of the machine. The tension load was applied on the sample in equal increments until failure, and the strains were measured from the four pairs of Demec gauge points and strain gauge at each load increment. It has to be noted that a direct application of a pure tension force free from eccentricity was difficult.

When the Demec gauge's readings were found to vary with a range of more than 20% the results of the sample were not used.

The tensile stress ( $\sigma_t = \text{load}/C.S.A$ ) was plotted against strain for the earlier stage of load (range of load of the elastic stage) for each sample giving acceptable

results, and the tension modulus was determined. All the results can be seen in table (3.4).

### 3.5 Modulus of rupture test

#### 3.5.1 Preparations of samples and testing

Moulds with dimensions of  $600 \times 100\text{mm}$  with different thicknesses (~~40-100mm~~) were constructed for producing the samples. 36 samples from each mix, which was designed previously (see 3.3.2) were cast with different agg/resin ratios. Half of the samples were reinforced by fibre glass mat which was placed at the top surface of each specimen, to investigate the effect of fibre glass on the properties of the polymer concrete. All the samples were cured at room temperature for 2 days and they were tested under two point loading in a rig, mounted in the Instron machine, so as to test each specimen under constant bending moment and stress between the point loads.

The specimens were deformed at a constant rate of deformation of  $20\text{mm}/\text{min}$  and an automatically plotted load/deformation diagram was produced by the Instron with a deflection scale of 1/1. From the plot, the slope of the elastic section of the graph was obtained and the load to cause failure was noted.

By using the Macaulays method (see Appendix 2) the value of ' $EI$ ' *w.r.t* the slope of the graph was calculated and by accurate measurement of the dimensions of the samples, the (I) value and hence the modulus of elasticity in bending for each

value would not be recommended as it will reduce the rate of curing in phenolic or polyester resin.

### 2.1.1 Type of sand and micro filler

The great majority of aggregate used in production of polymer concrete is silica sand.

Four different sizes of silica sand were used in this research and the following table is a summary of all the data relevant to the nomenclature of the standard sand used in the design of aggregate mixes for polymer concrete.

sand type	size nomenclature		description
	top size	bottom size	
1	2400	850	coarse
2	1200	600	medium coarse
3	600	300	medium fine
4	300	150	fine

11 different micro fillers were investigated in the experimental work for developing a mix with high performance and they are as follows:

#### 1. Tioxide (CR2):

Tioxide is a white powder in which the main component is titanium dioxide ( $TiO_2$  approximately 98%) but the following oxide may be present depending on grade:

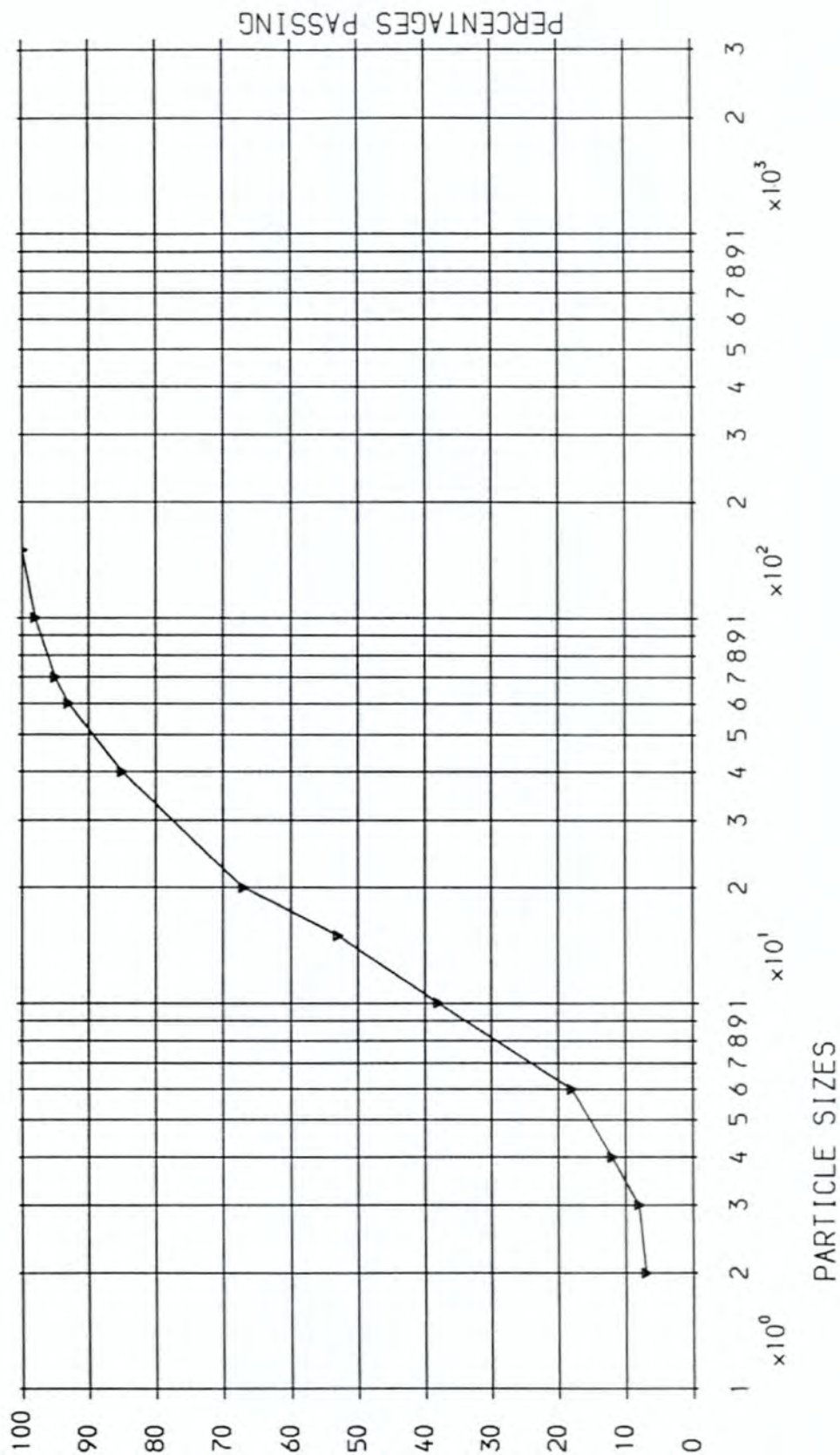
TYPE OF FILLER	BULK DENSITY Kg/m <sup>3</sup>	COLOUR,AFTER MIXING WITH RESIN (247)	REMARK
POZZOLAN	1400	Black	Cheap,good workability but disadvantage of colour
TIOXIDE	920	White	Expensive,good workability can be used as pigment
BALLOTINI	1500	Grey	Reasonably cheap & good workability
OMYA(B.L.H)	1350	White	Cheap,good workability, acceptable colour.
SILICA FLOURS	1000	Dark pink	Cheap,fair workability
TRIHYTE	900	Pink	Reasonably cheap & workable, flame retardant,difficult to cure @ room temperature.
CHINA CLAY GRADE(E& D)	590	Green	Cheap,fair workability, neutral PH value
PELLITE	1200	Black	Reasonably cheap but poor workability.
TALC	870	Dark grey	High PH value and poor workability.
FILLITE	400	Light grey	Cheap but poor workability
NEOSYL(ET)	240	Pink	Neutral PH value but poor workability.

Table(2.1).Determination of bulk density and selection of suitable filler.

SIEVE SIZE ( $\mu\text{mm}$ )	PERCENTAGE PASSING			
	TYPE OF SANDS			
	NQ(1)	NQ(2)	NQ(3)	NQ(4)
2400	100	100	100	100
1200	42	100	100	100
850	1	80	100	100
600	0	24	98	100
425		6	53	98
300		2	18	72
210		1	7	45
150		0	4	14
90			1	3
75			0	1
PAN				0

Table(2.2).Results of sieve analyses

# GRADING CURVE      FILLER: POZZOLAN



ELEMENTS TYPE	% OF THE ELEMENTS			
	SAND NO(1)	SAND NO(2)	SAND NO(3)	SAND NO(4)
Silica dioxide ( $\text{SiO}_2$ )	97.30	97.30	96.7	97.20
Alumina oxide ( $\text{Al}_2\text{O}_3$ )	0.28	0.28	0.64	0.79
Iron trioxide ( $\text{Fe}_2\text{O}_3$ )	1.65	1.65	2.15	0.40
Calcium oxide ( $\text{CaO}$ )	0.04	0.04	0.08	0.03
Magnesium oxide ( $\text{MgO}$ )	0.03	0.03	0.15	0.10
Sodium oxide ( $\text{Na}_2\text{O}$ )	0.05	0.05	0.08	0.05
Potassium dioxide ( $\text{K}_2\text{O}$ )	0.06	0.06	0.14	0.46
Titanium dioxide ( $\text{TiO}_2$ )	0.03	0.03	0.02	0.21
Sulphur trioxide ( $\text{SO}_3$ )	—	—	—	—
Phosphorus pentoxide ( $\text{P}_2\text{O}_5$ )	0.04	0.04	0.02	0.06
Manganat (iv)dioxide ( $\text{Mn}_3\text{O}_4$ )	0.01	0.01	0.01	—
Barium oxide ( $\text{BaO}$ )	0.01	0.01	0.01	0.01
Zirconium dioxide ( $\text{ZrO}_2$ )	—	—	—	0.06

Table(2.10A).Chemical analyses of the sands.

ELEMENTS TYPE	% OF THE ELEMENTS			
	POZZOLAN	OMYA(BLH)	SILICA FLOURS	CHINA CLAY
Silica dioxide ( $\text{SiO}_2$ )	49.80	—	99.5	48.0
Alumina oxide ( $\text{Al}_2\text{O}_3$ )	30.20	0.10	0.10	36.75
Iron trioxide ( $\text{Fe}_2\text{O}_3$ )	9.00	0.02	0.03	1.05
Calcium oxide ( $\text{CaO}$ )	2.80	—	0.02	2.25
Magnesium oxide ( $\text{MgO}$ )	1.10	0.10	0.02	1.10
Sodium oxide ( $\text{Na}_2\text{O}$ )	1.00	—	0.03	0.90
Potassium dioxide ( $\text{K}_2\text{O}$ )	2.90	—	0.01	1.50
Titanium dioxide ( $\text{TiO}_2$ )	1.10	—	—	1.25
Sulphur trioxide ( $\text{SO}_3$ )	0.72	0.06	—	—
Calcium carbonate ( $\text{CaCO}_3$ )	—	99.70	—	—

Table(2.10B).Chemical analyses of some fillers.

SAMPLE NO	S.G	M.C %	BULK DENSITY Kg/m <sup>3</sup>	PH VALUE
SAND NO(1)	2.66	0	1630	7.1
SAND NO(2)	2.65	0	1640	7.0
SAND NO(3)	2.65	0	1660	7.2
SAND NO(4)	2.63	0	1570	7.3
POZZOLAN	2.30	0.3	1400	10.3-7.8
B.L.H	2.70	0	1350	7.1
BALLOTINI	2.48	1.0	1500	6.0
SILICA FLOURS	2.65	0.1	1000	7.3
CHINA CLAY GRADE(E& D)	2.70	<1.5	590	5.5

Table(2.11).Results of the specific gravity, moisture content, bulk density & PH value

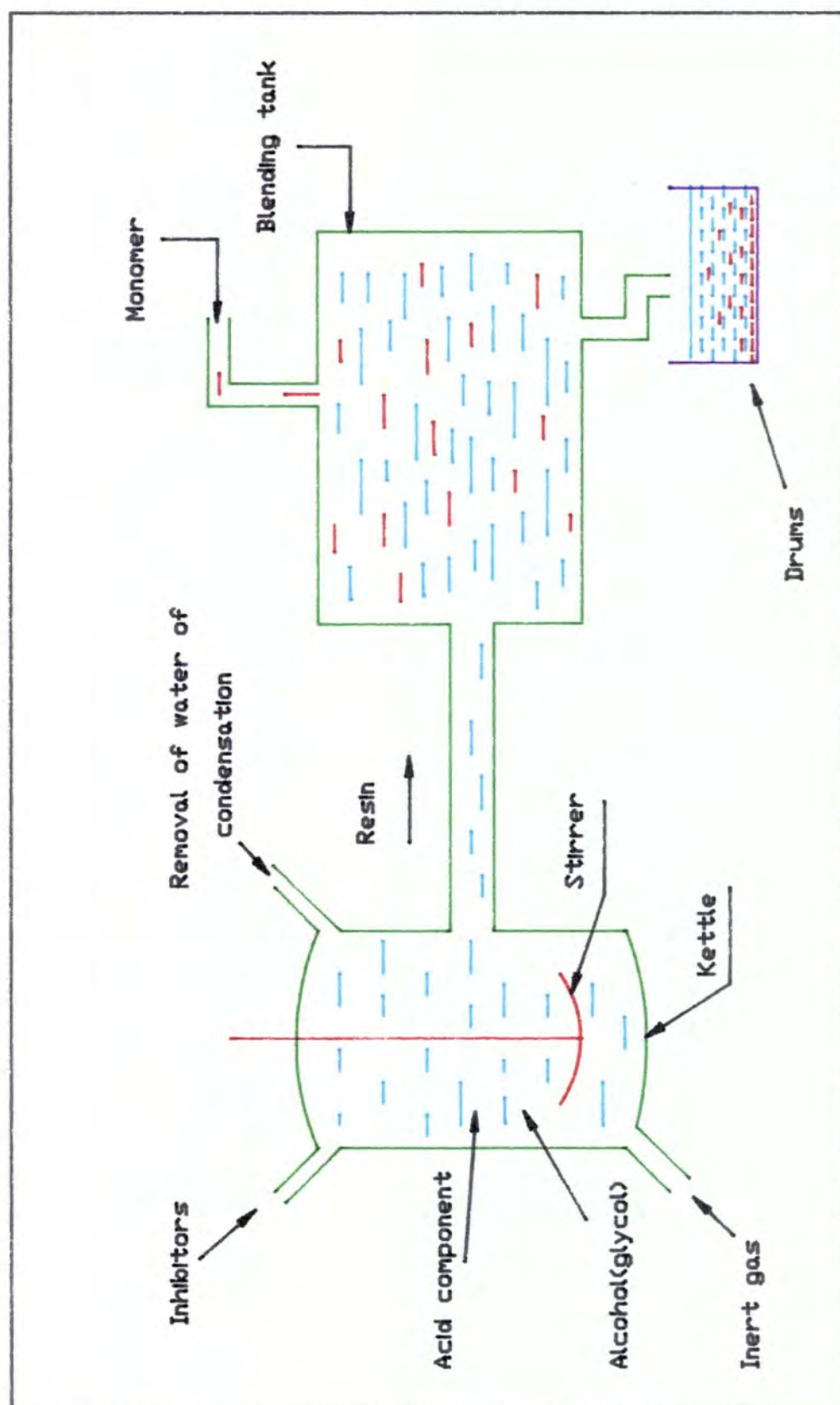



Fig.(2.12).Flow diagram for production of a polyester resin

NAME	TYPE	CHEMICAL FORMULA	REMARK
MONOMERS	Styrene	 $\text{CH}=\text{CH}_2$	Relatively cheap, reduces viscosity, compatible.
INHIBITORS	Hydroquinone	$\text{C}_{12}\text{H}_{10}\text{O}_4$	Relatively cheap, increase the potlife up to 6 months.
CATALYST	Methyl Ethyl Ketone Peroxide (M.E.K.P)	<p>Probably a mixture of:</p> <div style="display: flex; align-items: center; justify-content: center;"> <div style="text-align: center;"> <math display="block">\begin{array}{c} \text{O.OH} \\   \\ \text{C}_2\text{H}_5 - \text{C} - \text{CH}_3 \\   \\ \text{O} \end{array}</math> </div> <div style="margin: 0 10px;"> <math>\text{O} - \text{O}</math> </div> <div style="text-align: center;"> <math display="block">\begin{array}{c} \text{C}_2\text{H}_5 \\   \\ \text{C} \\   \\ \text{CH}_3 \end{array}</math> </div> <div style="margin: 0 10px;"> <math>\text{O} - \text{O}</math> </div> <div style="text-align: center;"> <math display="block">\begin{array}{c} \text{C}_2\text{H}_5 \\   \\ \text{C} \\   \\ \text{CH}_3 \end{array}</math> </div> </div> <p style="text-align: center;">&amp;</p> <div style="text-align: center;"> <math display="block">\begin{array}{c} \text{O.OH} \\   \\ \text{C}_2\text{H}_5 - \text{C} - \text{CH}_3 \\   \\ \text{O} \end{array}</math> </div>	Very active catalyst when used in conjunction with a cobalt accelerator.
ACCELERATORS	Cobalt	$(\text{C}_7\text{H}_{15}\text{COO})_2\text{CO}$	Relatively cheap, very active with (MEKP).

Table(2.18). Chemical formulas and general characteristics of some material used in conjunction with polyester resin.

curing cannot be stopped at an intermediate stage. However, the speed and onset of the reaction may be controlled by the use of heat, accelerators and inhibitors.

The overall curing action can be schematically represented as follows, where **A** represents the unsaturated acid (maleic anhydride), **G** the glycol, **P** the modifying acid (eg phthalic acid) and **S** the reactive monomer(styrene).



MIX NO.	RESIN TYPE	FILLER	RATIO	t (mm)	ULTIMATE STRESS (N/mm <sup>2</sup> )	E (N/mm <sup>2</sup> )
A	401	B.L.H	4:1	7.80	13.0	10850
			5:1	8.46	12.1	11500
			6:1	7.47	13.7	9140
S	401	POZZOLAN	4:1	8.47	19.2	11300
			5:1	9.41	16.4	11150
			6:1	7.85	11.5	10870
T	401	POZZOLAN	—	—	—	—
			5:1	8.63	9.5	9850
			6:1	7.82	7.8	8890
E	401	POZZOLAN	4:1	7.85	15.8	12150
			5:1	7.52	11.5	10800
			—	—	—	—
H	401	POZZOLAN	4:1	8.12	17.7	13820
			5:1	8.02	13.8	14100
			—	—	—	—
M	401	POZZOLAN	4:1	8.14	18.7	9780
			5:1	7.86	14.5	9650
			6:1	7.75	11.7	8600

Table(3.4A).Results of the direct tensile test.

MIX NO:	RESIN TYPE	FILLER	RATIO	t (mm)	ULTIMATE STREES (N/mm <sup>2</sup> )	E (N/mm <sup>2</sup> )
L	401	POZZOLAN	4:1	7.65	16.5	8050
			5:1	8.01	11.6	9870
			6:1	—	—	—
Q	401	POZZOLAN	4:1	8.21	14.4	11200
			5:1	7.47	13.1	11160
			6:1	8.18	10.9	10870
S101	401	POZZOLAN	4:1	8.02	16.0	13750
			5:1	7.96	16.0	13230
			6:1	7.84	12.6	11500
T102	401	POZZOLAN	4:1	—	—	—
			5:1	8.42	14.1	12650
			6:1	7.96	11.5	12730
SS	L.V.M	POZZOLAN	9:1	8.12	18.6	14350
			10:1	8.16	15.2	13760
			11:1	7.96	15.0	14110
TT	L.V.M	POZZOLAN	8:1	7.88	21.2	16790
			9:1	7.87	21.4	16260
			10:1	7.92	20.5	16870

Table(3.4B).Results of the direct tensile test.

MIX NO.	RESIN	FILLER	RATIO	FIBER GLASS	t (mm)	$\sigma_f$ (N/mm <sup>2</sup> )	$\sigma_u$ (N/mm <sup>2</sup> )	E (N/mm <sup>2</sup> )	DISPLACEMENT (mm)
A	401	POZZOLAN	4:1	NO GLASS	6.85	28.4	28.4	17600	8.5
				GLASS BOTTOM	7.32	23.8	42.3	8270	62
			5:1	NO GLASS	7.60	20.1	20.1	13525	7
				GLASS BOTTOM	8.90	24.7	39.7	11545	49
			6:1	NO GLASS	7.96	19.6	19.6	12130	7
				GLASS BOTTOM	8.83	32.9	43.4	11690	32
E	401	POZZOLAN		NO GLASS	8.47	21.0	21.0	14020	6
			4:1	GLASS BOTTOM	7.88	18.0	34.1	9690	41
				NO GLASS	7.85	18.2	18.2	12530	7
			5:1	GLASS BOTTOM	6.93	16.4	35.0	8050	60
				NO GLASS	—	—	—	—	—
			6:1	GLASS BOTTOM	—	—	—	—	—
H	401	POZZOLAN	4:1	NO GLASS	8.55	21.0	21.6	14930	7
				GLASS BOTTOM	9.04	18.1	34.1	10740	45
			5:1	NO GLASS	8.33	19.7	19.7	14580	7
				GLASS BOTTOM	7.52	16.6	34.2	10940	51
			6:1	NO GLASS	—	—	—	—	—
				GLASS BOTTOM	—	—	—	—	—
M	401	POZZOLAN	4:1	NO GLASS	9.24	23.9	25.6	12740	10
				GLASS BOTTOM	9.09	22.9	30.8	11280	26
			5:1	NO GLASS	8.51	20.4	21.9	11490	10
				GLASS BOTTOM	8.41	22.2	34.5	12870	28
			6:1	NO GLASS	8.55	16.2	17.4	10790	8
				GLASS BOTTOM	7.48	17.5	35.8	11530	41

Table(3.5A).Results of the rupture test for different mix's.

MIX NO.	RESIN	FILLER	RATIO	FIBER GLASS	t (mm)	$\sigma_f$ (N/mm <sup>2</sup> )	$\sigma_u$ (N/mm <sup>2</sup> )	E (N/mm <sup>2</sup> )	DISPLACEMENT (mm)
L	401	POZZOLAN	4:1	NO GLASS	8.47	25.1	26.2	14140	9
				GLASS BOTTOM	9.41	25.0	35.7	13380	22
			5:1	NO GLASS	8.38	23.7	24.2	13630	9
Q	401	POZZOLAN		GLASS BOTTOM	7.85	18.6	34.9	11320	39
			6:1	NO GLASS	—	—	—	—	—
				GLASS BOTTOM	—	—	—	—	—
S	401	POZZOLAN	4:1	NO GLASS	9.0	20.8	20.8	15000	7
				GLASS BOTTOM	8.91	23.2	32.4	13500	34
			5:1	NO GLASS	8.86	19.5	19.5	13300	8
T	401	POZZOLAN		GLASS BOTTOM	9.08	20.6	30.6	11400	35
			6:1	NO GLASS	9.36	16.7	16.7	12100	7
				GLASS BOTTOM	7.81	18.6	30.1	11800	44
	401	POZZOLAN	4:1	NO GLASS	8.35	25.2	25.2	14750	8
				GLASS BOTTOM	8.74	15.8	32.0	9460	49
			5:1	NO GLASS	8.84	20.4	23.4	14710	8
	401	POZZOLAN		GLASS BOTTOM	8.46	16.1	31.8	9865	49
			6:1	NO GLASS	8.67	16.0	16.9	11535	8
				GLASS BOTTOM	6.93	16.2	34.5	10110	81
	401	POZZOLAN		NO GLASS	—	—	—	—	—
			4:1	GLASS BOTTOM	9.09	19.4	32.0	9010	38
			5:1	NO GLASS	8.15	18.3	18.3	11425	9
	401	POZZOLAN		GLASS BOTTOM	8.57	18.6	34.4	10505	41
			6:1	NO GLASS	9.85	13.4	13.4	8280	7
				GLASS BOTTOM	7.47	14.4	35.5	9275	62

Table(3.5B).Results of the rupture test for different mix's.

MIX NO.	RESIN	FILLER	RATIO	FIBER GLASS	t (mm)	$\sigma_f$ (N/mm <sup>2</sup> )	$\sigma_{ue}$ (N/mm <sup>2</sup> )	E (N/mm <sup>2</sup> )	DISPLACEMENT (mm)
T102	401	POZZOLAN	5:1	NO GLASS GLASS BOTTOM	9.12	25.9	25.9	16200	9
			6:1	NO GLASS GLASS BOTTOM	8.21	23.8	34.2	12700	67
			7:1	NO GLASS GLASS BOTTOM	7.38	25.6	25.6	19400	8
	401	B.L.H	5:1	NO GLASS GLASS BOTTOM	8.45	24.4	35.7	13600	66
			6:1	NO GLASS GLASS BOTTOM	8.59	27.4	27.4	18800	8
			7:1	NO GLASS GLASS BOTTOM	6.98	23.2	39.0	13000	62
	401	B.L.H	5:1	NO GLASS GLASS BOTTOM	4.34	27.0	27.0	11030	22
			6:1	NO GLASS GLASS BOTTOM	4.49	29.4	45.9	12910	NOT FAILED
			7:1	NO GLASS GLASS BOTTOM	4.71	17.6	17.6	9970	20
	247	POZZOLAN	5:1	NO GLASS GLASS BOTTOM	4.25	24.3	39.0	10740	NOT FAILED
			6:1	NO GLASS GLASS BOTTOM	4.52	13.8	13.8	5800	20
			7:1	NO GLASS GLASS BOTTOM	4.93	24.5	39.0	12090	NOT FAILED
T102	247	POZZOLAN	5:1	NO GLASS GLASS BOTTOM	4.39	20.5	20.5	9520	21
			6:1	NO GLASS GLASS BOTTOM	4.15	21.3	38.4	10830	NOT FAILED
			7:1	NO GLASS GLASS BOTTOM	4.18	25.4	25.4	11120	21
	247	B.L.H	5:1	NO GLASS GLASS BOTTOM	4.32	22.8	38.4	10950	NOT FAILED
			6:1	NO GLASS GLASS BOTTOM	3.76	19.5	19.5	8910	23
			7:1	NO GLASS GLASS BOTTOM	4.11	25.0	43.5	11980	NOT FAILED
	247	B.L.H	5:1	NO GLASS GLASS BOTTOM	—	—	—	—	—
			6:1	NO GLASS GLASS BOTTOM	7.48	28.1	28.1	24000	8
			7:1	NO GLASS GLASS BOTTOM	8.03	19.2	19.2	16200	7
	247	B.L.H	5:1	NO GLASS GLASS BOTTOM	—	—	—	—	—
			6:1	NO GLASS GLASS BOTTOM	—	—	—	—	—
			7:1	NO GLASS GLASS BOTTOM	—	—	—	—	—

Table(3.6A). Results of the rupture test for mix (T102).

MIX NO.	RESIN	FILLER	RATIO	FIBER GLASS	t (mm)	$\sigma_f$ (N/mm <sup>2</sup> )	$\sigma_u$ (N/mm <sup>2</sup> )	E (N/mm <sup>2</sup> )	DISPLACEMENT (mm)
T102	L.V.M	POZZOLAN	7:1	NO GLASS	4.65	31.4	31.4	23770	12
				GLASS BOTTOM	4.60	20.9	41.5	13720	NOT FAILED
			8:1	NO GLASS	4.86	25.0	25.0	21530	11
				GLASS BOTTOM	4.40	19.1	36.2	10030	NOT FAILED
	L.V.M	POZZOLAN	9:1	NO GLASS	4.86	23.2	23.2	21200	11
				GLASS BOTTOM	4.80	19.4	22.6	13100	NOT FAILED
			10:1	NO GLASS	4.40	22.6	26.9	24070	10
				GLASS BOTTOM	—	—	—	—	—
	L.V.M	POZZOLAN	11:1	NO GLASS	8.52	26.9	26.9	23980	7
				GLASS BOTTOM	—	—	—	—	—
			12:1	NO GLASS	8.60	21.2	21.2	23160	6
				GLASS BOTTOM	—	—	—	—	—
	L.V.M	B.L.H	8:1	NO GLASS	7.79	25.6	25.6	18100	8
				GLASS BOTTOM	—	—	—	—	—
			9:1	NO GLASS	7.63	21.7	21.7	17850	7
				GLASS BOTTOM	—	—	—	—	—
	1077/6005	POZZOLAN	10:1	NO GLASS	7.89	18.5	18.5	16000	7
				GLASS BOTTOM	—	—	—	—	—
			6:1	NO GLASS	3.98	21.5	21.5	12760	16
				GLASS BOTTOM	4.15	22.2	35.5	9190	NOT FAILED
	1077/6005	POZZOLAN	7:1	NO GLASS	3.72	18.8	18.8	8830	21
				GLASS BOTTOM	4.17	21.3	33.4	8420	NOT FAILED
	1077/6005	POZZOLAN	8:1	NO GLASS	8.12	25.2	25.2	13960	11
				GLASS BOTTOM	—	—	—	—	—

Table(3.6B). Results of the rupture test for mix (T102).

MIX NO.	RESIN	FILLER	RATIO	FIBER GLASS	t (mm)	$\sigma_p$ (N/mm <sup>2</sup> )	$\sigma_u$ (N/mm <sup>2</sup> )	E (N/mm <sup>2</sup> )	DISPLACEMENT (mm)
S101	401	POZZOLAN	5:1	NO GLASS	8.05	22.2	22.2	16900	7
			5:1	GLASS BOTTOM	8.87	22.9	35.5	13900	45
			6:1	NO GLASS	7.63	22.6	22.6	16600	7
			6:1	GLASS BOTTOM	8.58	22.4	36.5	13600	49
			7:1	NO GLASS	8.48	19.4	19.4	15300	6
			7:1	GLASS BOTTOM	7.57	22.9	41.2	13700	71
	L.V.M	B.L.H	8:1	NO GLASS	7.82	20.1	20.1	15650	7
			9:1	NO GLASS	8.41	18.7	18.7	15400	6
	602	B.L.H	9:1	NO GLASS	8.13	19.9	19.9	16800	6
			6:1	NO GLASS	7.78	25.8	25.8	16350	8
	247	B.L.H	7:1	NO GLASS	7.65	25.3	25.3	16400	8
			8:1	NO GLASS	7.23	22.6	22.6	19100	7
			9:1	NO GLASS	8.03	25.9	25.9	17400	8

Table(3.6C).Results of the rupture test for mix (S101).

MIX NO.	RESIN	FILLER	RATIO	FIBER GLASS	t (mm)	$S_f$ (N/mm <sup>2</sup> )	$S_u$ (N/mm <sup>2</sup> )	E (N/mm <sup>2</sup> )	DISPLACEMENT (mm)
SS	L.V.M	B.L.H	8:1	NO GLASS GLASS@BOTTOM	7.89	19.7	19.7	17200	7
			9:1	NO GLASS GLASS@BOTTOM	7.54	19.1	19.1	14700	8
			9:1	NO GLASS GLASS@BOTTOM	8.62	20.5	20.5	17900	7
		POZZOLAN	10:1	NO GLASS GLASS@BOTTOM	8.10	28.4	48.8	19000	50
			10:1	NO GLASS GLASS@BOTTOM	4.11	16.6	16.6	12100	12
			11:1	NO GLASS GLASS@BOTTOM	7.62	31.4	48.2	21100	50
TT	L.V.M	B.L.H	6:1	NO GLASS GLASS@BOTTOM	7.32	16.8	16.8	24000	6
			6:1	NO GLASS GLASS@BOTTOM	7.52	32.6	49.1	26200	57
			7:1	NO GLASS GLASS@BOTTOM	4.69	17.1	17.1	15350	13
			7:1	NO GLASS GLASS@BOTTOM	8.51	21.4	41.4	12700	72
			7:1	NO GLASS GLASS@BOTTOM	7.68	19.4	19.4	19200	9
		POZZOLAN	8:1	NO GLASS GLASS@BOTTOM	8.05	21.4	41.4	12700	72
			8:1	NO GLASS GLASS@BOTTOM	8.00	18.1	18.1	16200	8
			8:1	NO GLASS GLASS@BOTTOM	8.06	21.9	37.9	15500	50
			8:1	NO GLASS GLASS@BOTTOM	7.38	32.1	32.1	27550	8
			9:1	NO GLASS GLASS@BOTTOM	7.19	32.3	53.0	19800	60
		POZZOLAN	9:1	NO GLASS GLASS@BOTTOM	3.91	26.7	26.7	27750	12
			10:1	NO GLASS GLASS@BOTTOM	7.11	28.0	49.4	17150	65
			10:1	NO GLASS GLASS@BOTTOM	7.92	23.5	23.5	26550	7
			10:1	NO GLASS GLASS@BOTTOM	7.60	28.2	46.6	19300	52

Table(3.7).Results of the rupture test for mix (SS) and (TT).

different type of sample was determined. By the knowledge of the load at failure the value of strength also was calculated, in terms of the extreme fibre stress in bending tension. The average of six samples for each mix with constant parameters was calculated.

Where the results for a specimen were different from others by 15%, the results of that sample were not used. All the results can be seen in fig (3.5).

For choosing a most suitable filler and resin, to give the highest modulus and strength in construction of polymer concrete, some samples were made, using mix **T102** and **S101**. The results can be seen in table (3.6).

After reviewing the results, resin L.V.M was chosen for further investigation and the mix T102 and S101 were slightly modified to new mixes, called (**SS**) and (**TT**). Samples were made in a previous manner and rupture tests were carried out and the results can be seen in table (3.7).

### **3.6 Effect of catalyst level**

#### **3.6.1. Effect of catalyst level on gel time (using penetrometer)**

Penetration test was carried out to investigate the effect of catalyst level on gel time. The % of accelerator (1%) remained constant throughout the test. The following apparatus was used:

A penetrometer, a flat glass plate, metal cup approximately 55mm in diameter and 40mm deep. 1mm diameter needle, stop watch.

From the moment the catalyst was mixed with polymer concrete, the stop watch was started. The metal cup was placed on the flat glass plate and was filled with the mix, and levelled off parallel to the base. The needle was loaded with 100gr. and it was positioned in such a way that it just touched the surface of the mix.

When the catalyst was added, the 1st reading was taken after 3 minutes. The needle was allowed to fall under gravity and penetration was measured. The needle was removed and cleaned and the test was carried out at 1 min intervals as before, until penetration was nil.

This test was repeated for different % of catalyst levels, a graph was drawn (fig 3.8) and the following conclusions were made:

1. to change the polymer concrete from the liquid state to the gel state in a reasonable time up to 2% of catalyst is required. However above 2% catalyst level in the mix, there is no evidence to prove that catalysts level has direct effect on the gel time of the mix.
2. Below 2% catalyst level, when the mix starts to gel, the rate of reaction is very slow and if any change of volume occurs during this stage, the molecular chains have time to move relative to each other before the final state. However above 2% catalyst level, as the rate of reaction is too fast, the chains cross link to each other in a short time, and if any change of volume occurs, internal stresses will develop, which may cause crazing.

It has to be noted that gel time depends on many factors, such as : room tem-

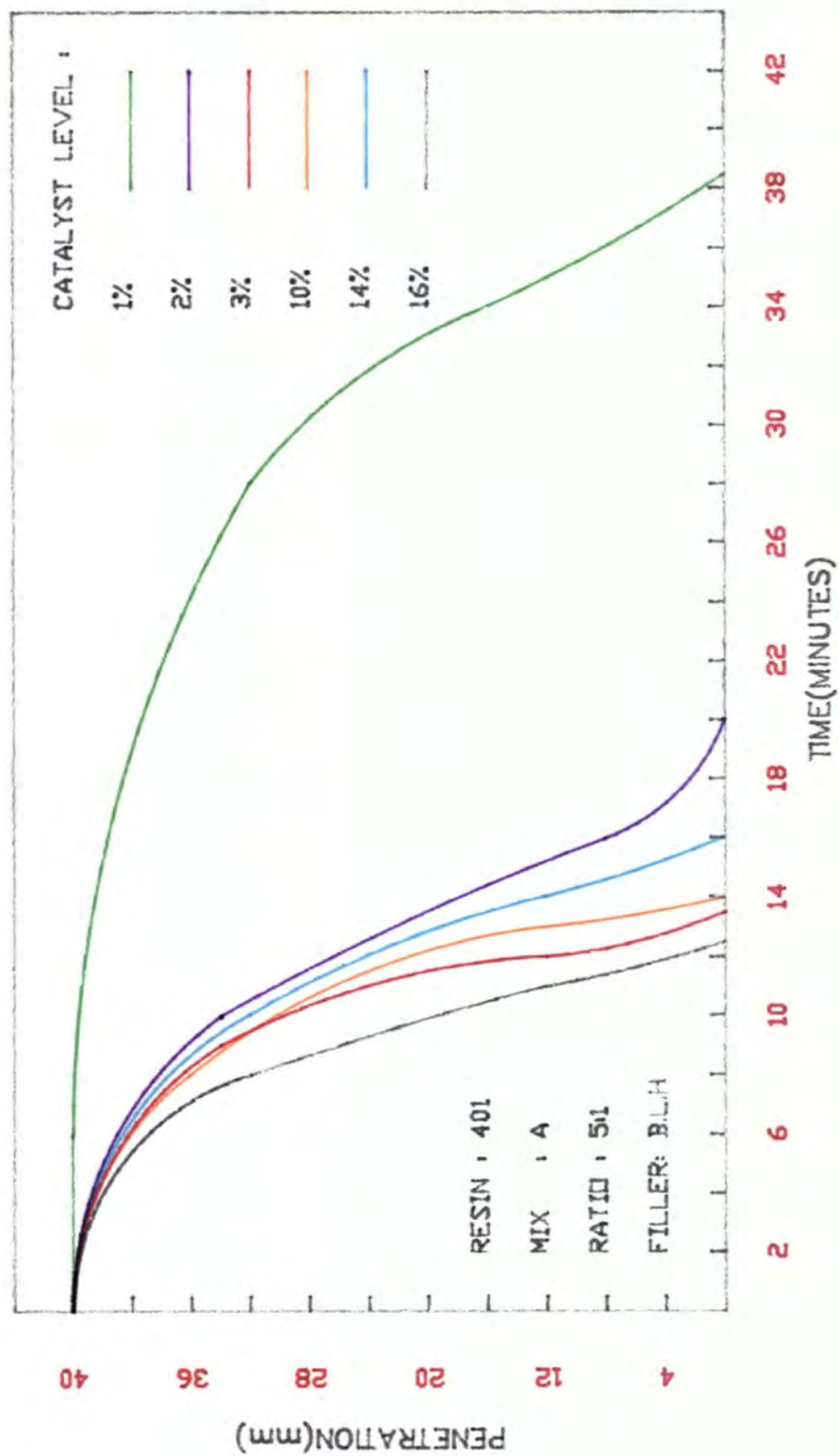


Fig.(3.8). Effect of catalyst levels on gel time.

MIX NO:	RESIN	FILLER	RATIO	% OF THE CATALYST LEVEL	% OF THE COBALT	GEL TIME (MINUTS)
TT	L.V.M	POZZOLAN	9:1	2	1	20
			8:1	1.5	1	19
			7:1	1.5	1	15
			9:1	2	1	21
SS	L.V.M	POZZOLAN	8:1	2	1	18
			7:1	2	1	17
A	401	B.L.H	5:1	2	0.35	15

Table(3.9). Time taken for the polymer concrete to be gel, with different % of catalyst.

perature, amount of filler, properties of the filler, amount and type of accelerator, monomer and resin, and, finally, the thickness of the samples.

Therefore, for each type of mix, the critical % of catalyst level and the gel time must be found.

This test was carried out on the TT mix with aggregate resin ratios of 9:1, 8:1, and 7:1; on the mix SS with aggregate resin ratios of 9:1, 8:1 and 7:1, using L.V.M resin and mix A (5:1) using 401 resin. The required amount of catalyst level and gel time for each mix was found. The results can be seen in fig (3.9).

It has to be noted that the direct comparison between mix A and TT or SS mix could not be made as the % of accelerator (cobalt) was different (the resins were supplied in pre-accelerated form by the manufacturers).

### **3.6.2 Effect of catalyst on curing time**

Resin 401 and L.V.M containing 0.35% and 1% cobalt respectively, were used to investigate the effect of catalyst level on curing time.

In a small glass container approx. 100mm in diameter, 200gr resin was poured and some % of catalyst on resin weight was added. The stop watch was started from the moment the catalyst was mixed with the resin. When the copolymerization started to form and the liquid reached its gel state, after a while some sort of vapour was observed and the mix became totally solid. This time was noted and the test was repeated for different % of catalyst level.

At the higher concentration of catalyst (peroxide initiator) two effects were

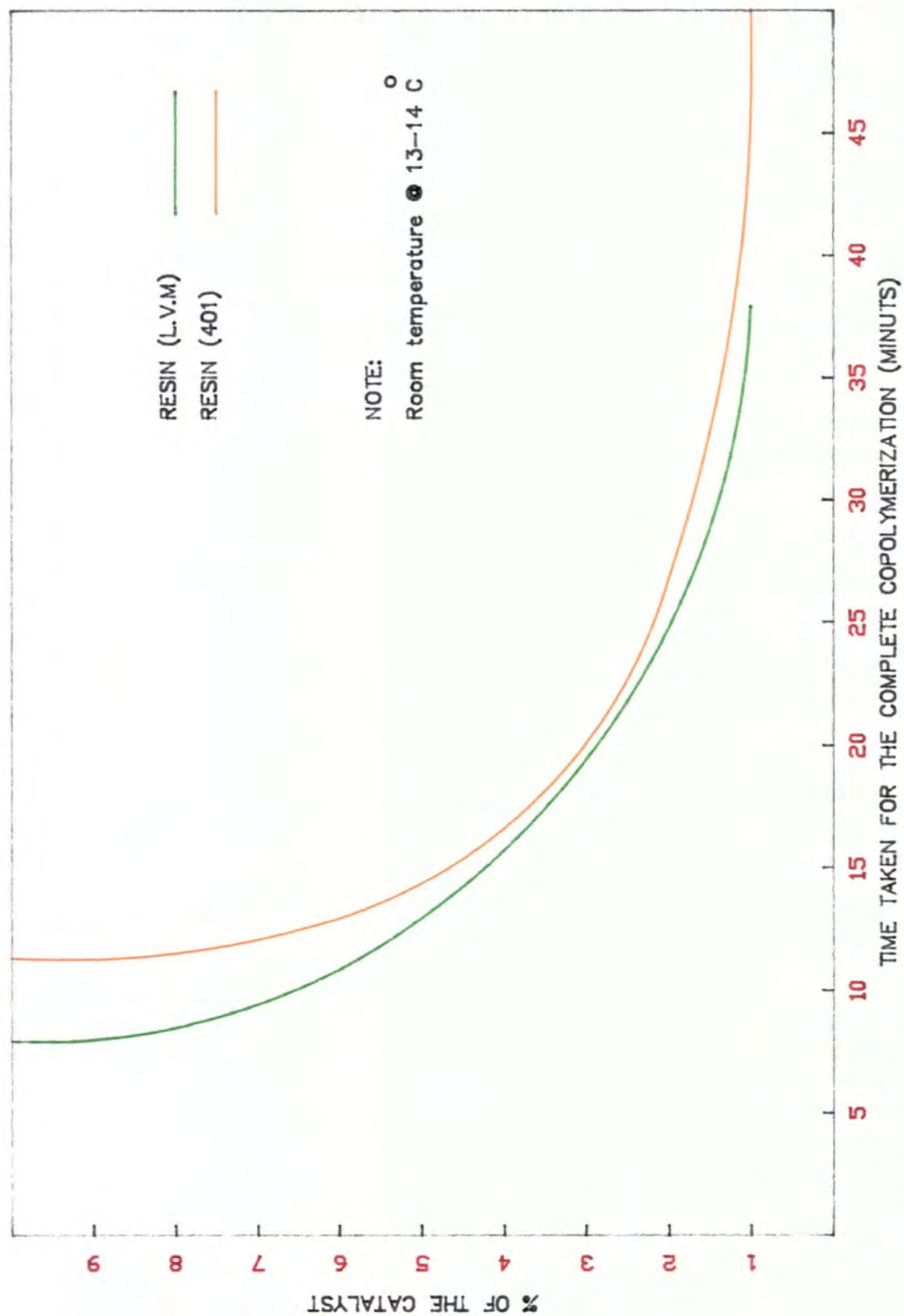


Fig.(3.10). Effect of the catalyst level on curing time of polyester resin @ room temperature.

observed. Large amounts of vapour were generated together with the resin system cracking immediately and extensively. This cracking was more obvious as the % of catalyst increased. Fig (3.10) shows that the catalyst level has a direct effect on curing time of the mix (ie; as the % of catalyst increases, the time taken for the mix to become totally solid got shorter).

The polymerization of styrene is exothermic to the extent of some 1500 calories per gram monomer, and this tends to give it a runaway characteristic. The higher the concentration of catalyst used, the larger the number of polymer cross links that are initiated which increase their runaway characteristic.(ie; doubling the concentration of the catalyst, double the amount of initiator double the amount of heat generated).

To understand the reason for cracking and vapour the temperature of the cross linking system was measured using a thermocouple probe, jacketed with a *p.v.c* tube to prevent damage to the probe. This was placed in a liquid resin prior to the addition of catalyst. The subsequent temperature of the cross linking reaction was then monitored (fig 3.11).

It was seen that the temperature of the reaction rose slowly followed by a rapid increase. Then the temperature stabilized at 148°C approx. It is thought that the vapour and the cracking in the bulk were caused by styrene boiling in the system (styrene boils at 145°C), although according to the thermocouple probe, this happened at the temperature near to 100°C and 30 seconds elapsed before reaching the maximum temperature (ie; 148°C), but however there would have been

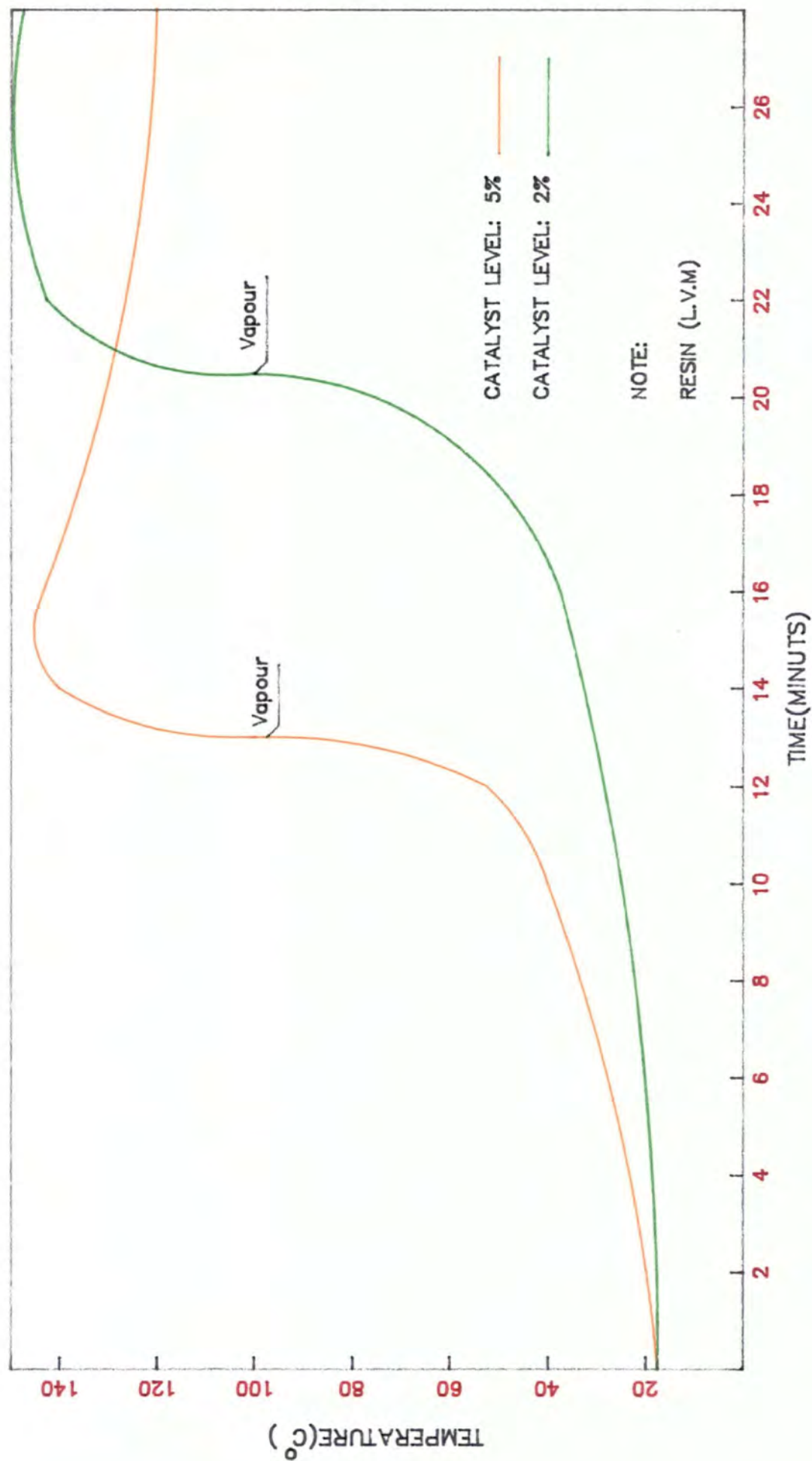


Fig.(3.11). Alteration of the temperature during the copolymerization.

a temperature lag between the thermocouple registered and the actual temperature of the system because of the insulating effect of the plastic *p.v.c* jacket around the probe.

However, it has to be mentioned that if the reaction was carried out in thin layers rather than in large bulk volumes, the vapour and cracking in the system could not have happened as the generated temperature could have escaped more easily.

### **3.6.3 Effect of filler addition on curing time for 6% catalyst level in polyester resin**

The same exercise as (3.6.2) was carried out in this test, except that this time the % of catalyst was kept constant throughout the test (6%) and some amount of filler was added.

Fig (3.1.2) shows the time taken for the complete reaction of the copolymerization for different % wt. added filler. When the reactive monomers polymerize, heat is generated and this heat accelerates the copolymerization of the system. Obviously, as the % of filler increase, it takes a longer time to cure as some of the generated heat is absorbed by the filler. This has been clearly shown in fig (3.12).

### **3.6.4 Effect of catalyst level on strength**

Several coupon samples were made with different % of catalyst level to find out the effect of catalyst level on flexural strength. All the samples were cured at

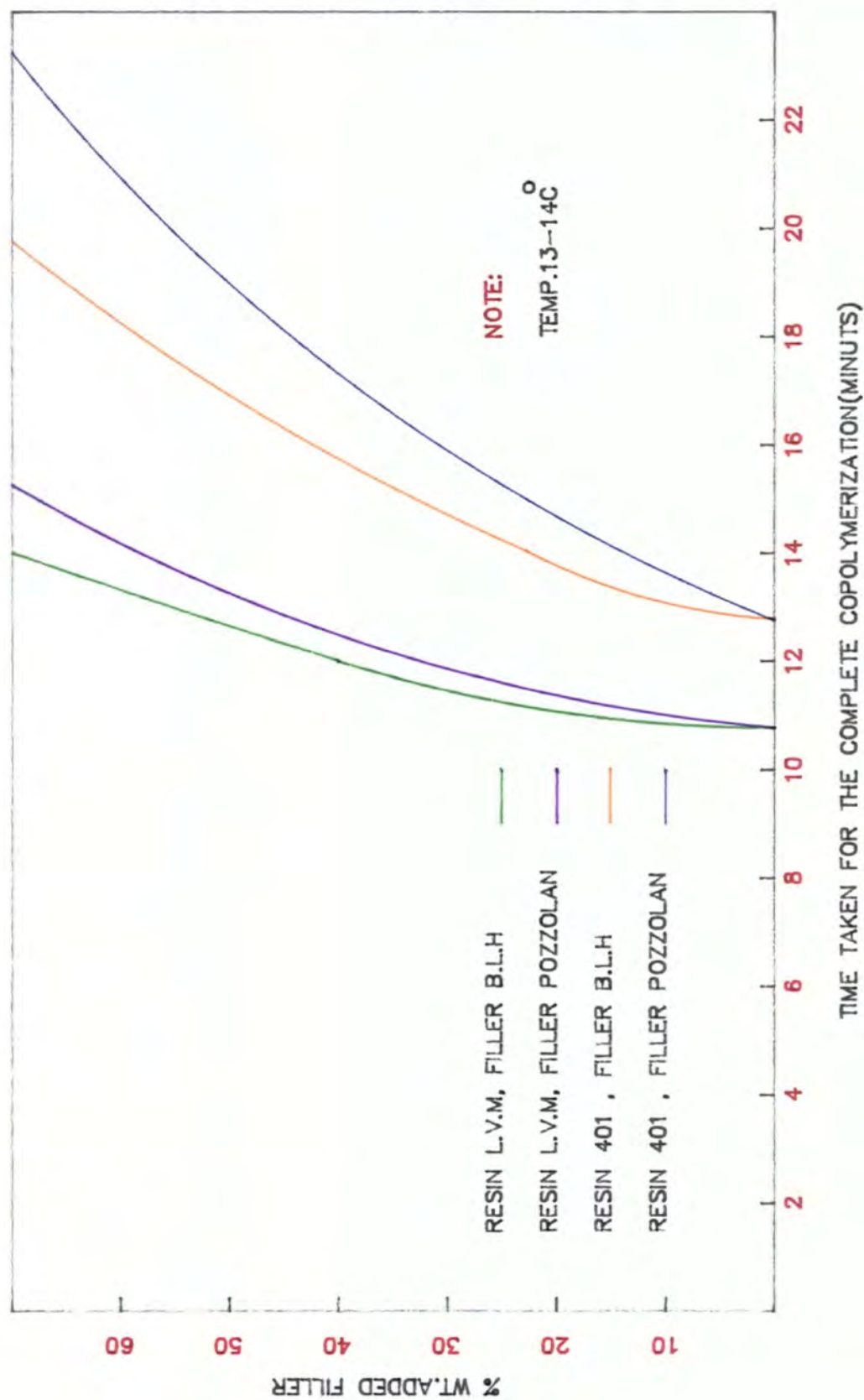
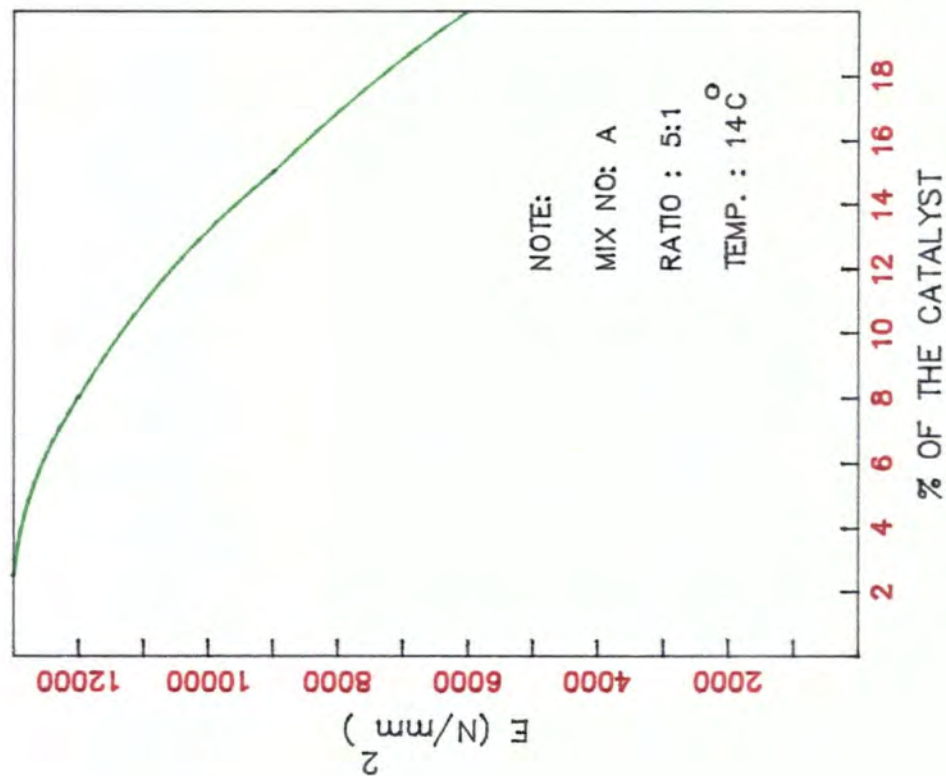
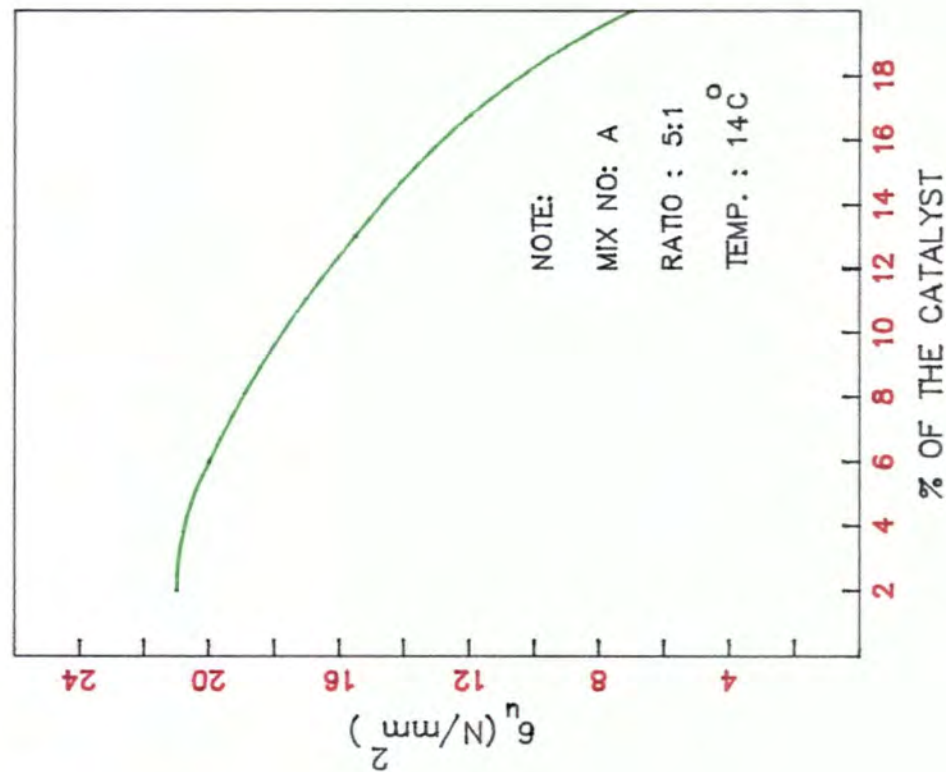


Fig.(3.12). Effect of filler addition on curing time for 6% catalyst level in polyester resin @ room temperature.



(a)



(b)

Fig.(3.13). Effect of catalyst level on elastic modulus & strength.

room temperature for two days and were tested by the Instron machine, and the results can be seen in graph (3.13). From the graphs it can be seen that with lower % of catalyst level a sample with higher  $E$ ,  $\sigma_u$ ,  $\sigma_f$  values can be made.

### 3.7 Relationship between time and development of the strength (curing time)

32 coupon samples were cast at room temperature ( $20^{\circ}C$ ) with the same mix (A) and the catalyst level (2%). Four samples at a time were tested in an Instron machine to determine the flextural modulus at that time. The average ( $E$ ) values were found out, and where the two successive ( $E$ ) values were approximately the same the system was declared as **fully cured**, this value was taken as 100% and the previous results were transferred to the % , relative to that value. The results can be seen in fig (3.14).

The curing time also can be controlled by many other factors, such as the amount of catalyst, accelerator, temperature, type and amount of filler etc. Therefore for each mix, type and amount of these factors together with curing time must be specified.

### 3.8 Water absorption test

Tests were carried out to determine the water absorption of the polymer concrete used to form the surface of the structural components. The tests were all

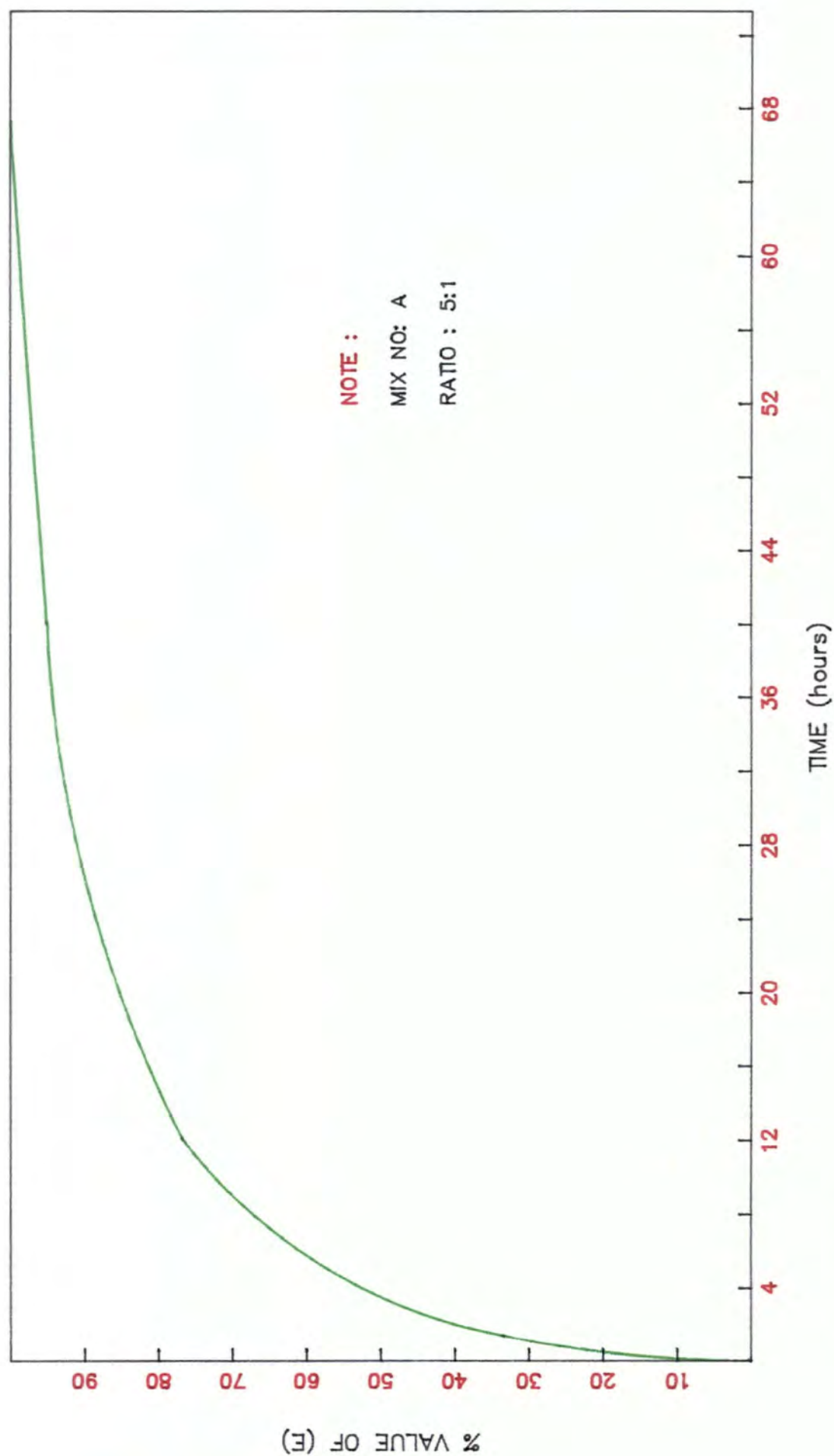


Fig.(3.14). Relationship between time & development of strength.  
(Curing time)

MIX NO:	RESIN	FILLER	RATIO	WATER ABSORPTION %	REMARK
A	401	B.L.H	4:1	0.18	Smooth surface
			5:1	0.21	Smooth surface
			6:1	0.27	Fair surface
S	401	POZZOLAN	4:1	0.23	Smooth surface
			5:1	0.22	Smooth surface
			6:1	0.47	Fair surface
S101	401	POZZOLAN	5:1	0.36	Smooth surface
			6:1	0.47	Fair surface
			7:1	0.98	Rough surface
SS	L.V.M	POZZOLAN	9:1	0.48	Smooth surface
			10:1	0.62	Fair surface
			11:1	0.98	Rough surface
T	401	POZZOLAN	4:1	0.52	Smooth surface
			5:1	0.61	Fair surface
			6:1	0.92	Fair surface
T102	401	POZZOLAN	5:1	0.48	Smooth surface
			6:1	0.87	Fair surface
			7:1	1.06	Rough surface
TT	L.V.M	POZZOLAN	8:1	0.14	Smooth surface
			9:1	0.36	Smooth surface
			10:1	1.01	Fair surface

Table(3.15). Results of the water absorption test.

conducted on the standard small flexural specimens, measuring  $600 \times 100$  mm, all specimens were approximately 8mm thick. Each test consisted of a cycle of drying to constant weight, wetting to constant weight and drying again.

The wetting was done by supporting the sample on 'knife edge' rails near their ends and immersing them in a water bath at  $20^{\circ}\text{C}$  for 3 days. Results of an average over eight tests on similar samples can be seen in fig (3.15).

Whenever a rich mix was used for casting any sample, the surface finish of that specimen was smooth but as the ratio of agg/resin increased a matt surface was produced and the water absorption of the latter samples seemed to be increased. This could be due to the fact that their surface was textured by tiny 'pin-hole' depressions, and that most of the water retained by these samples was held in these surface features, rather than in the body of the material. Therefore the results of the sample with the smooth surface finish is probably more representative of the true absorption of the material. However, the water absorption of all the samples proved to be less than 1%.

### **3.9 Density measurement of polymer concrete**

The tests were carried out according to B.S. 1377, immersion in water method. A cylindrical container was filled with water and placed on a scale and the weight was noted. All the specimens were weighed to the nearest 1g., and then they were suspended in the water without touching either the bottom or the sides of the

container. The density of the specimens were then calculated from the following formula:

$$\rho_s = \frac{M_s}{M_{ws}} \quad (3.3)$$

where:

$P_s$  is the density of the specimens ( $mg/m^3$ )

$M_s$  is the mass of the specimen  $agg.(g .)$

$M_{ws}$  is the mass of specimen when suspended in water ( $g .$ )

It is appreciated that as the polymer concrete has very low permeability (see 3.8) water absorption due to porosity has little effect on the measured densities. Theoretical density was also calculated from the densities of the component materials making up the polymer concrete as follows:

$$\rho_t = \rho_1 W_1 + \rho_2 W_2 + \rho_3 W_3 \quad (3.4)$$

where:

$\rho_1$  is density of resin + hardener

$\rho_2$  is density of sand

$\rho_3$  is density of filler ( $1350 \text{ kg/m}^3$  for B.L.H and  $1400 \text{ kg/m}^3$  for Pozzolan)

$W_1, W_2, W_3$ , are the fractional weights of the components in the polymer concrete.

From a knowledge of measured and theoretical densities, the approximate content of voids in the polymer concrete specimens was calculated as follows:

MIX NO:	RESIN	FILLER	RATIO	THEORETICAL DENSITY Kg/m <sup>3</sup>	DENSITY MEASUREMENT Kg/m <sup>3</sup>	VOIDE %	COMPRESSIVE STRENGTH N/mm <sup>2</sup>
A	401	B.L.H	4:1	2280	2069	9	84.8
			5:1	2341	1869	20	62.4
			6:1	2385	2009	16	72.7
S	401	POZZOLAN	4:1	2256	2082	8	79.0
			5:1	2316	2079	10	74.3
			6:1	2360	2053	13	70.4
T	401	POZZOLAN	5:1	2316	1951	16	63.8
			6:1	2360	1959	17	55.1
			7:1	2393	2036	15	60.8
E	401	POZZOLAN	3:1	2172	2101	3	80.6
			4:1	—	—	—	—
			5:1	2324	1975	15	65.9
H	401	POZZOLAN	3:1	2165	2064	5	82.7
			4:1	2256	2111	6	85.7
			5:1	2316	2022	13	73.1
M	401	POZZOLAN	4:1	2264	2004	11	75.8
			5:1	2324	1959	16	68.5
			6:1	2368	2026	14	71.7
L	401	POZZOLAN	3:1	2173	2113	3	78.3
			4:1	2264	2126	6	89.2
			5:1	2324	2121	9	85.8

Table(3.16A). The results of the compressive strength and density.

MIX NO:	RESIN	FILLER	RATIO	THEORETICAL DENSITY Kg/m <sup>3</sup>	DENSITY MEASUREMENT Kg/m <sup>3</sup>	VOIDE %	COMPRESSIVE STRENGTH N/mm <sup>2</sup>
S101	401	POZZOLAN	5:1	2308	2103	9	77.2
			6:1	2351	2100	11	73.7
			7:1	2384	2059	14	68.7
SW	247	POZZOLAN	6:1	2388	2106	12	83.6
			7:1	2417	2147	11	84.2
			8:1	2440	2190	10	87.1
Q	401	POZZOLAN	4:1	2264	1973	13	71.2
			5:1	2324	2023	13	69.9
			6:1	2368	2010	15	65.0
T102	401	POZZOLAN	5:1	2308	2053	11	97.1
			6:1	2351	2000	15	79.1
			7:1	2384	2142	14	—
TT	L.V.M	POZZOLAN	8:1	2398	2278	5	107.0
			9:1	2414	2221	8	96.0
			10:1	2427	2160	11	84.2
SS	L.V.M	POZZOLAN	9:1	2441	2319	5	93.2
			10:1	2454	2233	9	76.4
			11:1	2466	2219	10	

Table(3.16B). Results of the compressive strength and density.

$$\%voids = \frac{\rho_{theoretical} - \rho_{measured}}{\rho_{theoretical}} \times 100 \quad (3.5)$$

The results of measured and theoretical densities together with % voids are shown in table (3.16)

### 3.10 Compressive strength

The compressive strength of polymer concrete is taken as the maximum compressive load it can carry per unit area on specimens of standard geometry. All the specimens were cast in steel moulds, 100mm cube, keeping the type of resin, level of catalyst, and temperature constant throughout the casting.

A vibrator table was used to ensure a maximum density for a given mix. All the cubes were cured at room temperature for 2 days and they were tested on a standard concrete compression test machine, (ELC). The results can be seen in table (3.16).

### 3.11 Conclusions

Resin L.V.M proved to be the most suitable resin for producing polymer concrete. Not only did it improve the workability of any mix considerably, but also, as the results show, it produced a sample with a very high modulus.

From the results, also, it can be seen that filler pozzolan yielded a higher

strength than filler **B.L.H** for any given mix. For each mix at least three different agg/resin ratios were investigated. In most cases, the results varied by almost 10–15% from each other on a random pattern, ie; as the ratio of agg/resin increases the strength and modulus of elasticity decreases for the samples with the same parameters of filler, type of resin, thickness and reinforcement.

However, there is no evidence for some mixes to follow this pattern. This may be because the aggregate compacted particularly well for this mix, so that change in any other parameter, such as aggregate/resin ratio, could have little effect.

The (E) value of the samples with fibre glass reinforcement were less than the (E) value of the same sample without reinforcement by almost 15%. This reduction of E value can be due to the fact that as fibre glass absorbs some resin therefore the amount of resin to fill the voids between the particles of sand will be reduced and thus the void ratio increases. There may also be an increase in the void ratio within the reinforcement due to difficulty of wetting-out perfectly.

However, the effect of fibre glass reinforcement on strength was considerable. The increase over the previous sample with no reinforcement was between 40 to 100% and maximum deflection in some cases was greater than 100mm.

A number of formulae connecting tensile strength and compressive strength have been suggested for concrete, many of them of the type:

$$\sigma_t = K(\sigma_c)^n \quad (3.6)$$

Where 'K' and 'n' are coefficients.

A computer programme was written to analyse the results and to calculate a

value for K and n in polymer concrete.

The coefficient of n was given a value of 0.1 to 1.0 and K values for all the data were calculated. The minimum standard deviation for a particular value of n was determined. The output of the computer suggests that tensile strength is proportional to the compressive strength in a linear pattern with the following relationship:

$$\sigma_{t(in)} = 0.3(\sigma_c) \quad (3.7)$$

With the standard deviation of 0.035.

Where:

$\sigma_c$  is compressive strength resulting from the cube test (100 mm)

$\sigma_{t(in)}$  is tensile strength resulting from indirect bending tests.

The same procedure was repeated to find out the relationship between the tensile strength resulting from direct test and compressive strength. The relationship was found to be as follows :

$$\sigma_{t(d)} = 0.19(\sigma_c) \quad (3.8)$$

As we have gathered from the results, the modulus of rupture test yielded a higher value of strength than the direct tensile test for the same mix. This can be due to the following reasons, although they might not be of equal importance.

1. The accidental eccentricity in a direct test results in a lower apparent strength.
2. The influence of the loading arrangement on the value of the modulus of rupture. For instance, under flexure test, using a four-point load system, the bending moment distribution is in a trapezoidal shape so the maximum stress

- occurs over one section of the specimens only and the failure will generally occur only when strength immediately under a load point is exhausted. However under direct tension the entire volume of the specimen is subjected to the maximum stress, so that the probability of a weak element occurring is high.
3. When a local fracture starts at a point, the total failure depends on the behaviour and state of the material surrounding the critical point and the possibility of spreading of failure is affected by this state. In the flexure test, if any crack occurs it may be surrounded by less stressed material nearer to the neutral axis while in direct tension tests the propagation of fracture is not blocked by the surrounding material.
  4. In the calculation of the modulus of rupture, it is assumed that the stress is proportional to the distance from the neutral axis while the shape of the actual stress under loads nearing failure is parabolic in shape rather than triangular shaped.
  5. The rate of application of the load has a direct effect on strength. So the strain could have been increased with time, owing to creep while the reading was taken, but in the flexure test, the results were plotted automatically and the rate of applying load was constant throughout the test.

Voids contents were higher than had been hoped for and it is thought that this has been a major factor in producing the rather low measured strengths, in some cases, particularly at lower resin contents. For a given agg/resin ratio, the

compressive strength is higher for the mix which has a higher density, and therefore a lower void ratio: The compressive strength test was repeated on mix (S) but this time using resin (247,L.V.M) instead of the (401) resin. Although the void ratio was not changed significantly, the compressive strength was increased almost by 15%, and workability also was improved. Mix **SS** and **TT** were shown to have low void ratios and high compressive strength values.

# CHAPTER (4)

## CHAPTER FOUR

### 4. Sandwich Beams

#### 4.1 Introduction

The sandwich beam is a particular type of laminated structure. The simplest type of sandwich consists of two thin, stiff, strong sheets of dense material separated by a thick layer of low density material which may be much less stiff and strong.

The principles of sandwich construction were used first by the Egyptians many centuries before Christ. They spliced two types of wood together, where the strong and dense wood was put on the exterior of inferior wood to obtain strong members. As a crude guide to the proportions, an efficient sandwich is obtained when the weight of the core is roughly equal to the combined weight of the faces, obviously the bending stiffness of this arrangement is very much greater than that of a single solid plate of the same total weight made of the same material as the faces. This structural form, with suitable material for the faces and the core can be of great benefit for the purpose of insulation from heat loss, weather and sound as well as the light weight in the interior and external walls and the roofs of houses and other buildings.

The core used in a sandwich structure has to have several vital functions. It must be stiff enough in the direction perpendicular to the faces to ensure that they

remain the correct distance apart. It must be stiff enough in shear that when the beam is bent, the faces do not slide over each other. The core must also be stiff enough to keep the faces nearly flat; otherwise it is possible for a face to buckle locally under the influence of compressive stress in its own plane.

Beams of geometry similar to those tested here have a direct application. They are used in the construction of the sandwich panel housing as lintols over some windows and door voids, and in the construction of porches and verandas.

#### **4.2 Dimensions, construction and schedule of the beams**

All the sandwich beams made and studied in this research were cored by polyester foam. The faces were constructed using mix No.(A) or (SS) mix, (see Appendix 1) reinforced with fibre glass mat and in some cases with extra bar reinforcement. All the beams had a cross-section of  $200 \times 90\text{mm}$  and 1.5m long.

The upper and lower faces of all the beams were of 10mm thickness, and were joined together by 10mm 'ribs' along the sides and at the ends, the rest of the cross-section was the core, which, therefore, had dimensions of  $70 \times 180\text{mm}$  and 1.48m long. A mould was constructed using wood and polypropylene materials which could come apart very easily by means of 8 clasps.

Before casting, the foam and fibre glass mat were cut to the required dimensions. Mix was poured into the mould with the aid of a wooden 'screed', which was made to give 10mm clearance from the bottom face of the mould when it was placed

SET NO:	MIX NO:	RATIO	FIBRE GLASS REINFORCEMENT	BAR REINFORCEMENT (DIAMETER)
1	A	5:1	YES	—
2	SS	10:1	YES	—
3	A	5:1	YES	6 mm
4	A	5:1	YES	9 mm
5	SS	10:1	YES	9 mm
6	CONCRETE	2:1	NO	6 mm

Table(4.1). Beam specification's.

on the top surface of the mould. The 1st skin of the beam was laid down. The fibre glass mat was placed on the bottom face of the beam and the air trap between the mix and the fibre glass was removed by aid of a roller and vibrator (K20). After making sure all the air was removed and the fibre glass had been wetted thoroughly, the foam was placed in such a way as to give 10mm clearance in all directions from the mould. This gap was filled with mix and the second layer of fibre glass mat was placed on the top surface of the core. Finally the top face of the beam was laid and was levelled off with a flat wooden screed.

The schedule of the sandwich beam investigated in this experimental programme include six sets, each consisting of three beams, ie; 18 beams were made and tested in all. The three beams of each set were made to have the same faces, reinforcement, manufacture, curing conditions and testing procedures. The six sets were classified according to the properties of the mix and the type of reinforcement used to construct the beams of each set. The difference between each set can be seen in table (4.1).

During the construction of any beams, 4 flexural samples also were made as in (3.5), using the same mix as the faces in order to make sure a continous uniform mix for any set of beams.

### **4.3 Beams: preparation for testing and testing procedure**

After allowing three days for curing for each polymer concrete beam, they were

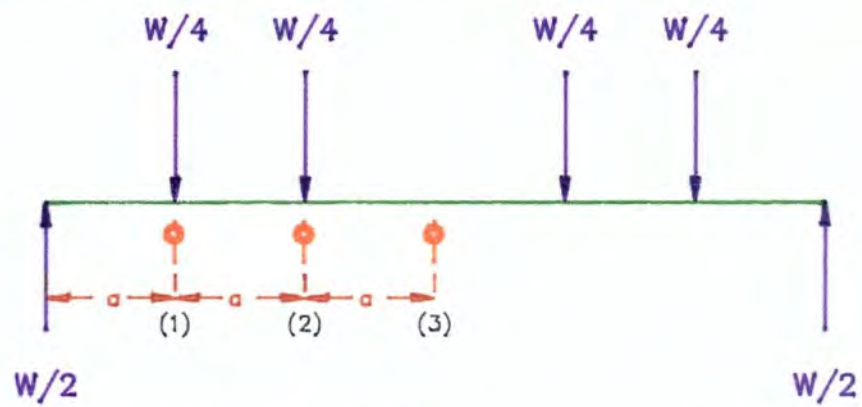


Fig.(4.2A). Position of the dial gauges & points load.

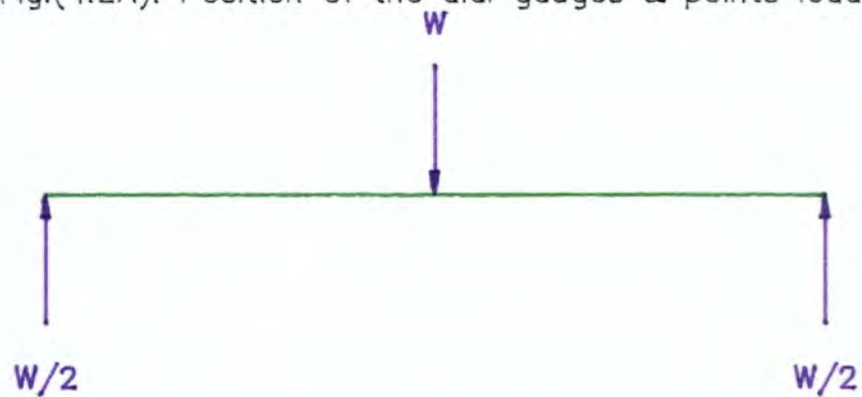


Fig.(4.2B). Arrangement of loading.(1 point loading)

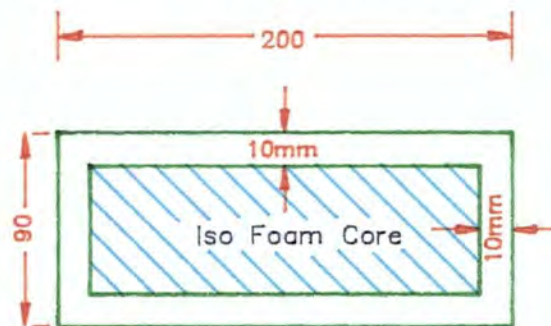


Fig.(4.2C). Cross section of the beam.

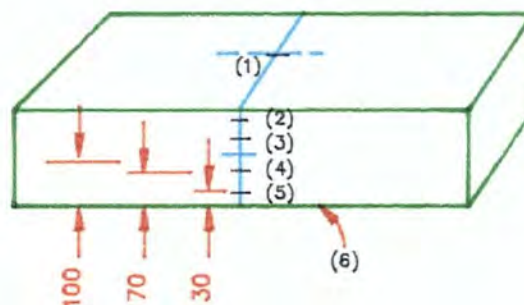


Fig.(4.2D).Position of the strain gauges.

removed from the mould. The need for exactly repeating the procedure of loading and deformation measurement, with each beam necessitated careful marking. Thus, all the beams were marked to have the same effective span (points of support) point of load, strain gauge points and the points of deflection measurements. The points of support were marked so as to be symmetrical from the centre of the beam with the total span of 1.26m. The beams also were marked to be loaded either at 4 points, at positions of:  $a$ ,  $2a$ ,  $4a$ ,  $5a$ , length from one of the supports ( $a=210\text{mm}$ ), or at the centre of the beam (fig 4.2).

All together ten strain gauges were fixed at the central cross-section of each beam of which two of them were positioned at each narrow side of the beam exactly at the centre and the rest were positioned on each wider side of the beam with the distances shown in fig (4.2) apart.

Tests were carried out on a Dension Testing Machine, model TLB/M.C 200 ton capacity of the flextural frame.

Three steel plates with 6 steel rollers, each 25mm diameter and 200mm length (equal to the beam width) were used to transfer the machine load to the beam. After the beam had been placed in the frame of the machine, its roller supports were adjusted to be lined with the points of beam supports as marked. In the case of four point loading, four of the steel rollers were placed in the loading positions and two of the steel plates were put over the rollers in a central position, making the steel rollers into two separate pairs. The other two rollers were positioned in the centre of these plates and the final steel plate was placed over the two upper

rollers. The load was transferred through the centre of this plate to the beam under testing.

Four gauges of 1/100 mm divisions were fixed under each point of load touching the bottom surface of the beam at the centre of its width, at the positions previously marked. Another two dial gauges were fixed at the centre of the beam. A load cell, of capacity ten thousand pounds, of which the calibration was confirmed from time to time, was used to control and measure the applied load precisely.

The initial reading from the strain gauges and the dial gauges were taken before the load application. The load was applied on each beam slowly with approximately constant rate of increase, which was controlled by Direct Reading Transducer Meter Type C52. At each 50 pounds increment, the load was kept constant for about 30 seconds until the reading of the dial gauges became constant. Then their values together with strain gauge readings were recorded.

The theoretical ultimate loads for the beams were calculated and each beam was tested 4 times with a different type of loading (4 point loading and central loading) on different faces with the maximum load of 1/4 of its ultimate load, before the final test which the failure load was applied. In the final test the beam was carefully watched before reaching the ultimate load and if any crack occurred, the load at that stage was recorded. Five or six hundred pounds before reaching the theoretical ultimate load, the dial gauges were removed and the strain measurements were no longer recorded. The load then continued slowly until the beams failed. The failure load and the type of failure were recorded.

MIX NO:	CEMENT	WATER/ CEMENT RATIO	AGGREGATE/ CEMENT RATIO	COMPRESSIVE STRENGTH <sub>2</sub> (N/mm <sup>2</sup> )
SS	PORTLAND CEMENT	0.45	1.5:1	60.0
SS	PORTLAND CEMENT	0.45	2.0:1	71.5
SS	PORTLAND CEMENT	0.45	2.5:1	62.6
SS	PORTLAND CEMENT	0.45	3.0:1	59.2
SS	PORTLAND CEMENT	0.45	3.5:1	56.5

Table(4.3). Concrete beam specifications.

After the total failure of the beams, the thickness of the ribs and the faces were measured carefully with a micrometer in order to find out the position of N.A and the values of the second moment of area of the beams in 'xx' and 'zz' directions.

#### **4.4 Sandwich concrete beams**

In order to compare the polymer concrete beams with concrete sandwich beam made with portland cement three beams were made in the previous constructional manner, reinforced with two 6mm diameter bars at the bottom face using (SS) mix with cement. With a water/cement ratio, of 0.45, several trial mixes were made using different aggregate/cement ratio, in order to find out a mix with the highest strength and with adequate workability. For each trial mix, five cube samples were made and after they were cured in a water tank for 28 days, they were tested in compression. From the results a value of aggregate/cement ratio of 2:1 was chosen. The results can be seen in fig (4.3).

#### **4.5 Theory of the sandwich beam**

The sandwich beam under transverse loading is usually designed on the assumption that the bending moment at the cross-section is taken by the facings, and the shear is taken by the core.

The deflection is obtained by super imposing the shearing deflection of the core on the bending deflections. However, since the shearing deflection would be several times the bending deflection due to the very low value  $G$  ( $20-2 \text{ N/mm}^2$ ) for

the low density core material which was used in this research, the edge ribs were constructed around the core to overcome this component of deflection, so in fact, the beams behaved as box beams rather than sandwich beams and at the same time could be said to enjoy the advantages of a sandwich beam, having good insulation and light weight.

However, in the theoretical calculation (see appendix 3), the shear deflection due to the core also has been considered, assuming no ribs on the beam, to see what differences it could have made in the total deflection.

The final formula derived from the appendix (3) has been tabulated in table (4.4) which includes the bending deflection, shear deflection and total deflection in different positions on the beam with different types of loading.

A formula has also been derived (see appendix 3) to determine the theoretical value of strain per unit load together with stress on the faces for different types of loading at the central cross-section and are as follows:

1. point load at the centre

$$\text{Strain/unit load} = \frac{L \times \hat{y}}{4 \times EI} \quad (4.1)$$

$$\sigma_y = \frac{W \times L \times \hat{y}}{4 \times I} \quad (4.2)$$

2. four points loading

TYPE OF LOADING	POSITION ON THE BEAM	BENDING DEFLECTION ( $\gamma_b$ )	SHEAR DEFLECTION ( $\gamma_s$ )	TOTAL DEFLECTION $\gamma = \gamma_b + \gamma_s$
4 POINTS LOADING	a	$\frac{1.43 \cdot 10^7}{D} \cdot W$	$\frac{W}{2AG} \cdot a$	$\left( \frac{1.43 \cdot 10^7}{D} + \frac{a}{2AG} \right) W$
	2a	$\frac{2.43 \cdot 10^7}{D} \cdot W$	$\frac{3W}{4AG} \cdot a$	$\left( \frac{2.43 \cdot 10^7}{D} + \frac{3a}{4AG} \right) W$
	3a	$\frac{2.78 \cdot 10^7}{D} \cdot W$	$\frac{3W}{4AG} \cdot a$	$\left( \frac{2.78 \cdot 10^7}{D} + \frac{3a}{4AG} \right) W$
CENTRAL POINT LOADING	a	$\frac{2.01 \cdot 10^7}{D} \cdot W$	$\frac{W}{2AG} \cdot a$	$\left( \frac{2.01 \cdot 10^7}{D} + \frac{a}{2AG} \right) W$
	2a	$\frac{3.55 \cdot 10^7}{D} \cdot W$	$\frac{W}{AG} \cdot a$	$\left( \frac{3.55 \cdot 10^7}{D} + \frac{a}{AG} \right) W$
	3a	$\frac{4.17 \cdot 10^7}{D} \cdot W$	$\frac{3W}{2AG} \cdot a$	$\left( \frac{4.17 \cdot 10^7}{D} + \frac{3a}{2AG} \right) W$

Table(4.4). Determination of deflection under various loads.

$$\text{Strain/unit load} = \frac{L \times \hat{y}}{8 \times EI} \quad (4.3)$$

$$\sigma_y = \frac{W \times L \times \hat{y}}{8 \times I} \quad (4.4)$$

#### 4.6 Results and discussions

All the flexural specimens were tested as beams in a rig mounted in the Instron 1995 testing machine as (3.5) and the  $E$  value was determined and tabulated in table (4.5). From careful measurement of the faces, thickness and ribs, the  $I$  value and hence the  $EI$  value was calculated. Knowing the relationship between the  $EI$  and  $W/y$  for positions 1,2,and 3 on the beam (from Appendix 3) theoretical values of were determined, (see table 4.5). A graph was plotted showing the values of the deflection at positions 1,2,3 due to the applied load for any beam at different face positions. A typical graph for any set of the beams on four point loading is shown in fig 4.6 (set no. 1-6, section 'A').

As the load-deflection diagrams indicate, the behaviour of the beams can be classified into two stages. The first stage, before the appearance of the crack, show the beams behaving elastically, and the second stage is after the cracks appeared, in which the load-deflection relationship is no longer linear. From the plots, the slope of the elastic section of the graph was obtained and it was compared with the theoretical value of  $W/y$  which was determined previously.

SET NO:	TYPE OF LOADING	FACE OF THE BEAM UNDER THE TEST	THEORETICAL VALUE										EXPERIMENTAL VALUE												FAILURE LOAD (lb)	CRACK LOAD (lb)
			E (N/mm <sup>2</sup> )	E (N/mm <sup>2</sup> )*10 <sup>-11</sup>	SLOPE OF THE GRAPH N/mm			STRAIN (u *10 <sup>4</sup> /N)			SLOPE OF THE GRAPH N/mm			E <sup>2</sup> N/mm	STRAIN (u *10 <sup>4</sup> /N)											
					POSITION			POSITION			POSITION				POSITION											
					1	2	3	1	6	1	2	3	1		2	3	4	5	6							
					1	CENTRE POINT	WIDER SIDE	15830	1.05	5248	2971	2530	1274		1486	5213	3084	2471	15797	1015	—	—	—	—		
1	CENTRE POINT	NARROW SIDE	15830	4.13	20549	11634	9904	787	738	18904	11155	9312	14900	823	560	303	259	450	590	—	—					
	4 POINTS	NARROW SIDE	15830	4.13	28931	16996	14869	394	369	27911	15790	14297	15111	341	294	172	122	197	348	4000 TENSION	1800					
	2	CENTRE POINT	WIDER SIDE	17430	1.07	5324	3014	2566	1314	1394	5485	3205	2659	18144	1146	—	—	—	—	—	—					
2	CENTRE POINT	NARROW SIDE	17430	4.21	20945	11859	10096	759	737	20476	12137	9830	17262	749	482	227	246	422	666	—	—					
	4 POINTS	NARROW SIDE	17430	4.21	29492	17325	15158	380	369	29620	17881	15171	17651	381	189	121	133	247	239	4400 TENSION	2000					
	3	4 POINTS	WIDER SIDE	11822	0.91	6373	3744	3276	878	715	5992	3576	3290	11571	725	460	577	791	—	—	3450 TENSION	1200				
4	4 POINTS	WIDER SIDE	11822	0.84	5874	3457	3022	968	719	4696	3432	2732	10634	892	—	336	612	—	—	5400 SHEAR	1200					
5	4 POINTS	WIDER SIDE	17430	1.42	9930	5843	5108	533	465	9918	5722	5400	17628	437	291	275	358	—	—	5800 SHEAR	1150					
6	4 POINTS	WIDER SIDE	20000	1.51	10559	6214	5432	467	471	10713	6624	5490	20636	392	314	380	392	—	—	2200 SHEAR	550					

Table(4.5). Comparison between the theoretical & experimental values of the beams.

The comparison between the two also can be seen in table (4.5) and fig (4.6 set no. 1-6 section B). Using the experimental values of  $W/y$ , the  $E$  values were determined and tabulated in table (4.5).

All the beams were failed under 4 point loading. The beam set no. (1 and 2) were tested on the narrow side of the beam while the beam set no.(3-6) were tested on the wider side. The average crack load for the first group appeared at 1800lb for the first set and 2000lb for the second set and the failure load at 4000lb and 4400lb respectively. All the beams failed due to the sudden tension failure of the bottom faces.

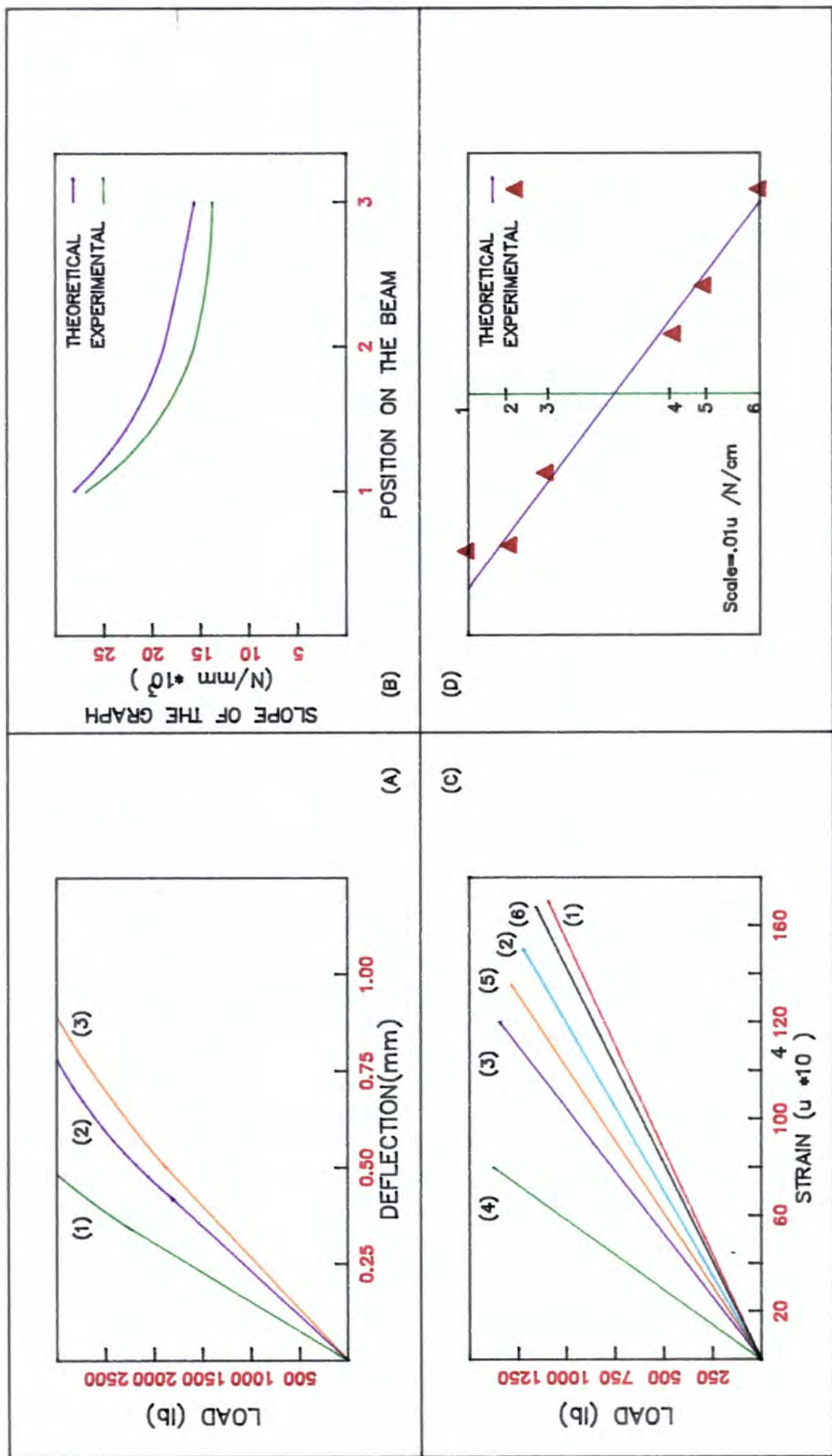
Beams set no. (3) which were cast using mix (A) and reinforced with two 6mm diameter bars at the bottom faces, were failed in the previous manner with the crack load and failure load at 1200lb and 3450lb respectively.

Beams set no (4) were the same beams as set no (3) except that they were reinforced with 9mm diameter bars. The type of failure was shear failure near the supports and although the crack load was the same as the beams set no (3), the failure load increased to 5400lb.

Beams set no (5) which were cast with mix (SS) and reinforced with two 9mm diameter bars were failed in the same manner as the beams set no (4) with crack load and failure at 1150lb and 5800lb respectively.

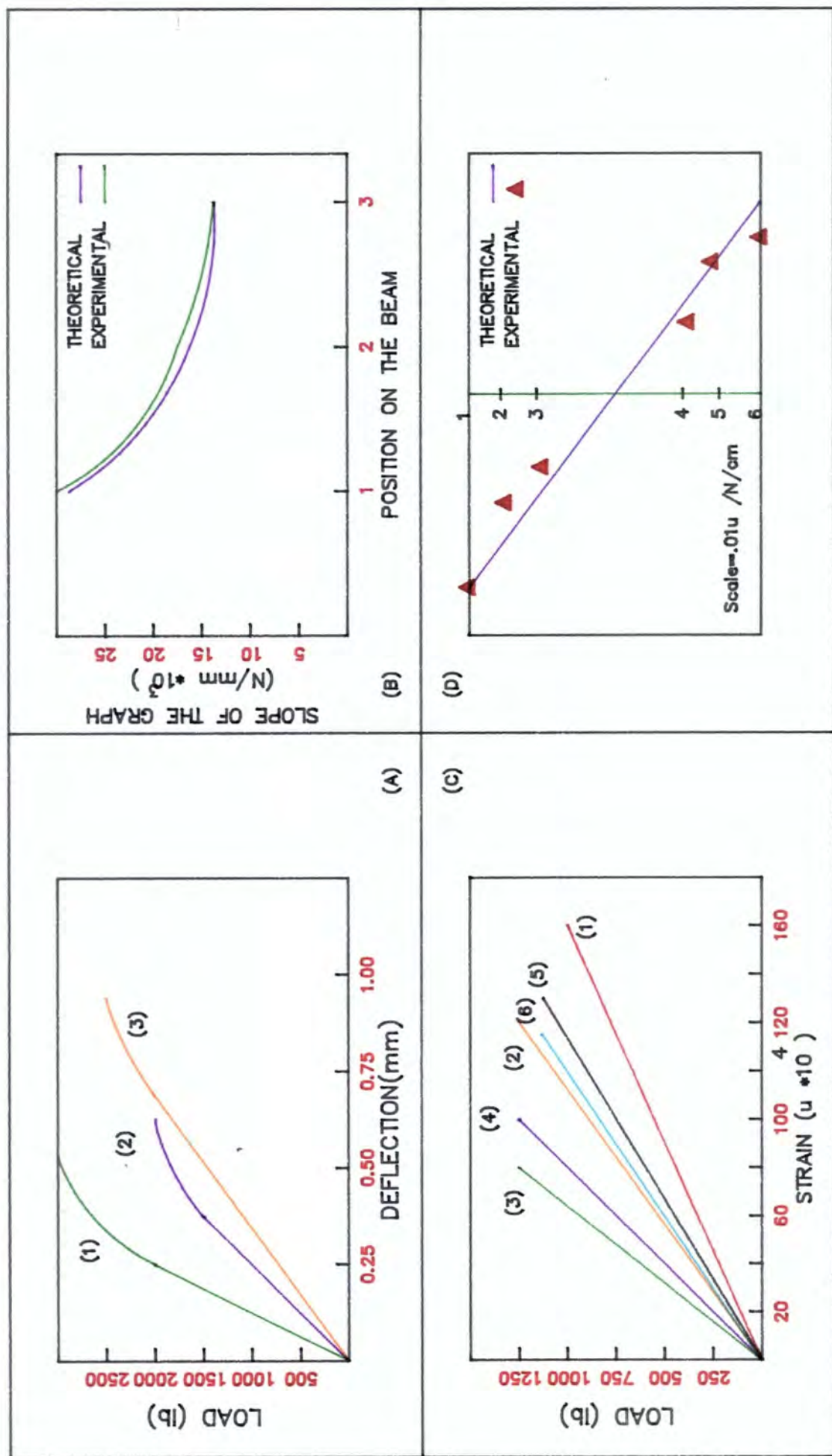
Beams set no (6) which were portland cement concrete and reinforced with 6mm diameter bars, failed in a shear manner near the supports at very low value of load (550lb crack load, and 2200lb failure load) compared with the previous polymer





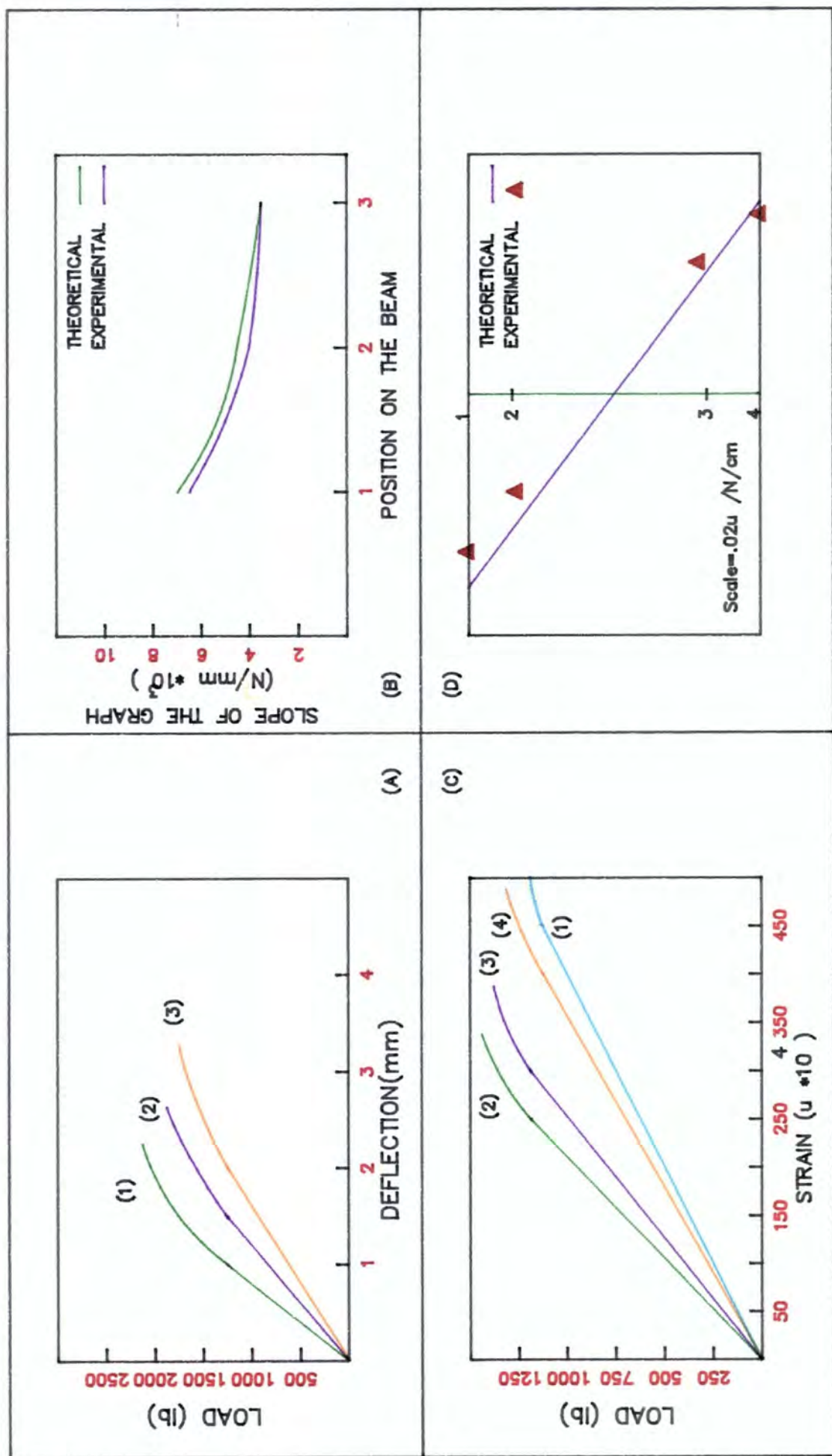
NOTE: 4 POINTS LOADING APPLIED ON THE WIDER SIDE OF THE BEAM.

Fig.(4.6). SET NO: 1



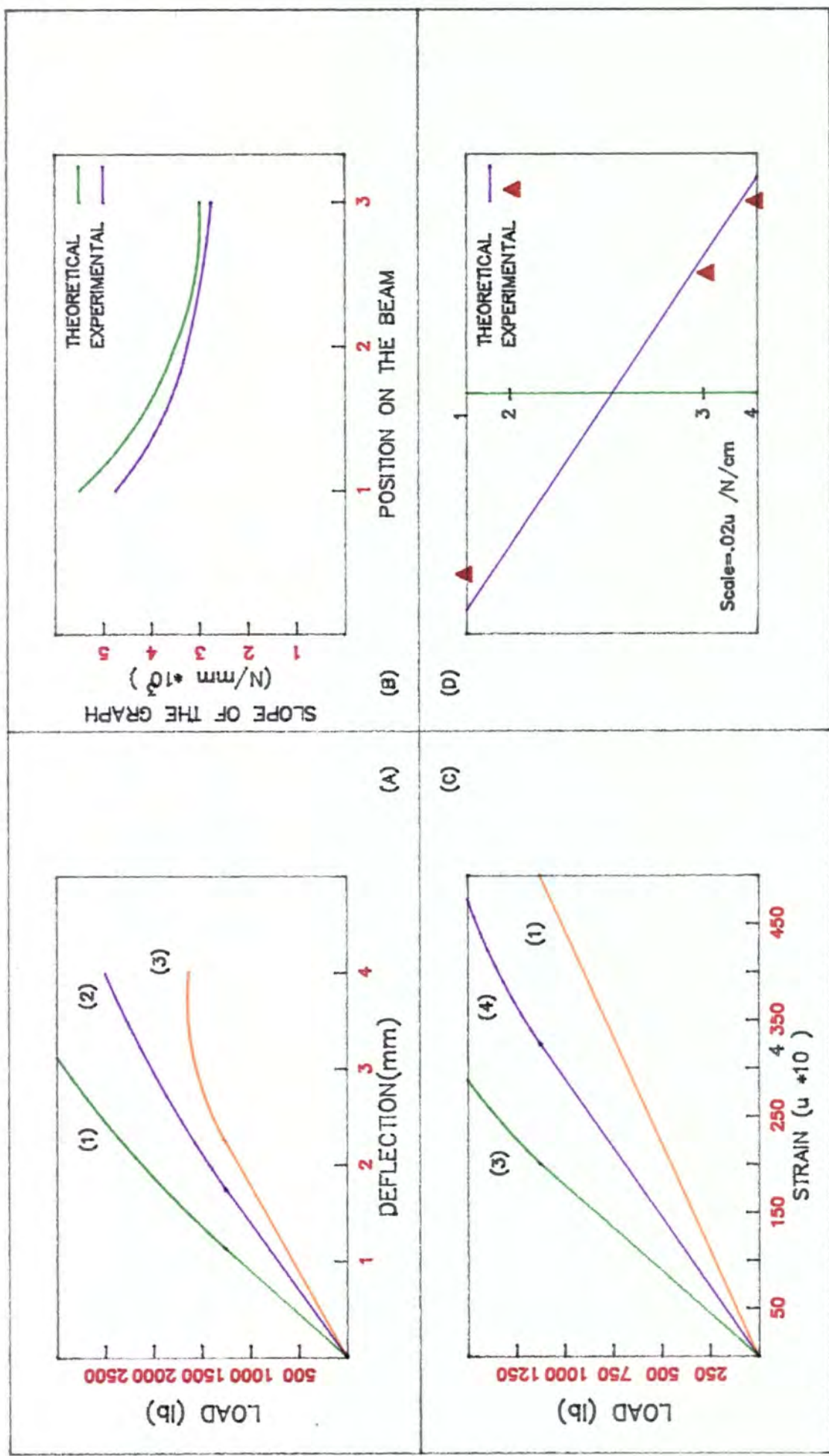
NOTE: 4 POINTS LOADING APPLIED ON THE WIDER SIDE OF THE BEAM.

Fig.(4.6). SET NO:2



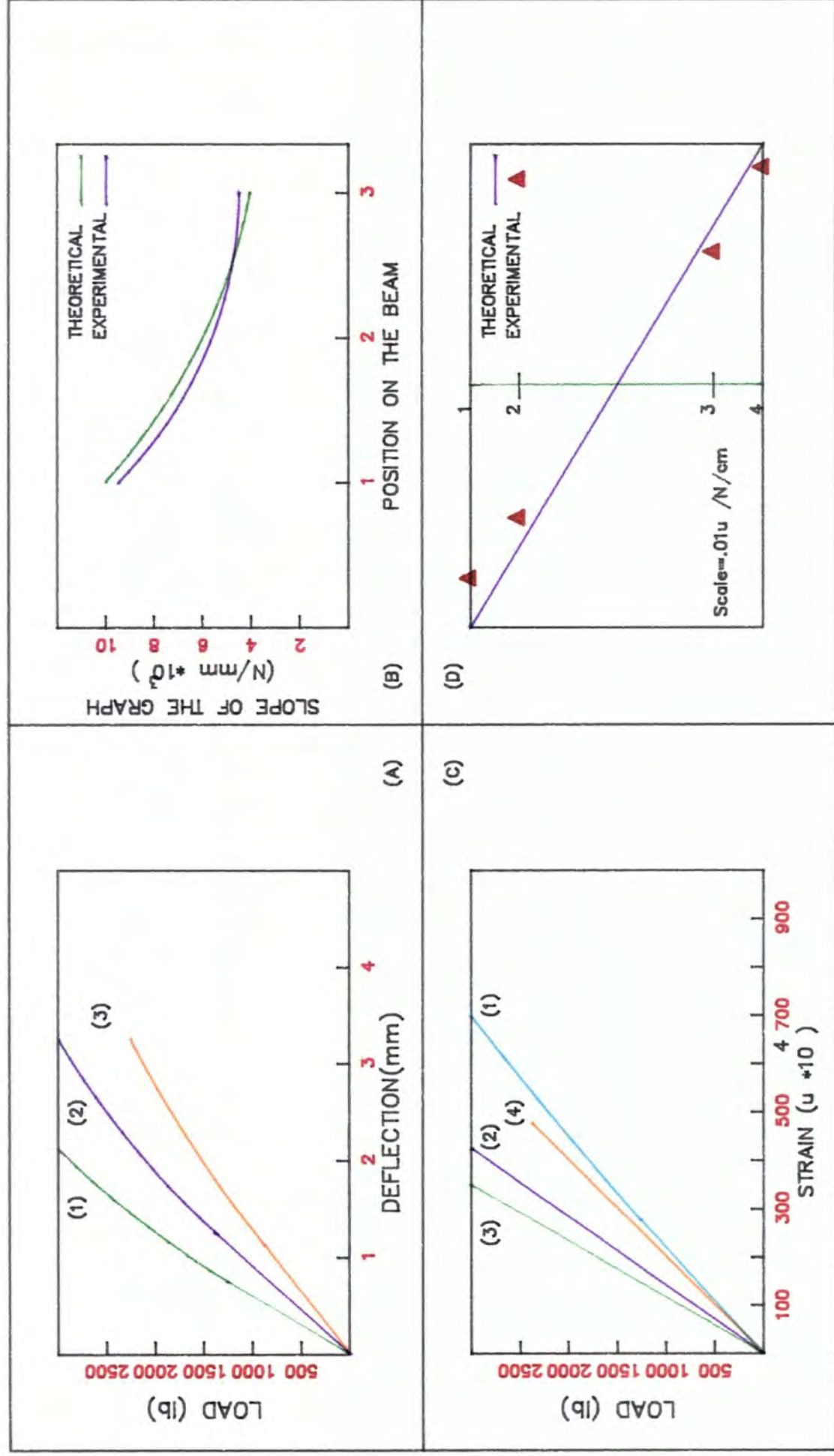
NOTE: 4 POINTS LOADING APPLIED ON THE WIDER SIDE OF THE BEAM.

Fig.(4.6). SET NO: 3



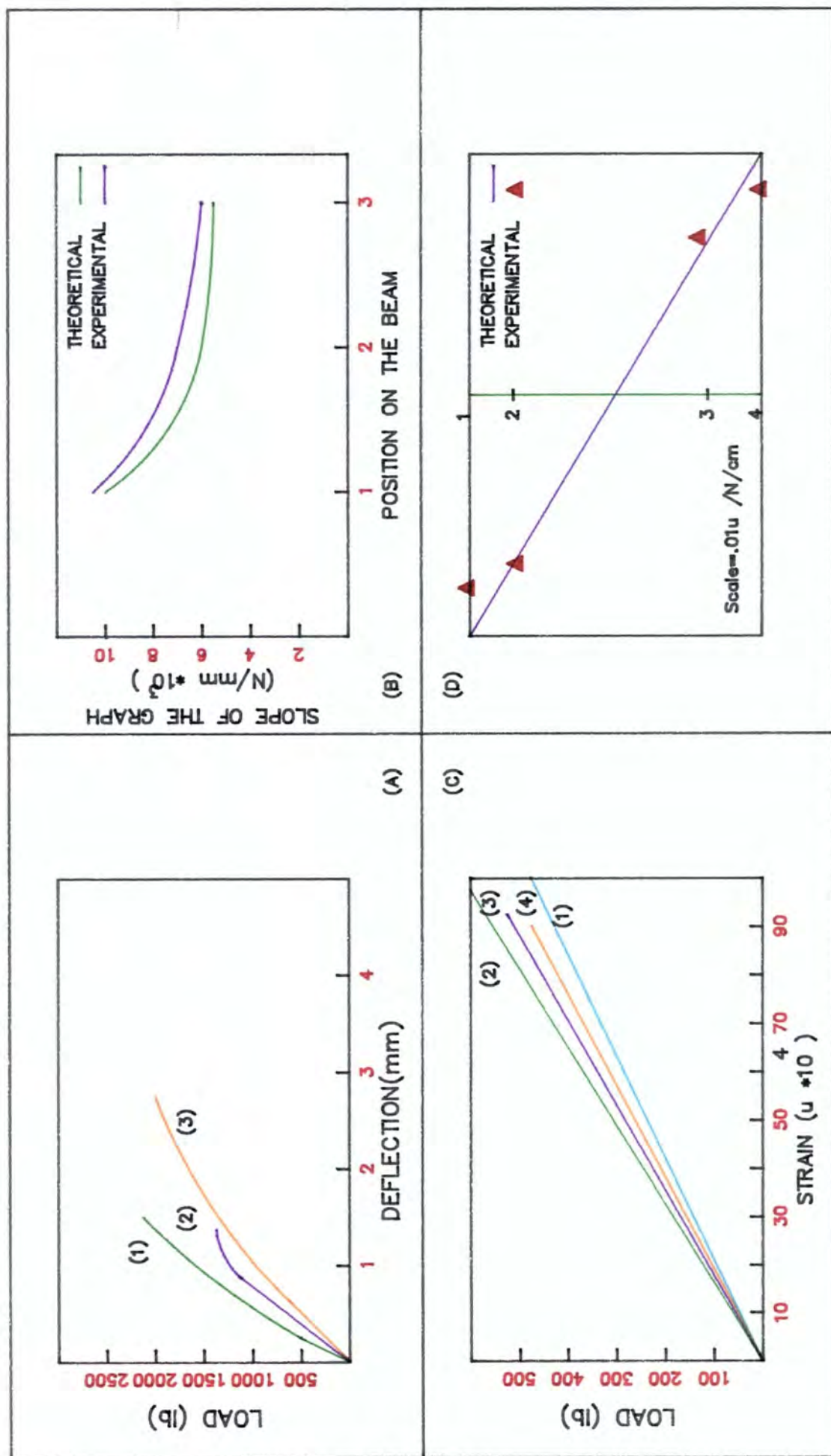
NOTE: 4 POINTS LOADING APPLIED ON THE WIDER SIDE OF THE BEAM.

Fig.(4.6). SET NO: 4



NOTE: 4 POINTS LOADING APPLIED ON THE WIDER SIDE OF THE BEAM.

Fig.(4.6). SET NO: 5



NOTE: 4 POINTS LOADING APPLIED ON THE WIDER SIDE OF THE BEAM.

Fig.(4.6). SET NO: 6

concrete beams.

The total strains measured ( $\epsilon_t$ ) on the faces of the beam were plotted against the total acting load ( $w$ ) for any set of beams tested in figures 6 (set no 1-6, section c).

All the strains measured above the N.A were compressive, and strains were found to be tensile on the bottom surfaces.

It can be seen from each figure that the rate of increase in the strain at the lower faces is greater than the upper faces. But in all cases, the load-strain relationship is linear in the stage of loading before crack appearance, ie; the beam behaved elastically in this stage, as considered before in deflection analysis.

Strain per unit <sup>load</sup> was taken from the straight line of the linear relationship throughout the elastic stage of each curve. The theoretical values of strain per unit load were calculated according to the equations (4.1 and 4.3) at the central cross-section in the elastic stage.

A vertical line was drawn and the position of strain gauges on the central cross-section of the beam were marked along this line. The theoretical value of strain per unit load at upper and lower faces were scaled off to  $(0.01\mu\epsilon/N/cm)$  and they were jointed together by a straight line. The experimental values also were scaled off opposite to its position on the beam. Graph 'D' in fig 4.6 (set no 1-6) illustrates this comparison between the theoretical and experimental value of strain per unit load.

Assuming that there were no ribs in the beams, the bending deflection of unit

SET NO:	TYPE OF LOADING	FACE OF BEAM UNDER TEST	POSITION ON THE BEAM	BENDING DEFLECTION/ UNIT LOAD ( $\gamma_b$ )	SHEAR DEFLECTION/ UNIT LOAD ( $\gamma_s$ )	TOTAL DEFLECTION ( $\gamma_T$ )	EXPERIMENTAL DEFLECTION/ UNIT LOAD (mm/N)	RATIO
1	4 POINTS	NAROW SIDE	CENTRE	$0.105 \times 10^{-3}$	$4.36 \times 10^{-3}$	$4.465 \times 10^{-3}$	$6.7 \times 10^{-5}$	66
2	4 POINTS	NAROW SIDE	CENTRE	$0.096 \times 10^{-3}$	$4.36 \times 10^{-3}$	$4.456 \times 10^{-3}$	$6.6 \times 10^{-5}$	68
3	4 POINTS	WIDER SIDE	CENTRE	$0.335 \times 10^{-3}$	$4.31 \times 10^{-3}$	$4.645 \times 10^{-3}$	$.31 \times 10^{-5}$	15
4	4 POINTS	WIDER SIDE	CENTRE	$0.327 \times 10^{-3}$	$4.31 \times 10^{-3}$	$4.637 \times 10^{-3}$	$.33 \times 10^{-5}$	14
5	4 POINTS	WIDER SIDE	CENTRE	$0.222 \times 10^{-3}$	$4.31 \times 10^{-3}$	$4.530 \times 10^{-3}$	$.20 \times 10^{-5}$	23
6	4 POINTS	WIDER SIDE	CENTRE	$0.197 \times 10^{-3}$	$4.31 \times 10^{-3}$	$4.507 \times 10^{-3}$	$.18 \times 10^{-5}$	24

Table(4.7). Comparison in deflection/unit load between the beams, assuming no ribs and the beams with ribs.

load and shear deflection/unit load for all the beams has been calculated and they are shown in table (4.7).

As we can see from the figures, the shear deflection mostly represents the total deflection due to the applied load. The previous results (beams with ribs) have been compared with these total deflections and their ratio has been found. Therefore we can conclude that, if the beams had no ribs, they would have failed well below the previous failure loads.

#### 4.7 Conclusions

From the results and observation during the test, the following conclusions have been made:

- i. Beams behave as box beams, and elastic behaviour can be predicted from **elastic** calculations.
- ii. The core has no discernable structural effect other than to ensure the local stiffness (stability) of the faces.
- iii. The effect of the bar reinforcement was to increase the stiffness and ultimate load of the beams greatly, and with the 9mm bars in this section the failure criterion was changed to a shear failure.

However, even without the steel, cracks appeared at a load substantially less than the failure load, so that potential failure could be diagnosed in practice before catastrophic collapse.

The polymer concrete beams were over twice as strong as the comparative reinforced concrete beams.

NB: In practice, the reinforced concrete would not have had sufficient durability because of the low bar cover, but the polymer concrete beams probably would have, because of the low permeability of the material.

# CHAPTER (5)

## CHAPTER FIVE

### 5: Access Floor Panels

#### 5.1 Introduction

A floor panel (slab) is a flat structural surface in which the length and breadth are large compared with the thickness. Slabs are able to carry loads acting perpendicular to their own plane by virtue of bending, twisting and shearing action.

In many buildings, such as computer rooms, there is a mass of cabling and ducting, and unhindered access to the under-floor services are required. In this case, pedestals or supporting props made from thick wall, galvanised steel tube, fitted with die-cast aluminium castellated head and base plate for adhesive bonding or screw fixing, are fixed to the sub floor at a spacing equal to the length of the panels (usually  $600 \times 600\text{mm}$ ).

The individual panels are locked firmly into the heads of the supporting props without the need for bolting or screwing to prevent movement. The props are fully adjustable to overcome variations in level of the sub-floor. The absence of independent stringers allows a completely free passage for ducting, cables and all other services.

Most of the panels used in this flooring system are constructed from galvanised

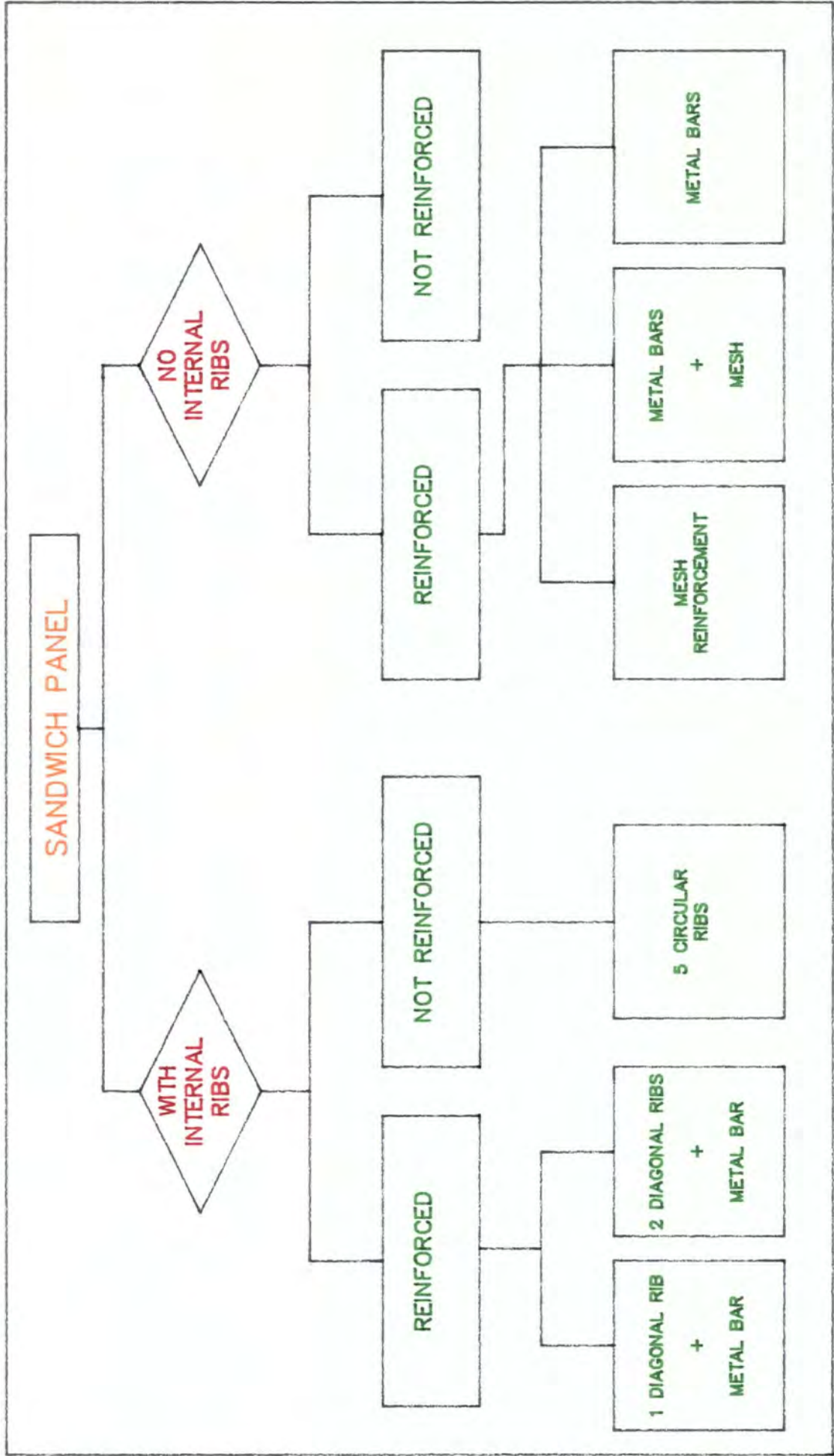
pressed steel, bonded to a high density, processed timber insulating core. However, they have many disadvantages, such as cost, deformation due to the heat, poor fire resistance, uncertain, possibly poor bonding between the steel and timber, excess of deflection under load, water absorption etc.

The objective of this exercise was to develop a filled polymer access flooring panel capable of :

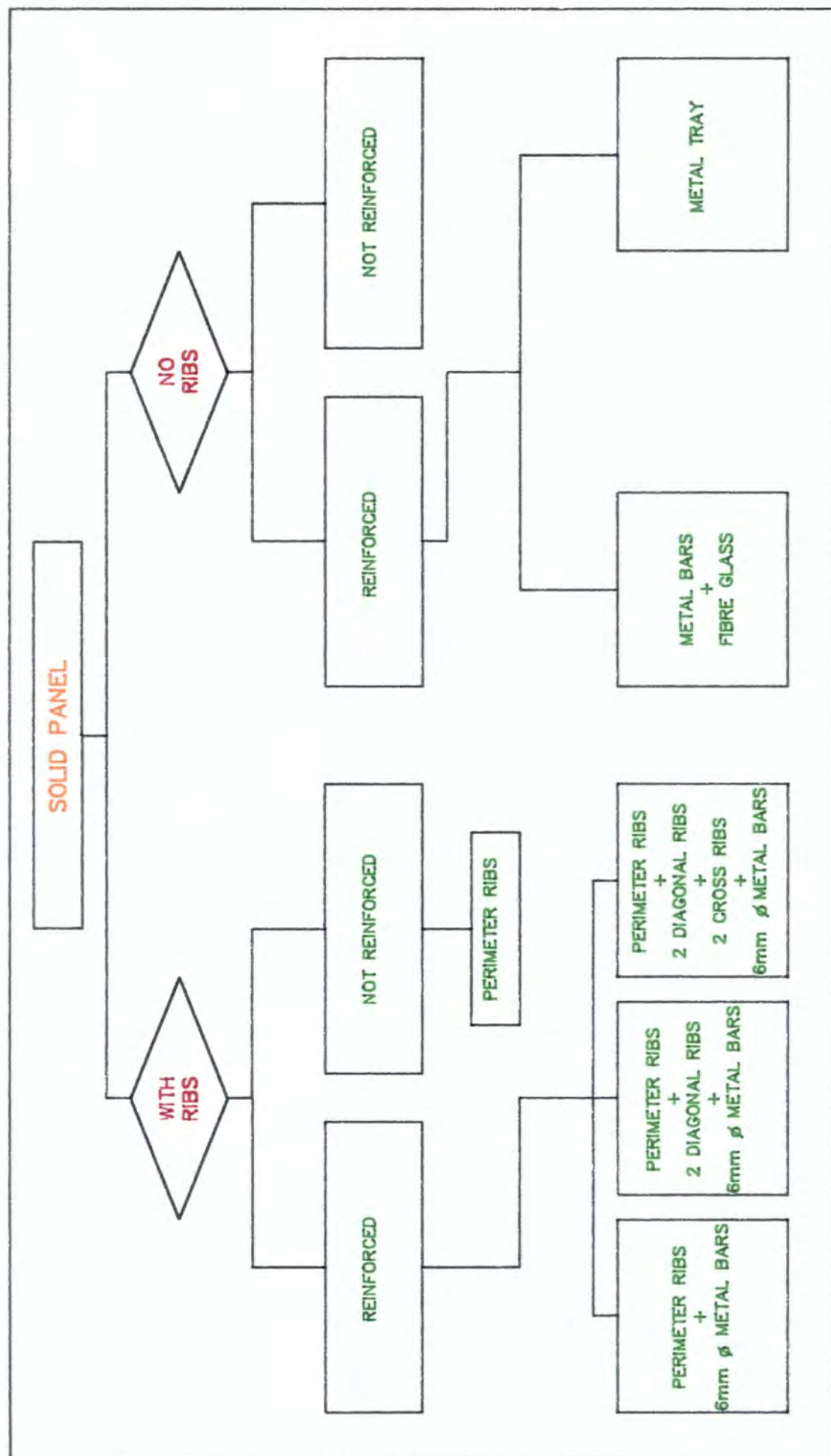
1. meeting DOE specification MOB 08/801 dated August 1985.
2. capable of being produced in volume.
3. unit cost of the end product to be within reasonable economic limits and also to be able to compete in the market with similar products currently available.

The most important factors which were considered in design of the panels in this research according to DOE specification MOB 08/801 dated August 1985 were as follows:

1. panels to be stringerless to a module of  $600 \times 600\text{mm}$
2. the maximum thickness must not be greater than 50mm
3. individual panels are not to exceed 20kg in weight
4. each panel shall be supported from below, at all four corners and shall be capable of bearing a load of 3 kN on a 25mm sq. area positioned anywhere on its top surface with <sup>x</sup>maximum deflection no greater than 2.5mm
5. each panel should sustain three times the working load ( $3 \times 3 \text{ kN}$ ) for 5 minutes without failure.



Table(5.1A). Schedule of the sandwich floor panels.



Table(5.1B). Schedule Of The Solid Floor Panels.

## **5.2 Dimensions and schedule of the panels**

All the dimensions of the panels were  $600 \times 600\text{mm}$  with the thickness between 20-50mm. They were divided into two main groups. The first group was sandwich panels which consisted of top and bottom faces of polymer concrete mix with 10mm thickness and were insulated with **Iso-foam** core. The second group were the solid panels, with no foam used in their construction. Perimeter ribs with diagonal ribs and/or cross ribs were constructed to join the top and bottom faces in some of the panels to reduce the deflection and maximise the critical load. Several types of reinforcement were used in these panels. These included fibre glass, 6mm dia. M.S bar, and galvanised steel tray.

The schedule of the panels with dimensions which were investigated in this research have been illustrated in table 5.1 and 5.2.

Note: mix TT(7:1) using resin (L.V.M) was used to construct all the panels used in this exercise.

## **5.3 Method of construction**

### **5.3.1. Sandwich panels**

#### **a1) Without internal ribs and without metal reinforcement**

This type of panel was constructed exactly in the same manner as the sandwich beams but in different dimensions, ie; polymer concrete was placed into the mould ( $600 \times 600 \times 50\text{mm}$ ) to the thickness of 10mm. After vibration, the fibre glass

(600 × 600mm) was laid over the first skin of the panel and the air trap between the mix and the fibre glass was removed by using a roller. The foam core with the dimensions of 590 × 590mm was placed in the middle of the mould and the gap between the foam and the mould was filled with the mix (10mm wide). The second layer of the fibre glass was placed on the top of the foam and mix was poured on top of that to give the 10mm thickness top skin. With the aid of vibrator and wooden screed, the top skin was levelled off. The cross-section of this type of panel can be seen in fig. (5.3).

**a2) Without internal ribs but with metal reinforcement**

Expanded metal mesh and M.S bar reinforcement was used to improve the performance of the above slabs.

**b1) with internal ribs and without metal reinforcement**

Ribs were used in the classic sandwich format to connect the top and bottom surfaces of the panel to minimise deflection and maximise the critical load.

**b2) With internal ribs and with metal reinforcement**

Bar reinforcement was used to improve the performance of the above panels. The dimension and shape of the bars are reported in fig. (5.4).

**5.3.2. Solid panels**

**a1) with ribs and with or without reinforcement**

These panels were constructed with 10mm top faces and 25mm perimeter ribs. Some of these panels had the addition of 2 diagonal ribs or 2 diagonal ribs plus

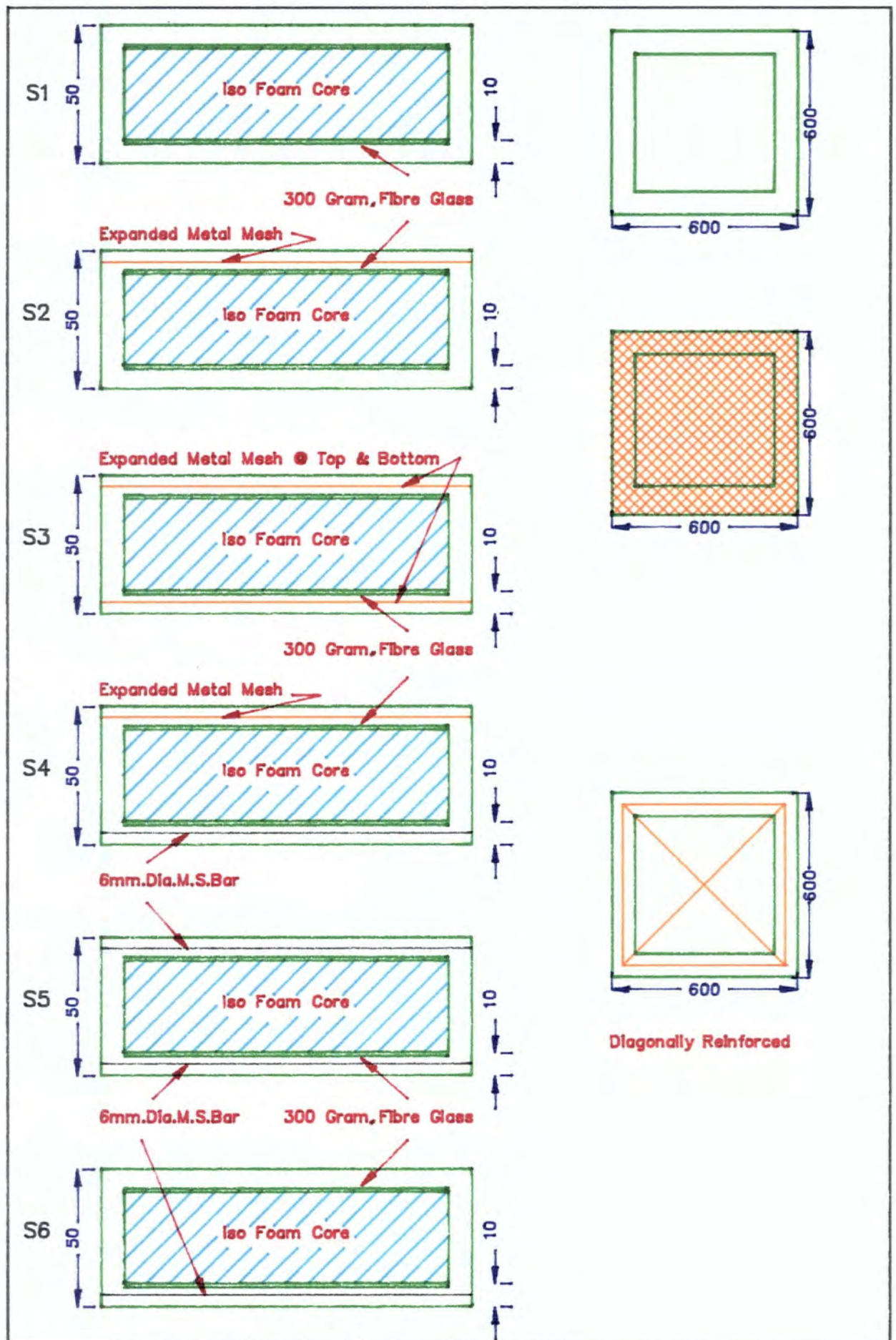


Fig.(5.3). Sandwich Panel With No Ribs.

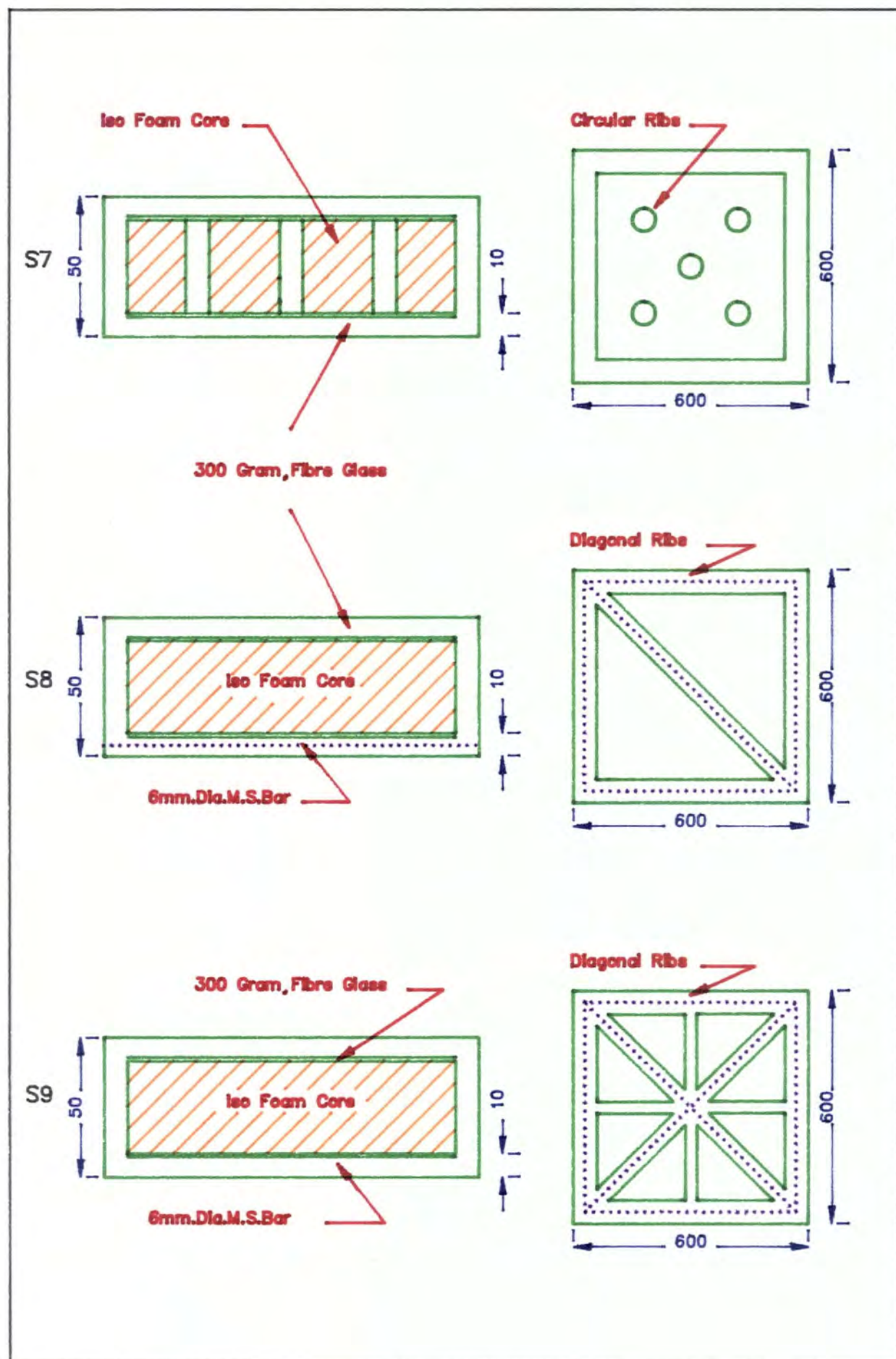


Fig.(5.4). Sandwich Panel With Ribs.

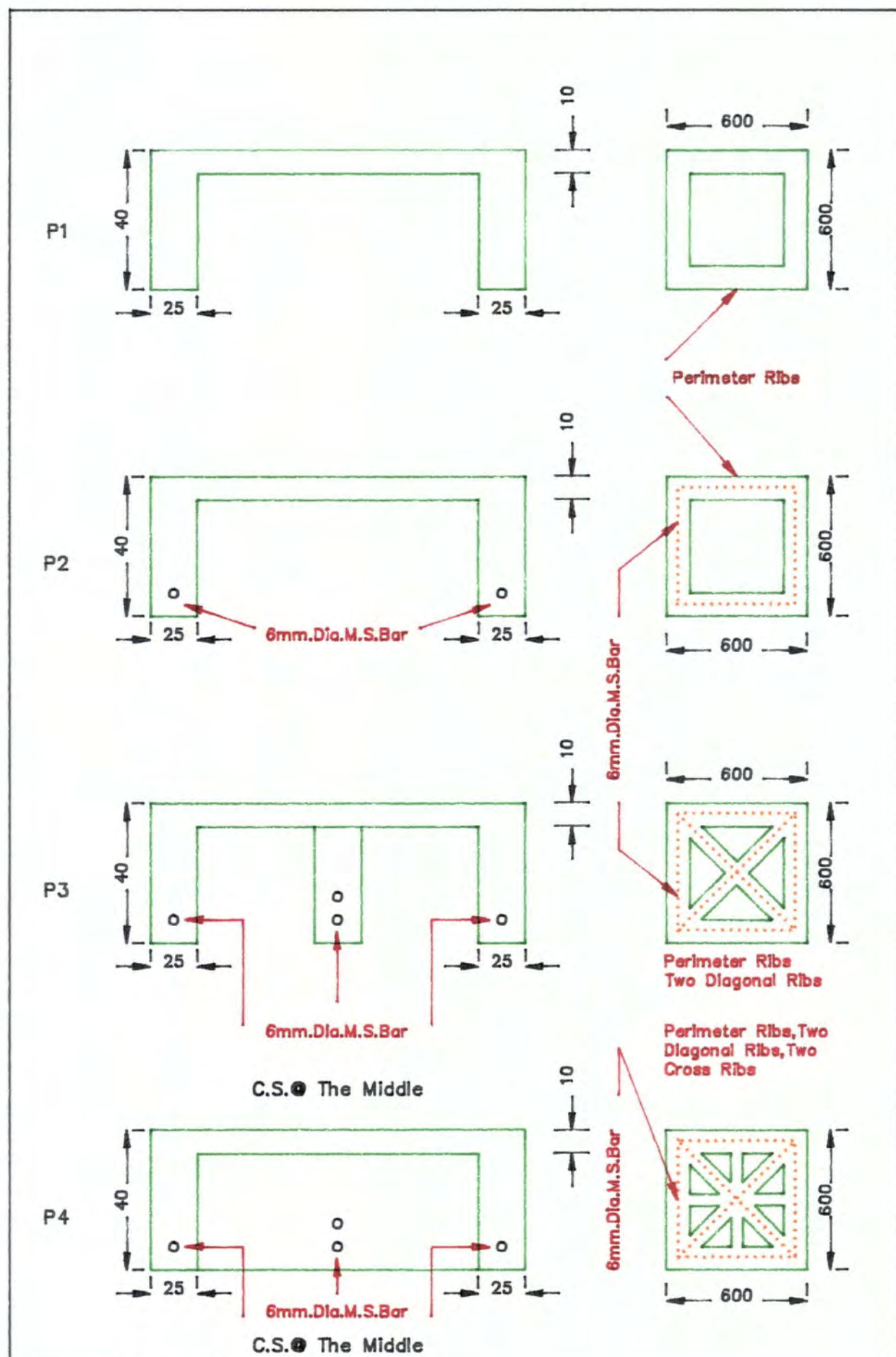


Fig.(5.5). Solid Panels With Ribs.

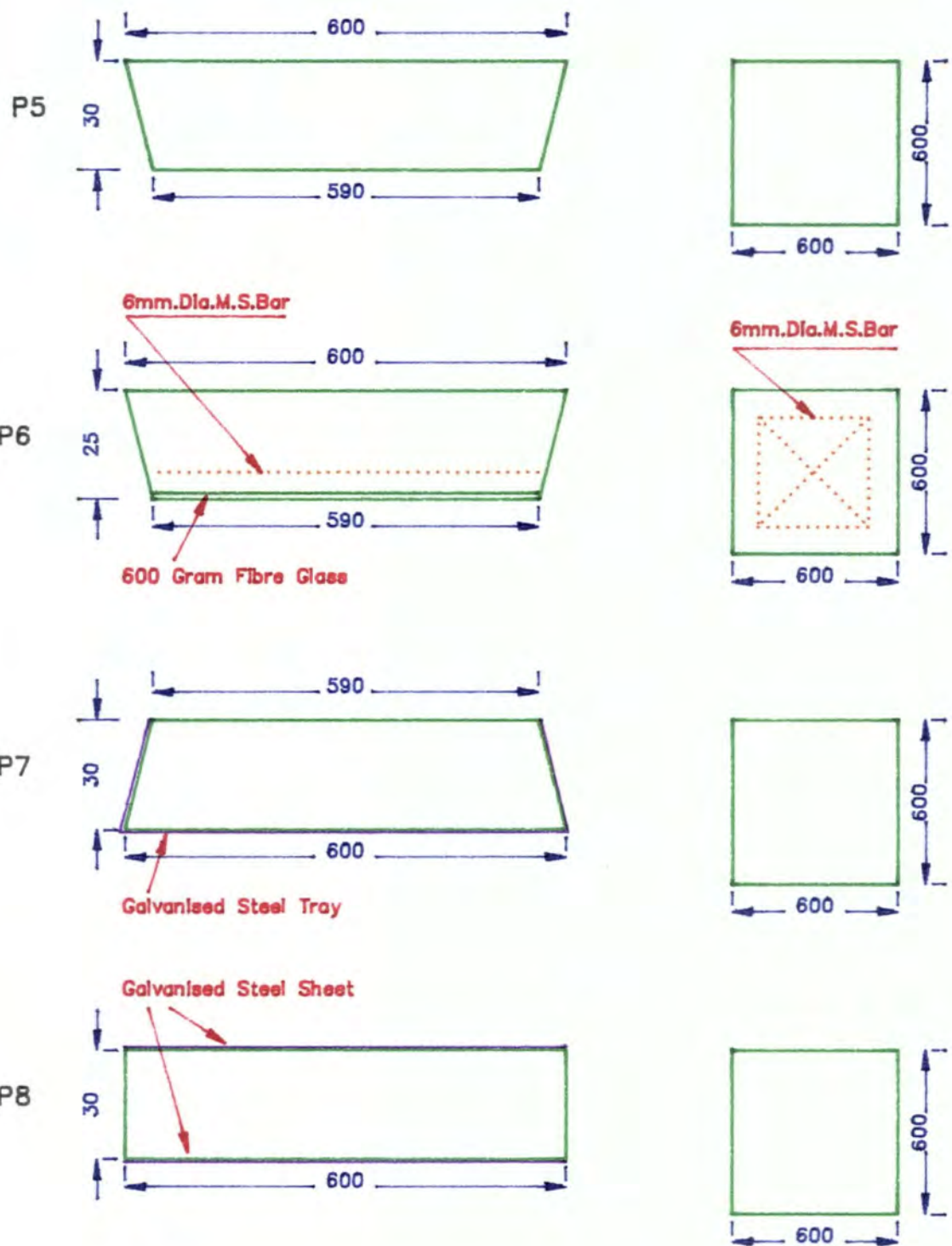


Fig.(5.6). Solid Panels With No Ribs.

two cross ribs, reinforced with 6mm dia. M.S bars inside the ribs. There was no problem of removing the panels from the mould, after the curing period as a result of the shrinkage. The cross-section of these panels can be seen in fig.(5.5).

#### **b1) Solid panels with no ribs**

The thickness of these panels varied between 25-30mm, construction was easy and fast as it was made in one operation. Mix was poured into the wooden mould or metal tray and after vibration, the top face was levelled off to the required thickness with the aid of the wooden screed. (see fig. 5.6).

### **5.4 Preparation for testing, and testing procedure**

After allowing three days for curing for each panel, they were removed from the mould and the positions at which to apply the loads were marked on the top surface of the panel, as shown in fig. (5.7).

The individual panels were placed in a standard test rig mounted on pedestal supports at four corners (see fig. 5.7). A monitored load was applied to predetermined critical points on the panel as a point load by <sup>a</sup>hydraulically operated ram with 25mm square head. The panel performance was observed and recorded, the following programme of test procedure was adopted for all specimens;

- i. A 3 kN load was applied at position (1) and maintained for 5 minutes. The deflection under the point load was recorded.
- ii. A 9 kN load was then applied at position (2) and maintained for 5 minutes

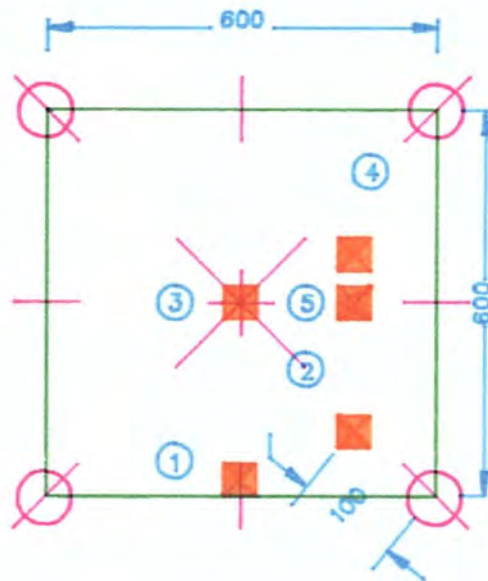


Fig.(5.7A). Position Of The Point Loads On The Panel.

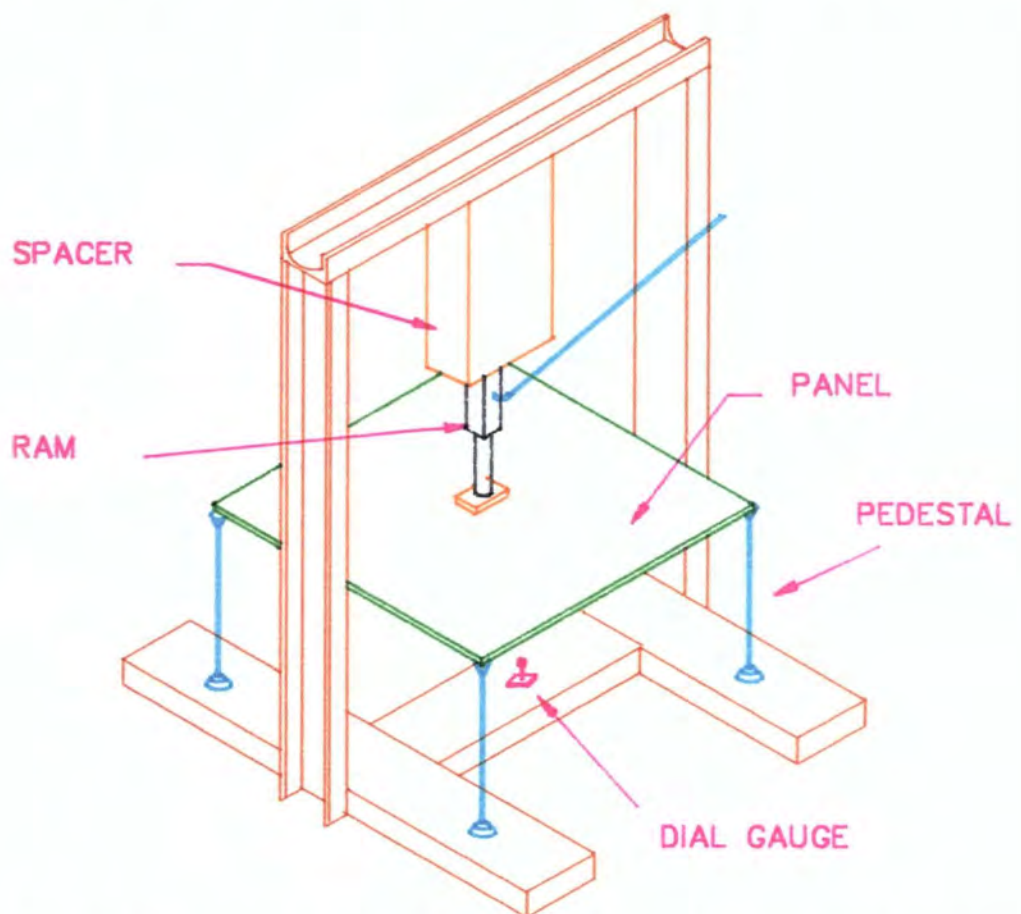


Fig.(5.7B). Illustration Of The Panel Under Testing.

and results were recorded.

- iii. A 9 kN load was then re-applied to the panel at position (1) and maintained for 5 minutes and the results recorded.
- iv. For some of the panels positions 3, 5 and 4 were critical. A 9 kN load also was applied in these positions and maintained for 5 minutes and performance was observed and recorded.

## **5.5 Results and discussions**

### **5.5.1 Sandwich panels**

#### **a1) Without ribs and without reinforcement**

Generally deflection in this type of slab was found to be greater than 2mm with a critical load of approximately 8.0 KN at position (4). However, there was a problem of local failure at the top surface due to punching.

#### **b1) Without ribs and with reinforcement**

Expanded metal mesh and M.S bar reinforcement was used to improve the performance of the slab. The <sup>x</sup>expanded metal was intended to prevent punching, but with no success. The M.S bar was used to reduce the deflection and increase the critical load, again with limited success. Neither provision is likely to meet the standard required.

Panel Ref.(S6) using a structural phenolic foam core with bar reinforcement at the bottom proved to be very satisfactory but the prospects of obtaining a good

bond between foam and the polyester matrix are very poor.

**c1) With ribs and without reinforcement**

Ribs were used in the classic sandwich format to connect the top and bottom surfaces of the panel to minimise the critical load. The object proved to be unattainable without some form of reinforcement.

**d1) With ribs and with reinforcement**

A slab with one diagonal or two diagonal ribs with bar reinforcement proved to be better than earlier examples, and the critical load was increased to 10.7 kN at position (4). However, the problem of punching in the top skin still occurred elsewhere on the panel.

**5.5.2. Solid panels**

**a2) With rib/perimeter rib**

Panels of this type were tested at position (1) they failed to achieve the design load before deflection could be considered. Failure occurred at 2.8 kN or thereabouts. At position (4), failure occurred at approximately 3.1 kN.

**b2) With ribs/perimeter rib plus two diagonal ribs/ with M.S bar reinforcement**

The 3.0 KN point load was applied at position 1, it induced a deflection less than 1.5mm. A 9.0 KN point load applied at position (2) and (4) was maintained satisfactorily without any type of failure. However, at position (5), it failed by punching through the surface of the panel under a load of 4.5 kN.

**c2) With rib/perimeter rib plus two diagonal ribs and two cross ribs**

These panels perform satisfactorily under the evaluation test at positions 1,4,5,2, with a 9 KN load. However, failure occurred at position (3) by punching through the surface of the panel at 6.9 kN. This problem may be overcome by using a 600 gramme fibre glass.

There are, however, other problems of greater significance with this panel. The geometry of the panel is complex and causes difficulty when releasing from the mould due to the shrinkage factor.

**d2) Solid panel with no rib/with M.S bar reinforcement/fibre glass bottom**

A slab 25mm thick was tested and satisfactorily resisted a 9.0 KN point load at any point on the surface. Deflection at design load was very satisfactory at 0.6mm.

**e2) With no rib/metal tray reinforced**

A galvanised tray 30mm deep was used as mould reinforcement. A satisfactory bond was obtained between the steel and the mix. A 9.0 kN point load was satisfactorily maintained at any point on the slab without any apparent signs of distress.

The applied load at position (4) was increased to 18 KN (ie; 6 times the design load) without any failure. However, there was a differential rate of shrinkage between the top and bottom surface due to the bonding of the bottom face of the tray and temperature difference between the two faces, resulting in a panel with concavity.

REF.	TYPE OF PANEL	DEPTH (mm)	WEIGHT (Kg)	POSITION OF LOAD	APPLIED LOAD (KN)	DEFLECTION (mm)	PERFORMANCE & REMARKS
	SANDWICH PANEL/NO RIBS						
S1	NO METAL REINFORCEMENT, STANDARD ISO FOAM CORE AND 300gr FIBRE GLASS @ TOP & BOTTOM OF THE CORE.	50	19.0	1	3.0	2.2	PASS
				4	8.0	—	FAILED/PUNCHED HOLE IN TOP SKIN.
S2	METAL MESH @ TOP FACE ONLY, STANDARD ISO FOAM CORE, 300gr.FIBRE GLASS @ TOP AND BOTTOM OF THE CORE.	50	18.5	1	3.0	1.7	PASS
				4	8.1	—	FAILED/CRACK @ BOTTOM.
S3	METAL MESH @ TOP & BOTTOM, STANDARD ISO FOAM CORE, 300gr.FIBRE GLASS @ TOP AND BOTTOM OF THE CORE.	50	18.1	1	3.0	1.5	PASS
				4	7.6	—	FAILED/PUNCHED HOLE IN TOP SKIN
S4	METAL MESH @ TOP + 8mm $\phi$ BAR @ BOTTOM.STANDARD ISO FOAM CORE.300 gr.FIBRE GLASS @ TOP & BOTTOM OF THE CORE.	50	17.2	1	3.0	1.54	PASS
				2	9.0	—	5 MINUTES/OK.
				5	6.7	—	FAILED/PUNCHED HOLE IN TOP SKIN.
S5	6mm $\phi$ BAR, REINFORCED @ TOP & BOTTOM. STANDARD ISO FOAM CORE. 300gr. FIBRE GLASS @ TOP & BOTTOM OF THE CORE.	50	17.2	1	3.0	1.2	PASS
				2	9.0	—	5MINUTES/OK.
				4	8.4	—	FAILED/PUNCHED HOLE IN TOP SKIN.

Table(5.8A). Results of the floor panel test.

REF.	TYPE OF PANEL	DEPTH (mm)	WEIGHT (Kg)	POSITION OF LOAD	APPLIED LOAD (KN)	DEFLECTION (mm)	PERFORMANCE & REMARKS
	SANDWICH PANEL/NO RIBS						
S6	6mm $\phi$ BAR, REINFORCED $\bullet$ BOTTOM, PHENOLIC FOAM CORE. 300gr. FIBRE GLASS $\bullet$ TOP & BOTTOM OF THE CORE.	50	17.4	1	3.0	1.50	PASS
				2	9.0	—	5 MINUTES/OK
				1	9.0	—	5 MINUTES/OK
				4	9.8	—	FAILED/PUNCHED HOLE IN TOP SKIN.
S7	SANDWICH PANEL/WITH RIBS  NO METAL REINFORCEMENT. 5 CIRCULAR RIBS, ISO FOAM CORE. 300gr. FIBRE GLASS $\bullet$ TOP & BOTTOM OF THE CORE.	50	17.2	1	3.0	1.50	PASS
				4	4.5	—	FAILED.
S8	6mm $\phi$ BAR $\bullet$ BOTTOM, ONE DIAGONAL RIB, STANDARD ISO FOAM CORE, 300gr. FIBRE GLASS $\bullet$ TOP & THE BOTTOM OF THE CORE.	50	16.1	1	3.0	1.00	PASS
				2	9.0	—	5 MINUTES/OK
				4	9.0	—	5 MINUTES/OK
				5	5.2	—	PUNCHED HOLE IN TOP SKIN.
S9	6mm $\phi$ BAR $\bullet$ BOTTOM, TWO DIAGONAL RIBS, STANDARD ISO FOAM CORE, 300gr. FIBRE GLASS $\bullet$ TOP & BOTTOM FACE OF THE CORE.	50	18.0	1	3.0	0.98	PASS
				2	9.0	—	5 MINUTES/OK
				4	9.0	—	5 MINUTES/OK
				5	6.7	—	PUNCHED HOLE IN TOP SKIN.

Table(5.8B). Results of the floor panel test.

REF.	TYPE OF PANEL	DEPTH (mm)	WEIGHT (Kg)	POSITION OF LOAD	APPLIED LOAD (KN)	DEFLECTION (mm)	PERFORMANCE & REMARKS
	SOLID PANEL/WITH RIBS						
P1	30mm PERIMETER RIBS	40	11.0	1	2.8	>2.5	FAILED/SUDDEN FAILURE ACROSS THE MIDDLE.
P2	30mm PERIMETER RIBS WITH 6mm $\phi$ BARS INSIDE.	40	12.6	1	3.2	2.64	FAILED
				4	3.1	—	FAILED/PUNCHED HOLE.
P3	DITTO P2 + TWO DIAGONAL RIBS.	40	12.8	1	3.0	1.40	PASS
				2	9.0	—	5 MINUTES/OK
				4	9.0	—	5 MINUTES/OK
				5	4.5	—	FAILED
P4	DITTO P3 + TWO CROSS RIBS.	40	14.1	1	3.0	1.00	PASS
				1	9.0	—	5 MINUTES/OK
				4	9.0	—	5 MINUTES/OK
				5	9.0	—	5 MINUTES/OK
				2	9.0	—	5 MINUTES/OK
				3	6.9	—	PUNCHED HOLE IN TOP SKIN.

Table(5.8C). Results of the floor panel test.

REF.	TYPE OF PANEL		DEPTH (mm)	WEIGHT (Kg)	POSITION OF LOAD	APPLIED LOAD (KN)	DEFLECTION (mm)	PERFORMANCE & REMARKS
	SOLID PANEL/NO RIBS							
P5	NO REINFORCEMENT		30	15.7	1 2	3.0 7.8	1.00 —	PASS FAILED @ THE CORNER
P6	6mmØ BAR @ THE BOTTOM PLUS 600gr. FIBRE GLASS @ THE BOTTOM FACE.		25	14.8	1 2 4 1	3.0 9.0 9.0 9.0	0.55 — — —	PASS 5 MINUTES/OK 5 MINUTES/OK 5 MINUTES/OK
P7	GALVANISED STEEL TRAY @ THE BOTTOM FACE.		30	19.6	1 1 2 4	3.0 9.0 9.0 18.0	1.00 — — —	PASS 5 MINUTES/OK 5 MINUTES/OK NOT FAILED--AXCESS OF LOAD IMPOSSIBLE.
P8	GALVANISED STEEL SHEET @ THE TOP & BOTTOM FACE.		30	21.6	1 1 2 4	3.0 9.0 9.0 14.0	1.00 — — —	5 MINUTES/OK 5 MINUTES/OK 5 MINUTES/OK

Table(5.8D). Results of the floor panel test.

## **f2) With no rib/galvanised steel at top and bottom**

In some panels, a satisfactory bond was obtained between the steel and the mix but it was not regular. Panels with good bonding, resisted a 9 KN point load at anywhere in the panel. The concavity problem was overcome.

A summary of all the results can be seen in tables (5.8-5.9).

## **5.6 Theoretical calculations**

The yield-line analysis (work method) was used to determine the theoretical ultimate load for slabs, as follow;

$$\text{Internal work done} = \sum M \times L \times \phi$$

Where

$M$  = plastic moment per unit width

$L$  = length of yield line

$\phi$  = relative rotation of two segments connected by yield line

$$\text{The external work done} = \int q \times dA \times \delta$$

Where

$q$  = intensity of load

$dA$  = element of area

$\delta$  = virtual displacement along line of action of load

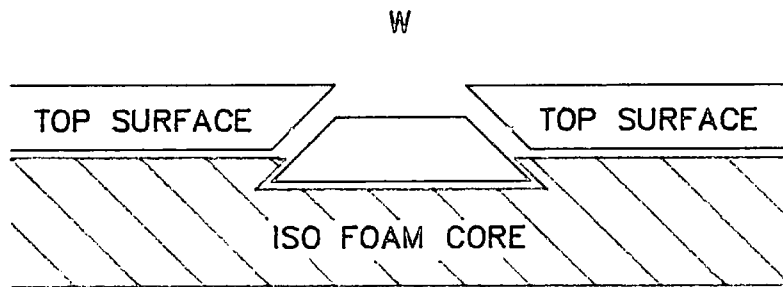
The external work done due to a point load is given by;

$$\text{external work done} = W \times \delta$$

The types of failure which were observed on all the slabs were as follows:

**a. Failure of top surface due to a punched hole**

This type of failure has been shown in Fig.(a)



Assuming the angle of failure is  $45^\circ$

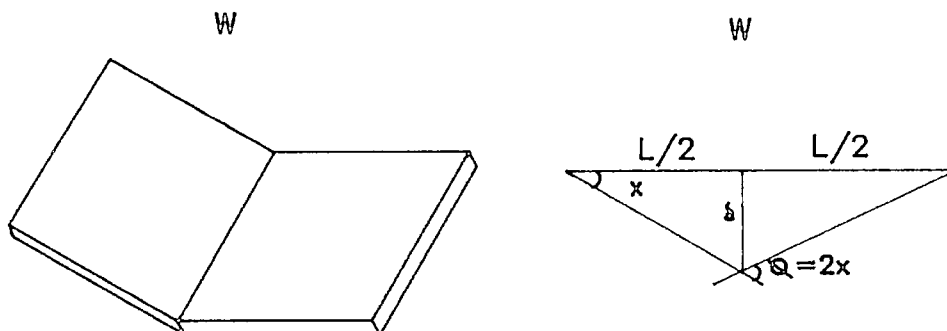
$$\text{The diagonal tension strength} = \frac{W}{A} = \frac{W}{4(25 + 53.28)/2 \times 10\sqrt{2}} = \frac{W}{2212}$$

The following slabs were failed under this action;

$$S_1, S_2, S_3, S_4, S_6, S_9, P_2, P_3, P_4$$

The results are shown in table (5.9)

**b. Failure across the middle**



$$\delta = x \times \frac{L}{2} \quad \text{then } x = \frac{2\delta}{L}$$

But  $\phi = 2x = (4\delta/L)$

$$\text{Internal work done} = \frac{4 \times M \times \delta \times L}{L} = 4M\delta$$

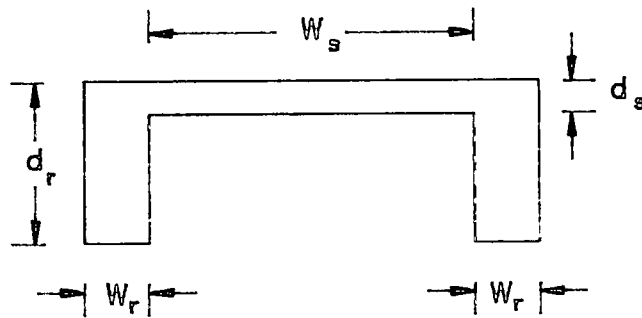
$$\text{External work done} = W \times \delta$$

Then

$$W \times \delta = 4 \times M \times \delta$$

$$W = 4 \times M$$

Slab no.  $P_1$  failed in this mode. The ultimate moment for the slab was calculated as follow;



The ultimate moment from the coupon test for the specimen of similar material with the thickness of  $7.66mm$  was found to be;

$$M_c = \frac{W}{2} \times a = \frac{315}{2} \times 113 = 17800 N.mm$$

Where  $M_c$  = ultimate moment of coupon specimen

$$M_c/\text{unit width} = \frac{17800}{100} = 178 N.mm/\text{unit width}$$

The total ultimate moment for the slab =

$$2 \times M_r \times W_r + M_s \times L_s$$

Where

$M_r$  = ultimate moment of ribs

$W_r$  = width of the ribs

$M_s$  = ultimate moment of the slab's face

$L_s$  = length of the slab's face

But

$$M_r = M_c \times \left(\frac{d_r}{d_c}\right)^2 = 178 \times \left(\frac{50}{7.66}\right)^2 = 7584 N.mm/unit \text{ width}$$

Where

$d_c$  = thickness of the coupon specimen

$d_r$  = thickness of the ribs

and

$$M_s = M_c \times \left(\frac{d_s}{d_r}\right)^2 = 178 \times \left(\frac{10}{7.66}\right)^2 = 303 N.mm/unit \text{ width}$$

Where

$d_s$  = thickness of the slab's face

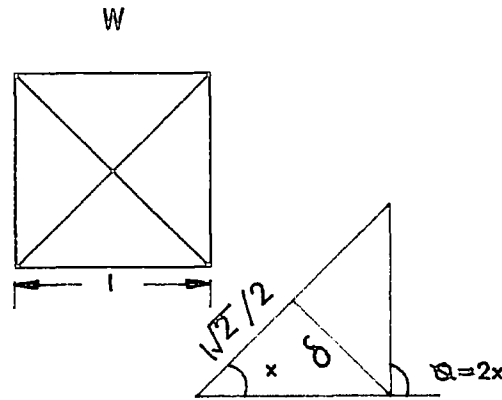
$$M_u = 2 \times 7584 \times 20 + 303 \times 560 = 4.7 \times 10^5 N.mm$$

$$M_u/unit \text{ width} = \frac{4.7 \times 10^5}{600}$$

but

$$W = 4M = \frac{4 \times 4.7 \times 10^5}{600} = 3.15 kN$$

c. Failure across the diagonal ribs



$$\delta = x \times \frac{l\sqrt{2}}{2} \quad \text{then } x = \frac{2 \times \delta}{l \times \sqrt{2}}$$

$$\text{Internal Work Done} = 2 \left( M \times l\sqrt{2} \times \frac{4\delta}{l\sqrt{2}} \right)$$

$$\text{External Work Done} = W \times \delta$$

Then

$$W \times \delta = 2 \left( M \times l\sqrt{2} \times \frac{4\delta}{l\sqrt{2}} \right)$$

So

$$W = 8M$$

Slab No:  $S_5$  failed in this mode. That was because the metal bar reinforcement around the edge prevented the slab from failing across the middle and the yield line was due to the bar reinforcement along the diagonal. Therefore the ultimate moment of the slab can be written as;

$$M_u = 2 \times A_s \times \sigma_y \times L_a$$

Where  $A_s$  = C.S.A of bar reinforcement

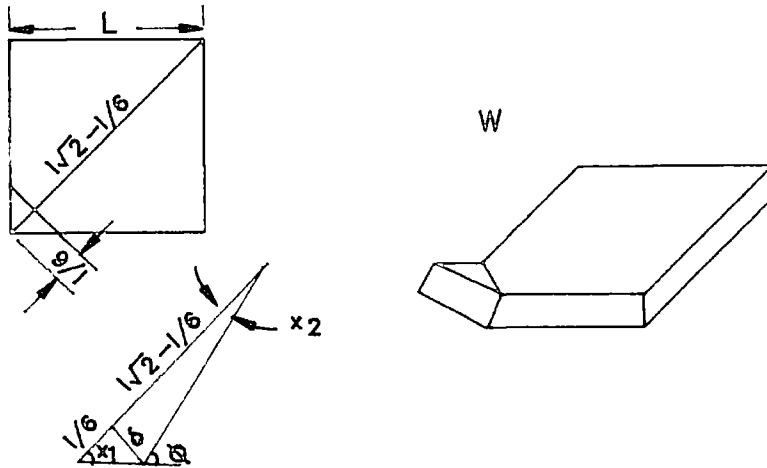
$\sigma_y$  = ultimate stress of the bar

then

$$M_u = 2 \times 28.27 \times 300 \times 45 = 763290 N.mm$$

$$W = 8M = \frac{8 \times 763290}{848.5} = 7.2 kN$$

#### d. Failure at the corner



$$\delta = x_1 \times \frac{l}{6} \quad \text{then } x_1 = \frac{6\delta}{l}$$

Also



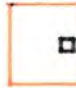





$$\delta = x_2 \left( l\sqrt{2} - \frac{l}{6} \right) \quad \text{then } x_2 = \frac{\delta}{l\sqrt{2} - \frac{l}{6}}$$

$$\phi = x_1 + x_2 = \frac{6\delta}{l} + \frac{\delta}{l\sqrt{2} - \frac{l}{6}}$$

$$\text{Length of the yield line} = \frac{l}{6} \times 2 = \frac{l}{3}$$

TEST NO:	POSITION OF THE POINT LOAD	ULTIMATE LOAD (EXPERIMENTAL) (kN)	ULTIMATE LOAD (THEORETICAL) (kN)	TENSION STRENGTH DUE TO THE PUNCH HOLE (N/mm <sup>2</sup> )	TYPE OF THE FAILURE
S1	4	8.0	—	3.6	PUNCH HOLE <input type="checkbox"/>
S2	4	8.1	—	3.7	PUNCH HOLE <input type="checkbox"/>
S3	4	7.6	—	3.4	PUNCH HOLE <input type="checkbox"/>
S4	5	6.7	—	3.0	PUNCH HOLE <input type="checkbox"/>
S5	4	8.4	7.2	—	DIAGONAL FAILURE <input checked="" type="checkbox"/>
S6	4	9.8	—	4.4	PUNCH HOLE <input type="checkbox"/>
S8	5	5.2	—	2.3	PUNCH HOLE <input type="checkbox"/>
S9	5	6.7	—	3.0	PUNCH HOLE <input type="checkbox"/>

Table(5.9A). Results of the ultimate load for the sandwich panels.

TEST NO:	POSITION OF THE POINT LOAD	ULTIMATE LOAD (EXPERIMENTAL) (kN)	ULTIMATE LOAD (THEORETICAL) (kN)	TENSION STRENGTH DUE TO THE PUNCH HOLE (N/mm <sup>2</sup> )	TYPE OF THE FAILURE
P1	1	2.8	3.1	—	ACROSS THE MIDDLE 
P2	4	3.1	—	1.4	PUNCHED HOLE 
P3	5	4.5	—	2.0	PUNCHED HOLE 
P4	3	6.9	—	3.1	PUNCHED HOLE 
P5	2	7.8	6.2	—	AT THE CORNER 
P6	—	NOT FAILED	—	—	NOT FAILED 
P7	—	NOT FAILED	—	—	NOT FAILED 
P8	—	NOT FAILED	—	—	NOT FAILED 

Table(5.9B). Results of the ultimate load for the solid panels.

$$\text{Internal Work Done} = M \times \frac{l}{3} \times \left( \frac{6\delta}{l} + \frac{\delta}{l\sqrt{2} - (l/6)} \right)$$

So

$$\text{Internal Work Done} = \frac{M}{3} \left( 6\delta + \frac{\delta}{\sqrt{2} - (1/6)} \right)$$

$$\text{External Work Done} = W \times \delta$$

Then

$$W = \frac{M}{3} \left( 6 + \frac{1}{\sqrt{2} - (1/6)} \right) = 2.27M$$

Slab no:  $p_5$  was failed in this mode. The ultimate moment for the slab was found using the coupon specimen's result.

$$M_s = M_c \left( \frac{d_s}{d_c} \right)^2 = 178 \times (30/7.66)^2 = 2730 \text{ N.mm/unit width}$$

$$W = 2.27 \times M = 2.27 \times 2730 = 6.2 \text{ kN}$$

The summary of all the calculation with the type of failure is shown in table (5.9).

## 5.7 Conclusions

Punching in the upper skin of the sandwich panel is the greatest problem to be overcome in this form of panel, when using low density foam with or without ribs or reinforcement. This problem may be overcome using a higher density reinforced foam in conjunction with heavier fibre glass reinforcement.

Since this panel technique employs a large number of manufacturing operations an alternative method of lay out will involve more costly materials, the sandwich-panel concept loses a lot of its attraction.

Furthermore, additional difficulties are envisaged on site where cutting and fitting at margins is required. Once cut the inherent structural properties of the sandwich panel will be lost. This will certainly demand **special** tiles for cutting at margins and thus extend the product range. Solid panels with ribs also have the problem of the punching in the upper skin. In general, panels requiring steel reinforcement will also create site difficulties when cutting is required. Since the filled polymer is extremely hard to cut it would be necessary to try to avoid any metal reinforcement located internally in the panel.

However, the filled metal trays acting both as moulds and reinforcement externally can be cut using existing site equipment, and they are simple and easy to cast with minimum labour. The filled metal trays showed variations of performance dependant upon the surface finish of the metal. It is essential that a good bond be achieved between the matrix and the metal.

The mould/reinforcement tray technique clearly offers a good chance of successful developement, but would require further facilities not available to the present investigation, ie;

1. trays of different gauges of thickness, and of different depths.
2. trays with different bonding surface finishes.
3. trays with pressed-in profile of ribs.

However, the present investigation gives a good base of knowledge, from which it may be seen in which direction the developement may proceed.

# CHAPTER (6)

## **CHAPTER SIX**

### **6. Sandwich panels**

#### **6.1 Introduction**

The polymer concrete sandwich wall panels discussed in this chapter are the structural elements of fundamental importance in the pre-fabricated building system. The panels have a rigid isocyanurate foam core, encapsulated in an 8mm thick outer skin consisting of glass fibre mat, and a mixture of polyester resin and mineral aggregate.

This forms a relatively light weight panel, with the edges profiled to form interlocking vertical joints. The range of panels includes corner, door and window panels, lintols, undercills and finally plain wall panels. A range of surface finishes may be applied to the panels either during or after manufacture to suit either internal or external applications.

#### **6.2 Schedule of the panels**

A programme of testing and analysis has been undertaken which has looked at the strength characteristics of three related types of panel:

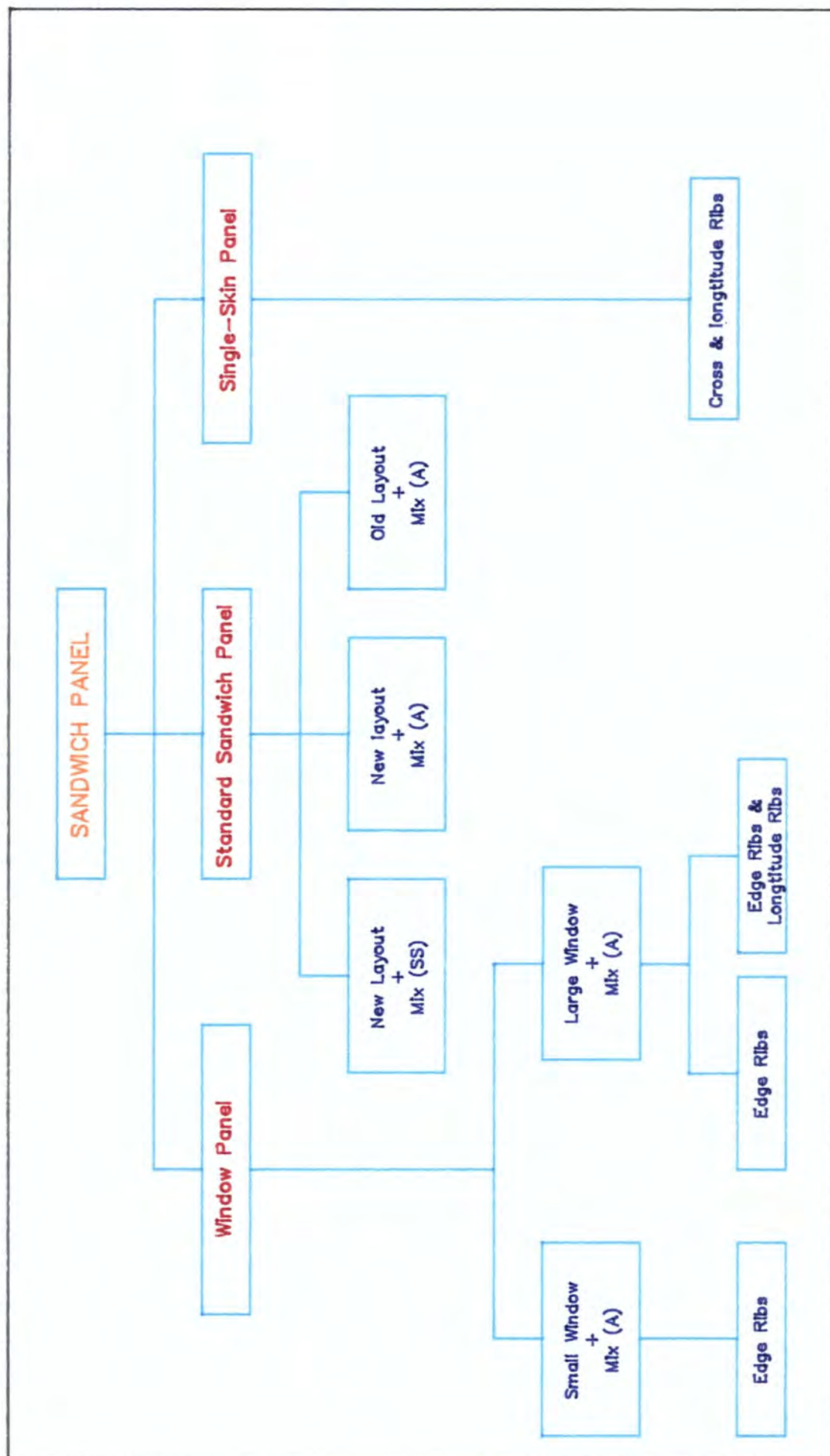


Fig.(6.1). Schedule Of The Panels According To The Type Of The Panels.

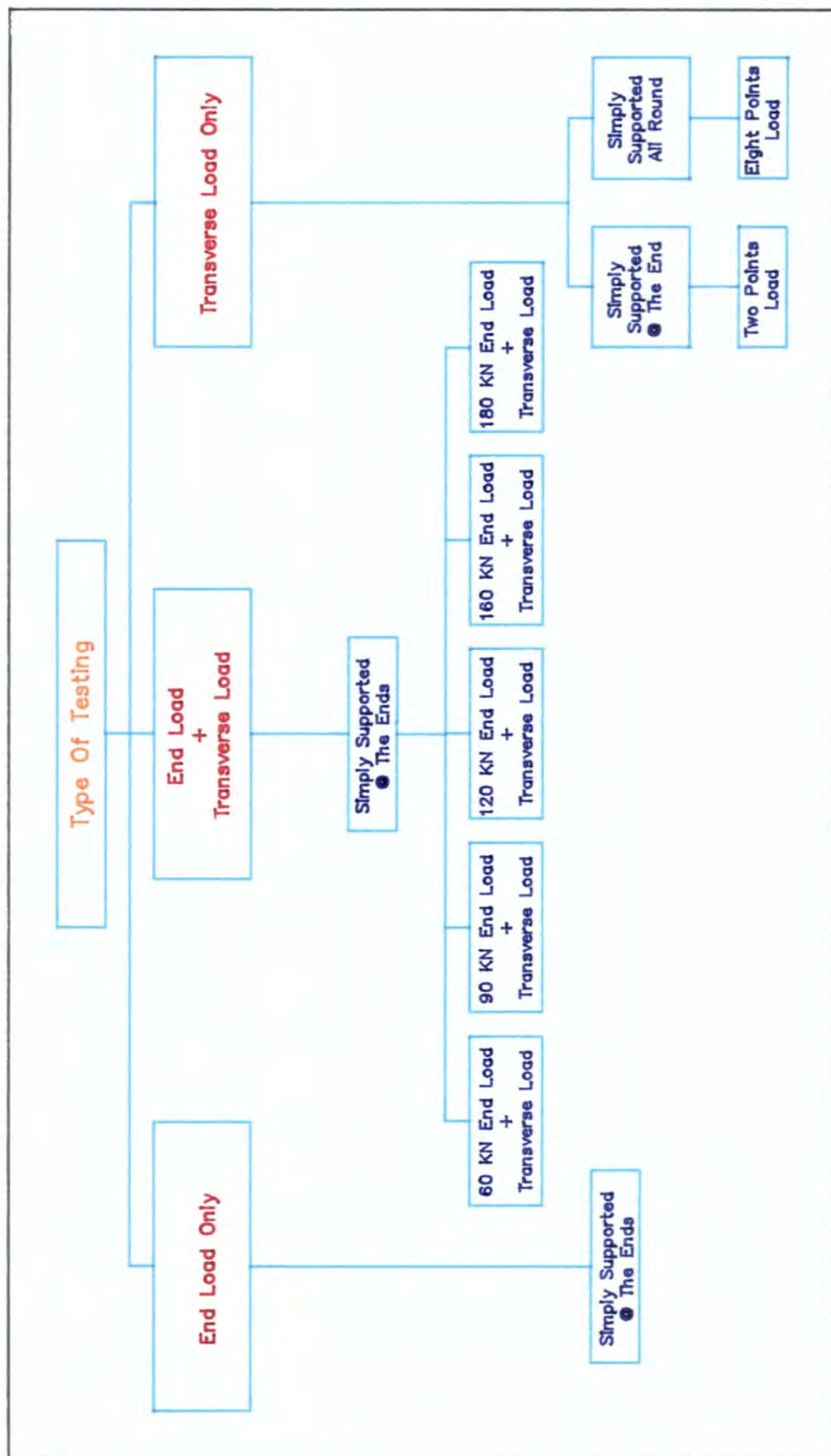


Fig.(6.2). Schedule Of The Panel According To The Type Of Testing.

### **6.2.1 The standard sandwich panel**

1. A set of panels were constructed in the original manner ie; with two longitudinal ribs as well as the edge ribs, and glass reinforcement at the middle of each face. Using mix (A) with resin 401, aggregate resin ratio of 4:1.
2. A set of panels were made using a new technique, ie; with no longitudinal ribs, only edge ribs, and with the glass reinforcement laid on the top and bottom surfaces of the foam, using the same mix as above.
3. A set of panels were cast using a new technique with the mix SS and resin L.V.M in a ratio of 10:1.

### **6.2.2 Window panels**

1. Large window. Two types of the panel have been investigated, one set with edge ribs only and the other set with one extra longitudinal rib in the middle. In both types mix (A) has been used.
2. Small window; panels with no ribs, using mix (A) have been constructed and investigated.

### **6.2.3 Single-skin panels**

In this type of the panel longitudinal and cross ribs have been constructed with a single skin using mix (A).

## **6.3 Manufacturing procedures**

### **6.3.1 Moulds and dimensions**

All the plain sandwich wall panels were cast in wooden moulds with the overall dimension of 2800mm in height and 1200mm in width and 90mm thickness. The base of the mould was supported on four wooden legs. Along the edges of the base, the edge moulds were fixed to the base by means of several butterfly screws. These defined the thickness of the panel and at the same time provided the tongue or groove along the side of the panel which provide the interlocking on the construction site.

In the case of the window panels, a wooden box with a thickness of 90mm and with the dimensions of 900mm wide by 1200mm height for the large window and 600mm wide by 900mm height for the small window was fixed in an appropriate place on the panel base to provide a rectangular void in the panel to receive the window frame. The details of the dimensions of the panels together with details of the joining are shown in fig.(6.4) and (6.3) respectively.

### **6.3.2 The casting process**

After assembling the mould, it was waxed thoroughly to ensure easy release of the panel after curing. A foam block and two sheets of glass woven roving were cut to size to give 20mm clearance from all sides of the mould. The mix was cast in a continuous pour, starting at one end and working along the panel. The continuous bottom skin was formed by screeding the mix with a board which had been recessed

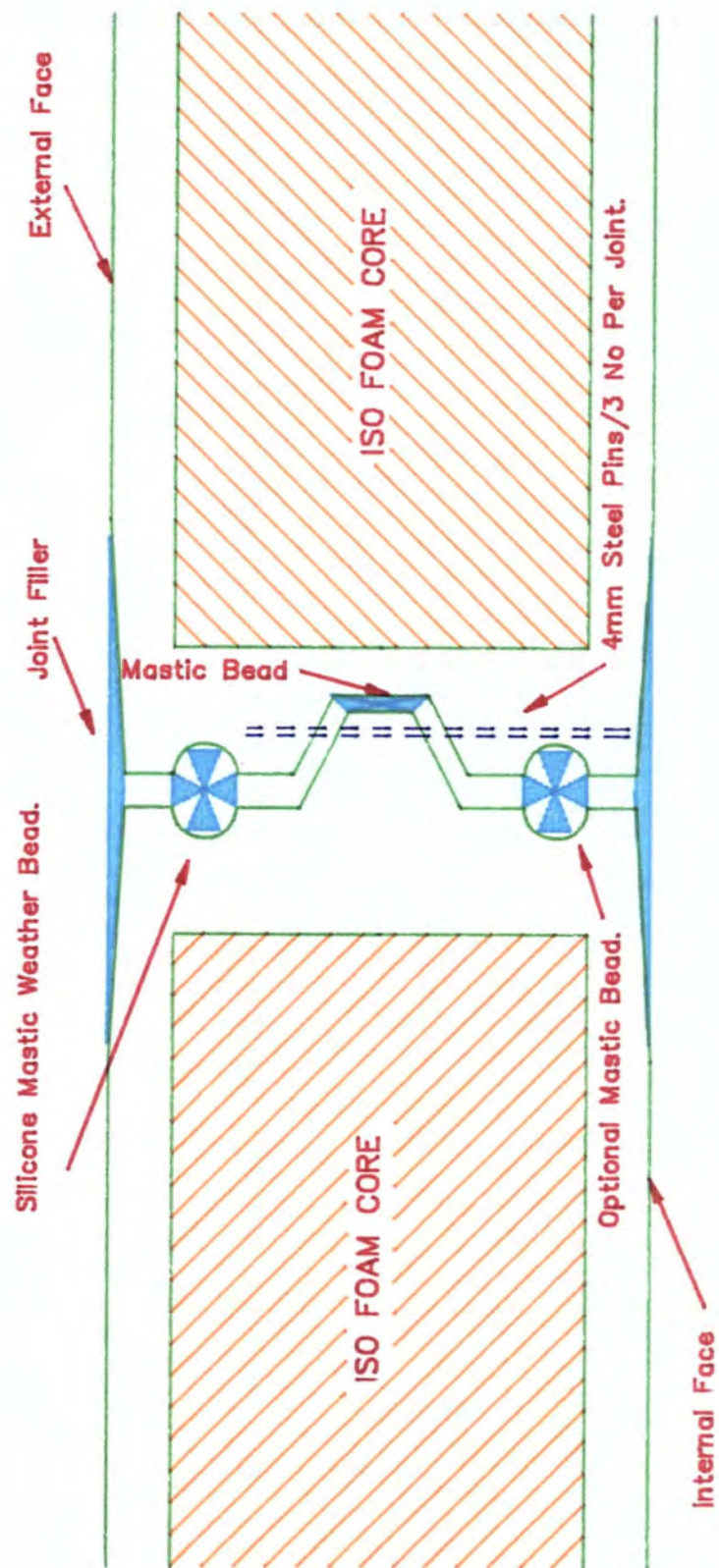
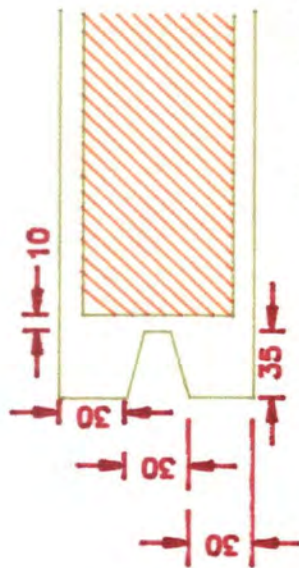
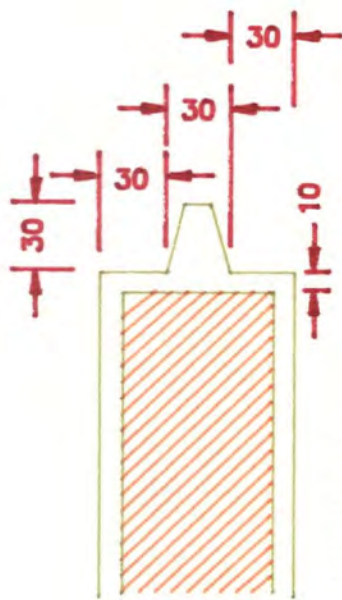
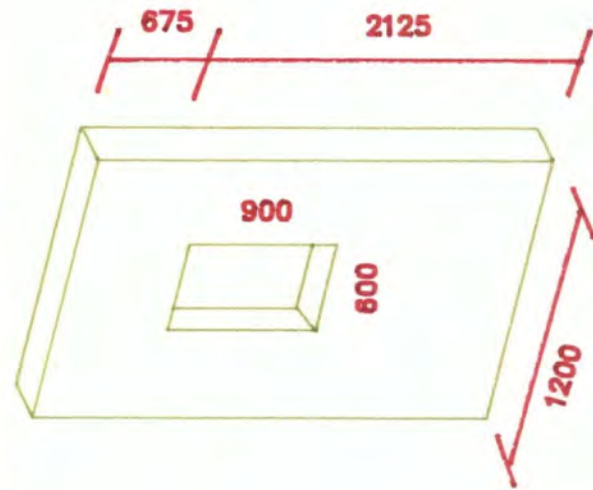


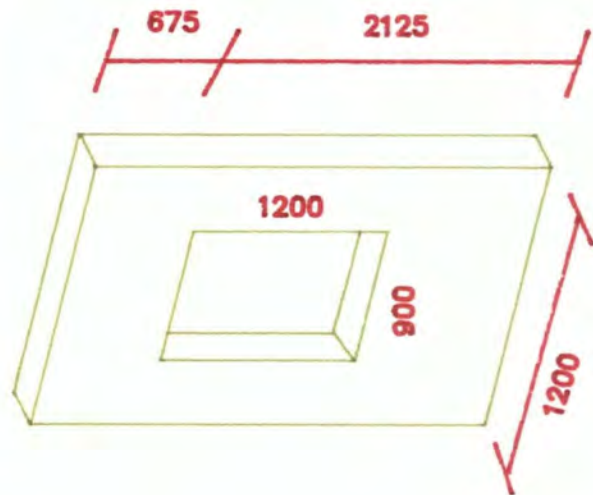
Fig.(6.3). Details Of The Standard Panel Junction.



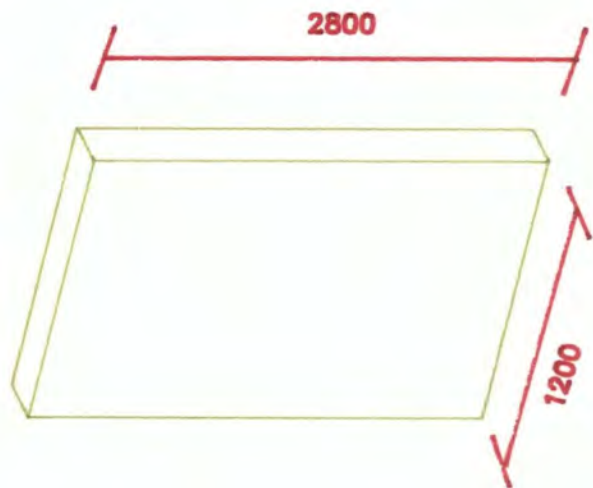
Details of the tongue & groove of the panels.



Small window panel



Large window panel



Standard panel

Fig.(6.4). Details of the dimensions of the panels.

to give 8mm clearance from the base of the panel when the ends of the screed board were in position on top of the mould edges. After vibrating the bottom skin with (k20) vibrators, the first continuous sheet of glass reinforcement was placed over the bottom skin and the trapped air was removed with the aid of a roller. The foam block was laid out in the mould so as to give 20mm clearance from all sides. The edge ribs were filled with the mix using a pallet knife and vibrator to ensure full compaction. The rib along the bottom edge of the wall panel was formed to provide a rebate of size 60mm high by 50mm deep. The mix laminate along one of the vertical edges of the wall panel was formed to provide a groove of size 30mm wide by 35mm deep, and the mix laminate along the opposite vertical edge was formed to provide a tapered tongue of overall size 30mm long by 30mm wide.

The top surface of the foam was wetted by use of a brush dipped in a bucket of resin and catalyst. The second layer of glass reinforcement was laid on the top surface of the foam using a roller, and, finally, the top skin of the panel was cast in a similar manner to the bottom skin except the mix was screeded over the foam with a flat board to give a smooth surface finish. The vibrator was used at all stages. In the original set of panels, the glass woven roving was laid in the middle of each skin and vertical stiffening ribs composed of similar material to the panel faces and of 20mm thickness were contained within the core of the wall panel at 375mm nominal centres.

Similar techniques were used as before to construct two trial single skin panels. Fig.(6.4B) shows the profile of one of the panels which were identical as far as

possible. Foam blocks were cut to size and laid out in the mould in the correct positions. The first sheets of glass woven roving were laid over the foam blocks from side to side, leaving gaps for the transverse ribs. Spacer boards of timber were lowered into the voids, and the foam blocks were held firmly in the correct positions. This helped to hold them down on to the base of the mould as well as in the correct position in plan. The ribs (30mm thick) and the top skin (12mm thick) were cast as previously described, and, finally, the second layer of the glass reinforcement was placed over the top of the skin. The rigid foam was used only as a means of moulding the ribs or fins onto the single skin. The foam had no effect on the panel strength, and it should not be assumed that any production model would have foam included in its construction, since the ribs could be moulded in rigid formwork in this case. Mix A with resin 401 in the ratio of (4:1) aggregate to resin, and mix SS with L.V.M resin with an aggregate to resin ratio of (10:1), were used to construct the panels. The cores of all the panels consisted of a polyisocyanurate foamed material *Nicflam* of 75mm thickness, as supplied by Coolag Limited.

### 6.3.3 Curing

All the specimens were made at a temperature of 20°C, and were left to cure over night. The following day they were stripped from the mould and stored on battens for more than 7 days at the same temperature before testing.

## **6.4 Testing**

A series of 39 slabs were tested altogether. They were classified according to the type of testing in the following groups:

### **a) With transverse load only**

1. simply supported at two ends (two point load)
2. simply supported all round (eight point load)

### **b) With end load only (simply supported two point load)**

### **c) With end-load as well as transverse loads (two point loads)**

1. 60. kN end load + transverse load
2. 90. kN end load + transverse load
3. 120 kN end load + transverse load
4. 160 kN end load + transverse load
5. 180 kN end load + transverse load

A summary of the schedule of the panels according to the type of panel and the type of test have been illustrated in fig. (6.1) and diagram (6.2)

## **6.5 Instrumentation and testing procedure**

### **6.5.1 Loading rig**

#### **1. The specification.**

There was a need for a testing frame which would be flexible enough in its range of utility to be able to test all the components within the field of enquiry,

but stiff enough to do so over the whole range of load and constraint to which they could be tested. The loading and constraint capability both had to be unusually variable. Loading could be either transverse or axial on both beams and slabs or shells. Constraint could either be such as to promote the mechanics of a single direction of span, as for a beam or a slab spanning in only one direction, or it could be multi-directional, as for a slab or shell supported all round its perimeter.

## **2. The frame design.**

The geometry of the main frame is shown in (fig. 1 appendix 7), which is an assembly drawing of the whole structure. The two longitudinal members of the frame are 4.5 m lengths of 300 x 150 mm hot-formed hollow rectangular section. Each of these is mounted on a pair of transverse plinths fitted with two heavy duty castors, so that each member can be moved about the laboratory floor independently. These two members can be stored side by side, and can be used separately or bolted directly together side by side to form the base of a beam testing rig.

In its normal, slab-testing configuration, the longitudinal members are separated by two cross-members, one near each end, attached to the longitudinal members by web cleats which are welded to the cross members and bolted on to the long members. The length of these cross members determines the width of the frame. Two pairs were obtained. The shorter pair provide the configuration for testing the standard wall panels with support on all four edges; the longer pair are for testing the wall panels simply supported along their ends. There are several sets of bolt-holes along the length of the long members, so that the cross members may

accommodate test specimens of different length.

Two heavy brackets, cut diagonally from the same 300 x 150 mm section, are bolted to the centre of each long member, on the outside of the frame. Into these are fixed the bottom ends of pairs of 30 mm steel rods, threaded at each end; the top ends of the rods pass through the ends of the upper cross beam on which is mounted the hydraulic jack used to apply the transverse load. The loading beam is another length of 300 x 150 mm hollow rectangle. The height of this above the top of the main frame is determined precisely by the pairs of steel tubes through which the tie-rods pass. The bottom ends of the tubes rest on the top surface of the brackets, while the cross-beam rests on their upper ends. The bolts on each end of the tie rods are tightened, so that the tubes and rods carry a small prestress which gives greater stability to the superstructure when it is not applying any load.

In order to apply end-load to the sandwich panel wall slabs, the cross beams were mounted on the outer-most connection points on the long members. The end-load hydraulic jack was attached to the inner side of one of them, and the reaction block was attached to the other. The specimens were supported, in this configuration, on rollers mounted in cleats bolted on to the inside of the long members at such a height that the end load was axial to the panel. The height of the panel could be adjusted by shims under the roller ends, or by shim plates between the panels and the rollers. Additional rollers were placed on the panels immediately above the lower, supporting rollers to constrain the panels against upward movement when they failed; these were held in place by additional cleats on the tops

of the roller guides. The end-load was transmitted to the panel ends by stiff hollow square steel beams to which were attached the wooden mouldings fitted into the channels moulded into the ends of the panels. These fittings are illustrated in figs.(2-5 appendix 7).

The frame and jacks were able to test the panels to destruction over the required range of support conditions and loads, the specimens being manouvered into place and subsequently removed with the aid of a small fork-lift, and a pair of additional hydraulic jacks for lifting the panels more precisely into position.

### **6.5.2 Method of testing**

A series of tests has been carried out in order to determine the deflection of the panels in service, the mode of failure, and stresses occurring at failure under the range of load conditions likely to be met in service. In general three types of testing were applied to all the panels and they were as follows:

#### **a) Transverse load only**

##### **i. Simply supported at two ends (two point loading)**

In this group of tests, panels were simply supported at their ends, rested on top of the main frame members, and were subjected to transverse load from the jack mounted in the cross beam over the rig. The load was distributed uniformly at the quarter points of span. The deflection was measured with the aid of 3 dial gauges of mm divisions (see fig.6.5), to determine the curvature, as well as the deflection of the centre section. Also, four strain gauges were fixed within the centre section

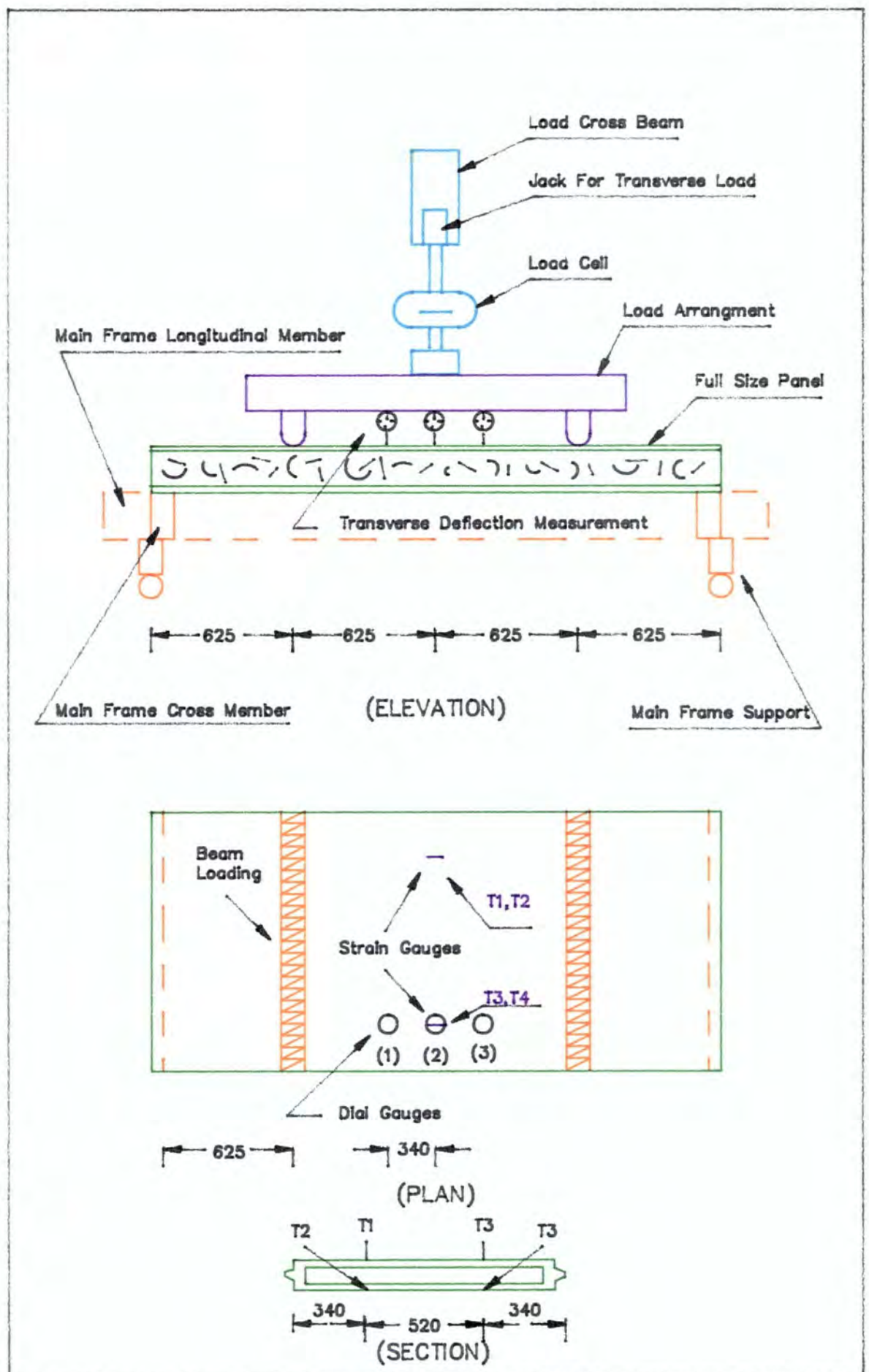


Fig.(6.5). Test Arrangement (Transverse Loading—Two Points Loading).

of the panel on both sides to measure the strain in compression and tension under load.

A load cell, of capacity ten thousand pounds (45KN), of which the calibration was confirmed from time to time, was used to control and measure the applied load precisely. The initial readings from the strain gauges and the dial gauges were taken before the load application. The load was applied slowly in increments of 200lb, but was kept constant for about 30 seconds until the reading of the dial gauges became constant. Then their values, together with strain gauge readings, were recorded. The panels were carefully watched when nearing the ultimate load. The load continued to increase slowly until the panel failed. The failure load and type of failure were recorded.

## **ii. Simply supported on four sides (uniform loading).**

Two panels with internal ribs were tested in this exercise, being supported on their four sides, with the load arranged to approximate to a uniformly distributed load, using a lever and roller system. Nine dial gauges together with ten strain gauges were used to determine the deflection and strain at different positions on the panel, under the various loads. Fig.(6.6) shows the position of the dial gauges and strain gauges. The first panel was loaded up to 2500lb, in increments of 200lb, and readings were taken at each load increment. This load was maintained on the panel for 24hrs, and during this time, the panel was watched carefully, and change in deflection was recorded. The load was then removed in increments of 200lb, and again the readings were taken. The panel was loaded once more in the same manner

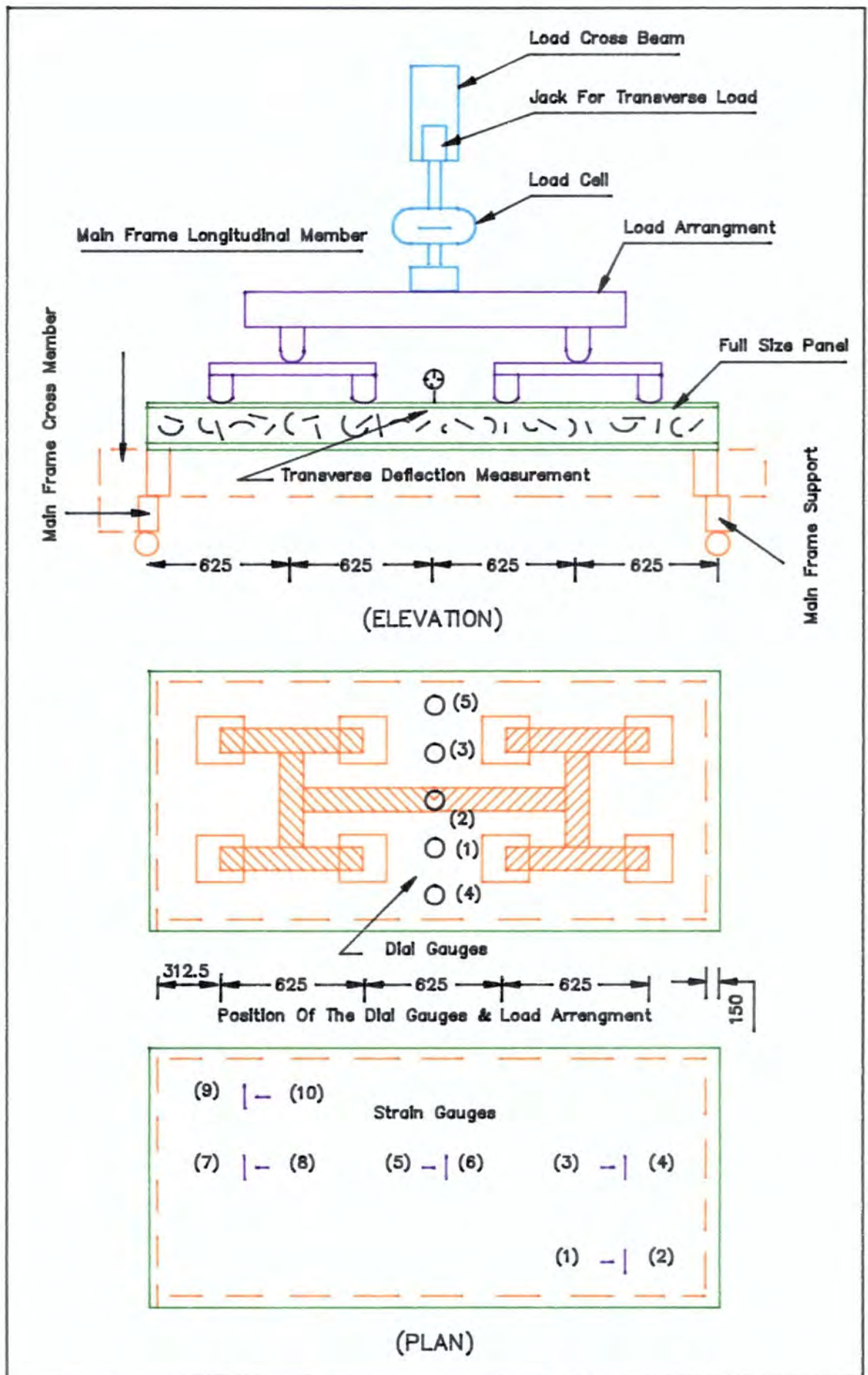


Fig.(6.6).Test Arrangement.(Transverse Loading—  
All Sides Supported)

up to 5000lb (max load) and stayed under this load for 48hrs, and readings were taken during this period. The second panel also was loaded up to 10000lb, and stayed under this load for 48hrs. There was no sign of failure in any of the panels.

**b) End load only (two point load)**

In this group of tests, the panels were supported on rollers mounted within the rig in such a way that an end-load was applied by a second hydraulic jack of maximum capacity 50 tonnes acting on one of the main-frame cross-members, while the other end was restrained by the other cross-member. The load magnitude was read from the hydraulic gauge of the jack, which was calibrated at intervals not exceeding one month on the Dennison Testing Machine. The end load was distributed to the specimen by means of a heavy flanged plate bearing on to the hollow rectangular steel edge beams, which in turn rested on the timber fillets engaged with the notches on each end of the specimen.

A pair of dial gauges was registered on to the upper surface of the specimen about 100mm from each side, on the lateral centre-line of the panel, so that they detected transverse displacement of the slab in either direction.

**c) Transverse load together with end load (two point load)**

The transverse load (two point load) and end load were applied to the panels in the manner described in preceeding sections, *proving loads* were applied to all the panels (see chapter 9) in this set with the following loading cycles:

The load magnitudes were chosen to relate to the design loads of the wall panel under the various conditions encountered in service.

The maximum axial load per panel in single storey construction is about 8.7kN (see chapter 9). This was rounded up to 10kN for stage (1). The load encountered by the wall panel in the lower storey of a two storey house is about 20kN, as stage (2). Stage three, therefore, represented the maximum service load times a load factor of 2. The maximum predicted wind load on a wall panel is about 3.75kN (see chapter 9) this was rounded up to 4kN for stage (4). Stage 5, again, represented maximum transverse load times a load factor of 2. Through each stage of the test deflection gauge readings were recorded at the centre section. The deflection readings during stages (1) to (3) were used to check on the concentricity of the load. If significant readings were obtained during these stages the test was interrupted while the slab was adjusted up or down to ensure reasonable concentricity of load. This could be achieved without harm to the specimen since it was clear that the early stages of the test were achieving no more than the bedding in of the end rails. The adjustment of the slab level was achieved satisfactorily by the use of shims on the support rollers. At the end of the load cycle the loads were removed slowly, while the deflection gauge readings were watched, and any residual deflection recorded.

After removing the *proof loading* all the panels in this set were subjected to the following loading.

1. 60. kN end load + transverse load up to the failure
2. 90. kN end load + transverse load up to the failure
3. 120 kN end load + transverse load up to the failure
4. 160 kN end load + transverse load up to the failure

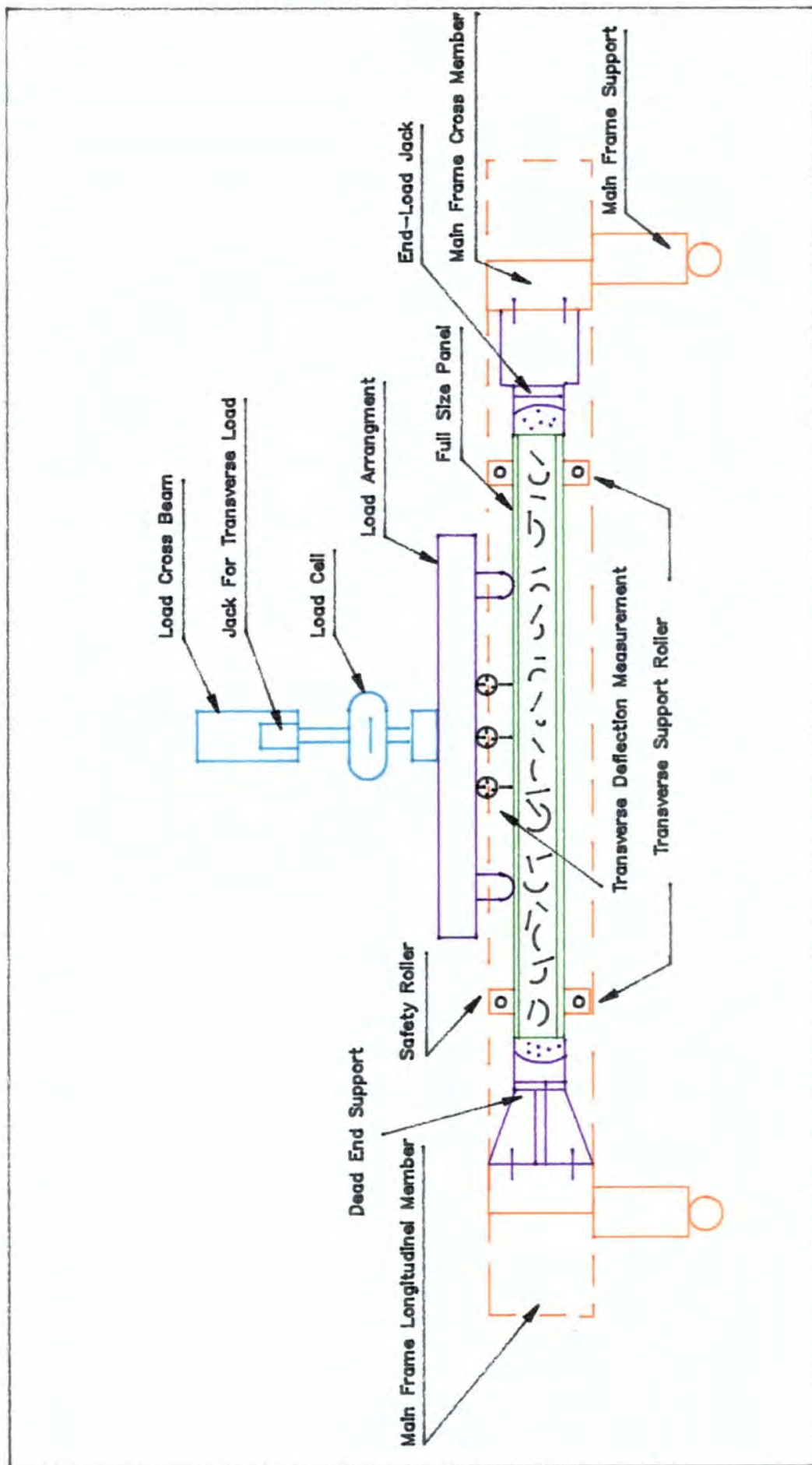


Fig.(6.7).General Arrangement Of The Test Rig For The Panels In End-  
Load & Transverse Load. ( Supported @ Ends. )

#### 5. 180 KN end load + transverse load up to the failure

The transverse load was delivered to the slab through a system of beams which applied two line loads at the quarter points of the span, so that the maximum bending moment had the same magnitude as would be caused by a uniformly distributed load of the same value as the load applied by the jack, and the movement was constant over the centre section of the specimen.

The ultimate transverse load and type of the failure were recorded for all the panels.

### 6.6 Results and calculations

#### a) Bending of sandwich panel (transverse load)

##### i. Simply supported at two ends

A series of twelve panels were tested altogether in this exercise. After the total failure, the dimensions of all the panels were measured carefully with a micrometer, to check the face thicknesses. A computer programme was written to calculate the  $I$  value and position of the neutral axis for all the panels. The dial gauge and strain gauge readings were plotted against the transverse load and the slopes of the graphs were determined.

Using these values, together with the ultimate load and  $I$  value of the panels, the modulus of elasticity and ultimate stress were calculated. A typical calculation for one of the panels is shown below. Also the representative load/deflection and

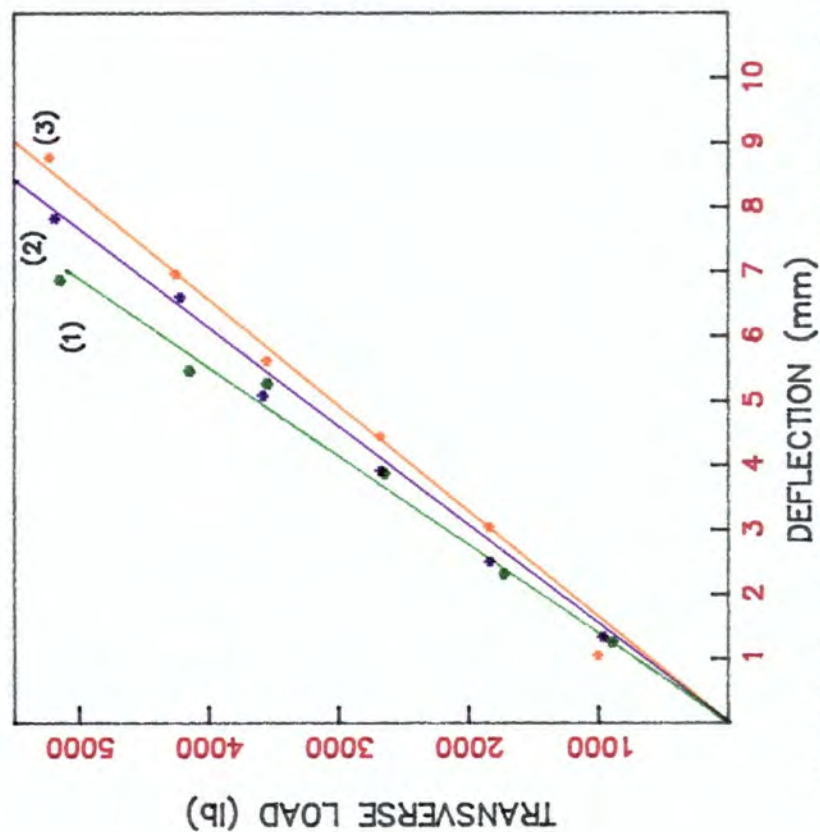


Fig.(6.8). Deflection of the panel under the transverse load @ position 1,2 & 3.

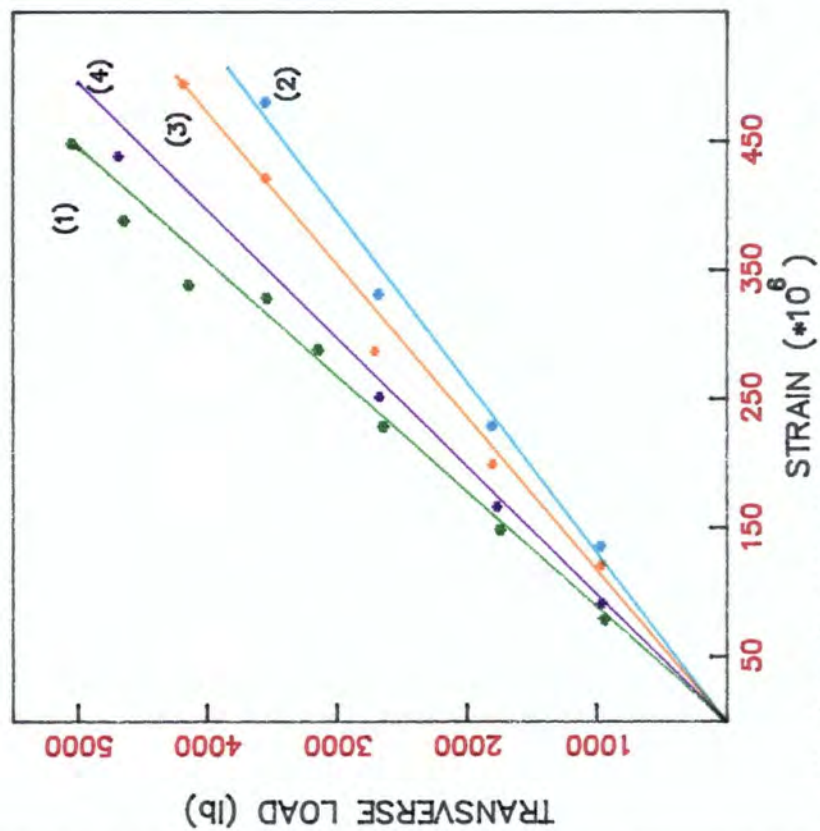
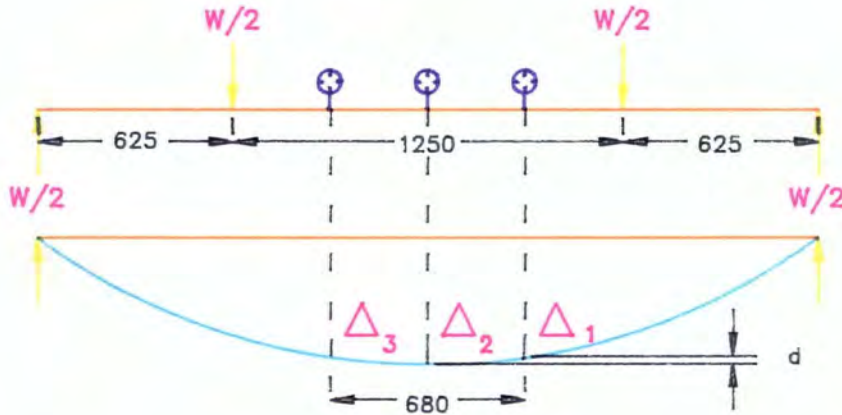


Fig.(6.9). Strain @ the central cross section under the transverse load.

load/strain graphs are shown in fig.(6.8) and (6.9) respectively.



$$I = 33.9 \times 10^6 \text{ mm}^4$$

moment per unit load is equal to

$$\frac{W \times a}{2} = \frac{625}{2} = 312.5 \text{ lb.mm}$$

$$\frac{M}{I} = \frac{\sigma}{\hat{y}}$$

$$\sigma = \frac{M \times \hat{y}}{I}$$

Then stress per unit load is equal to;

$$\frac{312.5 \times 45}{33.9 \times 10^6} = 4.15 \times 10^{-4} \text{ lb/mm}^2$$

From the graph (strain / load)

$$\text{Strain per Unit load} = 0.11 \times 10^{-6} / \text{lb}$$

$$E = \frac{\sigma}{\epsilon} = \frac{4.15 \times 10^{-4}}{0.11 \times 10^{-6}} = 3771 \text{ lb/mm}^2 = 16.4 \times 10^9 \text{ N/m}^2$$

Since load at failure = 6000lb

Then:

$$\text{The ultimate stress} = 4.15 \times 10^{-4} \times 6000 = 2.49 \text{ lb/mm}^2 = 10.9 \text{ N/m}^2$$

The  $E$  value also has been calculated using the deflection reading as follow;

$$R = \frac{c^2}{2d}$$

Where

$$d = \Delta_2 - \frac{\Delta_3 + \Delta_1}{2}$$

and  $c = 340 \text{ mm}$

From the graph (load / deflection);

$$\Delta_2 = 1.66 \times 10^{-3} \text{ mm/lb}$$

$$\Delta_3 = 1.57 \times 10^{-3} \text{ mm/lb}$$

$$\Delta_1 = 1.34 \times 10^{-3} \text{ mm/lb}$$

$$d/\text{unit load} = 1.66 \times 10^{-3} - (1.57 \times 10^{-3} + 1.34 \times 10^{-3})/2 = 2.05 \times 10^{-4} \text{ mm/lb}$$

Then

$$R = \frac{340^2}{2 \times 2.05 \times 10^{-4}} = 2.82 \times 10^8 \text{ mm/lb}$$

But

$$\frac{M}{I} = \frac{E}{R}$$

or

$$E = \frac{R \times M}{I}$$

TEST NO:	MIX	INTERNAL RIBS	LOAD AT FAILURE (lb)	$(mm)^4 \times 10^{-6}$	DEFLECTION @ CENTRE (mm/lb) $\times 10^3$	strain per unit load at centre (1/lb) $\times 10^6$	EXPERIMENTAL "E" VALUE, USING THE STRAIN GAUGES $(N/mm^2) \times 10^{-9}$	EXPERIMENTAL "E" VALUE, USING THE DIAL GAUGES $(N/mm^2) \times 10^{-9}$	ULTIMATE STRESS $(N/mm^2)$	TYPE OF THE FAILURE
1	A	YES	6000	33.9	1.66	0.11	18.4	11.3	10.9	TENSION FAILURE ON THE BOTTOM FACE
2	A	YES	6400	38.3	2.31	0.11	14.9	13.6	10.5	"
3	A	YES	5000	37.5	2.28	0.10	16.3	13.3	8.40	"
4	A	YES	4000	39.5	2.32	0.12	12.9	12.1	6.40	"
5	A	YES	5500	37.2	2.10	—	—	12.6	9.20	"
6	A	YES	4500	41.4	2.02	—	—	10.9	7.00	"
7	A	NO	4000	33.3	3.08	—	—	10.2	7.50	"
8	A	NO	3000	33.8	3.16	—	—	9.8	5.60	"
9	A	NO	3000	33.8	2.73	0.12	15.1	15.2	5.60	"
10	A	NO	2500	31.6	3.40	0.18	10.8	9.30	4.90	"
11	SS	NO	2750	33.6	1.31	—	—	22.4	5.00	"
12	SS	NO	2500	29.3	1.74	—	—	19.1	5.20	"

Table(6.10). Results of the panels under the transverse load.(simply supported @ the ends)

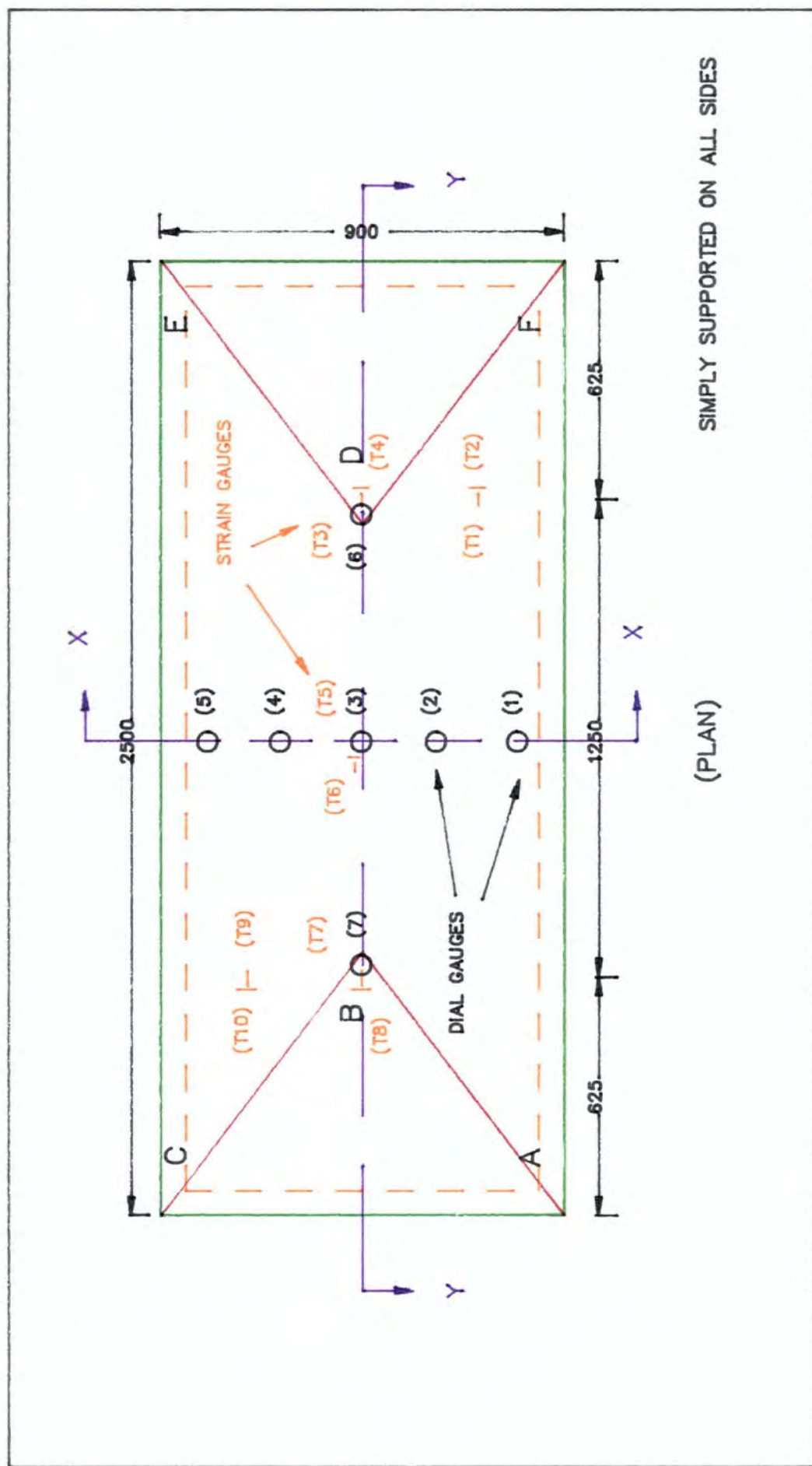


Fig.(6.11). Position of the dial gauges & strain gauges on the panel.

therefore

$$E = \frac{2.82 \times 10^8 \times 313.5}{33.9 \times 10^6}$$

$$E = 260 \text{ lb/mm}^2$$

or

$$E = 11.3 \times 10^9 \text{ N/m}^2$$

Table (6.10) shows the summary of all the deduced properties together with the specification of the panels.

## **ii. Simply supported on four sides**

The arrangement of the dial gauges and strain gauges on the panel are shown in fig.(6.11)

The dial gauges and strain gauge readings were plotted against the applied load and the slopes of the graphs were determined. Typical graphs for the deflection and strain gauge readings are shown in fig.(6.12) and fig.(6.13) respectively. A summary of all the slopes of the graphs is tabulated in table (6.14).

The deflection profiles of the panel at the XX and Y-Y sections under the various loads for one of the tests are shown in fig.(6.15) and fig.(6.16) respectively. To determine how the load is spread between the X-X and Y-Y direction, the following calculation has been made:

The max deflection is at the centre of the panel where;

$$y = b/2, \quad x = L/2$$

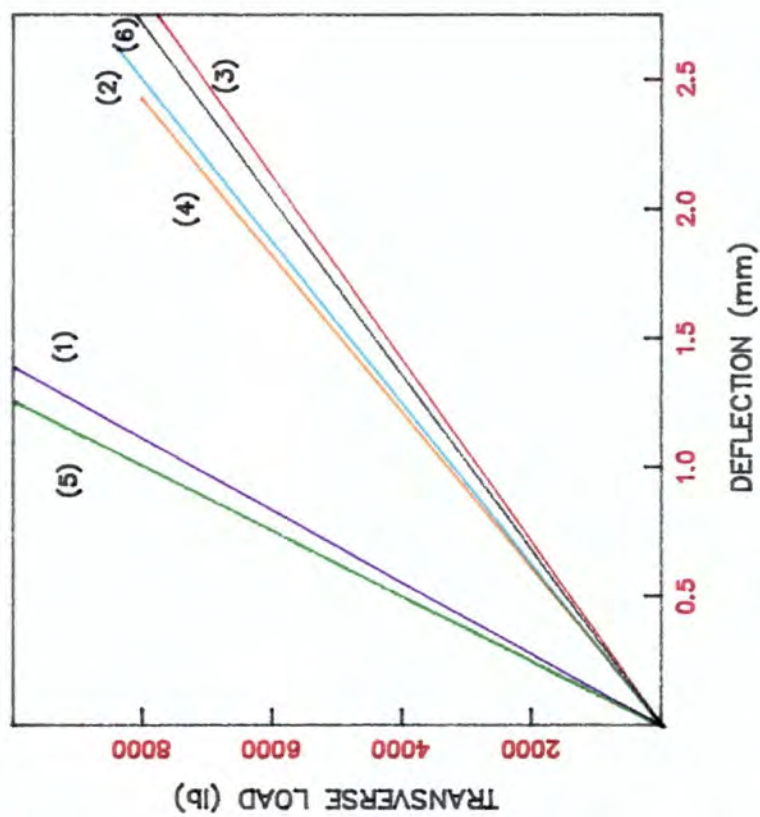


Fig.(6.12). Variation of the deflection for different position on the panel under the transverse load.

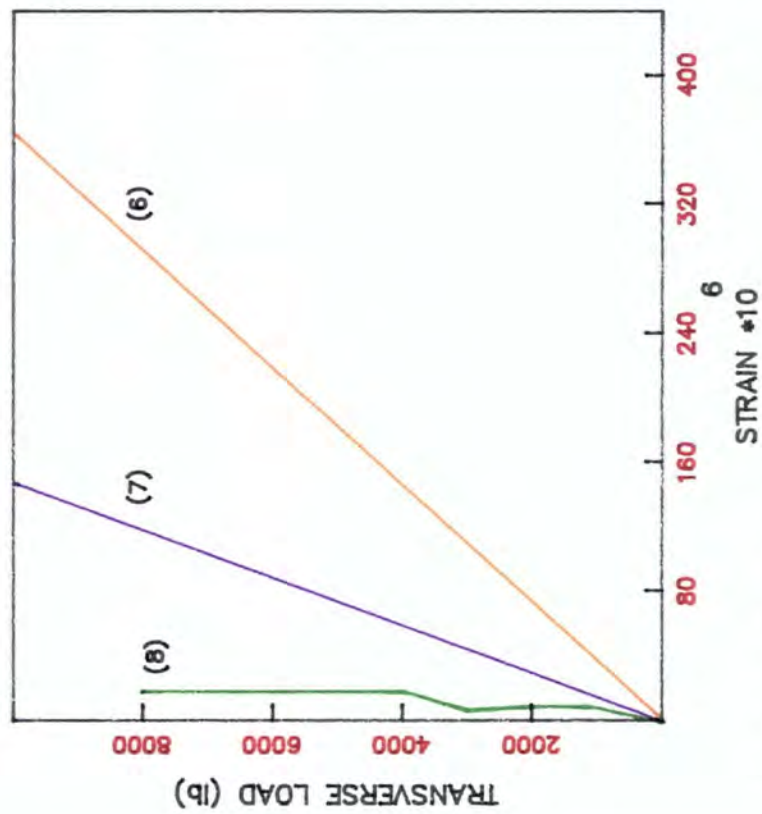


Fig.(6.13). Variation of the strain for different position on the panel under the transverse load.

test no:	SLOPE OF THE GRAPH (LOAD/DEFLECTION) lb/mm						SLOPE OF THE GRAPH (LOAD/STRAIN) lb/strain $\times 10^6$									
	POSITION OF THE DIAL GAUGE						POSITION OF THE STRAIN GAUGE									
	(1)	(2)	(3)	(4)	(5)	(6)	(1)	(2)	(3)	(4)	(5)	(6)	(7)	(8)	(9)	(10)
1	6667	3333	3125	3375	7143	3225	—	48	50	—	—	25	60	—	—	54
2	5980	3421	3015	3510	6565	3106	—	46	50	—	—	21	50	—	—	52

NOTE: SLOPE OF THE GRAPHS FOR THE STRAIN GAUGES OF WHICH ARE NOT SHOWN, ARE NEGLIGABLE.

Table(6.14). Results of the panel, under the transverse load, supported on all the sides.

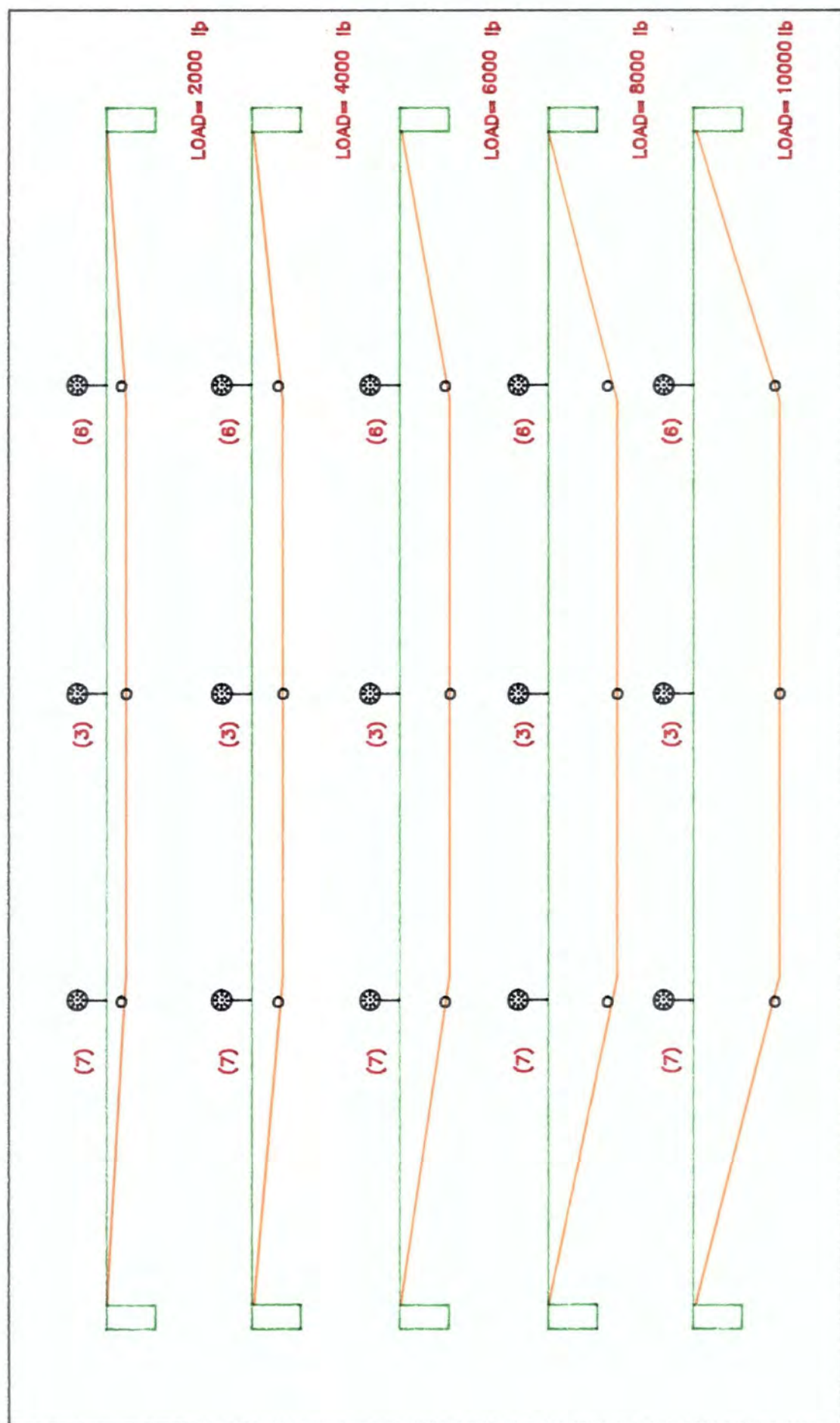


Fig.(6.15). Profile of the panel @ X-X section, showing the deflection under the various loads.

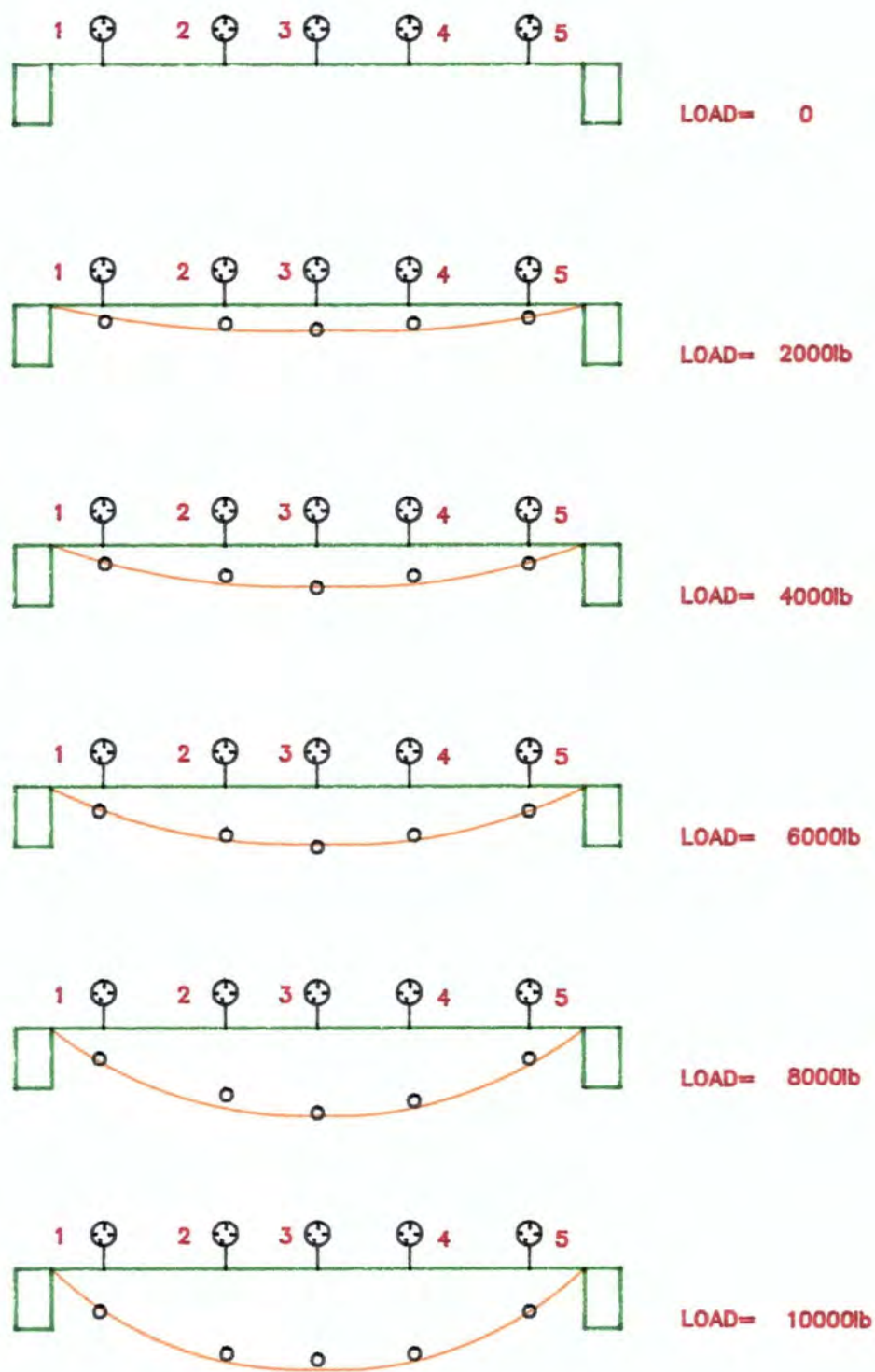


Fig.(6.16). Profile of the panel @ Y-Y section, showing the deflection under the various loads

and is given by the general form of

$$\Delta_{max} = \alpha \left( \frac{qb^4}{EI} \right)_y = \alpha \left( \frac{qL^4}{EI} \right)_x \quad (1)$$

Where

$\alpha$  = constant coefficient

$q$  = uniformly applied load ( $N/mm^2$ )

$L$  = length of the panel

$I$  = the second moment of area per unit length  $mm^4/m$

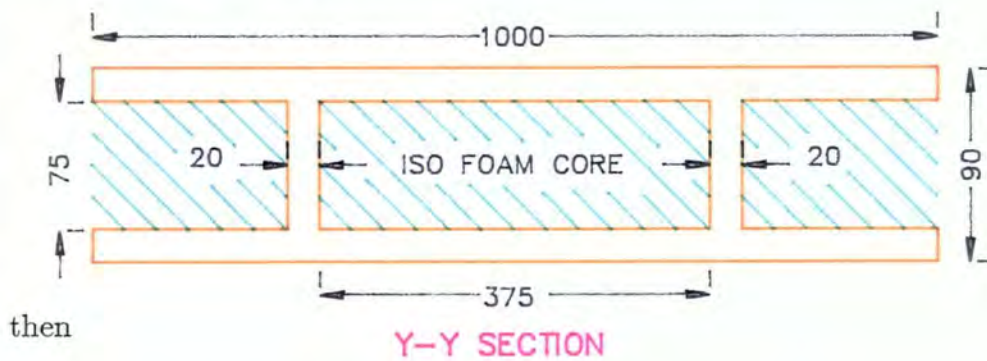
$b$  = width of the panel

$y$  and  $x$  denote the above values in the short and long length of the panel respectively.

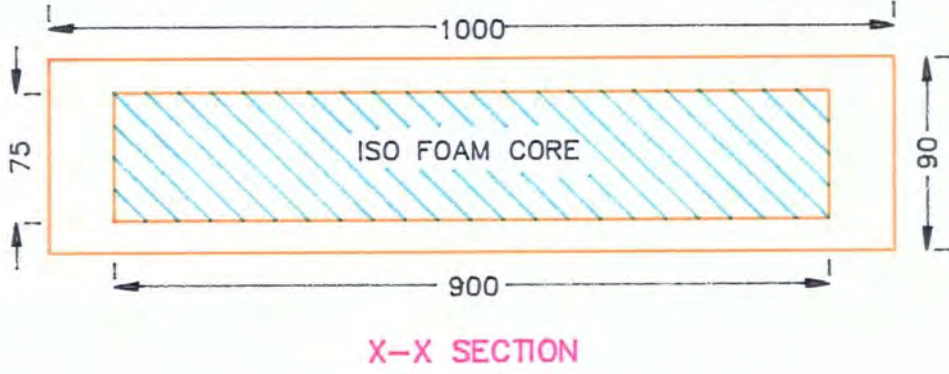
Therefore from the previous equation;

$$\frac{q_y}{q_x} = \frac{\left( \frac{L^4}{I} \right)_x}{\left( \frac{b^4}{I} \right)_y}$$

but  $L_x = 2500mm$ , and  $b_y = 1100mm$



$$I_{yy} = \frac{1 \times 90^3}{12} - \frac{2 \times 0.2925 \times 75^3}{12} - \frac{0.375 \times 75^3}{12} = 27000 \text{ mm}^4/m$$



$$I_{xx} = \frac{1 \times 90^3}{12} - \frac{1 \times 75^3}{12} = 25600 \text{ mm}^4/m$$

and

$$\frac{q_y}{q_x} = \frac{2500^4/25600}{1100^4/27000} = \frac{1.526 \times 10^9}{0.054 \times 10^9} = 28.1$$

ie; if  $29.1 \text{ N/mm}^2$  uniformly load, apply on the panel,  $28.1 \text{ N/mm}^2$  load would be spread along the  $Y - Y$  section and  $1 \text{ N/mm}^2$  along the  $X - X$  section. Therefore

$$q_y = \frac{28.1}{29.1} q_t$$

Where  $q_t$  is the total uniform load.

Therefore from Equation (1)

$$\frac{\Delta_{max}}{q_t} = \frac{28.1}{29.1} \times \alpha \times \left( \frac{b^4}{EI} \right)_y \quad (2)$$

$$\frac{\Delta_{max}}{q_t} = \frac{28.1}{29.1} \times \alpha \times \left( \frac{1100^4}{(15000 \times 27000)} \right) = 3491 \times \alpha \text{ mm/N/mm}^2$$

From the graph

$$\Delta_{max}/W_t = 7.10 \times 10^{-5} \text{ mm/N}$$

where  $W_t$  = total load

$$\Delta_{max}/q_t = 7.10 \times 10^{-5} \times 2500 \times 1100 = 195.0 \text{ mm/N/mm}^2$$

Then  $\alpha = \frac{195.0}{3491} = 0.056$

Putting the value of  $\alpha$  in general formula;

$$\Delta_{max} = 0.056 \left( \frac{qL^4}{EI} \right)_y = 0.056 \left( \frac{qL^4}{EI} \right)_x$$

Therefore

$$\frac{\Delta_{max}}{q_y} = 2.02 \text{ mm/N/mm}^2$$

and

$$\frac{\Delta_{max}}{q_x} = 5.66 \text{ mm/N/mm}^2$$

From equation (2);

$$\begin{aligned} \Delta_{max} &= \frac{q_t b^4}{D} \times \left( \frac{28.1}{29.1} \times 0.056 \right) \\ \Delta_{max} &= \frac{q_t b^4}{D} \times 0.054 \end{aligned} \quad (3)$$

where  $D = EI_y$  per unit length

However, the maximum deflection in the panel in equation (5.35a of reference 20) is given by;

$$\Delta_{max} = \frac{q_t b^4}{D_2} (\beta_1 + \rho \beta_2)$$

where

$$\begin{aligned} \rho &= \frac{\pi^2}{2(1 - \nu_f^2)} \times \frac{E_f t d}{E_c b^2} = \frac{\pi^2 \times 15000 \times 7 \times 81}{2(1 - 0.2^2) \times 15 \times 1100^2} = 2.41 \\ D_2 \text{ ( per unit length )} &= \frac{E_f t d^2}{2(1 - \nu_f^2)} = \frac{15000 \times 7 \times 81^2}{2(1 - 0.2^2)} = 359 \times 10^6 \text{ N.mm}^2 \\ \frac{a}{b} &= \frac{2500}{1100} = 2.27 \end{aligned}$$

from fig.(5.6 of reference 20)

$$\beta_1 = 11 \times 10^{-3}$$

$$\beta_2 = 12 \times 10^{-3}$$

then

$$\begin{aligned}\Delta_{max} &= (11 \times 10^{-3} + 2.41 \times 12 \times 10^{-3}) \left( \frac{q \times b^4}{D_2} \right) \\ \Delta_{max} &= 0.04 \times \frac{qb^4}{D}\end{aligned}\tag{4}$$

Putting the values of  $b$  and  $D$

$$\frac{\Delta_{max}}{q_t} = \frac{0.04 \times 1100^4}{359 \times 10^6} = 163.0 \text{ mm}/N/mm^2$$

The maximum direct stresses in the faces and maximum shear stresses in the faces and core are given in Appendix(4), and are as follow,

The maximum direct stresses in the faces at  $x = L/2$  and  $y = b/2$  is;

$$\begin{aligned}\sigma_x &= \frac{qb^2}{dt}(\beta_3 + \nu\beta_4) \\ \sigma_y &= \frac{qb^2}{dt}(\beta_4 + \nu\beta_3)\end{aligned}$$

The maximum shear stresses in the faces at  $x = 0$  and  $y = 0$  is;

$$\tau_{xy} = \frac{qb^2}{dt}(1 - \nu)\beta_5$$

The maximum shear stresses in the core at  $x = 0$ , and  $y = b/2$  is;

$$\tau_{zx} = \frac{qb}{d}\beta_6$$

The maximum shear stresses in the core at  $x = L/2$  and  $y = 0$  is;

$$\tau_{zy} = \frac{qb}{d}\beta_7$$

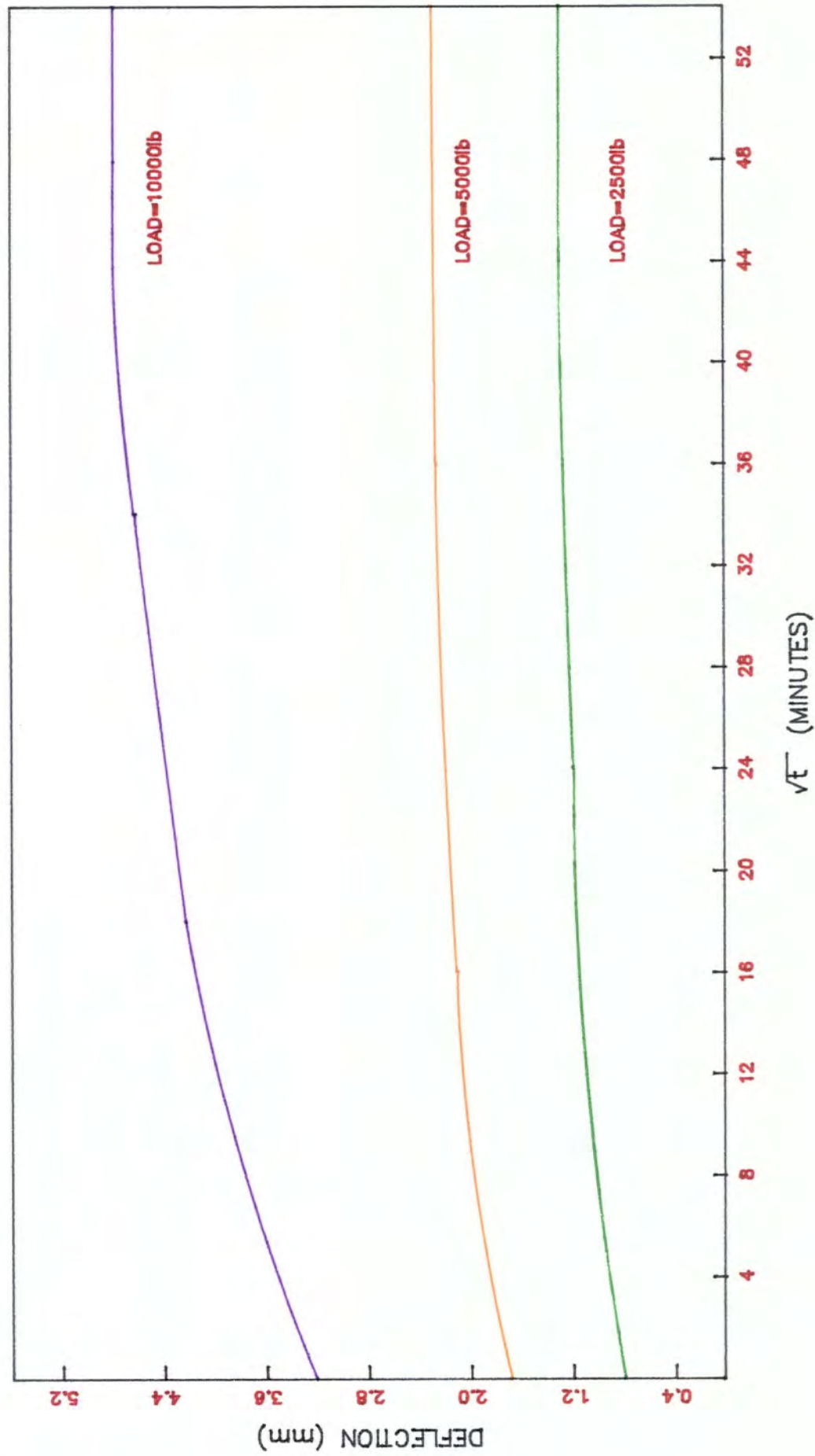


Fig.(6.17). Creep test for the panel, simply supported on all sides, under the transverse loading.

But

$$\frac{L}{b} = \frac{2500}{1100} = 2.27$$

From fig.(5.5, of Reference 20)

$$\beta_3 = 1.3 \times 10^{-2}$$

$$\beta_4 = 10.7 \times 10^{-2}$$

$$\beta_5 = 6.7 \times 10^{-2}$$

$$\beta_6 = 0.35$$

$$\beta_7 = 0.47$$

Therefore

$$\sigma_x = \frac{q \times 1100^2}{8 \times 82} (0.013 + 0.2 \times 0.107) = 63.5 \times q_t \text{ N/mm}^2$$

$$\sigma_y = \frac{q \times 1100^2}{8 \times 82} (0.107 + 0.2 \times 0.013) = 202.2 \times q_t \text{ N/mm}^2$$

$$\tau_{xy} = \frac{q \times 1100^2}{8 \times 82} (1 - 0.2) \times 0.067 = 98.9 \times q_t \text{ N/mm}^2$$

$$\tau_{zx} = \frac{q \times 1100}{82} \times 0.35 = 4.7 \times q_t$$

$$\tau_{zy} = \frac{q \times 1100}{82} \times 0.47 = 6.3 \times q_t$$

Finally, increase in deflection *w.r.t* the time under constant loads are shown in fig.(6.17).

#### **b) Buckling of sandwich panel (axial load)**

The critical load for a pin - ended axially loaded compression member of length **L** and minimum flexural rigidity **EI** according to Euler formula is:

$$P_{cr} = \frac{\pi^2 EI}{L^2}$$

In a sandwich member in which the core material is of low modulus it is likely that shear deformation within the core will occur. This reduce the stiffness of the member. The critical load per unit length for a thin face sandwich panel is given by :

$$P_{cr} = \frac{\pi^2 \times D_2}{b^2} \times K \text{ (see appendix 4)}$$

Two panels supported on two sides with the total length of 2800mm were tested to failure under axial load and the following results were determined:

TEST NO:	TYPE OF PANEL	$I$ (mm <sup>2</sup> × 10 <sup>-6</sup> )	LOAD AT FAILURE (KN)	TYPE OF FAILURE
1	ordinary panel with no internal ribs	19.7	150	local failure at the bottom face near the end load
2	ordinary panel with no internal ribs	22.2	170	local failure at the bottom face near the end load

The critical load for various length according to the Euler formula has been calculated and fig.(6.18) was drawn to show the relationship between the critical load and (L/r) where  $r = \sqrt{\frac{I}{A}}$ .

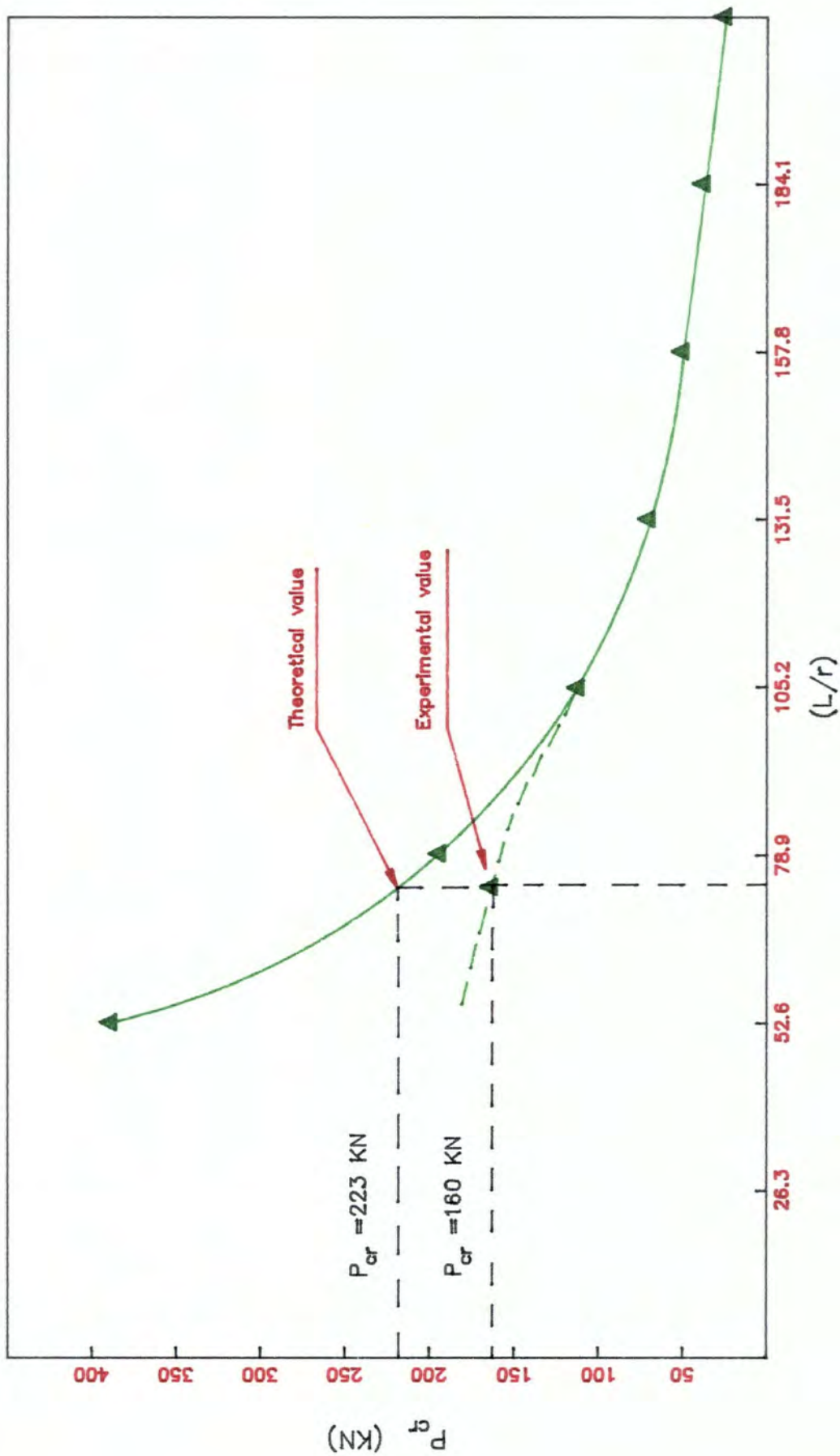


Fig.(6.18). The relationship between the critical load for a pin-ended axially loaded compression member and  $(L/r)$ .

The theoretical value of critical load for a thin face sandwich panel (assuming no edge ribs) supported on four sides has been calculated with the following average dimensions and modulus of rigidity for the faces and core material for all the panels.

For  $a = 2800mm$ ,  $b = 1200mm$ ,  $t = 8mm$ ,  $c = 74mm$ ,  $d = 82mm$ ,

$E_f = 15000N/mm^2$ ,  $E_c = 15N/mm^2$ , and  $\nu = 0.2$ .

From equ.(2.2 of appendix 4);

$$P_{cr} = \frac{\pi^2 D_2}{b^2} \times K$$

Where  $K$  is function of  $a/b$  and  $\rho$

But

$$\rho = \frac{\pi^2}{2(1 - \nu^2)} \times \frac{E_f t d}{E_c b^2}$$

$$\rho = \frac{\pi^2 \times 15000 \times 8 \times 82}{2 \times (1 - 0.2^2) \times 15 \times 1200^2} = 2.34$$

$$\frac{a}{b} = \frac{2800}{1200} = 2.33$$

From fig.(5.4 of reference 20),  $K = 0.40$

$$D_2/\text{unit length} = \frac{E_f t d^2}{2(1 - \nu_f^2)} = \frac{15000 \times 8 \times 82^2}{2(1 - 0.2^2)} = 420 \times 10^6 N.mm^2$$

Therefore,  $P_{cr}$ (per unit length) is;

$$p_{cr} = \frac{\pi^2 \times 420 \times 10^6}{1200^2} \times 0.4 = 2.9kN$$

Fig.(5.4 of reference 20) may only be used if  $D_f/D$  and  $D/L^2 D_q$  give a point in figure(6.5 of reference 18) which is close to the line ABCG.

It is therefore necessary to check this condition;

$$D_f = \frac{I_f E_f}{(1 - \nu^2)}$$

Where  $I_f = 8^3/6 = 85.33mm^4$

So

$$D_f = \frac{15000 \times 85.33}{(1 - 0.2^2)} = 1.33MN.mm^2$$

$$D = I_{total} \times \frac{E_f}{(1 - \nu_f^2)} = 420 \times 10^6$$

Then

$$\frac{D_f}{D} = \frac{1.33}{420} = 0.00317$$

$$D_q = \frac{E_c d^2}{c} = \frac{15 \times 82^2}{74} = 1363Nmm^2$$

$$\frac{D}{L^2 D_q} = \frac{420 \times 10^6}{2800^2 \times 1363} = 0.039$$

The above values of  $D_f/D$  and  $D/L^2 D_q$  give a point on the line ABCG of fig.(6.5 of reference 18).

### **c) Sandwich panels simply supported on two ends with axial load and transverse load**

#### **i. Ordinary panels**

A series of 18 panels were tested in this type of loading. Initially a set of proving loads were applied to every panel to prove its adequacy for its commercial duty. There was no sign of any failure in any of the panels under this loading. Then the panels were failed under the transverse load, together with different values of axial load.

TEST NO:	MIX	INTERNAL RIBS	AXIAL LOAD (KN)	C.S.A (mm <sup>2</sup> )	$I$ (mm <sup>4</sup> * 10 <sup>-6</sup> )	TRANSVERSE LOAD (lb)	$W/A$ (N/mm <sup>2</sup> )	$M/Z$ (N/mm <sup>2</sup> )	TOTAL STRESS AT FAILURE (N/mm <sup>2</sup> )	TYPE OF THE FAILURE
1	A	YES	60	25585	39.15	4500	2.34	7.05	9.39	TENSION FAILURE @ THE BOTTOM FACE
2	A	YES	60	26105	39.81	5000	2.30	7.70	10.00	TENSION FAILURE @ THE BOTTOM FACE
3	A	NO	60	26814	39.20	5000	2.24	7.82	10.06	TENSION FAILURE @ THE BOTTOM FACE
4	A	NO	60	26887	36.88	4000	2.23	6.65	8.88	FACE BUCKLING NEAR THE END LOAD.
5	SS	NO	60	23946	32.44	4000	2.51	7.56	10.07	FACE BUCKLING NEAR THE END LOAD.
6	A	YES	90	24259	35.29	4800	3.71	8.34	12.05	TENSION FAILURE UNDER THE POINT LOAD
7	A	YES	90	24465	36.07	5000	3.68	8.50	12.18	TENSION FAILURE
8	A	NO	90	26627	35.73	5000	3.38	8.58	11.96	TENSION FAILURE
9	A	NO	90	23684	31.40	4000	3.80	7.81	11.61	FACE BUCKLING NEAR THE END LOAD.
10	A	NO	90	23077	33.50	4000	3.90	7.32	11.22	FACE BUCKLING NEAR THE END LOAD.

Table(6.19A). Results of the simply supported panels under the axial load & the transverse load.

TEST NO:	MIX	INTERNAL RIBS	AXIAL LOAD (KN)	C.S.A (mm <sup>2</sup> )	$I$ (mm <sup>4</sup> * 10 <sup>-6</sup> )	TRANSVERSE LOAD (lb)	$W/A$ (N/mm <sup>2</sup> )	$M/Z$ (N/mm <sup>2</sup> )	TOTAL STRESS AT FAILURE (N/mm <sup>2</sup> )	TYPE OF THE FAILURE
11	A	YES	120	24155	37.85	6000	4.97	9.72	14.69	TENSION FAILURE
12	A	YES	120	24316	35.85	6800	4.93	11.63	16.56	TENSION FAILURE
13	A	NO	120	26091	35.13	5000	4.60	8.73	13.33	LOCAL COMPRESSION FAILURE NEAR THE END BAY.
14	A	NO	120	26476	34.93	5500	4.53	9.65	14.18	LOCAL COMPRESSION FAILURE NEAR THE END BAY.
15	A	YES	160	26446	41.50	9000	6.05	13.30	19.35	TENSION FAILURE AT THE MIDDLE
16	A	YES	160	25600	39.00	7500	6.25	11.80	18.05	TENSION FAILURE AT THE MIDDLE
17	A	YES	180	23965	31.60	5500	7.51	10.67	18.18	TENSION FAILURE AT THE MIDDLE
18	A	NO	180	25083	34.58	6700	7.17	11.88	19.05	TENSION FAILURE AT THE MIDDLE

Table(6.19B). Results of the simply supported panels under the axial load & the transverse load.

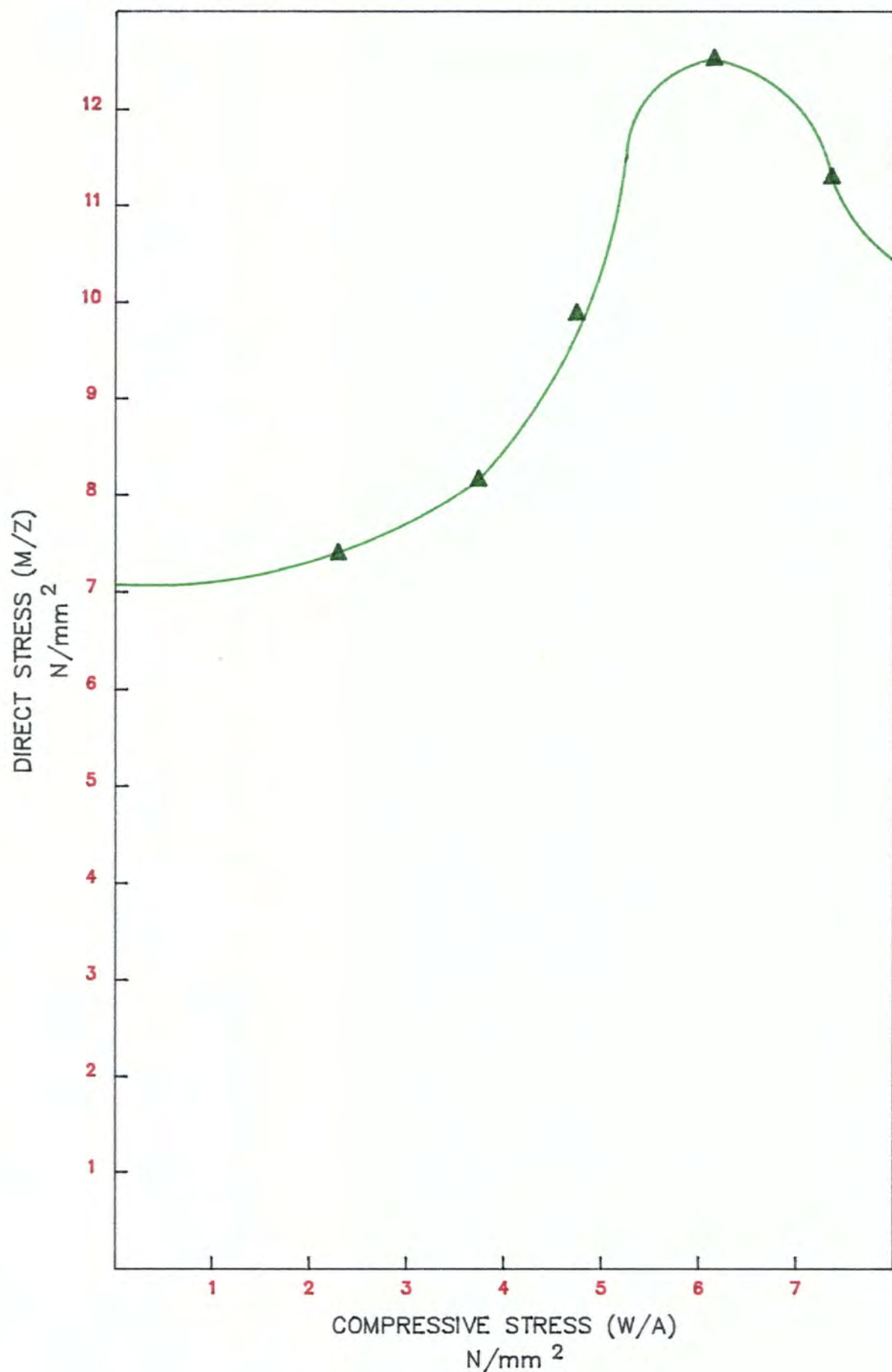


Fig.(6.20). The relationship between the direct stress and the compressive stress for the panel, simply supported on its two ends.

After the failure, the dimensions of the panel were measured using a micrometer in order to calculate the cross sectional area,  $\hat{y}$ , and  $I$  values. The compressive stress  $W/A$  and direct stress  $M/Z$  were calculated and these are shown in table (6.19).

A graph was drawn to show the variation of  $M/Z$  due to the axial load. This can be seen in fig. (6.20)

## **ii. Panels with window voids**

Three different types of panels with window voids were tested under transverse load and axial load, and were as follows:

1. Panel with window voids of dimension 900 mm by 1200 mm with internal centre ribs.

The 'proving' loads were applied to the panel, and there was no sign of any kind of failure. Finally the panel was failed under a 2500lb transverse load, together with a 60 kN axial load.

2. Panel with window voids of dimension 900 mm by 1200 mm with no internal rib.

The panel failed at the end of the 'proving load' cycle, ie; 40 KN axial load plus 8 KN transverse load.

3. Panel with window voids of dimension 900 mm by 900 mm with no internal rib.

The panel could resist the 'proving loads' without any problem and failed under a 2000 lb transverse load together with a 60 KN axial load. The position of the failure for all the panels were at one of the corners of the window voids.

### **iii. Single-skin panels**

Two panels were made and tested. This was done to develop construction techniques and made it possible to test the panels in either direction of transverse loading with the face on the compression side and the tension side in bending.

Both specimens survived the proof loading cycles. The panels with the skin on the compression side failed at a 2350 lb transverse load together with a 40 KN axial load. The second panel, with the skin on the tension side, failed under a 4000 lb load with the same value of axial load as before.

## **6.7 Conclusions**

### **a) Bending of sandwich panel**

#### **i. Simply supported at two ends**

As expected the ribbed panel gave better results than the unribbed, but it is important to note that even the unribbed panel, gave results which would suggest the mechanical strength of this sort will not be critical design criterion for panels with these dimensions in this service situation.

As the graph of load against deflection indicates, all the panels behaved elastically up to the failure. The modulus of elasticity of the panels using the 'SS' mix, once again proved to be better than the others. All the specimens showed ultimate failure of a similar kind, ie; tension failure on the bottom face. However, the ultimate stress of the panel seems to be less than was predicted.

## ii. Simply supported on four sides

From the experimental result the following expression was determined:

$$\Delta_{max} = \frac{q_t b^4}{D} \times 0.054$$

where  $D = EI_x$  and the value of  $\Delta_{max}/q_t$  was found to be  $195\text{mm}/\text{N}/\text{mm}^2$ . However, from the theoretical work a similar expression of;

$$\Delta_{max} = \frac{q_t b^4}{D} \times 0.04$$

Where

$$D = \frac{E_f b d^2}{2(1 - \nu^2)}$$

With the value of  $\Delta_{max}/q_t$  of  $165\text{mm}/\text{N}/\text{mm}^2$  was obtained.

A panel simply supported on four sides with a uniform transverse loading probably can be divided into four sections (see fig. 6.11).

Sections ABC and DEF which are rotated about the X-X axis and sections CBDE and ABDF which are rotated about the Y-Y axis. Using the yield line method the position of band D was found to be 637mm from the end supports, and thus the position of the strain gauges of no. 3,4,7 and 8 were found to be in ABC and DEF sections. As these sections are rotated about the X-X axis, there must not be any significant reading in strain gauges no.(8) and (4) and similarly with strain gauges no.(1,5,and 9) as they are in a section which is rotated about the Y-Y axis.

The result of the strain gauge reading supported the above theory as the strain gauge reading of no. 1,4,5,8,9 were found to be negligible. From fig.(6.17) it can

be seen that the increasing deflection of the panel under constant lower transverse load would settle sooner than the panel with the higher value of transverse load. eg; the deflection of the panel under 2500lb transverse load became steady after 24hrs while the deflection for the second and third panel became steady 36hrs and 48hrs respectively. From the fig.(6.17) also can be seen that the initial rate of increase in deflection for the panel with higher transverse loading is greater than the ones with lower transverse loading.

#### **b) Buckling of sandwich panel (axial load)**

As we can see from the graph (6.18) the average experimental value of critical load is less than the theoretical Euler crippling load. However, in practice, the critical load for members with a small value is always less than the value determined from the Euler formula. The shape of the graph is likely to be similar to the dotted line shown in fig (6.18).

The theoretical value of the critical load for a thin faced sandwich panel (assuming no edge ribs) also has been calculated and found to be in the region of 2.4 KN (see chapter 9). It is clear that the presence of edge ribs in the panel increases the value of the critical load greatly. For the same length of a member, the value of critical load according to the Euler formula is almost 75 times more than the value of critical load for a thin faced sandwich panel without edge ribs.

**c) Simply supported sandwich panels at two ends with axial load and transverse load**

**i. Ordinary panel**

The type of failures of all the internal ribbed panels were similar to those in the previous test series (transverse load only) but however there was another kind of failure for some of the unribbed panels under the axial load together with transverse load. Most of the unribbed panels showed signs of compression face local buckling near the load line, especially at a higher value of axial load (above 120 KN) where they are approaching the local buckling stress. As the test series no.(2) suggests this type of panel would buckle approximately under 160 KN axial load.

An important phenomenon shown clearly by the test is the increase in the slab flexural strength produced by the 'prestressing' effect of the load. Some strengthening could have been predicted on the grounds that since the failure mode is likely to be due to tension strain for all the ribbed panels, then the failure will be delayed by introducing an overall compressive stress, as happens due to the end load.

However, fig.(6.20) shows that this strengthening effect does not continue to increase beyond an axial-stress value of  $6.15\text{N/mm}^2$ . At higher axial stresses the failure occurs at reducing values of transverse bending stress.

This test series has shown that slabs of these specifications have a load factor of at least 5 when used in the most demanding structural environment to which they can be subjected in practice. ie; as the lower storey in a two storey house. This applies to the unribbed slab. Ribbed slabs have a higher load factor.

## **ii. Panels with window voids**

From the test result it is clear that the inclusion of small voids will make little difference to the end load performance and that even relatively large openings are accommodated without much loss of strength in this mode, but that the voids will make some difference to the performance in the transverse loading mode.

The panel with the opening of dimensions 900 mm by 1200 mm with internal ribs and the panel with the opening of dimensions 900 mm by 900 mm with no ribs survived the proof loading cycles. However, the panel with opening of dimensions 900 mm by 1200 mm with no ribs failed at the end of the proof loading cycle. This suggests that internal ribs are necessary for the panels with openings as large as this.

## **iii. Single skin panels**

Both single skin panels survived the 'proof load' cycles, but with very little to spare. Obviously the transverse bending strength is significantly less than that of the compatible sandwich panel.

It may be deduced from the description of the manufacturing procedure that the panels take rather more time and trouble to make than the sandwich panel. It seems likely from this brief experience that such a single-skin panel could not be produced commercially more cheaply than the sandwich panel, especially since it would have to be reinforced with glass on both faces to cope with likely local loading from either direction. This is particularly true if the sandwich panels can be produced without ribs, as seems to be the case, since the single-skin panel would

always need its face stiffened by ribs, though perhaps not as many were used here.

This last remark also implies that it would not be simple to produce single-skin panels with the range of surface finishes and appearance possible with the sandwich panel.

In general it can be concluded that with its lower strength, very poor insulation and relatively high cost the single-skin panel does not look to be a promising prospect for production. This is especially true since it must always be compared with the sandwich panel, which is in every way, a more efficient building component.

# CHAPTER (7)

## CHAPTER SEVEN

### 7. Polymer concrete Bridge-Deck

#### 7.1 Introduction

Polymer concrete *Bridge-Deck* consists of a flat sheet stiffened on one side by an array of ribs. The assembly is initially reinforced on the top and bottom faces with layers of glass-fibre woven roving. The ribs may be not reinforced, or may be reinforced with flat steel bars cast vertically in the ribs, or with a pair of plain round bars cast into the top and bottom of each rib.

The plain polymer concrete Bridge-Deck, usually in width of 900mm, and usually with only three ribs per sheet may be used as roofing sheet. The steel reinforced Bridge-Deck, in widths of up to 1200mm, may be used either as permanent form-work for reinforced concrete or as a self-supporting floor structure.

#### 7.2 Dimensions and schedule of polymer concrete Bridge-Deck

Two sets of samples were made with two identical samples in each set.

**Set(1)** consisted of sections of Bridge panel, 1400mm long and approx. 280mm wide, so that each contained two ribs, symmetrically disposed. In this set each rib was reinforced with one length of steel strip 4mm wide and 40mm deep.

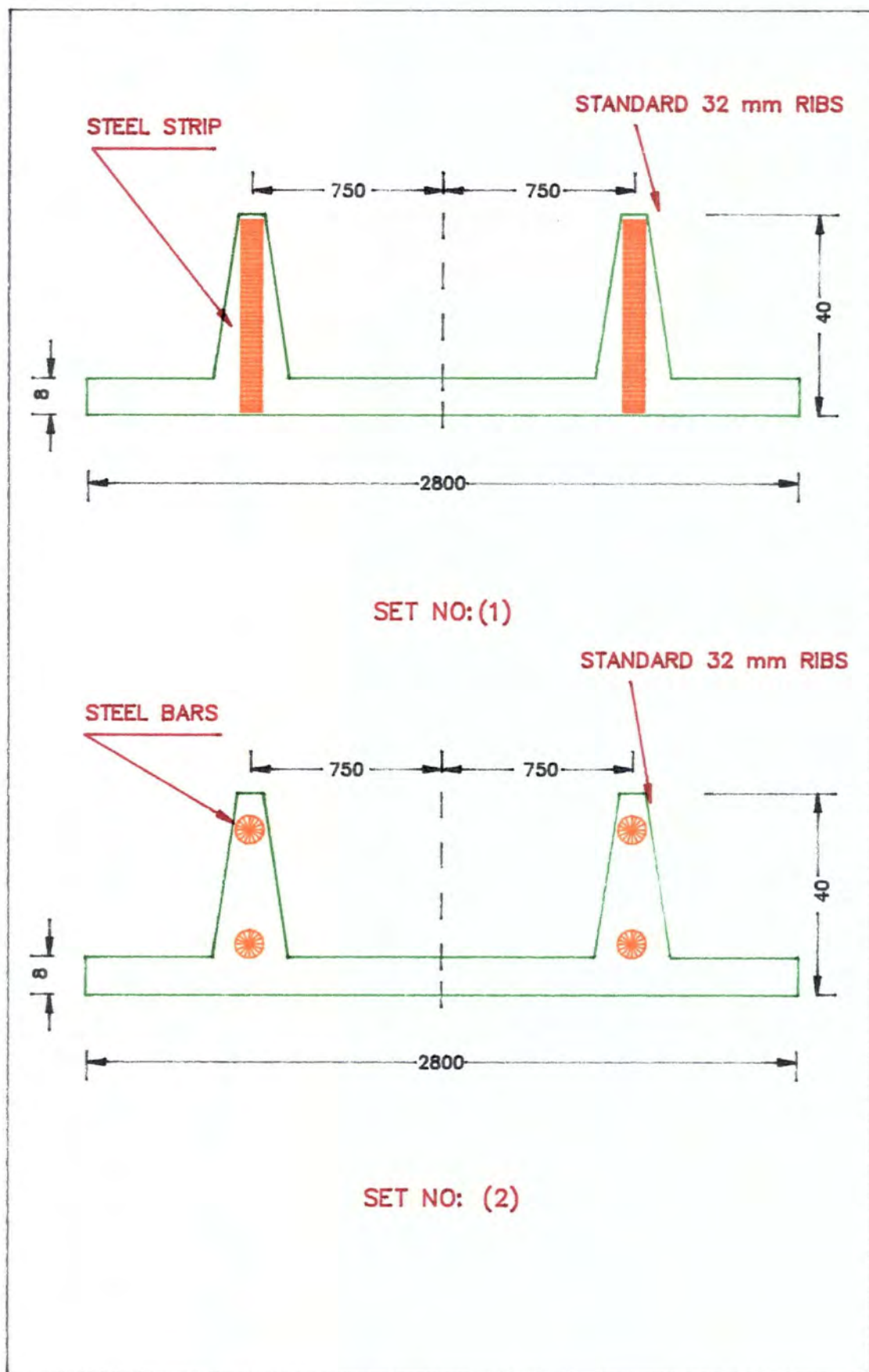


FIG.(7.1). Typical section BRIDGE-DECK.

**Set(2)** was similar to set (1) except that the reinforcement in each rib consisted of a pair of 9mm steel bars, one at the top of the rib and the other approximately at the centre of depth of the slab.

All the samples were made with mix 'A' (3.5:1) using resin (401) and filler (B.L.H). The cross sections of the two types are shown in fig.(7.1).

### **7.3 Method of construction**

After the wooden mould was waxed thoroughly, the fibre glass mat, which had previously been cut to size, was placed over the mould and pushed down into the ribs. The steel reinforcement were placed in position in the ribs. The mix was poured onto the mould and then levelled off with a flat screed. The second layer of fibre glass mat was placed over the mix and the air trap was removed with the aid of a roller.

### **7.4 Test procedure**

The samples were made slightly longer than was necessary for the test so that a section could be cut off the end of each specimen to expose the section, and show the position of the reinforcement. Thus, a length of 200mm was cut from the end of each specimen, making the remaining overall length 1200mm so that they were suitable for testing over the 1100mm span. The dimensions of each of the specimens were obtained, notably the slab thickness, and the arrangement of the bars.

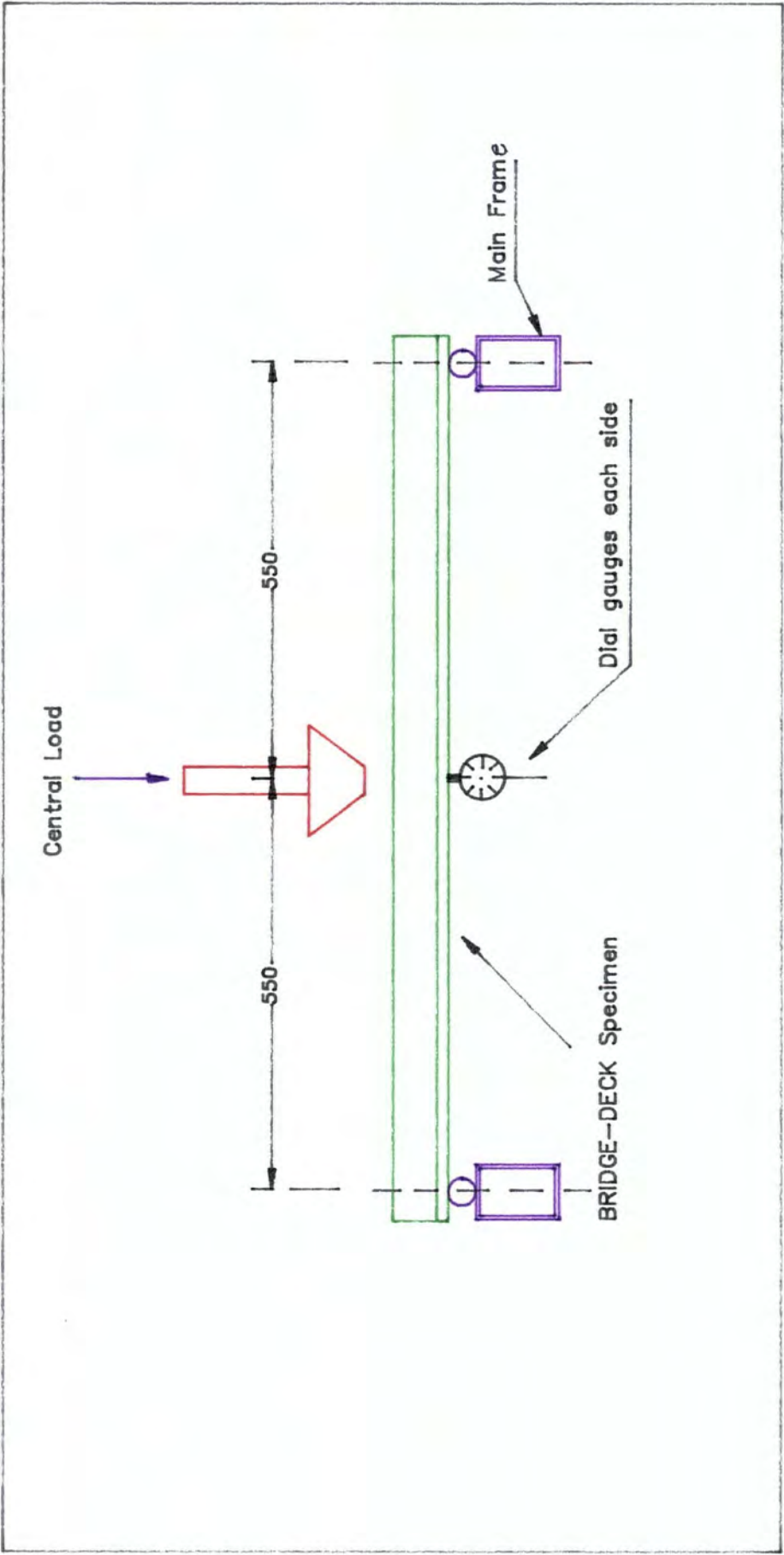


Fig.(7.2). Test configuration.

The samples were placed, in turn, onto the test rig and loaded hydraulically with a central point load and the load intensity was measured by means of an electronic load cell. The deflections were measured by dial gauges placed at each side of the specimen on the line of the load. The load arrangement are shown in fig.(7.2).

## 7.5 Results and calculations

Graphs were drawn of load against deflection for each specimen. A typical graph is shown in fig.(7.3).

The principle features of curve are:

1. A steep straight-line section indicating linear elastic behaviour.
2. A short curved section indicating the onset of yield in the reinforcement leading to a long horizontal section where the steel is yielding.
3. A sudden drop in the graph indicating the tension cracking of the polymer concrete across the bottom of the specimen under the load.
4. A continuation of the graph at a much lower load, showing the continued deflection of the specimen, with the tensile force component provided by the yielding lower steel and the compression still being provided by the uncracked polymer concrete together with the compression steel at the top of the specimen in a similar manner to the yielding of a reinforced concrete beam.

From each graph the following data was obtained:

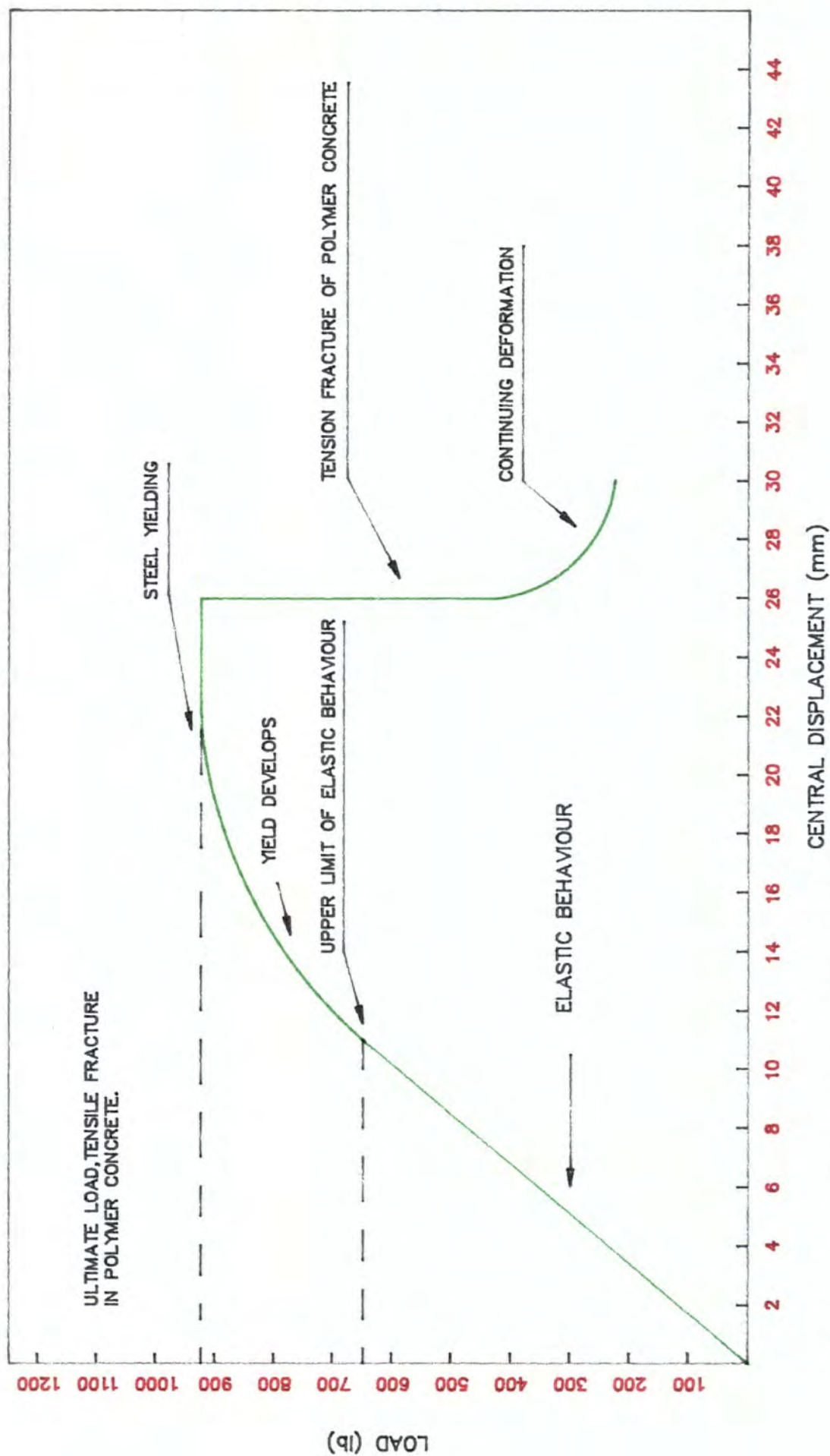


Fig.(7.3). Typical load/deformation graph.

1. The slope of the graph
2. The load causing the first change of slope of the graph
3. The ultimate load.

These are tabulated in table (7.5). Using the slope of the graph, the experimental  $EI$  value was found from the expression of:

$$EI = \frac{L^3}{48} \times \text{slope}$$

Assuming the modulus of steel to be  $E_s = 2 \times 10^{11} \text{ N/m}^2$ , and using the equivalent section method, and reducing the polymer concrete to the equivalent steel area, the second moment of area of the specimens with respect to the steel was found.

A computer programme, *B DECK* (see appendix 5), was written to provide a numerical model of a specific bridge panel specimen. From this it was possible to plot the graph in fig.(7.4), which showed the theoretical prediction of the second moment of area of the specimens, compared to the second moment of area in the tests.

The theoretical  $I$  value was plotted for a range of modular ratios from 10 to 35, so that the effective modular ratio in the tests could be determined. Also a programme made it possible to calculate the theoretical stress at the change of slope of the graph (see Appendix 5).

The theoretical model is based on the assumption that;

1. Perfect bond is maintained between the polymer concrete and the steel.
2. The section properties assume an uncracked section.

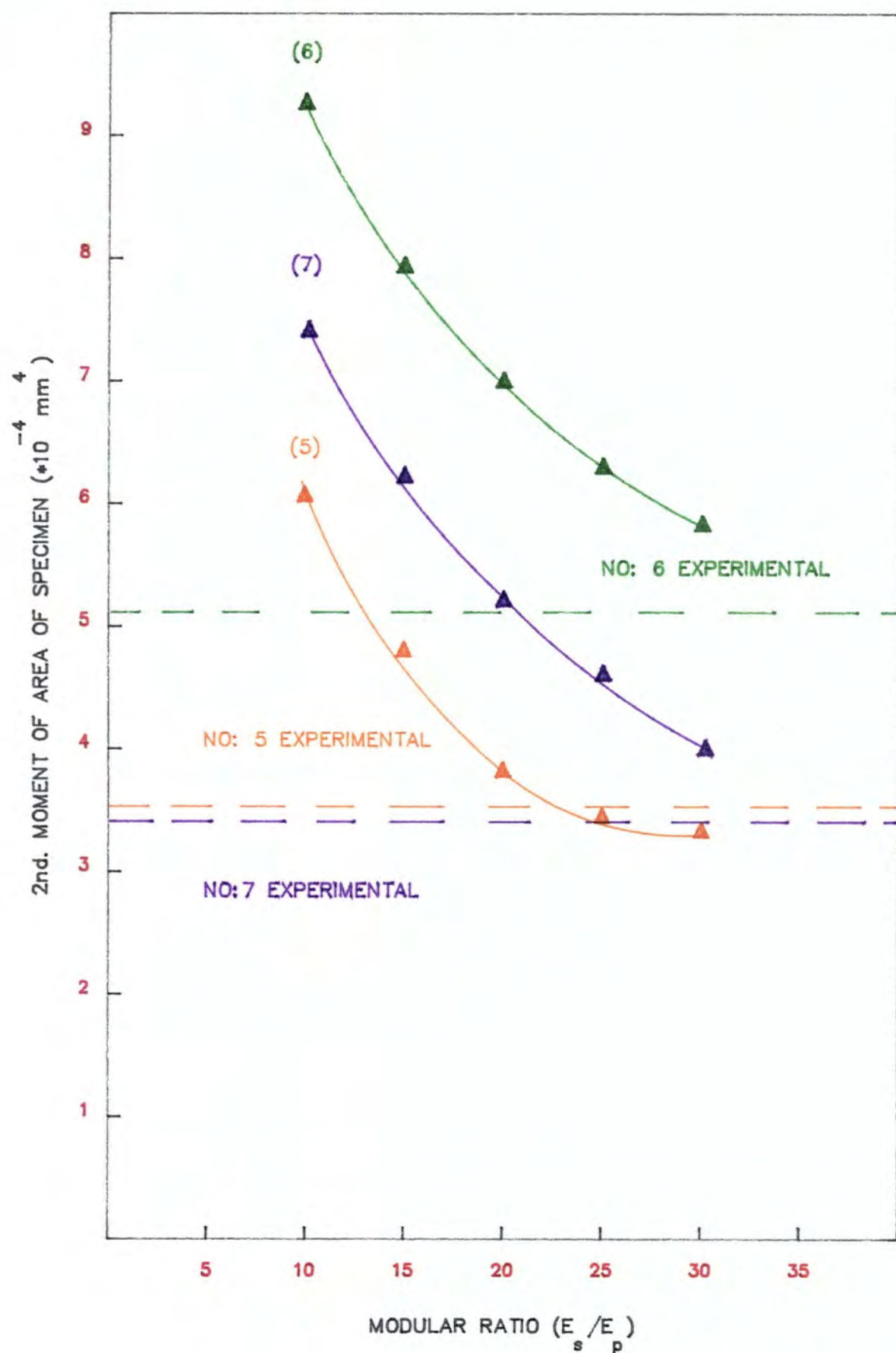


Fig.(7.4). Modular ratio comparison.

3. The tension and compression elastic moduli are the same for both polymer concrete and steel, and the steel modulus remains throughout such that:

$$E_s = E_p \times m$$

where

$E_s$  is the steel modulus,

$E_p$  is the polymer concrete modulus,

$m$  is the modular ratio.

From the graph in fig.(7.4), it is clear that a modular ratio of 30 is a reasonable general approximation to make for all the tests. Therefore the calculations were made and tabulated in table (7.6) with the assumption of  $E_s = E_p \times 30$ .

It was seen from the elastic-plastic behaviour of the test samples that the *Bridge-Deck* failed on all occasions, when the steel reinforcement reached its yield stress, when an effective plastic hinge developed under the load. When the hinge had flexed some way the polymer concrete failed in tension along a line across the bottom of the sample immediately under the load. This confirmed that the polymer concrete itself did not fail until some time after the steel had yielded, as would be predicted by comparing the strains at which each material is known to fail in plain bending.

*ie*; Steel strain at yield;

$$\epsilon_s = \sigma_s / E_s = 3 \times 10^8 / 2 \times 10^{11} = 1.5 \times 10^{-3}$$

TEST NO:	SLOPE OF THE GRAPH (N/mm)	LOAD @ THE END OF THE ELASTIC SECTION (lb)	ULTIMATE LOAD (lb)	$EI \cdot 10^{-9}$ (Nmm)	$I_s \cdot 10^{-4}$ IN TERM OF THE STEEL (mm)
5	225	650	920	7.07	3.53
7	249	625	1100	6.91	3.45
6	366	900	1200	10.2	5.07

Table(7.5). Results of the test on BRIDGE-DECK specimens.

TEST NO:	$I_y$ (mm)	MODULAR RATIO $E_s/E_p$	$I_p \cdot 10^{-8}$ (mm)	$E$ (N/mm)	$E_f$ (N/mm)	$E_u$ (N/mm)
5	top 23.8	30	0.99	7141	23.9	33.8
	bottom 16.2				16.3	23.0
7	top 21.8	30	1.21	5707	17.2	30.3
	bottom 18.2				14.4	25.3
6	top 23.1	30	1.69	6006	18.8	25.1
	bottom 16.9				13.4	17.8

Table(7.6). Calculation values for the BRIDGE-DECK.

TEST NO:	$\sigma_s$ (N/mm <sup>2</sup> )	$I_s \times 10^{-4}$ (mm <sup>4</sup> )	$\bar{Y}_t$ (mm)	$\bar{Y}_b$ (mm)	$M_t$ (Nmm)	$M_b$ (Nmm)	$W_f$ THEORETICAL (KN)	$W_f$ EXPERIMENTAL (KN)
5	300	3.53	10.78	3.22	9.82	32.9	TOP 3.57	2.90
							BOTTOM 12.0	
7	300	3.45	21.8	18.2	4.75	5.69	TOP 1.73	2.79
							BOTTOM 2.07	
6	300	5.07	23.07	16.9	6.59	8.98	TOP 2.40	4.02
							BOTTOM 3.27	

Fig.(7.7). The comparison between the experimental & theoretical, value of the ultimate load.

Polymer concrete strain at tensile fracture;

$$\epsilon_p = \sigma_p / E_p = 25 \times 10^6 \times 30 / 2 \times 10^{11} = 3.75 \times 10^{-3}$$

It can be seen that the strain in the polymer concrete at the steel yield load was not high enough to cause complete tensile failure.

The tests showed that the failure load of the reinforced polymer concrete panel could be predicted by calculating the moment to cause the development of the yield stress in the reinforcement, using the section modulus, calculated from the 'equivalent section' method. The comparison between the predicted failure load and experimental failure load can be seen in table (7.7).

## 7.6 Conclusions

From the test results and observations during the test the following conclusion has been made.

The effective failure of each panel was caused by the development of yield throughout the steel reinforcement, causing the formation of a plastic hinge under the load. The hinge effect then suffered considerable deformation before the next and final event of the test.

The ultimate failure of each specimen was due to tensile failure of the polymer concrete/glass reinforcement mat at the base of the slab. The high value of the modular ratio and the crack stopping capability of the glass mat allows the polymer concrete to remain intact until after the steel has yielded considerably. The polymer

concrete/steel bond also remains viable until the steel yield.

It will be seen that the design philosophy of reinforced polymer concrete must be different from that used in the design of reinforced concrete, since in the latter the equivalent section method cannot be used in the same way, because of the earlier failure of the concrete in tension. For this reason the prediction of deflection in a reinforced polymer member is much simpler and more reliable than is the case with the equivalent reinforced concrete section.

However, it has to be noted that if a higher value of polymer concrete modulus was used (ie; using mix **SS** or **TT**), it would have altered the above behaviour fundamentally, causing the polymer concrete to crack in tension before steel yield, but of course at higher failure load. The design procedures together with the output of the computer programme *B DECK* are shown in Appendix (5).

# CHAPTER (8)

## CHAPTER EIGHT

### 8. Polymer concrete sheeting

#### 8.1 Introduction

By and large the roofing industry has seen little or no change in the last few years. However fairly recent events concerning the health hazards of asbestos have brought about a radical change in the roofing market. Government legislation in the UK in 1982 meant that asbestos producers and fitters had to be licenced and strict safety procedures had to be observed. The consequences of the 1982 legislation are far reaching, causing many industries extra cost in reducing the risks and hazards of asbestos building products. Some industries have been able to replace these products with suitable substitutes, while others have had to demolish areas containing a high element of asbestos and have had to pay a premium for extra safe-guards.

However, the polymer concrete sheeting described here which is for use as roofing and wall cladding and is manufactured by a pulltrusion process developed for continuous mass production. It contains no asbestos fibre or similar product and can generally be regarded as 'safe' material and therefore can be regarded as an asbestos substitute.

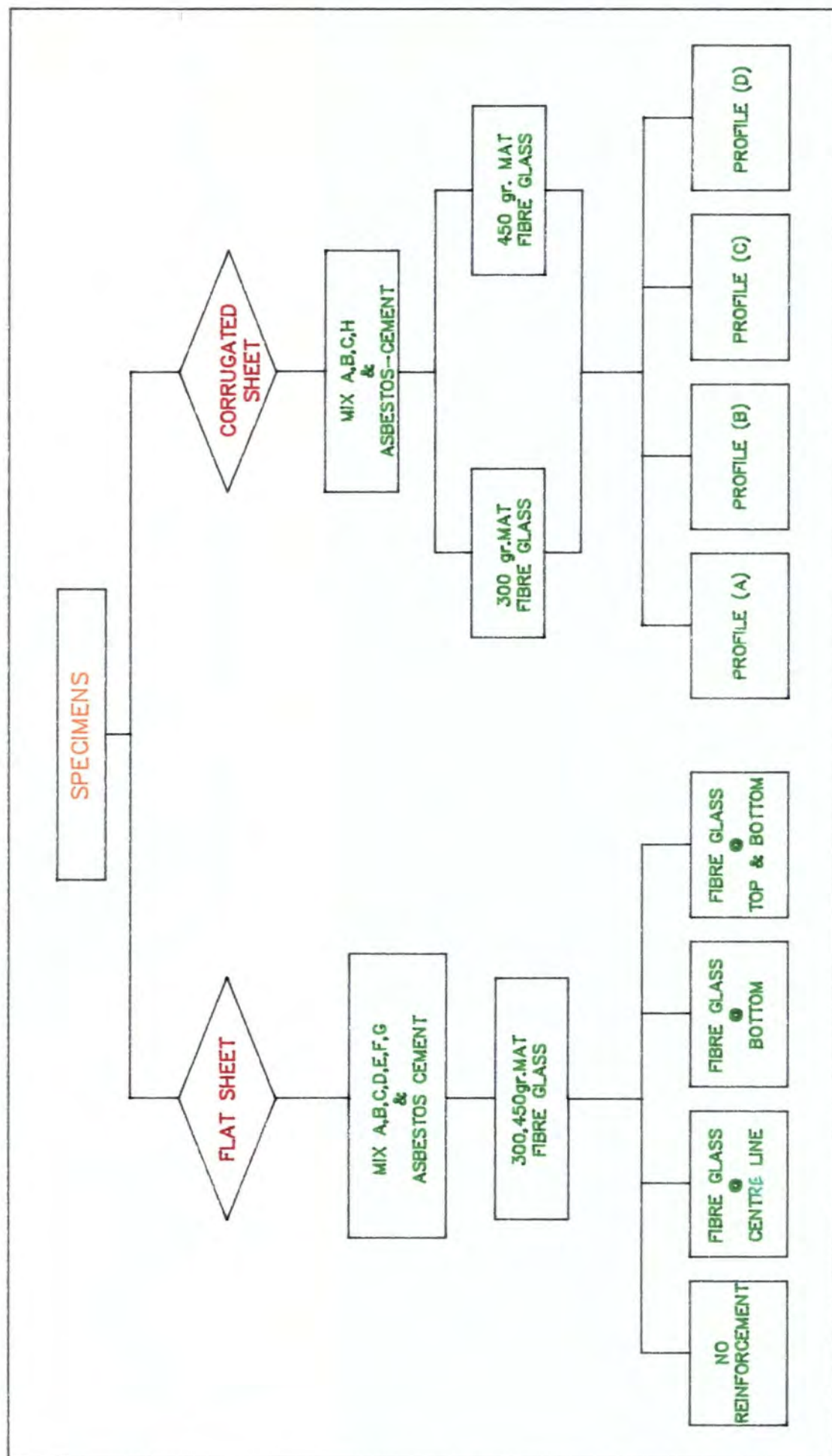
A series of specimens of both flat sheet and corrugated sheet from an ex-

perimental '*pulltrusion*' machine were produced at Alton during the latter part of November 1983. As the research in polymer concrete only started in October 1983 at Durham University the new mix **SS** or **TT** and new filler (**pozzolan**) or resin (**L.V.M**) were not available at that time so all the specimens were produced using a variety of different techniques and trial mixes.

In 1985 the firm that supported this research had to withdraw due to financial reasons and the production of more corrugated sheet specimens with the new mix was impossible. However the initial trial demonstrated that, first of all, the product can be produced continuously by a '*pulltrusion*' method, and secondly, the results were encouraging compared with other similar specimens of commercially available asbestos - cement sheet, and other alternative products.

## **8.2 Dimensions and schedule of polymer concrete sheeting**

Two kinds of specimen were cut from the flat sheet and corrugated sheet. Small flexural specimens of a size similar to that described in (3.5), were cut from the flat sheets and were tested in the *Instron rig*. Larger flexural specimens were cut from the corrugated sheet. In this instance they were tested in the *beam rig* as in (4.3). The width of the support stirrups of the beam test machine and the width of the available sample sheet both suggested that the bending specimens should be cut so that they consisted of three complete corrugations of the '*big six*' profile. Thus the range of samples of this profile were all about 420mm wide and 1170mm long.



Table(8.1). The schedule of the test on sheeting.

MIX NO:	RATIO	RESIN	% OF THE AGGREGATES			TYPE OF THE FILLER	% OF THE CATALYST
			SAND NO(2)	SAND NO(4)	FILLER		
A	3:1	602	32	59	9	TALC	1.75
B	2:1	401	—	91	9	B.L.H	2.0
C	2:1	401	—	100	—	—	2.0
D	2:1	401	—	91	9	B.L.H	1.75
E	3.25:1	602	24	70	6	TALC	2.0
F	3.5:1	602	65	27	8	B.L.H	1.75
G	3.25:1	602	70	20	10	TALC	1.75
H	4:1	LV	65	27	8	B.L.H	1.75

Table(8.2). The specification of the initial trial mix's.

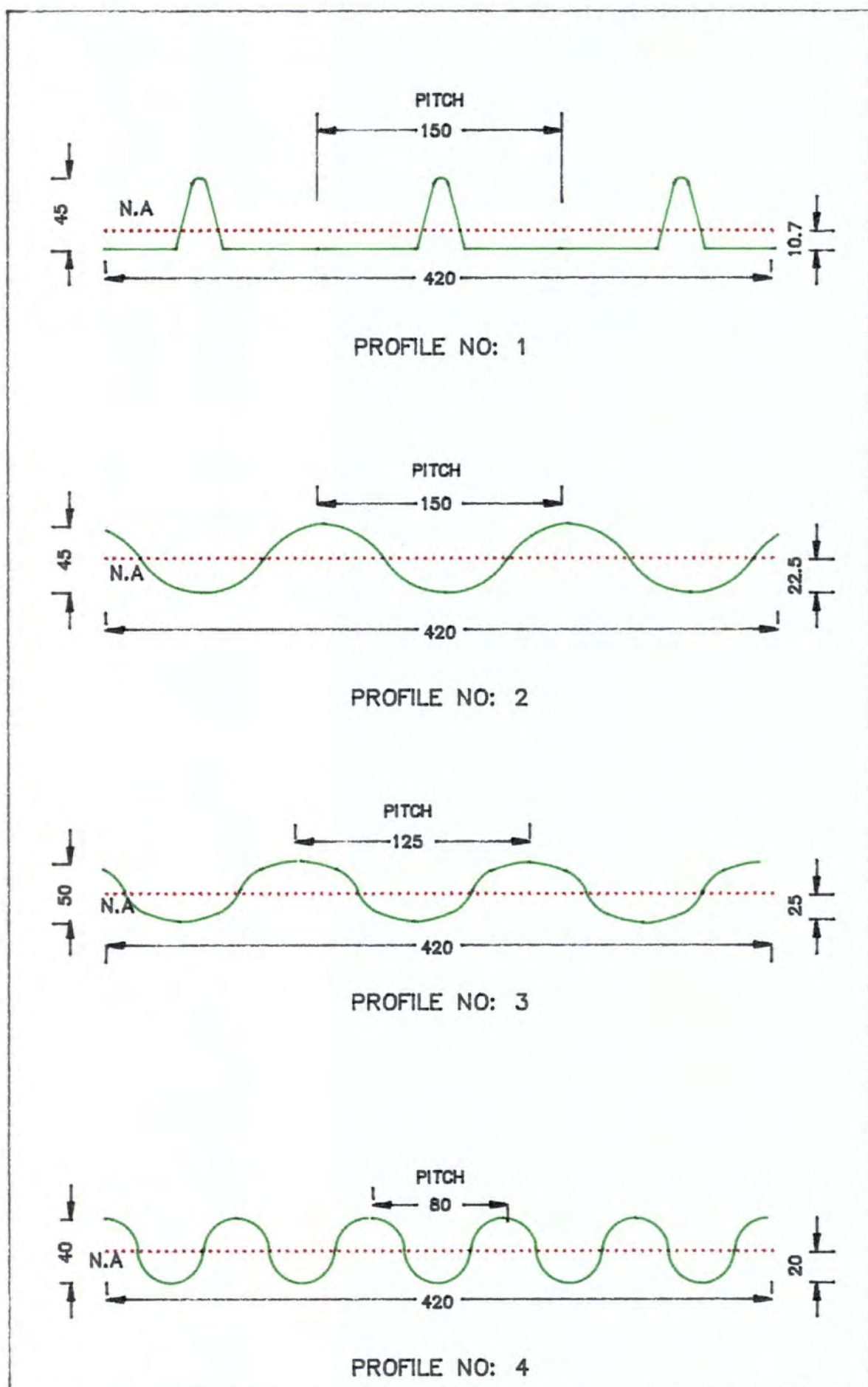


Fig.(8.3). The profile of the corrugated sheets.

The schedule of the test and the specification of the mixes are shown in tables (8.1) and (8.2) respectively. Also the profiles of the corrugated sheets are shown in fig.(8.3).

### 8.3 Method of construction

All the corrugated sheets were constructed in one continuous process from the experimental 'pulltrusion' machine.

A thin film carrier(melanex sheet), was arranged to pick up the mix when passing under the mixing head. The lay up was spread evenly and to the required thickness by passing under a '*doctor blade*' and over a vibrating table. This operation was arranged at two points simultaneously on two independent carrier films travelling in opposite directions during the actual laying down process.

The two films were brought together in such a way that they sandwich a glass fibre mat in the process. At this point both carriers films are travelling in the same direction ie; the direction of the main flow. The result of this operation was to have a sandwich of reinforced matrix between two carrier films, top and bottom. The compacted sheet was then passed through thicknessing rollers to control the finished thickness of the sheet. The lay-up then passed over a preheated table at  $60^{\circ}C$ , which started the gelation process. As the gelation commenced, the sheet was moved forward into the oven section of the machine and over formers where it was formed into profiled sheet as required. After a predetermined time gelation was

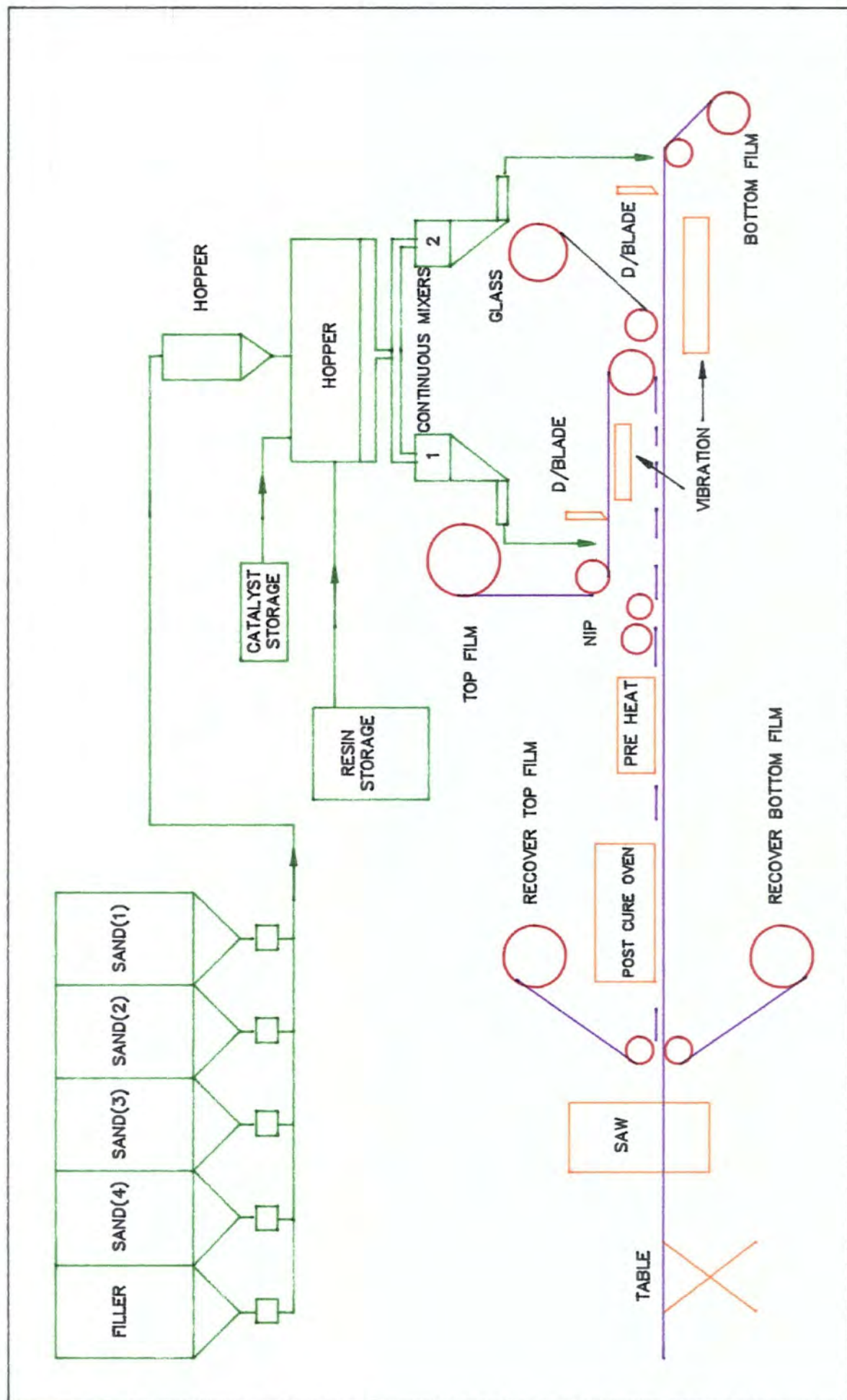


Fig.(8.4). The layout of a sheeting plant.

completed as the sheet left the last former. At this point the sheet passed into a hot oven at  $100^{\circ}\text{C}$  and was hardened due to the presence of the heat-reacting catalyst before leaving the ovens. Finally, the sheet was passed through an air cooled section to allow the sheet to be handled.

On emerging, the carrier film was stripped from the sheet. It was then edge trimmed and cut into standard lengths. Fig.(8.4) shows a lay out of the sheeting plant.

## **8.4 Test configurations**

### **8.4.1 Tests on small flat specimens**

All the specimens conformed to the geometry used in the tests previously explained in (3.5). They were 10mm wide, and were tested on a span of 450mm in four-point bending, with a pair of loads applied 113mm on either side of the centre of the specimen.

Load and deflection were recorded graphically by the Instron testing machine.

### **8.4.2 Bending tests on corrugated sheet**

All the specimens were tested in three point bending, over a span of 1170mm, with a central point load. The ends were supported on timber templates cut to fit the profile and the load was applied on a similar (female) template fitting into the corrugations. Both end supports and load were padded with dry sand so that differences between the templates and the sheet profiles were evened out smoothly.

The load was applied hydraulically, but measured by a proving ring. In some of the tests, deflections were measured by a pair of dial gauges mounted at equal distances on either side of the load template. Subsequently, in order to cope with the relatively large deflections, and also to monitor the horizontal as well as the vertical displacements of the specimens' outer edges, another technique was used; Theodolites **Kern DKMls** were set up 2m from the centre of span of the specimens so that they were sighting along one edge of the specimen. They were focused onto demec buttons attached to the specimen edges with adhesive, and were able to measure the vertical and lateral movement of the edges of the specimen.

Subsequent tests have been performed on similar specimens of asbestos reinforced cement, so that comparisons could be drawn between the mechanical properties of the two materials. The tests on the asbestos-cement used the same geometry of test specimen and the same loading procedure as before, except that the asbestos-cement specimens were thicker. This has been taken into account in the calculation of the mechanical properties.

## **8.5 Results and calculations**

The test results on small, flat specimens are shown in table (8.6), and the results in corrugated sheets are summarized in table (8.7). The deflection of the specimens which were measured using the theodolite was calculated as follows:

SPEC.NO	MIX NO:	REINFORCEMENT	$t$ (mm)	$W_f$ (N)	$W_u$ (N)	$\delta_f^2$ (N/mm)	$\delta_u^2$ (N/mm)	$E^2$ (N/mm)	DISPLACEMENT (mm)
2130	C	—	6.01	194	194	18.6	18.6	7940	15.5
2143	E	300 gr.MAT TOP & BOTTOM	6.54	338	640	26.7	50.6	7216	59.8
2146	D	300 gr.MAT TOP & BOTTOM	6.24	294	528	26.6	47.7	8350	54.4
2149	D	—	5.44	131	131	14.9	14.9	6618	14.3
2147	D	300 gr.MAT ● BOTTOM	4.54	76	125	12.4	20.4	8582	>70
2145	E	—	6.54	147	187	11.9	15.2	7554	14.9
2128	D	300 gr.MAT ● CENTER	7.85	254	484	14.4	27.4	7560	50.4
2141	E	300 gr.MAT ● CENTER	5.87	90	183	9.0	18.3	6721	>70
2142	E	450 gr.MAT ● CENTER	5.37	97	143	14.2	20.9	8091	>70
2184	A	300 gr.MAT ● BOTTOM	4.22	25	88	5.2	18.3	5321	>70

Table(8.6A). Test results on the small, flat specimens.

SPEC.NO	MIX NO:	REINFORCEMENT	$t$ (mm)	$W_f$ (N)	$W_u$ (N)	$\delta_f^2$ (N/mm)	$\delta_u^2$ (N/mm)	$E^2$ (N/mm)	DISPLACEMENT (mm)
2187	E	450 gr.MAT TOP & BOTTOM	4.48	95	141	16.7	24.8	9608	>70
2188	B	300 gr.MAT ● CENTER	4.67	83	114	13.1	18.0	8534	>70
2186	A	450 gr.MAT ● CENTER	4.29	40	65	7.9	12.6	4683	>70
2183	A	300 gr.MAT ● CENTER	4.53	32	64	6.0	12.0	2913	>70
4	G	300 gr.MAT ● CENTER	6.24	222	399	20.1	36.0	19110	>70
4.1	G	300 gr.MAT ● CENTER	5.44	156	239	17.7	27.1	15050	>70
4.2	F	450 gr.MAT ● CENTER	4.33	200	290	31.4	45.6	23000	>70
ASBESTOS CEMENT	—	—	6.30	270	290	26.9	28.9	22000	18
A	TT 10:1	300 gr.MAT ● CENTER	7.60	480	793	28.2	46.6	19300	52
B	SS 10:1	300 gr.MAT ● CENTER	7.62	538	826	31.4	48.2	21100	50

Table(8.6B). Test results on the small, flat specimens.

SPEC.NO	GROUP NO	MIX NO:	TYPE OF PROFILE	L (mm)	REINFORCEMENT	t (mm)	WIDTH (mm)	$\bar{Y}$ (mm)	I PER PITCH (mm <sup>4</sup> × 10 <sup>-8</sup> )	I TOTAL (mm <sup>4</sup> × 10 <sup>-8</sup> )
2163	1	A	1	1170	450 gr.MAT ● CENTER	4.98	420	34.3 TOP 10.7 BOTTOM	0.1673	0.4685
2170	2	B	2	"	350 gr.MAT ● CENTER	4.29	"	25.0	0.1766	0.4945
2171	"	"	"	"	"	4.42	"	"	0.1823	0.5104
2172	"	"	"	"	"	5.14	"	"	0.2115	0.5922
2173	"	"	"	"	"	5.31	"	"	0.2185	0.6118
2174	"	"	"	"	"	4.27	"	"	0.1757	0.4920
2175	3	A	"	"	"	4.89	"	22.5	0.2103	0.5636
2176	"	"	"	"	450 gr.MAT ● CENTER	4.26	"	"	0.1753	0.4908
2180	"	"	"	"	350 gr.MAT ● CENTER	4.19	"	"	0.1724	0.4827
2182A	4	C	"	"	"	4.67	"	"	0.1922	0.5382

Table(8.7A1).The results of the second moment of area & the position of the N.A. for the corrugated sheet specimens.

216

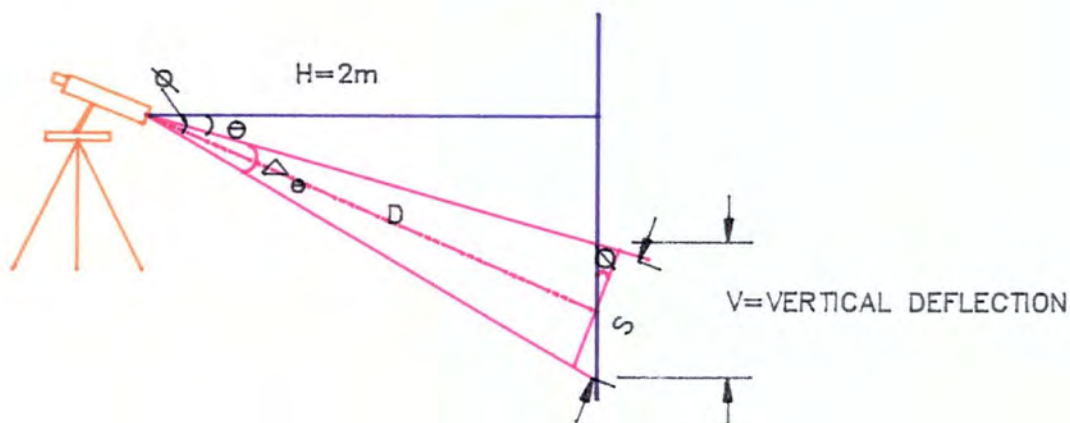
SPEC.NO	GROUP NO:	MIX NO:	TYPE OF PROFILE	L (mm)	REINFORCEMENT	t (mm)	WIDTH (mm)	$\bar{Y}$ (mm)	PER PITCH (mm $\times 10^{-6}$ )	TOTAL (mm $\times 10^{-8}$ )
2182G	4	C	2	1170	300 gr.MAT @ CENTER	5.19	420	22.5	0.2136	0.5981
2190	5	B	3	"	"	4.48	"	25.0	0.2190	0.7370
2191	"	"	"	"	"	4.79	"	"	0.2350	0.7890
2201	6	A	4	1420	"	4.56	415	20.0	0.1925	1.0000
2202	"	"	"	"	"	4.86	385	"	0.2051	0.9500
2203	"	"	"	"	"	4.74	405	"	0.2000	1.010
2204	"	"	"	"	"	4.86	380	"	0.2051	0.9700
2132 WRC A	7	H	2	1170	"	5.46	420	22.5	0.2247	0.6290
2132 WRC B	"	"	"	"	"	5.78	420	"	0.2378	0.6658
ASBESTOS CEMENT	8	—	"	980	"	6.53	450	"	0.2828	0.8100

Table(8.7A2). The results of the second moment of area & the position of the N.A. for the corrugated sheet specimens.

SPEC. NO:	SLOPE OF THE GRAPH (N/mm)	FAILURE LOAD (N)	ULTIMATE STRESS <sup>2</sup> (N/mm )	E <sup>2</sup> (N/mm )	ULTIMATE DEFLECTION (mm)
2163	59.26	1722	36.88 TOP 11.5 BOTTOM	4226	>70
2170	64.82	1567	23.18	4368	35
2171	80.81	1722	24.67	5290	44
2172	34.19	1278	15.78	1925	73 \$
2173	79.37	1945	23.24	4331	52
2174	67.64	1333	19.81	4593	25
2175	41.67	1389	16.22	2466	45
2176	43.70	1639	21.98	2975	60
2180	39.07	1556	21.21	2693	56
2182A	66.07	1667	20.38	4125	45
2182G	39.69	1389	15.28	2207	40
2190	49.39	1500	19.88	2239	36
2191	51.29	1611	14.93	2167	38
2201	32.02	1017	7.22	1912	>70
2202	28.33	842	6.10	1728	>70
2203	34.03	1189	8.36	2013	>70
2204	32.35	1276	9.34	1986	>70
2132WRC A	296.3	2498	26.13	15692	57
2132WRC B	309.4	2387	23.59	15500	50
ASBESTOS CEMENT	525.29	2500	17.01	12716	7

\$=Specimen slightly damaged and distorted.

Table(8.7B). The results of the ultimate stress & the modulus for the corrugated sheet specimens.



$$\phi = \theta + \frac{\delta\theta}{2}$$

$$D = \frac{H}{\cos \phi}$$

$$\tan\left(\frac{\delta\theta}{2}\right) = \frac{S}{2 \times D}$$

Therefore:

$$S = 2 \times D \times \tan\left(\frac{\delta\theta}{2}\right)$$

But

$$\cos \phi = \frac{\frac{S}{2}}{\frac{V}{2}}$$

Or

$$V = \frac{S}{\cos \phi}$$

Or

$$V = \frac{2H \tan\left(\frac{\delta\theta}{2}\right)}{\cos^2 \phi} \quad 8.1$$

Also

$$\text{Horizontal deflection} = 2 \times \tan \theta \quad 8.2$$

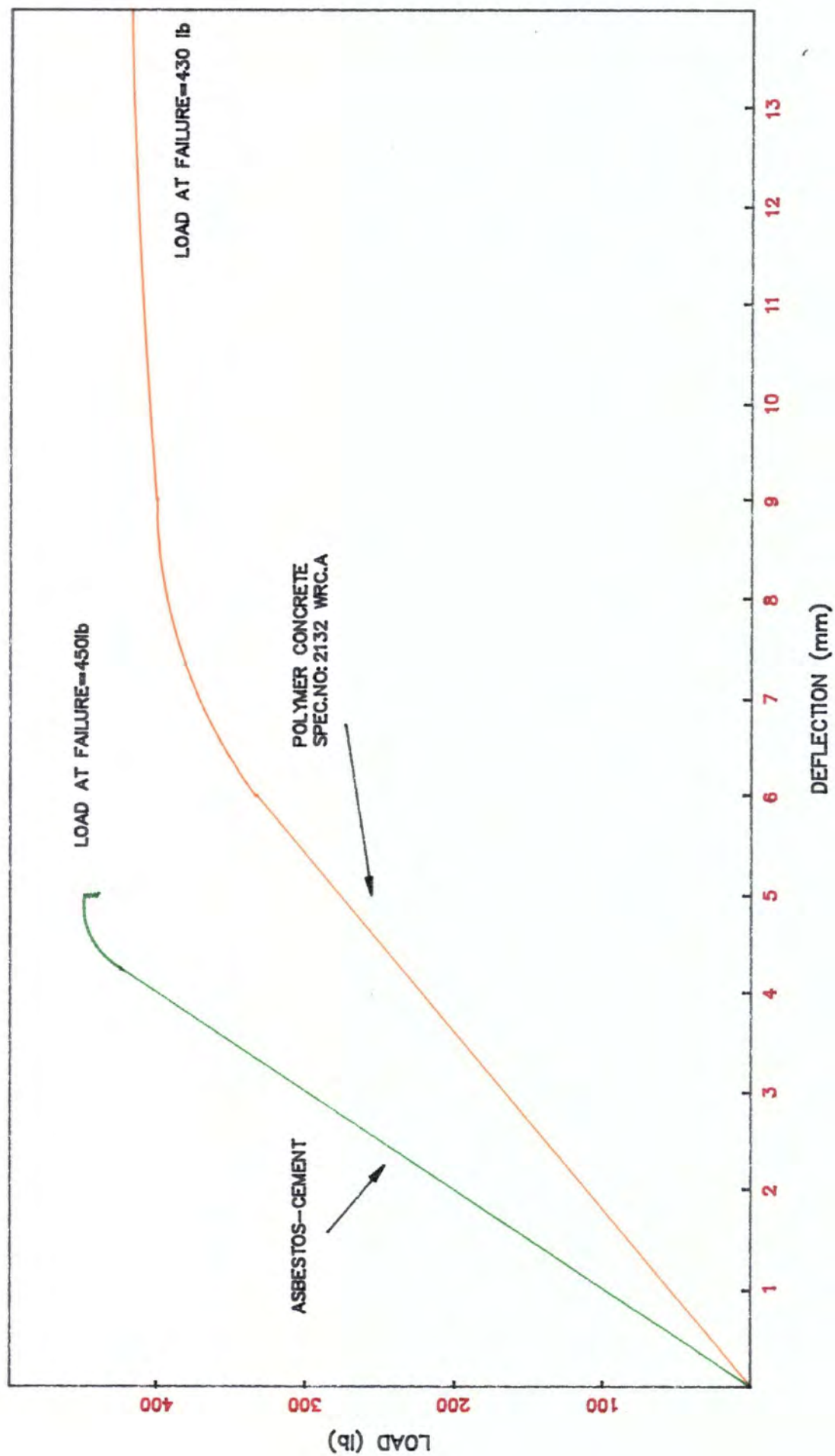


Fig.(8.8). Comparison between the Asbestos-cement & the Polymer concrete sheets.

The elastic moduli were calculated by obtaining the value of EI from the slope of the load-deflection graph. A specially written computer programme was used to calculate the 2nd moment of area of the profile from the measured geometry, and the elastic modulus was deduced from the following expression:

$$E = \frac{WL^3}{48 \times I \times \delta}$$

Or

$$E = \text{slop of the graph} \times \frac{L^3}{48 \times I} \quad 8.3$$

and the stress from:

$$\sigma = \frac{M}{I} \times \hat{Y}$$

Or

$$\sigma = \frac{WL}{4I} \times \hat{Y}$$

A typical load-deflection graph for specimens no: 2173,2132 WRC and asbestos-cement are shown in fig.(8.8).

## 8.6 Commentson the results

### 8.6.1 Small flat specimens

After reviewing the results of the tests on the small flat samples cut from sheets made in the pilot runs at Alton, the following comments can be made, (Again it has to be born in mind that the specimens were made from the initial trial mixes.)

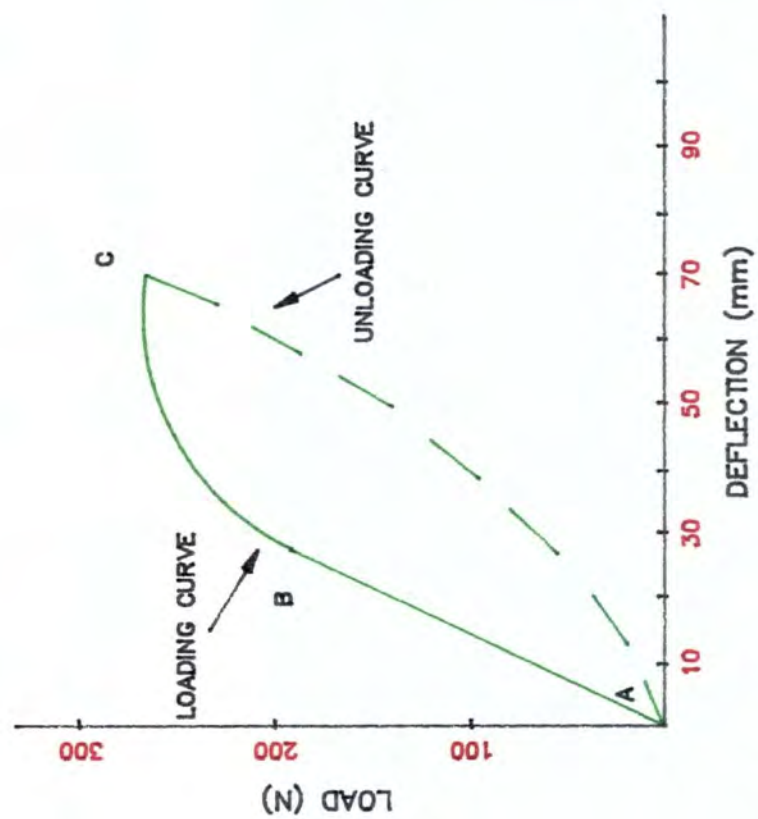
The results showed the wide variation in properties over the range of samples. Sample 2183 had a low modulus and much the best result was from sample 2187 giving a modulus of  $9.6 \times 10^9 N/m^2$  and an ultimate stress of about  $25 N/mm^2$ . Another significant factor that has to be noted is the range of displacement of the specimens reinforced with fibre glass before failure. In most cases the displacements were greater than 70mm without any type of failure.

However, these results should be compared with the specimens No 4, 4.1, 4.2 (ratio 3.5:1) which had their mixes designed at Durham University during the initial stage of this research and were constructed in a previous manner, and also with specimens No A and B (hand made, ratio 10:1) which were designed later as a final recommended mix. The modulus and ultimate stresses were in the range of  $22 \times 10^9 N/m^2$  and  $46 N/mm^2$  respectively.

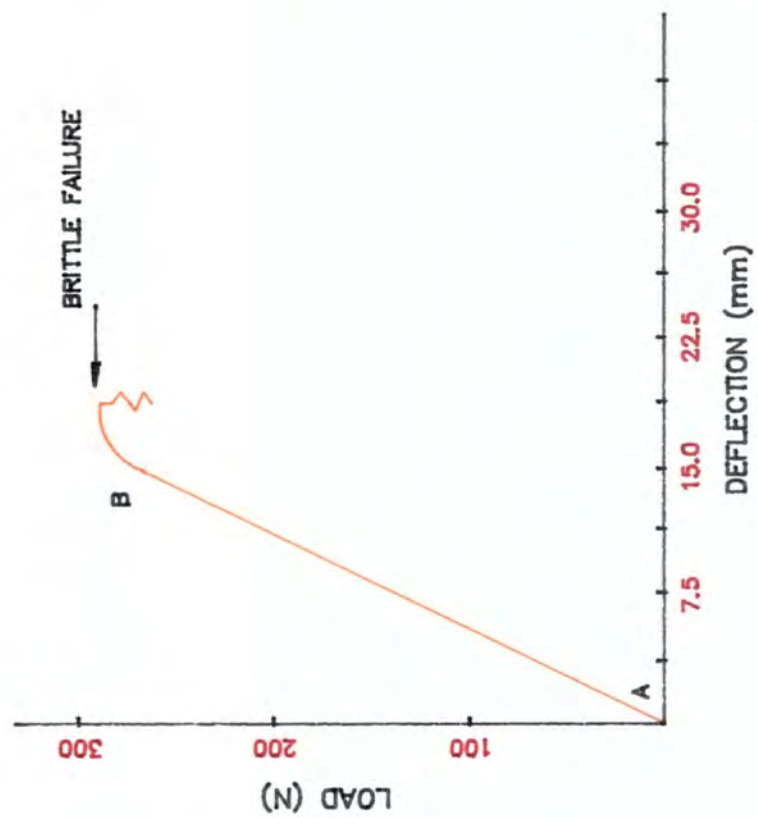
The two load/displacement curves for specimen 4.2 and asbestos-cement are shown in fig (8.9).

It will be seen that the polymer concrete specimens exhibited the familiar properties of the 'elastic' section of the curve (AB), the cracking failure at B and then the continued flexure (BC) to a large displacement under a lower rate of increase of the load, and eventually recovered to almost zero extension along a 'visco-elastic' curve. A further test of the same specimen would have produced a repeat of the curve with a smaller elastic slope and a lower 'cracking stress'.

The asbestos-cement specimens all behaved in a typically brittle fashion. The curve shows only 'elastic' behaviour (AB), with a complete fracture of the specimen



Fig(8.9A). Polymer concrete,specimen(4.2)



Fig(8.9B). Asbestos-cement specimen.

at B. Of course, there can be no plastic extension, no recovery, and no possibility of repeat loading.

A comparison will show that the bending stiffness of the two materials was similar, with modulus values of about  $22 \times 10^9 N/mm^2$  for both, but the failure stress of the polymer concrete was 1.6 times as high as that of the asbestos-cement;  $45.6 N/mm^2$  against  $28.9 N/mm^2$ .

### 8.6.2 Corrugated specimens

In discussing the results one must notice, first, the wide variation in modulus and in stress for each of the groups of specimens. Next it can be seen that whereas the stresses lie well within the range of the previous set of results (small, flat specimens), the moduli are constantly much lower. This is probably attributed to a combination of two major effects.

- i. the tendency for the relatively flexible corrugated samples to 'spread' as they deformed, and
- ii. the effect of the difference in the compression and tension elastic moduli.

This shows the importance of using the tests, as far as possible, to compare like with like, and is the reason for the separate test on a section of corrugated asbestos-cement sheet of the same profile.

Specimen 2163 was of the profile which consists of quite long, flat sections separated by stiff, narrow ridges, and was tested with large flats on the bottom and the ridges protruding upwards. The section was obviously very stiff laterally, in the

sense that it would have little or no tendency to 'spread' like the more conventional profiles. In the event, it did not do so, and the modulus value was exactly in the range of values shown by the flat specimen or similar material. The specimen failed in tension, like the others. The neutral axis was about one third of the way up the section, indicating that the compressive stress in the tops of the ridges was in excess of  $36N/mm^2$  when the flats failed in tension at about  $11.5N/mm^2$ . (the ultimate stress for the small flat specimen with the same mix was  $12.8N/mm^2$ ).

The bending elastic modulus for one of the groups of specimens, those numbered 2170 to 2174, was in about the same proportion to that of asbestos-cement, as had been shown in the small-specimen tests, ie; about 2.5 times lower; while their ultimate stress was about 40% higher. The advantage of the greater strength is obvious. However, the greater flexibility may also be viewed as being not really detrimental, since the relatively large deflections which would be felt under a human foot load would serve to deter a person straying onto a roof without proper local support, and the deflections would be largely recoverable without fracture.

The profile of specimens group (3) were similar to group (2) but using mix no.(A). The bending elastic modulus were quite low compared with the previous groups.

The two specimens 2190 and 2192 of group (5) are examples of the quasielliptical profile. The appearance of these specimens under the test suggested that their moduli are both quite low. In fact the specimens were of a profile which could be expected to be quite flexible laterally if not constrained. However, the specimens

in group (7) which were made with the mix no.(H), appeared to be better than the others. The moduli were about 20% and the ultimate stress about 50% higher than the asbestos - cement sheet.

## 8.7 Conclusions

Possibly the greatest significance is the extreme brittleness of the asbestos-cement compared with the ability of the polymer concrete to deform plastically long after the onset of cracking. Of course, this is the purpose and function of the glass mat reinforcement in the polymer concrete, without which it would probably be stronger than the asbestos-cement but equally brittle.

In practice, the great advantage given to the polymer concrete by its comparative lack of brittleness is its ability to accept conditions producing local failure without the failure 'running away' and producing a total catastrophic collapse. Thus a local impact, such as that given by a falling tile or a local failure under heavy sustained load, such as that under a man's boot, causes catastrophic failure in an asbestos-cement sheet. On the other hand, the polymer concrete sheet would dent temporarily, even be permanently weakened, but would not collapse suddenly, and may not even collapse at all if the offending load were to be removed.

The later development work produced mixes (eg. TT mix) from which some small flexural specimens were made and tested and gave results which demonstrated clearly how successful the product can be from the points of view of ease of pro-

duction and technical performance.

Finally a finite element analysis was carried out by means of the available **PAFEC 75** computer programme (see appendix 8), to see first of all, if there is any tendency for the corrugated sheets to spread as they deformed, and secondly by what ratio it would effect the calculated 'I' values before loading.

A sample with profile No. (2) and with thickness of 8mm with 'E' value of  $22000 \text{ N/mm}^2$  was considered at this analysis. The results of the computer analysis (see appendix 8) show that, there is a tendency for the corrugated sheets to spread, causing the I value before loading, to be reduced by a factor of (0.61). Therefore the previous calculated 'E' values for the corrugated sheets with the same profile have to be adjusted by a factor of 1.64 (ie;  $1/0.61$ ), for taking into account the effect of spreading under this load.

# CHAPTER (9)

## CHAPTER NINE

### 9. Racking tests on a bungalow

#### 9.1 Introduction (prefabricated housing system)

The prefabricated housing system (polymer concrete) comprises a range of interlocking panels which are erected within a 600mm planning grid to form a simple structure of variable perimeter. The range of panels includes corner, door and window panels and plain panels.

The wall panels are joined together by fitting the tongue of one of the wall panels within the groove of the adjacent panel (fig.9.1). The groove of the joint is coated with an intumescent mastic 'Nullifire' prior to fitting the wall panels. A soft-wood horizontal rail of overall section size 60mm by 50mm is fitted across the top of the wall assembly within the rebate at the top edge of the wall panels. The rail is fixed to each wall panel by a total of three expanding steel anchors which are passed through the top edge of the wall panels and into the core material.

A mild steel angle of size 150mm long by 50mm flanges by 4mm thick is fixed to the bottom of the internal face of each wall panel at a nominal distance of 200mm from each vertical edge of the wall panel. The upstanding flange of the angle is fixed to the wall panel with two steel multi connectors and the other flange is fixed to the concrete load-spreading beam with a single expanding steel bolt.

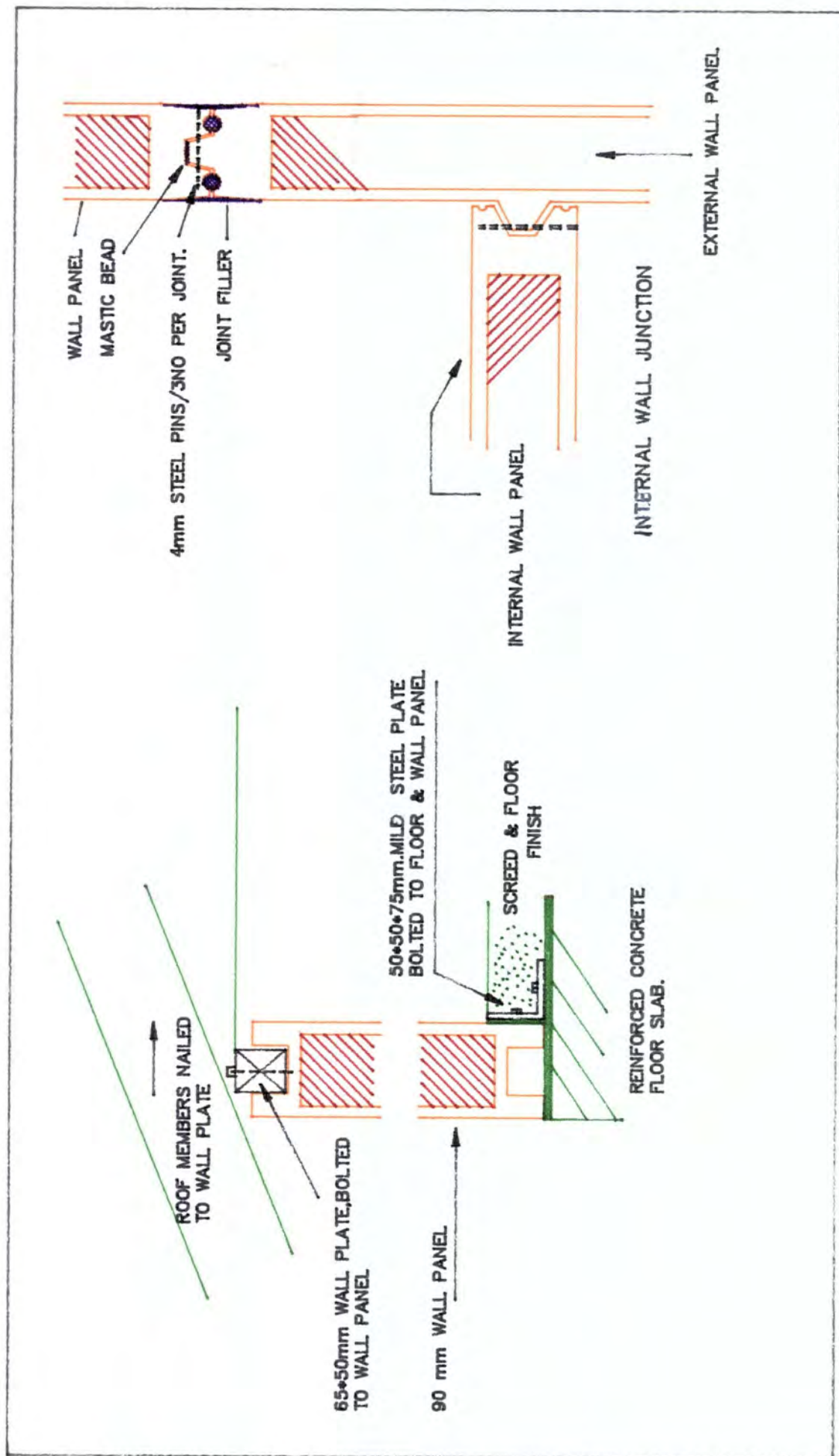
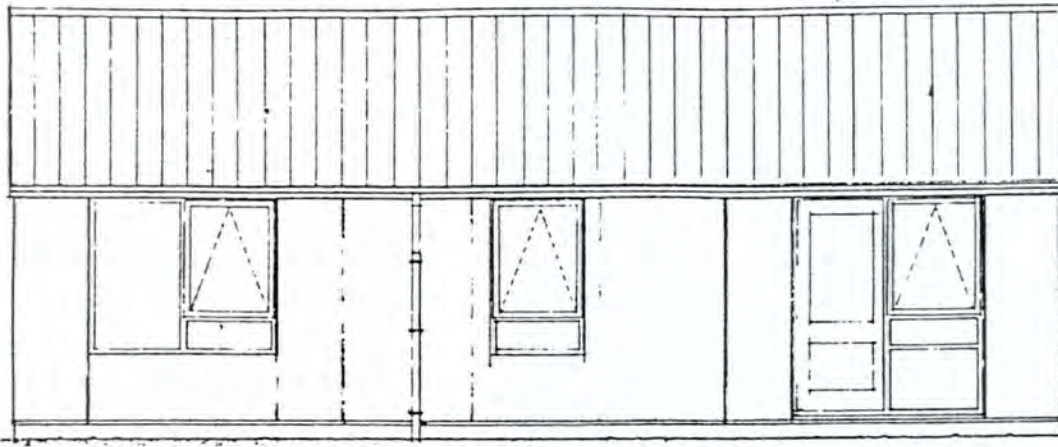


Fig.(9.1). Typical junction.



Front Elevation

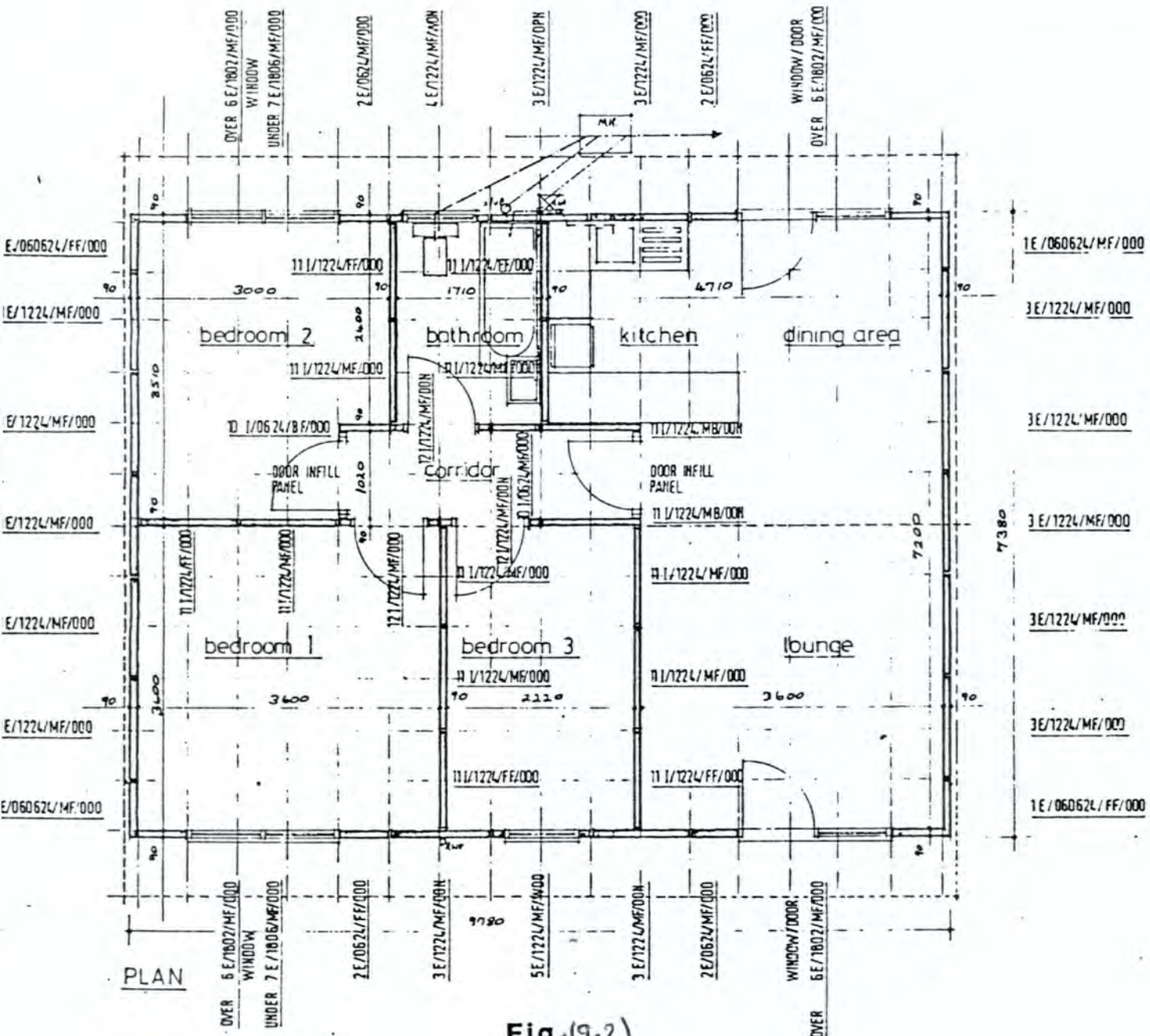


Fig.(9-2)

Plan and Elevation

A range of surface finishes may be applied to the panels either during or after manufacture to suit either internal or external applications.

## **9.2 The test structure**

The test structure was originally built as a 'show house' in February, 1981, but has been used for most of its life as an office and laboratory. The house rested on a site-concrete slab which projected about 200mm clear of the walls on all sides. The walls were surfaced to resemble a rendered and pebble-dashed finish, with 9mm single size limestone chippings. The roof was a conventional timber-frame structure, using prefabricated timber trusses, concrete tile cladding and a plaster-board ceiling throughout. Large window openings were cast into the panels at the front and back, and at each end of the main room, which was at one end of the building, french-window openings were spanned by reinforced box beam lintols.

The two gable walls were left plain, with no interruption of the standard, plain sandwich panels. The interior space was divided in a way suitable for a three bedroomed dwelling, and had been fully equiped as such. Fig (9.2) shows the plan and elevations diagrammatically.

The building was situated in the forecourt of a typical Northern heavy industrial site and therefore subjected to considerable aerial polution but was well protected from wind and weather by surrounding structures.

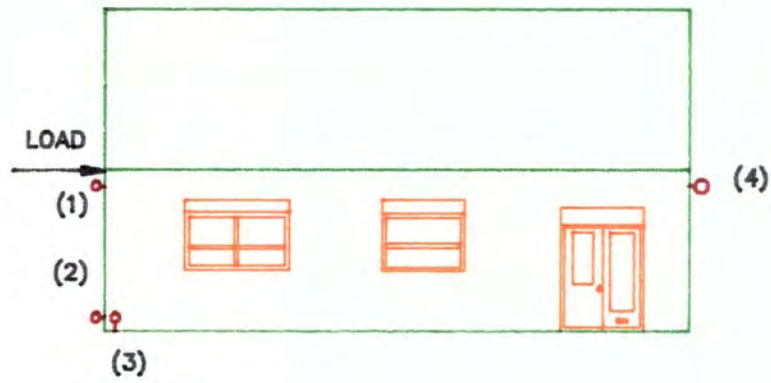


FIG.(9.3A)  
GAUGE LOCATIONS  
LOAD IN LINE WITH EAVES



FIG.(9.3B)  
GAUGE LOCATIONS  
LOAD IN LINE WITH GABLE

### 9.3 Test conditions

It was decided that horizontal loads would be applied at eaves level, on the gable end with the load applied along the eaves direction, and on the rear wall with the load applied along the gable wall at eaves level. The required load magnitude was assessed by calculating the optimum wind force on the gable and allocating a proportion of this to each gable at eaves level. This was considered to be the optimum working load for the test. The load was increased slowly up to this magnitude and then released slowly. This was repeated once, and then the load was increased slowly up to 3 times this value as a proof load. Throughout each load cycle the deflections of the building were measured at a series of locations. The position and orientation of the deflection gauges are shown in fig.(9.3A) for the loading along the eaves and fig.(9.3B) for the loading along the gable.

An abstract of the calculations to determine the load magnitudes is given below. In the event it was found that the load cell was still calibrated in pounds and some rounding up of the test figures was allowed for convenience on the site.

Wind conditions; (see Appendix 6)

$$V = 52m/sec$$

$$V_{s(roof)} = 43.16m/sec \quad , \quad q_{roof} = 1.14KN$$

$$V_{s(wall)} = 40.56m/sec \quad , \quad q_{wall} = 1.01KN$$

Gable forces;

Total force on gable (wind ward)=18.6 KN

Total force on gable (lee ward)=5.31 KN

Total force=23.91 KN

Approximate force applied along eaves= $\frac{23.91}{4}=5.98$  KN

=1339 lb

3 × working load, ie; proof load=4000 lb (approx.)

Eaves forces;

Maximum horizontal force from roof wind loading = 0.1 KN/m

$load/panel = 0.1 \times 1.2 = 0.12$  KN

maximum horizontal force on a wall panel= $2.8 \times 1.2 = 3.36$  KN

With maximum spacing of cross-walls being 3 panels:

load at eaves level of cross-wall (or gable)= $(\frac{3.36}{2} + 0.12) \times \frac{3}{2} = 2.7$  KN

Although this is much less than the working load calculated for the gable it was decided that the higher load should be applied in each case. For convenience on site, the following load cycle was applied in each case:

1. load slowly increased to 2000 lb and then released

2. repeat
3. load slowly increased to 4000 lb
4. load slowly increased further to seek first sign of failure.

## 9.4 Test equipment

Two frameworks were constructed to carry the hydraulic jacks used to apply the horizontal loads. These were designed and built by a local scaffold erector (Deborah Scaffolding Teesside Ltd). The principal members were made from scaffold ladder frame. A pair of vertical members were supported at their tops by racking members at  $30^\circ$  to the horizontal. The vertical members were held down by Kentlidge supported pairs of ladder-frames spanning between the verticals near to the ground, and the horizontal load jack was held by a universal beam section between the tops of the verticals. The frame is illustrated diagrammatically in fig.(9.4).

Loads were generated by a 50 KN hydraulic jack operated by a hand pump mounted on the base of the frame. Load measurement was achieved by a load-cell attached to the jack and read from a meter mounted by the pump. The load was applied onto a stiff steel plate attached to the wall, so that there would not be a problem with the local crushing of the sandwich material of the wall.

All the deflections were measured by large dial gauges, which were supported on independant scaffold frames and registered on to steel angle brackets screwed onto the walls. In each case gauge No:1, which recorded the displacement proximate to

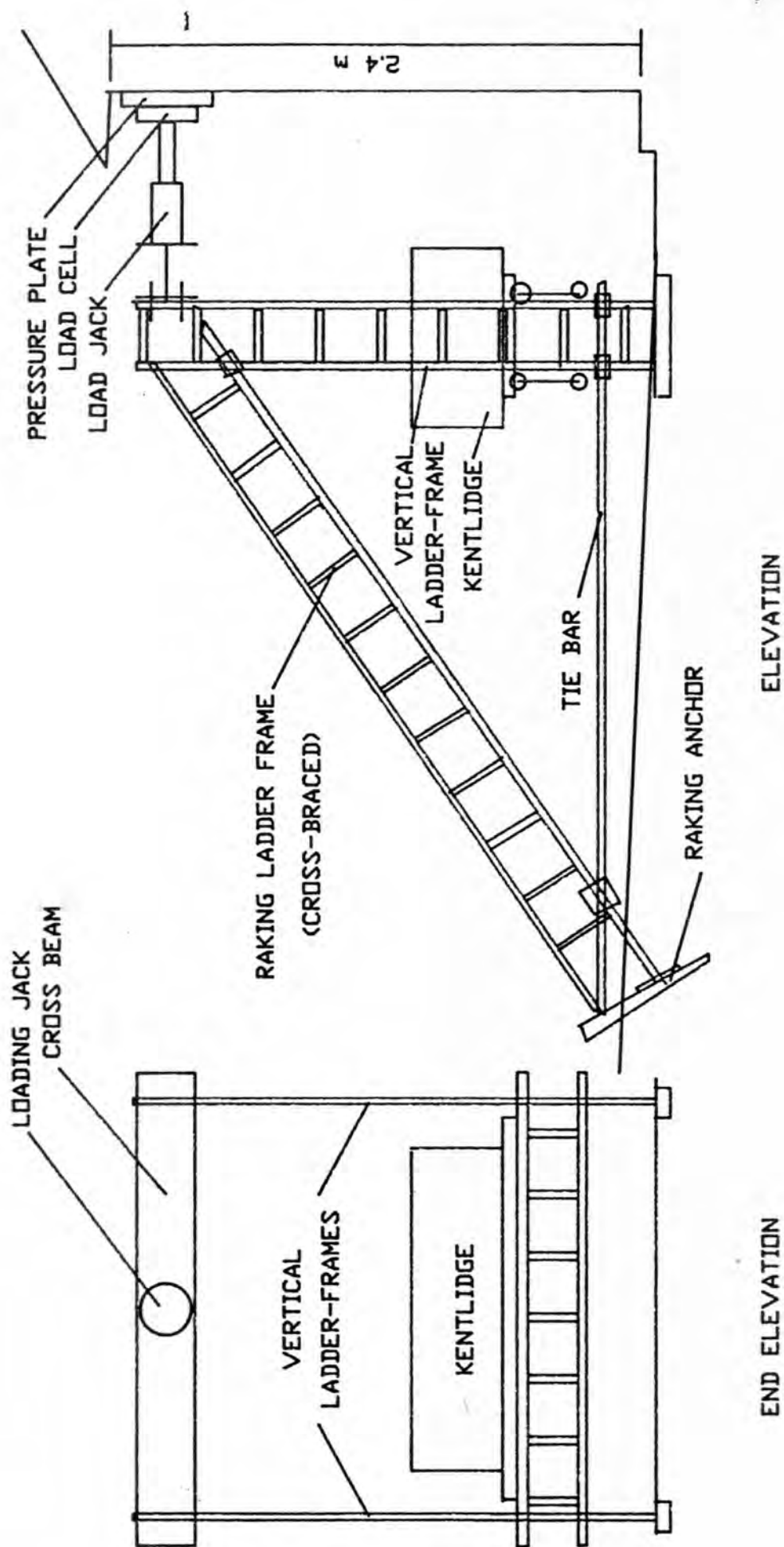


FIG. (9.4)

DIAGRAM OF LOADING FRAME

the load, was registered on a separate plate from the load itself, so that it did not show any local crushing under the load plate.

## 9.5 Test results

Table (9.5A) refers to the test with the load directed along the eaves and shows the values of displacement recorded by all the gauges tabulated against the applied loads. Table (9.5B) shows the values for the test with load along the gable.

The results are further illustrated in graph (9.6) which displays the load/displacement behaviour for the load-point gauge in the first test, and also shows the behaviour of the gauge at the base of the wall at the loaded end in the second test.

All the displacement readings represent the stable condition of displacement, when all observable movement has ceased.

## 9.6 Conclusions

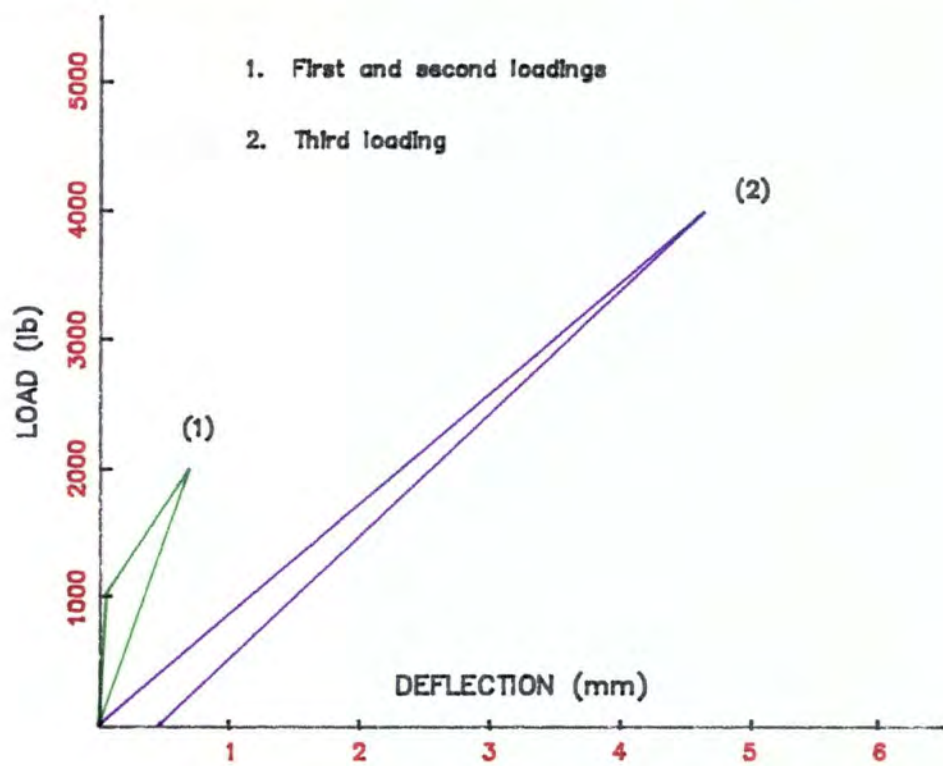
It is seen that within the limits of accuracy available, and apart from small 'bedding-in' displacement, the deflections of the building under repeated working load are small and recoverable. The behaviour of the building in the highest winds predicted would be entirely satisfactory. Interpretation of the results for the proof loading shows that at loads near proof load there appears to be some slight adjustment of the building components. The results are commensurate with the effect of the closing up of the joints and general small settling movements of the individual

LOAD (lb)	DISPLACEMENT (mm)			
	gauge(1)	gauge(2)	gauge(3)	gauge(4)
0	0	0	0	0
1000	0.02	0.01	0.10	0.10
2000	0.72	0.35	0.38	0.27
0	0.01	0.12	0.10	0.05
1000	0.02	0.24	0.20	0.14
2000	0.71	0.38	0.40	0.27
0	0.01	0.15	0.12	0.07
4000	4.65	1.10	1.60	0.91
0	0.48	0.65	0.28	0.21

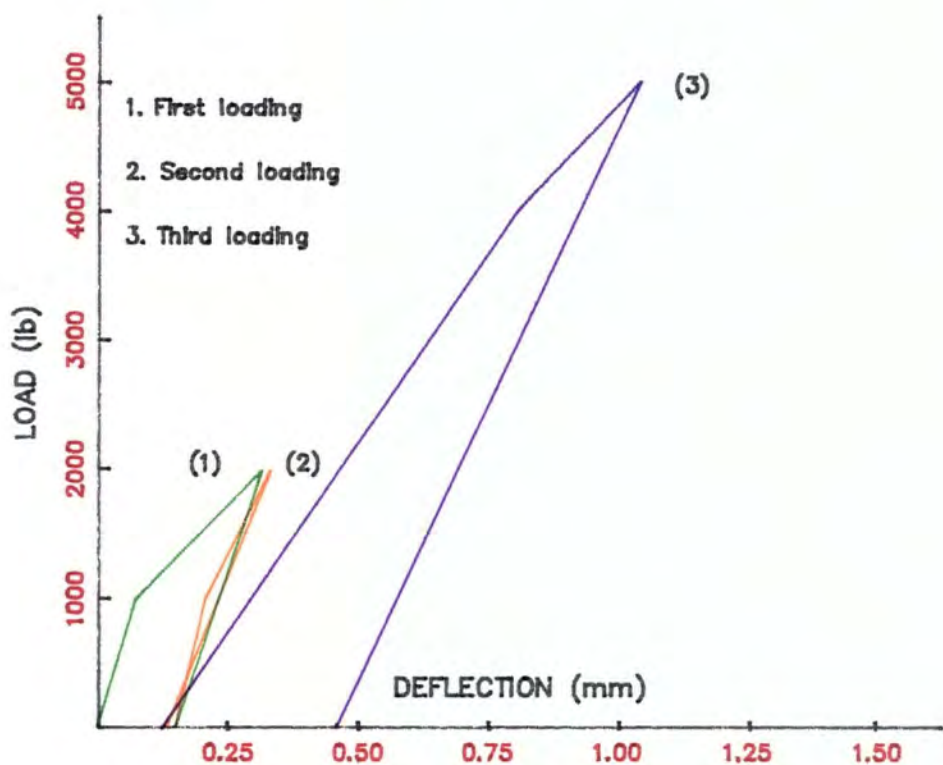
Table(9.5A). Loads and displacement (Load along the eaves)

LOAD (lb)	DISPLACEMENT (mm)				
	gauge(1)	gauge(2)	gauge(3)	gauge(4)	gauge(5)
0	0	0	0	0	0
1000	0.09	0.01	0	0	0
2000	0.31	0.02	0.04	0.01	0.01
0	0.16	0	0.02	0	0.02
1000	0.21	0.01	0.02	-0.01	0.02
2000	0.34	0.02	0.04	0.01	0.03
0	0.14	0	0.02	-0.14	0.03
4000	0.82	0.06	0.14	0.13	0.03
5000	1.05	0.12	0.21	0.40	0.03
0	0.47	0.04	0.06	-0.03	0.03

Table(9.5B). Loads and displacement (Load along the gable)



LOAD ALONG THE EAVES.



LOAD ALONG THE GABLE.

Fig.(9.6).Racking tests (Displacement for dial gauge NO:1)

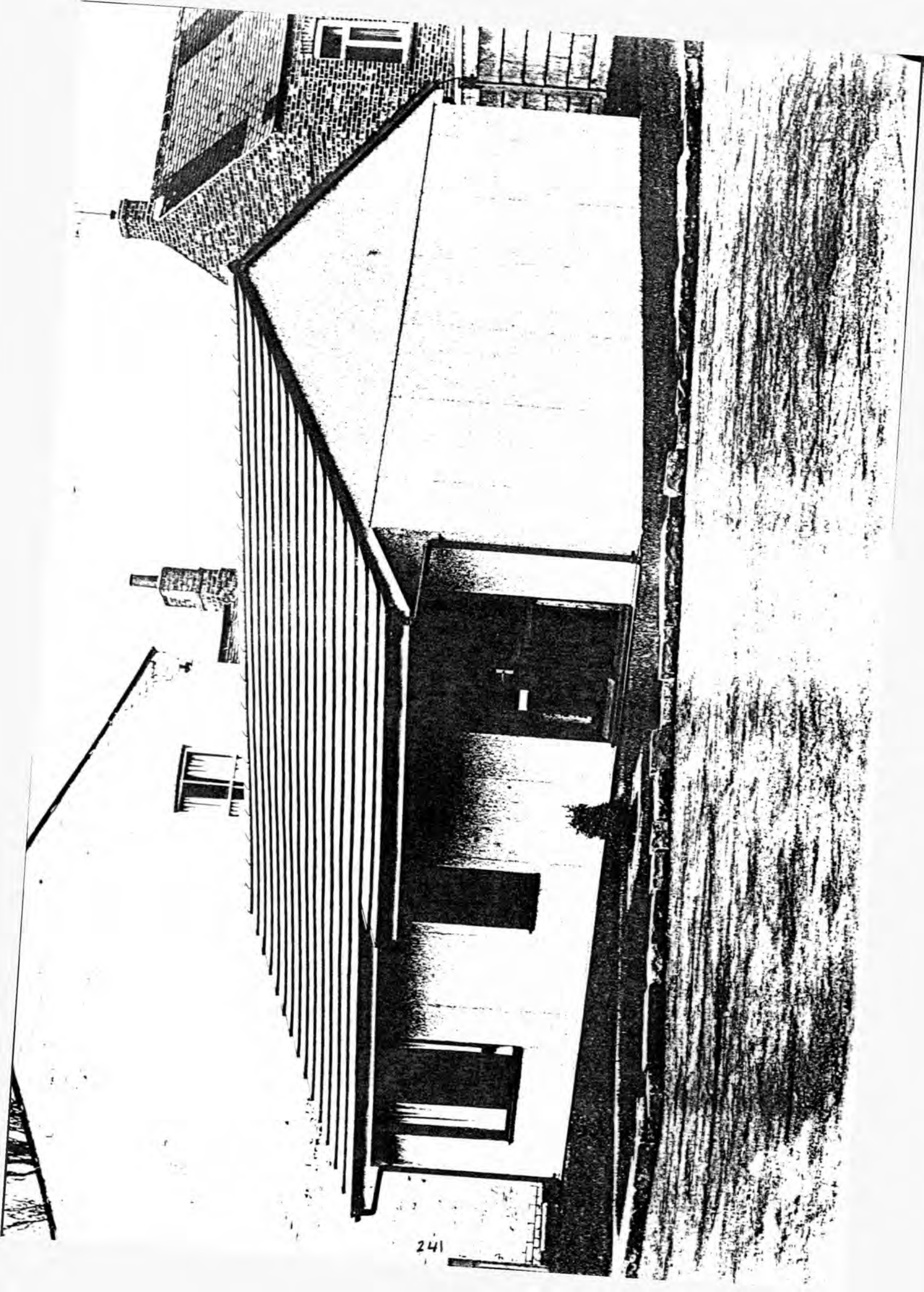
components. However, even under the highest load of 5000 lb (over 22.25 KN) the deflections settled down almost instantaneously to a steady state. The movements were having the effect of locking the structures more firmly together.

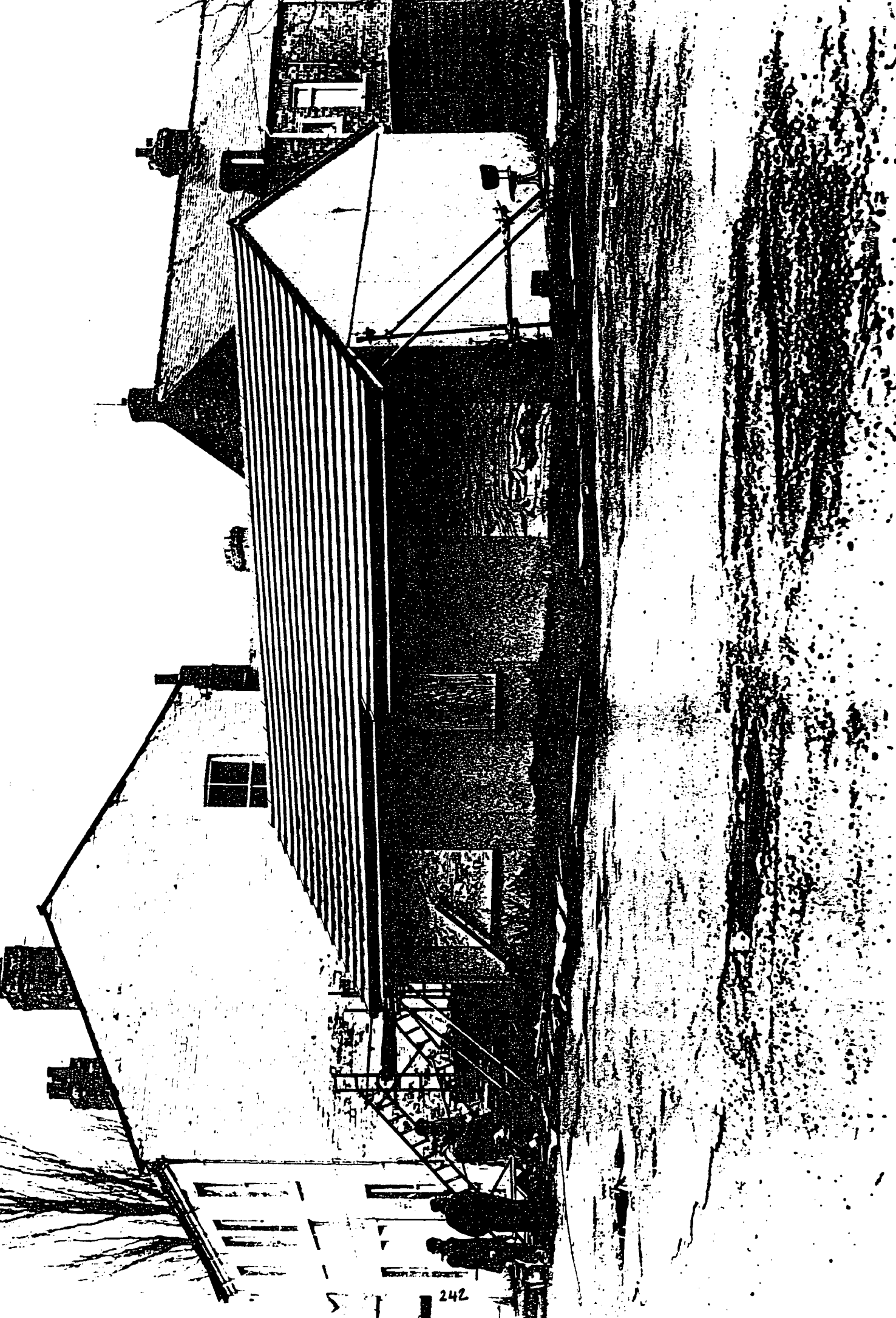
It is worth noting, at this juncture, that when this bungalow was built it was not intended that it should remain permanently in its present location and in consequence the tongue-and-groove joints between the wall slabs were left dry, instead of being grouted, as would be done in a more permanent construction. The proof loading must be seen, therefore, as a test on the worst possible state of this kind of structure. Some tightening of the components would be inevitable at some stage, and would be less likely to happen in the grouted building.

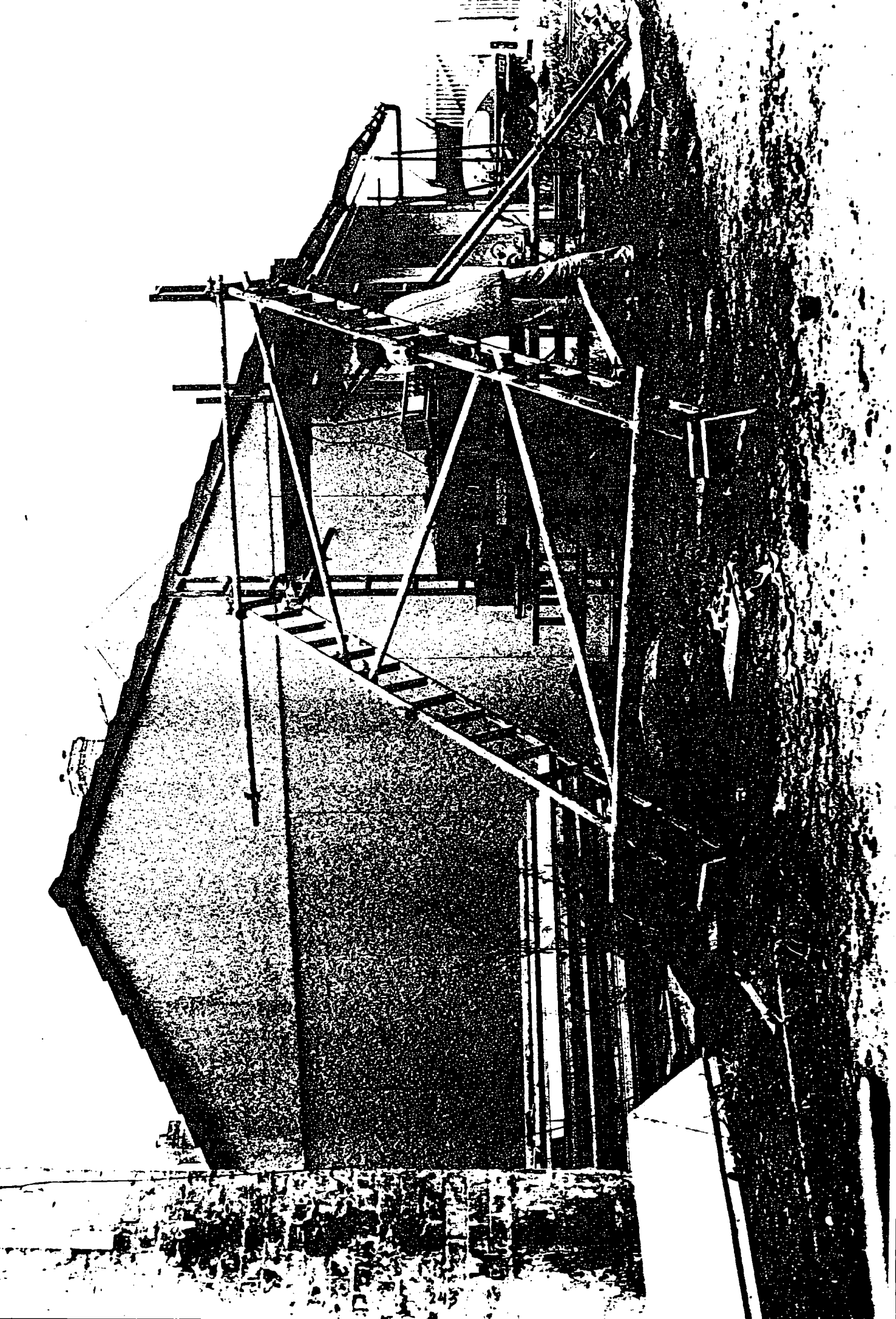
The building has performed very well in these tests, which have shown that there is a satisfactory resistance to racking in an array of the wall slabs, when they are under normal amount of superimposed loading from above, ie; from the roof load.

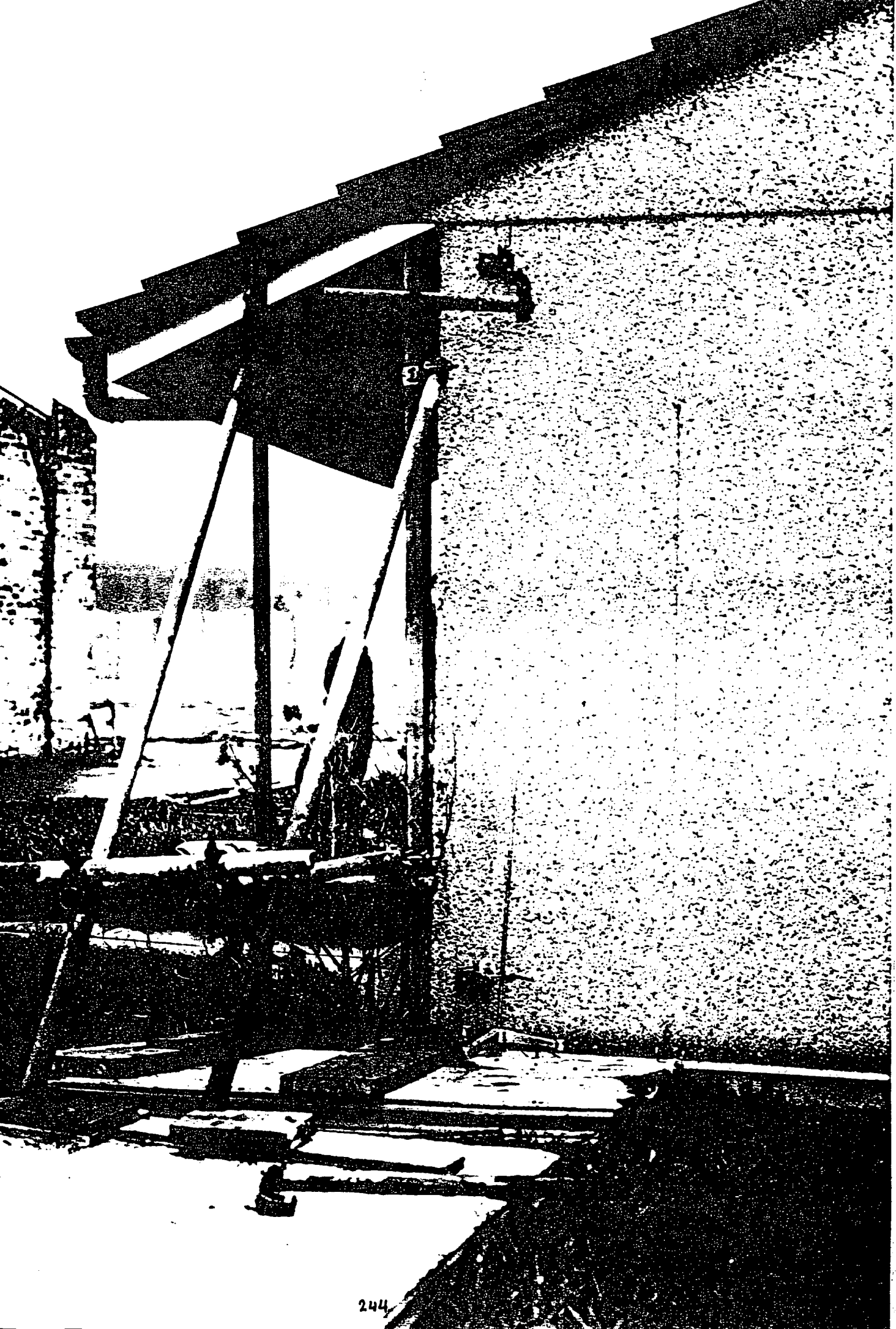
The building remained apparently undamaged after these tests. It was the original intention to increase the load until some damage was apparent. It is unfortunate that this intention was thwarted by the slipping of the loading frame at about 5500 lb(22.5 KN) in the first test and about 4500 lb(18.45 KN) in the second test because of the reorganisation of the frame required in order to mount the Kentledge.

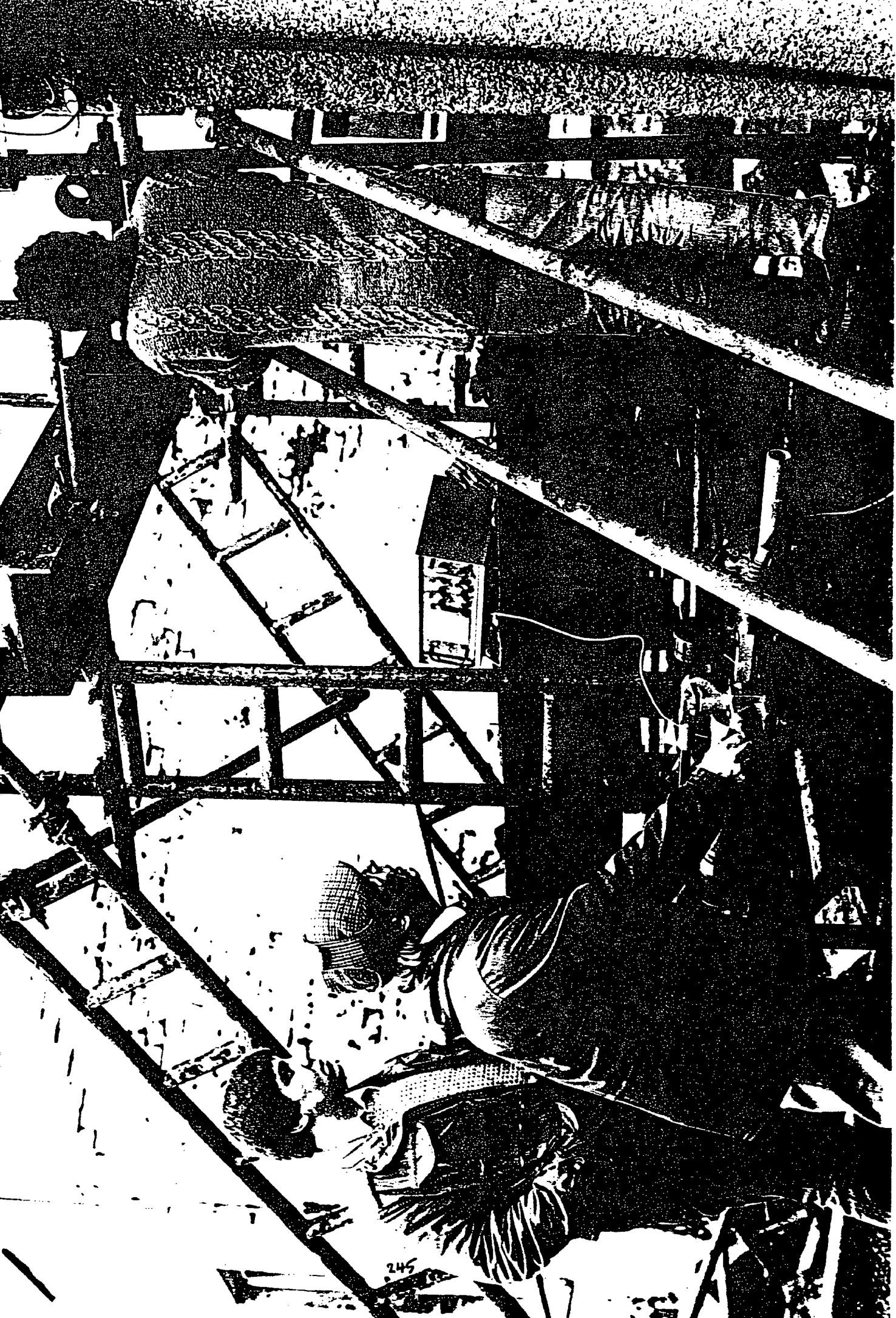
The following photos were taken during the racking test on the bungalow.











# CHAPTER (10)

## CHAPTER TEN

### 10. Phenolic resin

#### 10.1 Introduction

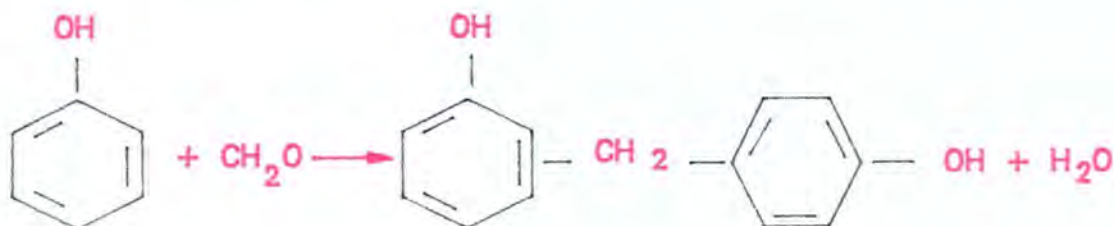
Phenolic resins are the oldest known plastic material (1872), and yet they are equally applicable to the most recent of techniques, such as reinforced reaction injection moulding. The phenolics are rigid, strong, and have excellent resistance to moisture, and very good high-temperature properties. When combined or alloyed with other adhesive systems, they become excellent structural adhesives and are widely used in this manner throughout the aerospace industry.

#### 10.2 Chemical nature of phenolic resin systems

Phenolic resin fall into two categories. These are normally termed **resol** or 'one step' resins, and **novolak** or 'two step' resins.

Resol resins may be cured by the application of heat alone, or at ambient temperature, if a strong acid catalyst is used, whilst novolaks require the addition of an aldehyde donor to complete their cure. Both are made by the condensation of a **phenol** and an **aldehyde**; the commonest *phenol* being itself and the commonest aldehyde being *formaldehyde*.

The reaction may be written as follows:



### 10.3 Test results and comments

Because of the very good high-temperature properties of the phenolic resins, attempts were made to construct a polymer concrete using this resin. In the first attempt, filler (pozzolan) or (B.L.H) was used with no success of curing.

After an inspection it was discovered that the problem was due to the high 'PH' value for these fillers. Some of the fillers which were found to be suitable for this application were; *silica flour, china clay and ballotini*.

Samples as (3.5) were made and tested with a little success (maximum ratio of agg/resin 7:1). The maximum modulus values were somewhere between 2000 – 7000  $\text{N/mm}^2$  with the ultimate stress of 4 – 12  $\text{N/mm}^2$ .

All the samples were cured for 24 hrs.in an oven at  $70^\circ\text{C}$ . Some of the samples were tested after removing them from the oven while some were left for another 3 days at room temperature. It was puzzling that the result of the test for the latter group were lower than for the first group. It seemed that their stiffness decreased with respect to time and they became plastically flexible at room temperature. Some of these samples were placed in the oven for a second time and they seemed

to gain some strength.

All the samples were not reinforced with fibreglass as almost all the available glasses had been coated, bound or surface treated. Interaction of the chemicals used in such treatment with resol/acid system retard cure of the resin. However, suitable glasses for the system do exist and the glass manufacturers are, in general, aware of the problem.

Due to the above problems further investigations are required for using phenolic resin which are not in the scope of this thesis.

# CHAPTER (11)

## CHAPTER ELEVEN

### Conclusions

In selecting the material for making the polymer concrete, care must be taken to achieve the following requirements:

- a. High ratio of aggregate to resin
- b. Workable mix for ease of flow
- c. High strength and modulus
- d. Curing time within a reasonable time

It should be remembered that in practice the aggregate available locally or within an economic distance has to be used. Both gap-graded and continuously graded aggregate can be used to make a good workable polymer concrete, but in each case the right % of aggregate and micro filler has to be chosen. Thus it can be seen that we should not aim at any ideal grading but find the best combination of the available aggregate.

In a mix, the ability to take fillers is a matter of chemical surface interaction of polyester resin and filler, and inter-particle forces in the dispersed filler. Some fillers agglomerate and precipitate, some stay finely dispersed. The **pozzolan** proved to be of latter sort, and resin **L.V.M** was the most suitable one for mixing with this filler.

Mix **SS** and **TT** with the maximum aggregate size of  $2400\mu m$  and  $1200\mu m$

respectively, using resin(L.V.M) and filler pozzolan, proved to be the best combination for producing the polymer concrete with the agg/resin ratio as high as 11:1 with reasonable workability, and maximum modulus value of  $27000N/mm^2$  and ultimate stress of  $49N/mm^2$ , when reinforced with fibre glass. Filler (B.L.H) proved to be the second best filler, after pozzolan for using in polymer concrete.

The catalyst level has direct effect on curing time and strength of the polymer concrete. The correct ratio of catalyst to resin will depend upon the reactivity of the particular commercial resin and catalyst system chosen. The optimum % of the catalyst using (MEKP), was found to be between 1% to 2% of resin weight, depending on the room temperature and the requirement of the rate of curing time and gel time.

The amount of accelerators (cobalt) was constant throughout the test, as it was premixed with the resin by the manufacturers (0.35% on resin 401, and 1% on resin L.V.M)

Temperature has a direct effect on the viscosity of the resin, and thus the workability of the mix. As the temperature increases the viscosity of the resin decreases.

However, an increase in temperature causes the resin to gel and cure without any addition of the catalyst. Thus, for increasing the pot life of the resin, it must be kept in a cold place and must be preheated before use, to reduce viscosity and hence improve the ease of flow. The room temperature at the time of mixing and placing the polymer concrete must not fall below  $15^{\circ}C$ .

The sandwich beams behaved as box beams due to the presence of the ribs along the sides and at the ends, so that the deflection under the load was due to the bending only, and had little shear component. The polymer concrete beams proved to be much stronger than the comparative reinforced concrete beams with the same dimensional cross-section. The bar reinforcement increased the stiffness and ultimate load of the beams greatly and the crack load was substantially less than the failure load, so that there was a long warning time before the final collapse of the beam.

The investigation seeking to develop an access floor panel using polymer concrete was worthwhile, as the last design stage of the panel, using the mould/reinforcement tray, proved to resist the required load with a safety factor of 6.

However, further investigation is required to develop better casting techniques and to improve the bond between the panel and the tray. Facilities were not available for this at the time of the research.

Tests on all the sandwich panels for housing, suggested that firstly, there is no need for internal ribs in the plain panels, even when they are subjected to the maximum service load with a factor of 2 in a lower storey of a two storey house. Secondly, all the panels resist the maximum predicted wind load with a minimum load factor of 2.

Therefore this suggests that the mechanical strength of this sort of panel will not be a critical design criterion for such panels in this service situation.

For the design and construction of bridge panels, there are two separate criteria

of design, the flexural stiffness and the steel yield stress. The latter has to be used, rather than the ultimate failure due to tensile cracking of the polymer concrete, since permanent deformation of the panel has to be considered an unacceptable service condition. If this is accepted, the bridge panel must be considered a very good structural component since its failure due to collapse gives a long warning period before catastrophe. However, the placing of the steel is of paramount importance. If the bars or strip are displaced by only a few millimeters from their assumed position, the section properties will be altered unacceptably. A device must be employed to maintain the steel in position during production.

The use of the glass reinforced polymer concrete in the production of profiled sheeting for the cladding of roofs and walls is an obvious development. Mechanical testing has demonstrated that the material has much greater flexural resilience than conventional non-metallic materials used in this way. Glass reinforced polymer concrete sheets used for roof cladding would be much less fragile than traditional components, and less likely to fail catastrophically under live loads, typically those applied by the occasional human presence. The sheets would be capable of much greater flexural deformation without failure.

In determination of wind pressure on the building the location of the building was assumed to be in open country with no obstructions with the maximum speed of wind in UK (52 m/sec) and a factor of safety of 3.

However, the test on the bungalow performed very well, which showed that there is a satisfactory resistance to racking in an array of the wall slabs when they

are under their normal amount of superimposed loading from above, ie; from the roof load.

### **Further work**

The polyester polymer concrete products have been fire-tested at the Warrington research centre to British standard 476 (parts 6,7 and 8) and have been granted certificates of half hour resistance, and one hour with more sophisticated treatment. However, during the fire test a good deal of black smoke was generated. Therefore a possible step in searching for a better polymer concrete with regard to its fire resistance, would be the replacement of the polyester resin by a phenolic resin. As a result of low modulus and the problem of curing, the phenolic resin produced by B.P Chemicals Ltd, at the time of writing, is not a suitable substitute unless there is a chemical modification of the resin, to overcome these problems. The requirements for phenolic resin will be :

1. low viscosity (achieved by degree of condensation)
2. Rapid cure (reactivity control by the level of methylphenols present)
3. Good wetting of glass/other reinforcement
4. ability to take fillers
5. low free formaldehyde (for health and safety)
6. low free phenol (for health and safety)

Using phenolic resin means that a new type of fibre glass, filler, catalyst and

different curing technique must be implied for construction of the polymer concrete.

Reinforcing the polymer concrete was achieved by using a specific kind of fibre glass or/mild steel (30 grade). It would be advisable to try different types of fibre glass, eg. different mass/unit area for the matt fibre glass, and short chopped fibre glass. Also since the steel yield was the stress criterion in some components (eg. Bridge-Deck), it would be sensible to consider whether it would be sufficiently economical to replace the existing mild steel reinforcement (30 grade) by a high yield steel (say 40 grade).

This would cause a proportionate increase in the strength calculated on the stress criterion. Also it would be desirable to have a close look at the bonding between the polymer concrete and steel.

# APPENDIX (1)

## **Appendix 1**

**Synopsis: Draws sets of aggregate grading curves on a log. graticule**

### **1. General description:**

- 1.1 This programme will produce drawings of several aggregate grading curves on the same log - plane graticule.
- 1.2 Up to ten curves may be drawn together, though this would appear to be rather congested, and usually not more than about four would be displayed.
- 1.3 Up to 14 particle sizes may be specified, using the same units for all the sizes.  
B.S. sieve size numbers cannot be used. It is usual to specify all sizes in microns.

### **2. Running the programme:**

- 2.1 The object module of the programme is held in MTS file ESK5:OGRAW. The programme sets up its own temporary files, but requires subroutines from the \*GHOST80 package, so that the run command is:-

RUN ESK5:OGDRAW+\*GHOST80

- 2.2 The programme is entirely interactive, and displays messages on the VDU screen which prompt for the next required data, and show the format in which it must be supplied.
- 2.3 A typical data set is shown in the next page;

Record No:	Format	Data	Description
1	I3	154	Job Number
2	I3	-3	Number of particle sizes to be specified.
3	10F6.0	2400. 1200. 600.0 300.0	Particle sizes.
4	I3	-2	Number of grading curves.
5a	10f6.0	100.0 25.00 0.000 0.000	Aggregate gradings to be
5b		100.0 100.0 70.00 20.00	plotted.
6	2F6.0	100.0 3000.	Lower and upper limit of particle sizes for the graph graticule.

2.4 The gradings curves may be inspected, if you are on a graphics terminal, by the command:

RUN \*PLOTSEE

and giving the plot-file name as '-PLOT'.

2.5 A hard copy of the grading curves will be produced on the computer unit flat-bed graphics device when you give the command:

RUN \*MTSPLOT SCARDS=-PLOT

2.6 A hard copy of the data may be recovered by printing the file '-RESULT' A copy of the input data is placed in this file automatically. The command is:

COPY -RESULT \*PRINT\*

## **Efficiency in Aggregate Mix Design:**

**Synopsis:** A computer programme permits up to 14 granular materials of known grading to be combined into the closest possible approximation to a defined target grading. The best proportions for the mix are computed using a least-squares algorithm.

### **1. Introduction:**

1.1 The routine described here is an attempt to arrive at the proportions which will produce the best possible approximation to a proscribed grading, using the matrix formulation of the least-squares solution. An equation is written in such a way that the variation from the desired grading is quantified, and this is minimised by differentiation. Given the existence of the programme, the routine has been found to take most of the work and aggravation out of the aggregate design procedure.

### **2. Programme procedure:**

2.1 First the programme asks for the fractions or particle sizes which are to be used in defining the gradings in the task. Up to 15 sizes may be specified. Thereafter all the aggregates must be specified using these sizes. For example, a typical fine aggregate may be defined by the sizes :-

2400, 1200, 600, 300, 150;

where the sizes are specified in microns.

2.2 At this point the user is asked to choose an option; he may either choose to follow the procedure which optimises the design of a specified grading, or he may choose, simply, to enter the gradings of his components and specify mix proportions, the programme then producing the grading data and grading curve of the specified mix. The latter option is a trivial but useful facility.

2.3 If the first (design) option is chosen, the next data to be supplied must be the grading of the target mix; i.e. the mix to be achieved when the components are mixed in the proportions to be defined by the programme. This may be achieved in either of two ways, by entering an explicit target grading, (para.2.2.1) or by taking the option to request the programme to calculate the 'Fuller' grading for the specified top size, (para 2.2.2). The option is given by an instruction on the VDU at this point in the programme run.

2.3.1 Grading specified by the user. This must be entered as the weight percentages passing the specified particle sizes. For a good, compactable grading the specified target will be either something approximating to a 'Fuller' grading or a 'gap' grading.

2.3.2 When the 'Fuller Curve' option is chosen, the programme calculates the grading curve which is defined by Fuller's expression :-

$$P_n = 100 \times \sqrt{\frac{D_n}{D_{max}}}$$

where  $P_n$  = the percentage passing size  $D_n$

and  $D_{max}$  = the maximum particle size.

2.3.3 Experience with the Fuller grading option will make the user aware of a characteristic of the grading produced by this procedure which, sometimes, is not desirable. The procedure often produces a grading which has too high a proportion of fines passing the lowest specified size. In order to cope with this an additional procedure is available to modify the Fuller curve so that the grading has a similar shape but has only a specified percentage passing the smallest size. The example No.5 includes an illustration of the use of this facility. In practice, if the smallest component aggregate has, say, 12 % passing the smallest size, and it is anticipated that this component will make up about one third of the total aggregate, then it would be sensible to specify that, say, 4 % of the resultant 'Fuller' grading should pass this size.

2.3.4. As a useful check on the potential workability of the mix, the programme works out and tabulates the 'surface area indices' of each weight fraction of the aggregate, and then sums these to obtain the surface area index of the whole aggregate. Subsequently the 'S.A.I.' of the designed mix is calculated and the two values are quoted together at the end of the run, for easy comparison.

2.4 The number of components must then be specified, and their gradings will be quoted in the same way as the target grading. Up to 14 components may be used, though it is more usual for there to be, say, four or five.

2.5 In the case of both the target grading and the components the programme converts the percentage-passing data into weight-fraction data and this is printed

in the output. All subsequent calculations are performed on the weight fractions . Having obtained the weight fractions an additional routine calculates the surface area index of each fraction, and these are listed with the grading data for the target grading. At the end of the procedure the surface area indices of the target and the designed grading are listed together, to show how these compare.

2.6 The algorithm then proposes a set of proportions by weight, of such a nature that if the components are to be mixed in these proportions the resulting grading will approximate as closely as possible to the target grading. These may be identified as  $r_1, r_2, \dots, r_n$ , so that we may write a series of equations to define the weight fractions of the resultant mix as:-

$$a_1 \times r_1 + b_1 \times r_2 + c_1 \times r_3 \dots + z_1 \times r_n = B_1 + D_1$$

where  $a_1, b_1, \dots, z_1$  are the weight fractions of the top size of the various component aggregates,

and  $B_1$  is the weight fraction of the top size of the target fraction, with  $D_1$  being the amount by which the mix resultant differs from the target.

When similar equations are assembled for all the weight fractions the set may be quoted as a matrix equation :-

$$[A] \times \{r\} = \{b\} + \{d\}$$

If the equation is differentiated so as to minimise the sum of the squares of the

differences, d, the equation becomes :-

$$[B] \times [A] \times \{r\} = [B] \times \{b\}$$

Where  $[B]$  is the transpose of  $[A]$ , so that the 'normalised' equation:-

$$[G] \times \{r\} = \{X\}$$

where  $[G] = [B] \times [A]$ ; and  $\{X\} = [B] \times \{b\}$

may be solved to give the best values of the mix proportions 'r'.

2.7 The programme prints both the fractional proportions 'r' and the percentage fractions 'p' which should be used to give the best mix. Initially, these are quoted as weight fractions, but on the assumption that all the bulk densities are the same. However, the user is given the chance to specify the bulk unit weight values in the case where these are different, and the programme will, then, give the mixing proportions by volume and by weight. This is followed by information about the solution obtained. First the weight fractions and the percentage-passing grading of the resultant mix are quoted, and then the programme calculates and quotes the differences between the target mix and the resultant, so that any gross differences may be identified. This is of great assistance to the designer, since it usually allows him to decide what further addition should be made to the mix to achieve a better resultant. Usually one further iteration is all that is necessary to achieve a satisfactory result. Finally the programme calculates and quotes the standard deviation of the resultant

from the target.

2.8 The output from the programme is displayed on the V.D.U. and at the same time an image of this is stored in a temporary file. This output file may be printed subsequently to give a permanent record of the solution.

2.9 At the end of the programme a plotting routine establishes the data to enable the resident graphics package to be invoked for the purpose of plotting the grading curves of the target and computed gradings, as well as the individual grading curves of the component aggregates.

### **3. Data Sets and Formats:**

3.1 The programme is designed to be interactive, so that each new section of the data set is prompted as it is required, and the data format is quoted in the prompt. However, if the required data set is large, as it might be, for example, if there were a large number of particle sizes to be specified, then it would be worth while to assemble a data set in a separate file before the programme run.

### 3.2 Specimen data set:

Record No:	Data	Format	Comments
1	100	I3	Job No.
2	5	I3	No. of particle sizes
3	2400. 1200. 600.0 300.0 150.0	10F6.0	Sizes in microns
4	0	I1	Prompt for the design option.
5	0	I1	Prompt for the user-specified grading.
6	100.0 63.00 35.00 20.00 5.000	10F6.0	Target grading.
7	3	I3	No. of component aggregates.
8a	100.0 15.00 0.000 0.000 0.000	10F6.0	Component gradings.
8b	100.0 100.0 15.00 15.00 0.000		
8c	100.0 100.0 100.0 15.00 0.000		
9	100.0 3000.	2F6.0	Particle size limits for graph graticule

## 4. Discussion:

4.1 The programme was written to simplify the aggregate mix design for workers researching in the use of polymer-bound micro-concrete, who were making up mixes of aggregate using four or five 'single-size' component aggregates and a fine filler, and were seeking a mix to give low voids with high workability. It has proved very useful, and in these circumstances speeds up the mix selection very greatly.

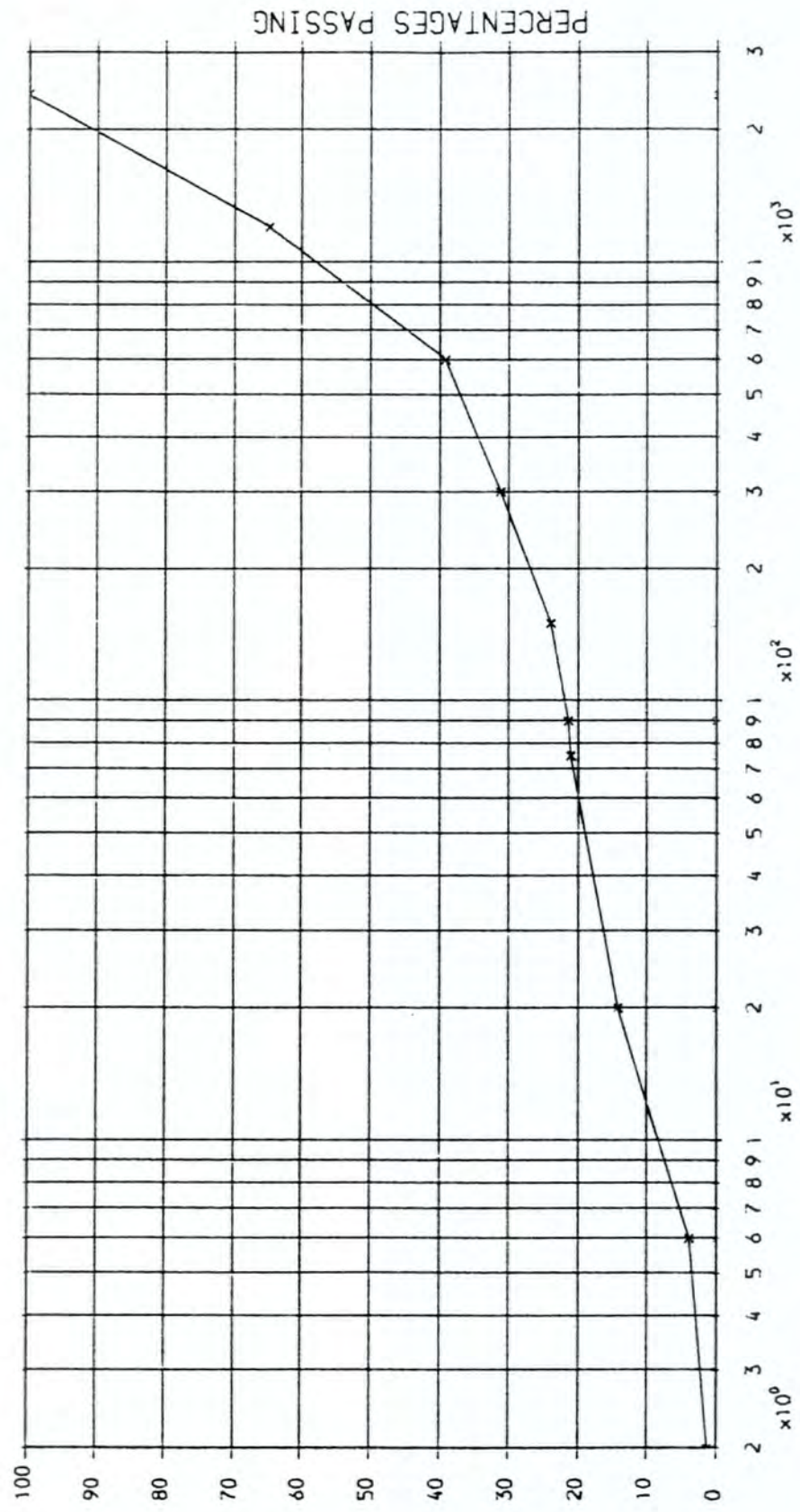
4.2 It has been interesting to compare the mix designed by the programme with mix proportions deduced by other means ( using a mixture of trial-and-error and graphics). The other methods may arrive at a mix of very similar proportions and properties to the one produced by the programme. However, in some cases the 'ad hoc' procedure has arrived at mix proportions quite different from those produced by the programme, but having similar properties. It is clear that there are many viable solutions to the mix design problem. However, there seems to be little doubt that the programme produces the required solution every time, and does so with minimum effort on the part of the designer, which may be regarded as not the least important facility offered by the 'least work' principle.

GMP/jan.1987

MIX NO.	TYPE OF FILLER	PERCENTAGE OF AGGREGATE				
		SAND NO(1)	SAND NO(2)	SAND NO(3)	SAND NO(4)	FILLER
A	B.L.H	43	15.5	18	15.5	8
H	POZZOLAN	65	—	—	27.5	7.5
L	POZZOLAN	66.5	—	—	26.5	7
E	POZZOLAN	65	—	27.5	—	7.5
M	POZZOLAN	66.5	—	26.5	—	7
Q	POZZOLAN	66.5	—	18.5	7.5	7.5
S	POZZOLAN	64	—	18	7	11
S101	POZZOLAN	64	—	16	7	13
SS	POZZOLAN OR B.L.H	64	—	10	8	18
T	POZZOLAN OR B.L.H	—	65	—	27.5	7.5
T102	POZZOLAN OR B.L.H	—	64	—	18	18
TT	POZZOLAN OR B.L.H	—	64	—	11	25

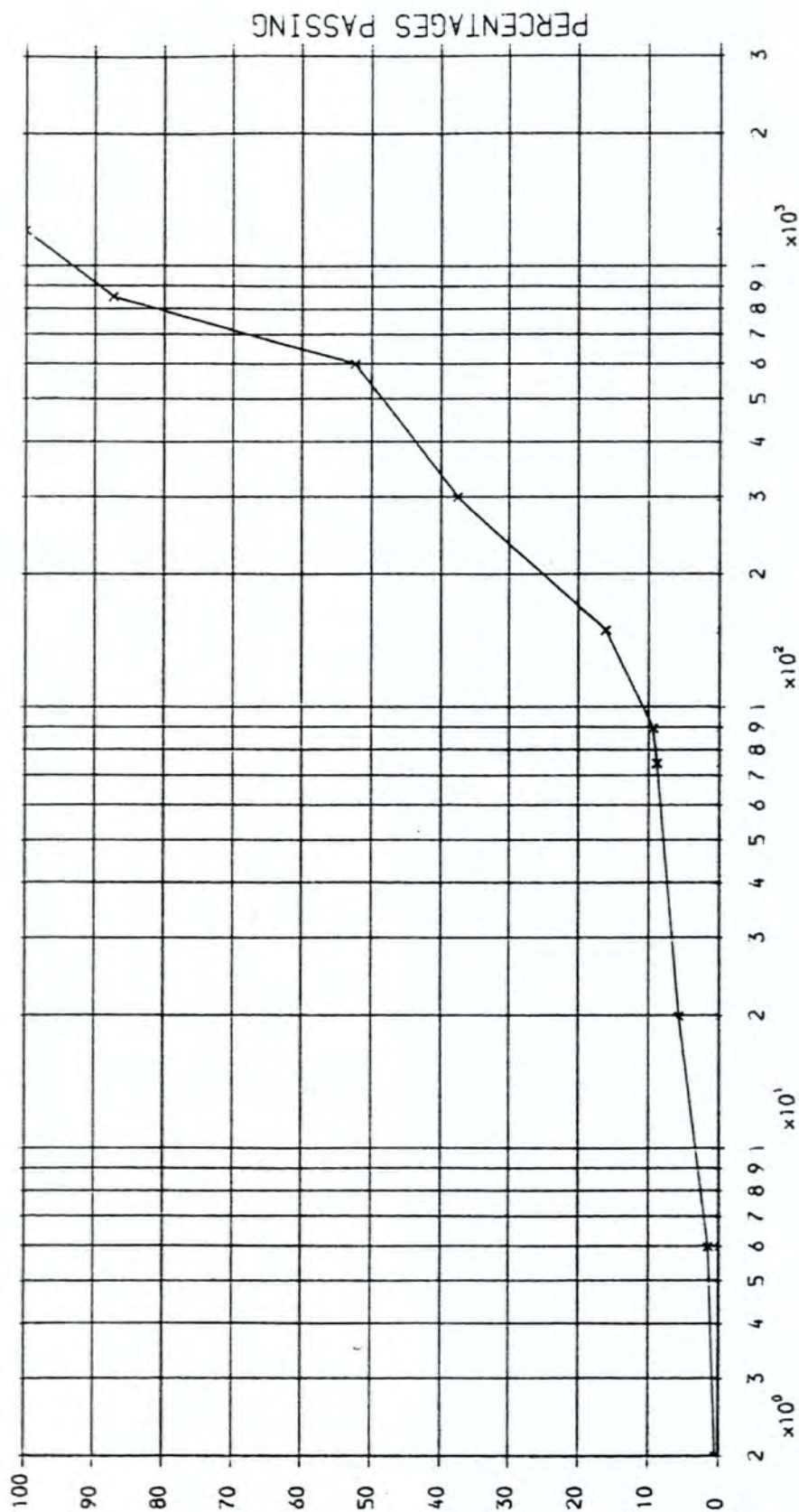
The combination of individual aggregates for producing the particular mix.

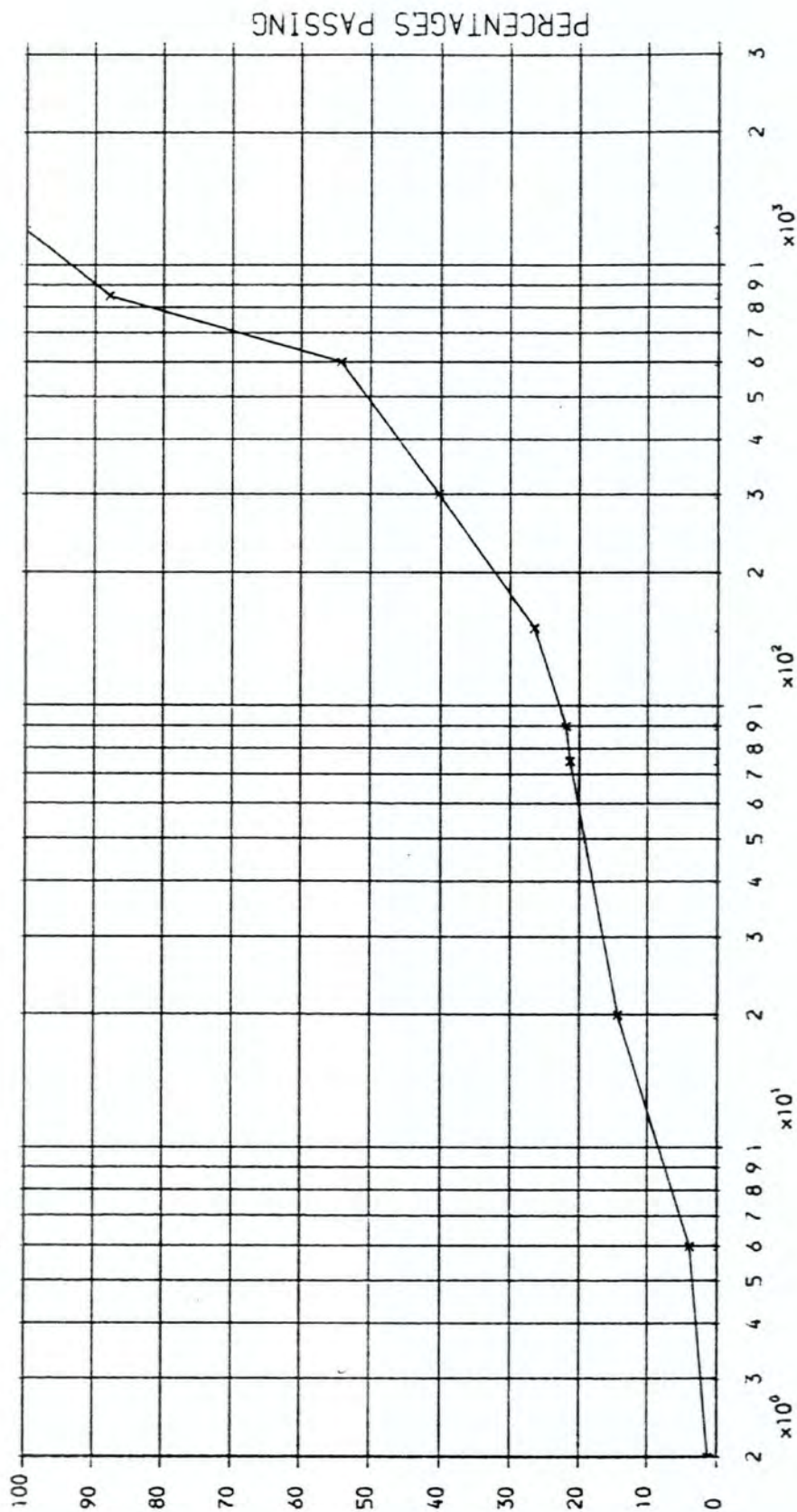
GRADING CURVES MIX: (SS); FILLER: POZZOLAN



PARTICLE SIZES  
 TARGET GRADING DOTTED  
 COMPUTED GRADING FULL

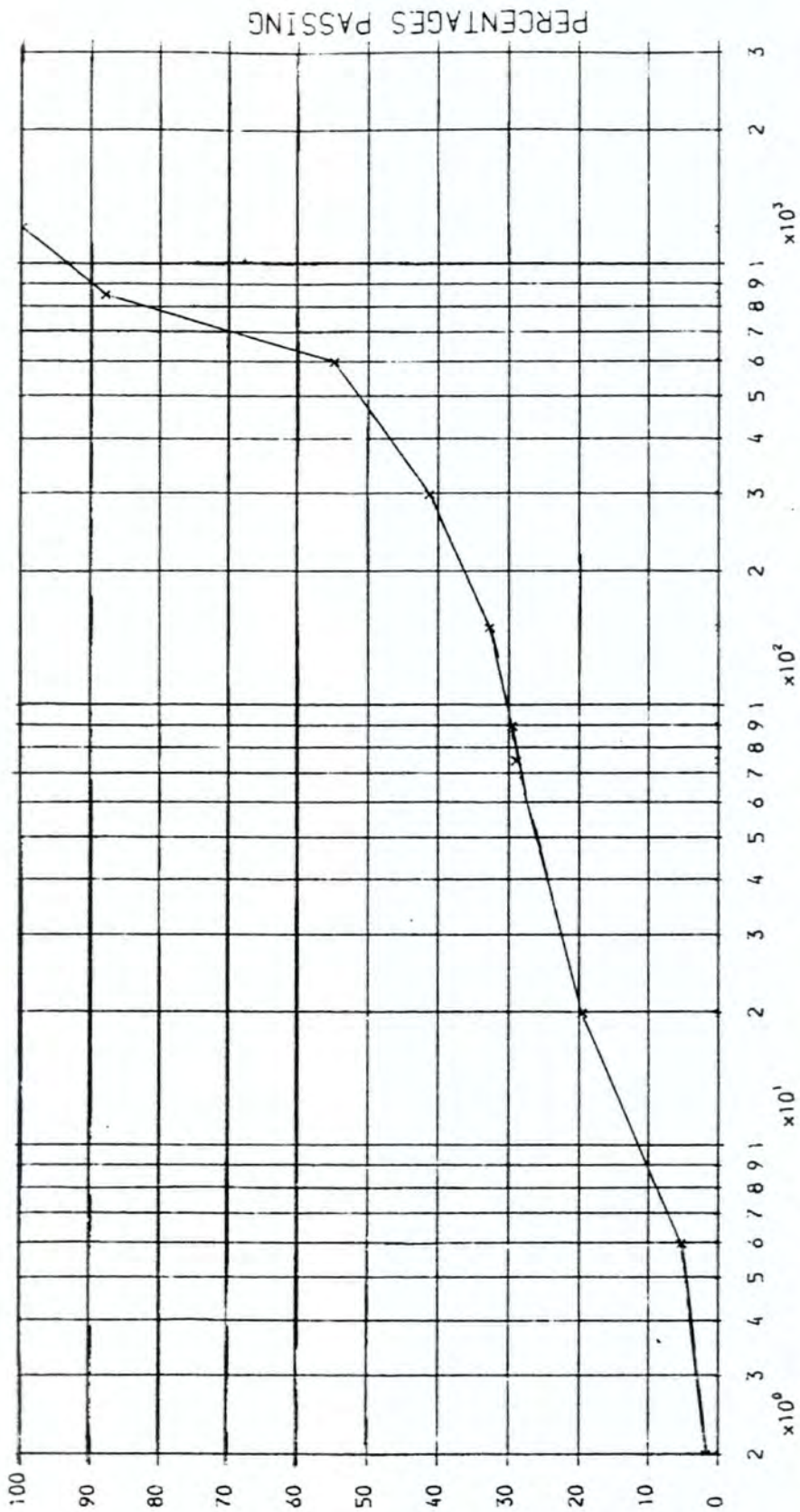
GRADING CURVES      MIX:(T):      FILLER:POZZOLAN



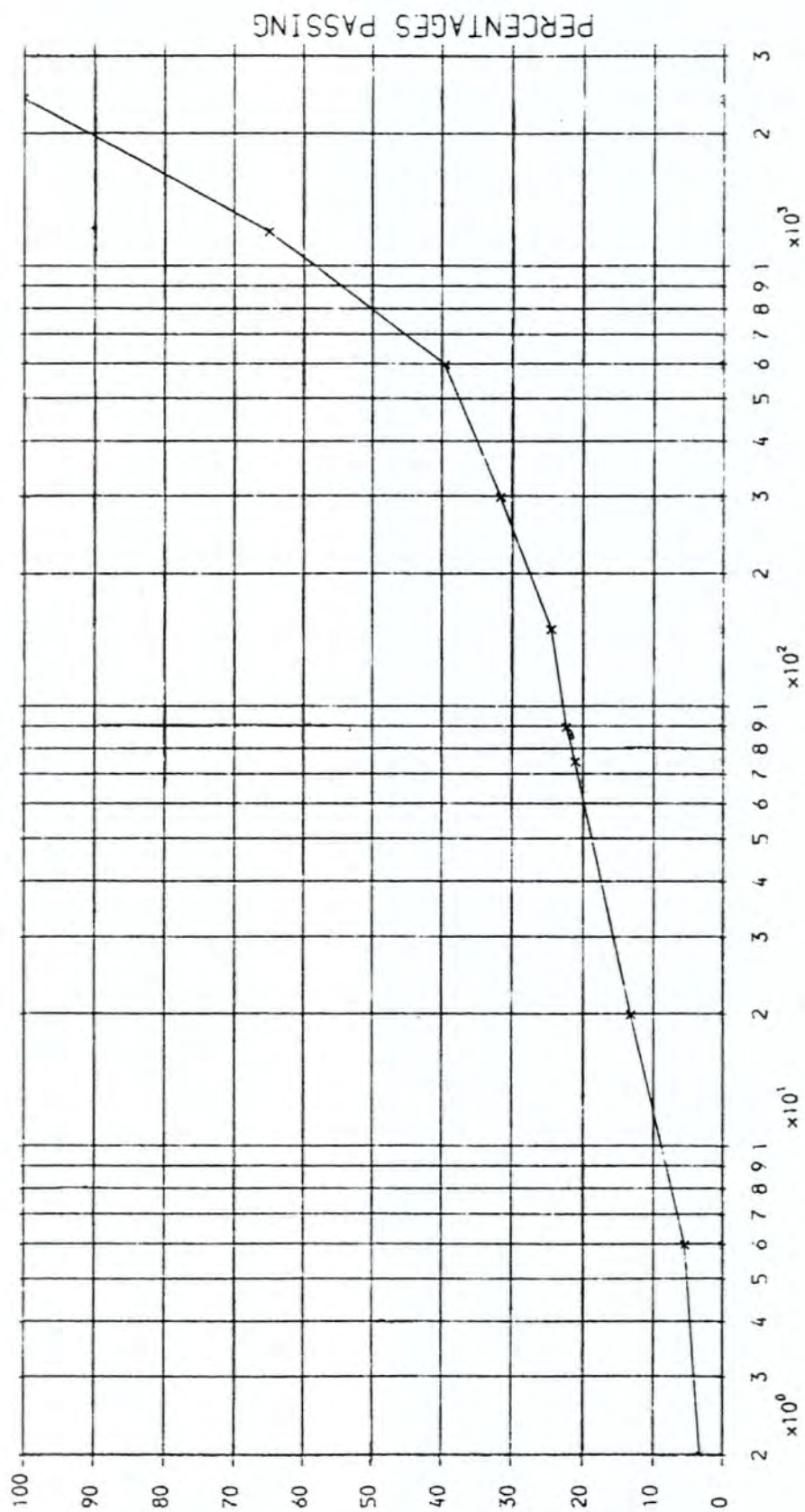


PARTICLE SIZES  
 TARGET GRADING DOTTED  
 COMPUTED GRADING FULL

GRADING CURVES      MIX:(TT);      FILLER:POZZOLAN



TARGET GRADING DOTTED  
COMPUTED GRADING FULL



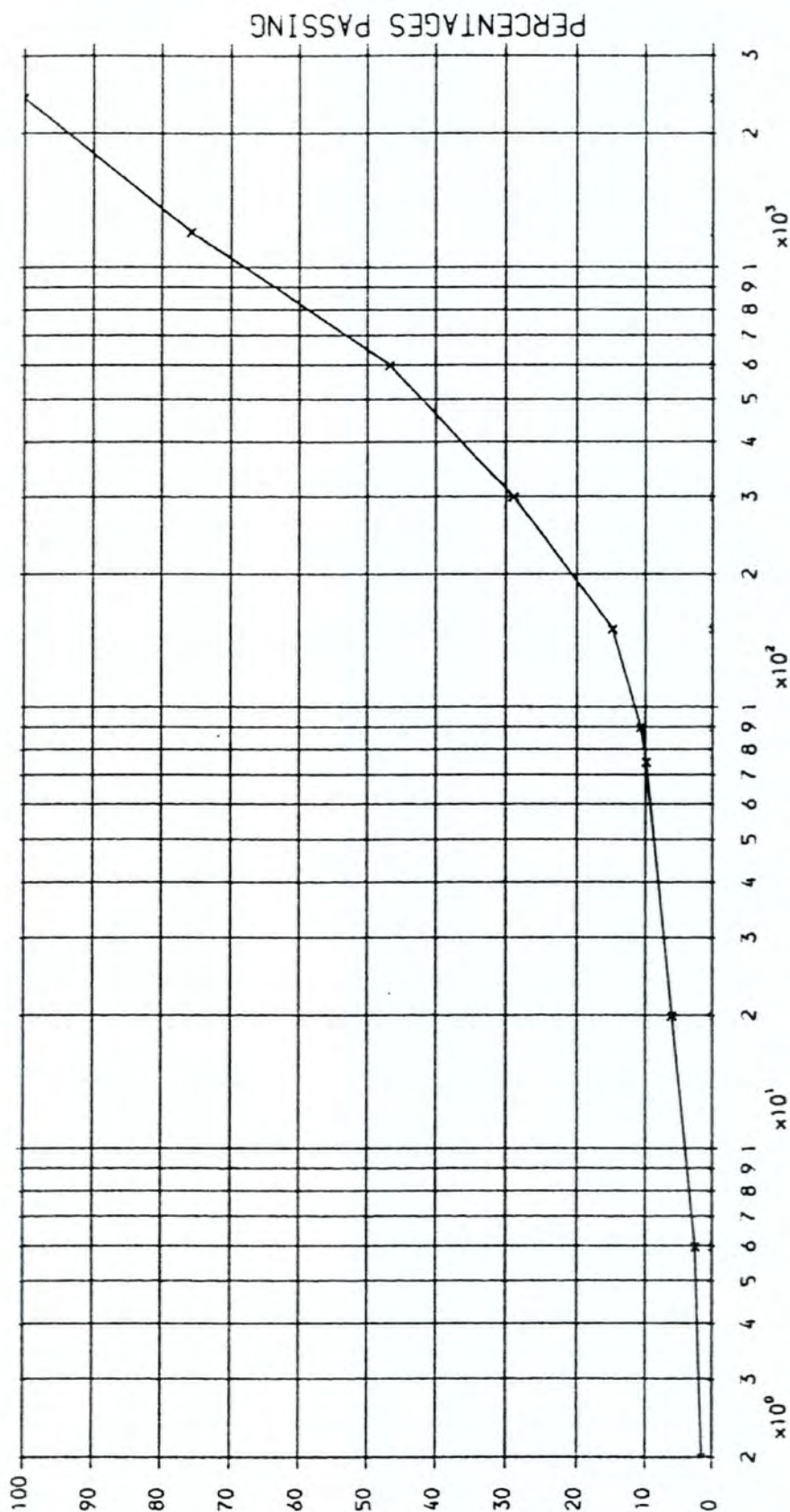
## PARTICLE SIZES

TARGET GRADING DOTTED

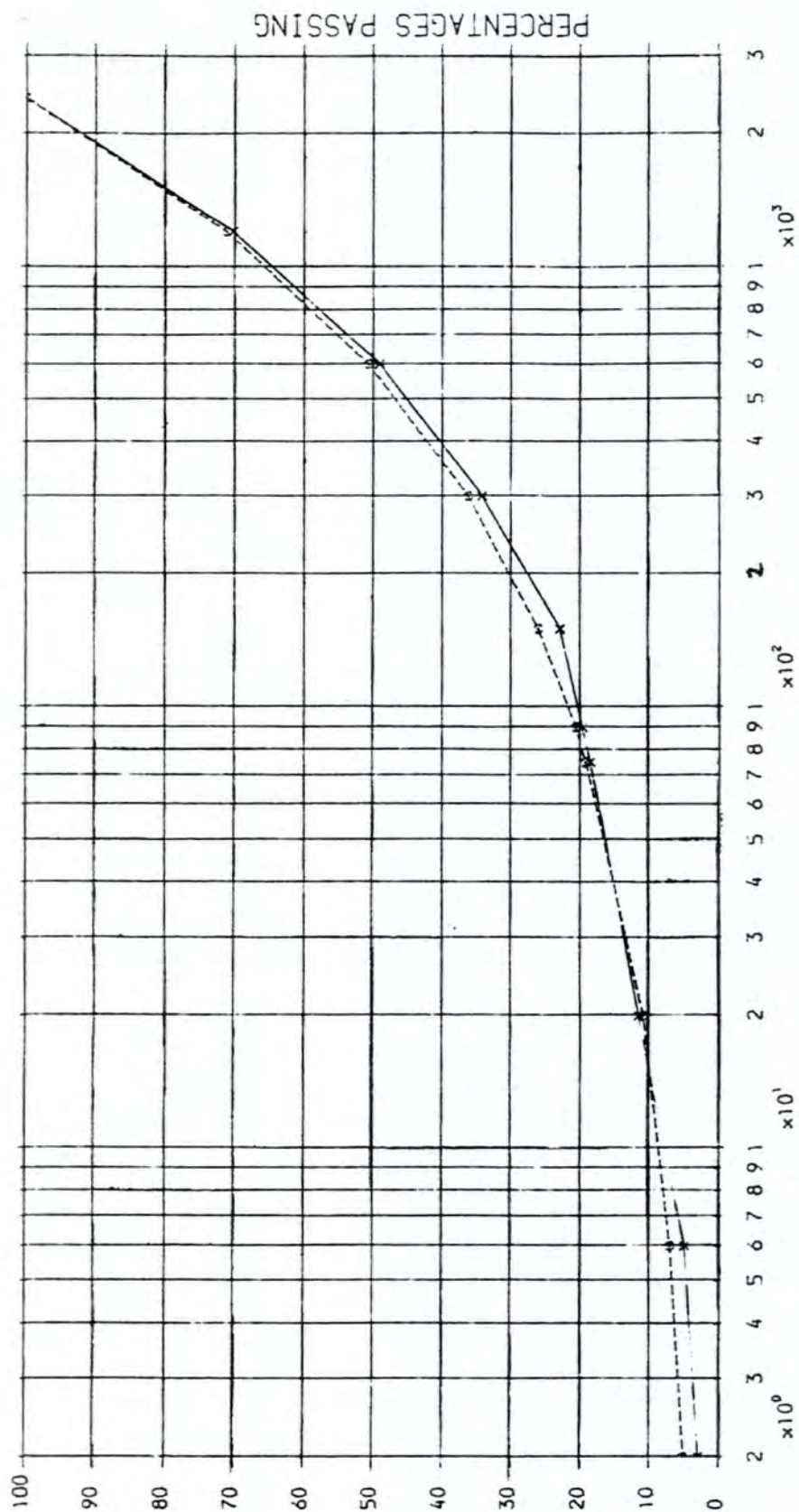
COMPUTED GRADING FULL

# GRADING CURVES

MIX: (A); FILLER: B.L.H

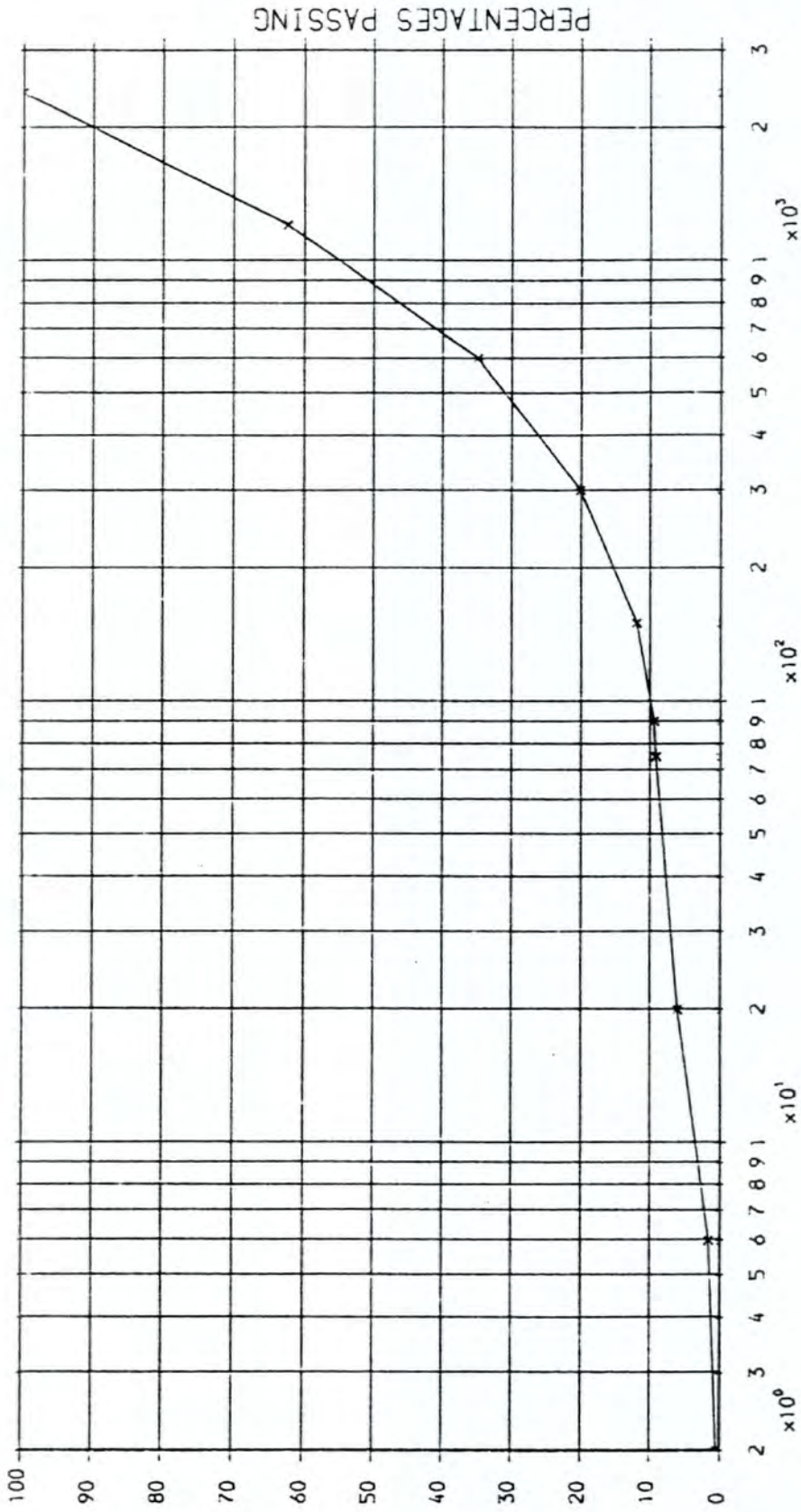


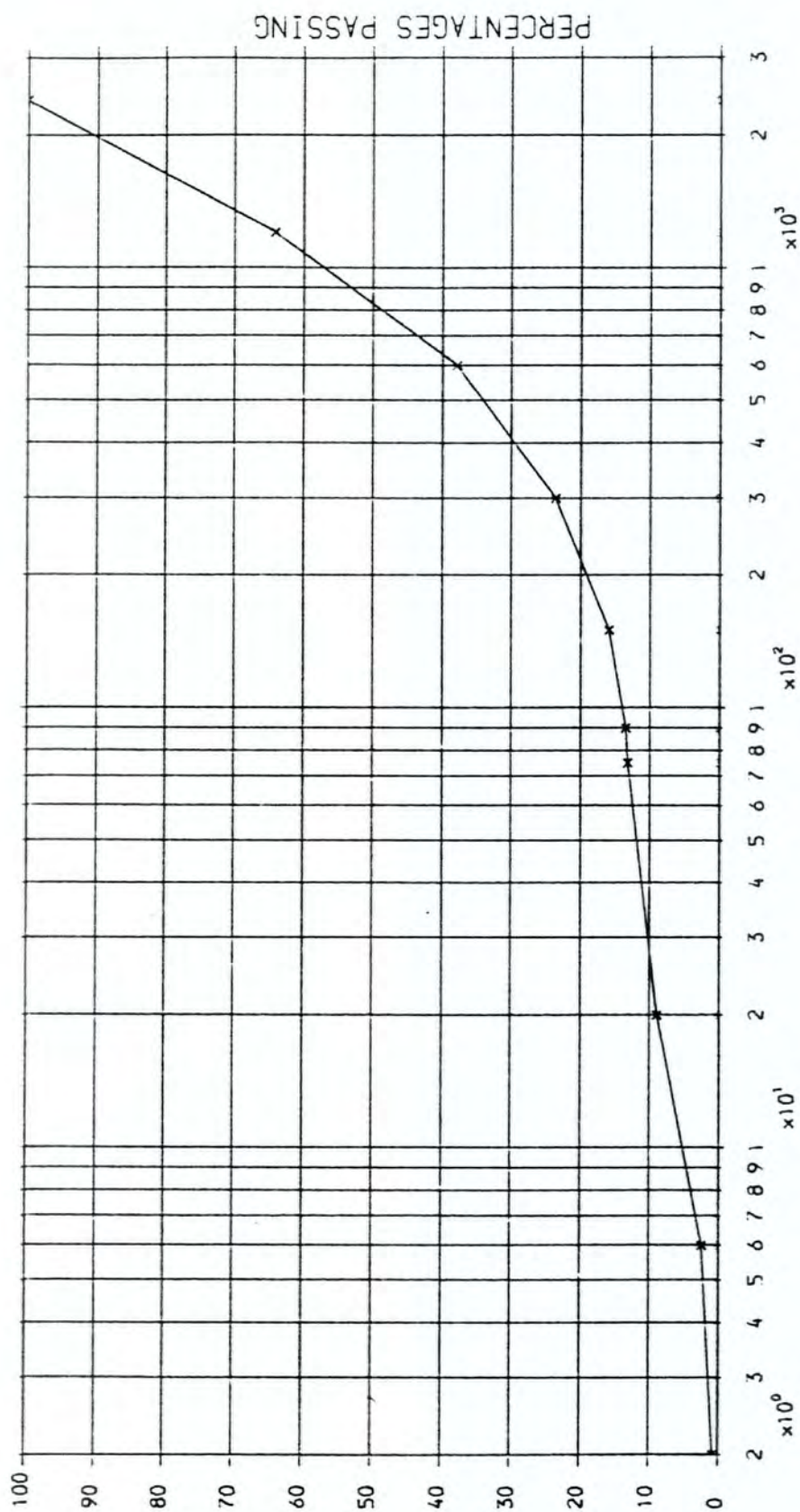
GRADING CURVES      MIX:(A): FILLER:B.L.H  
 &  
 FULLER GRADING



# GRADING CURVES

MIX: (Q); FILLER: POZZOLAN



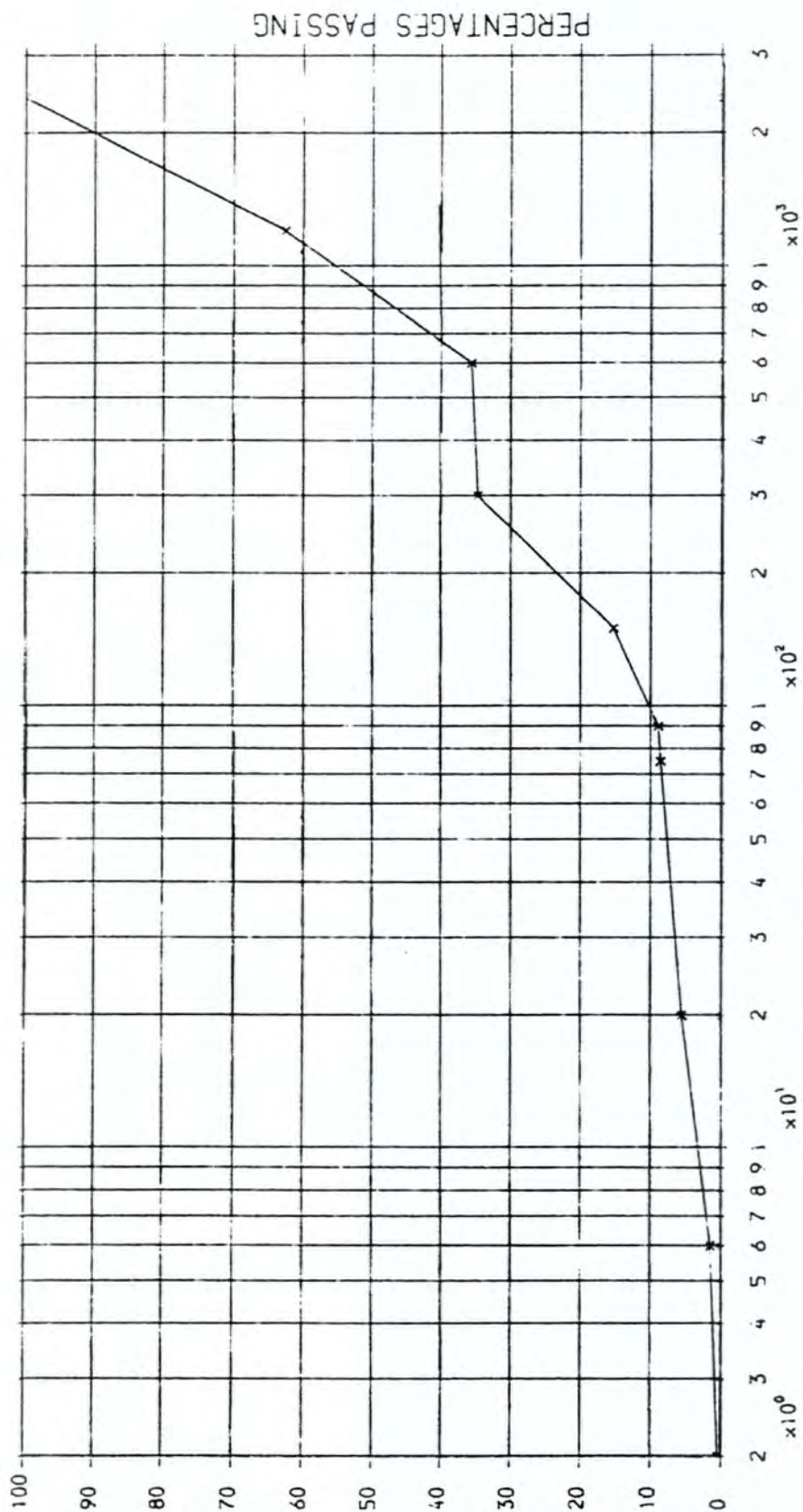


## PARTICLE SIZES

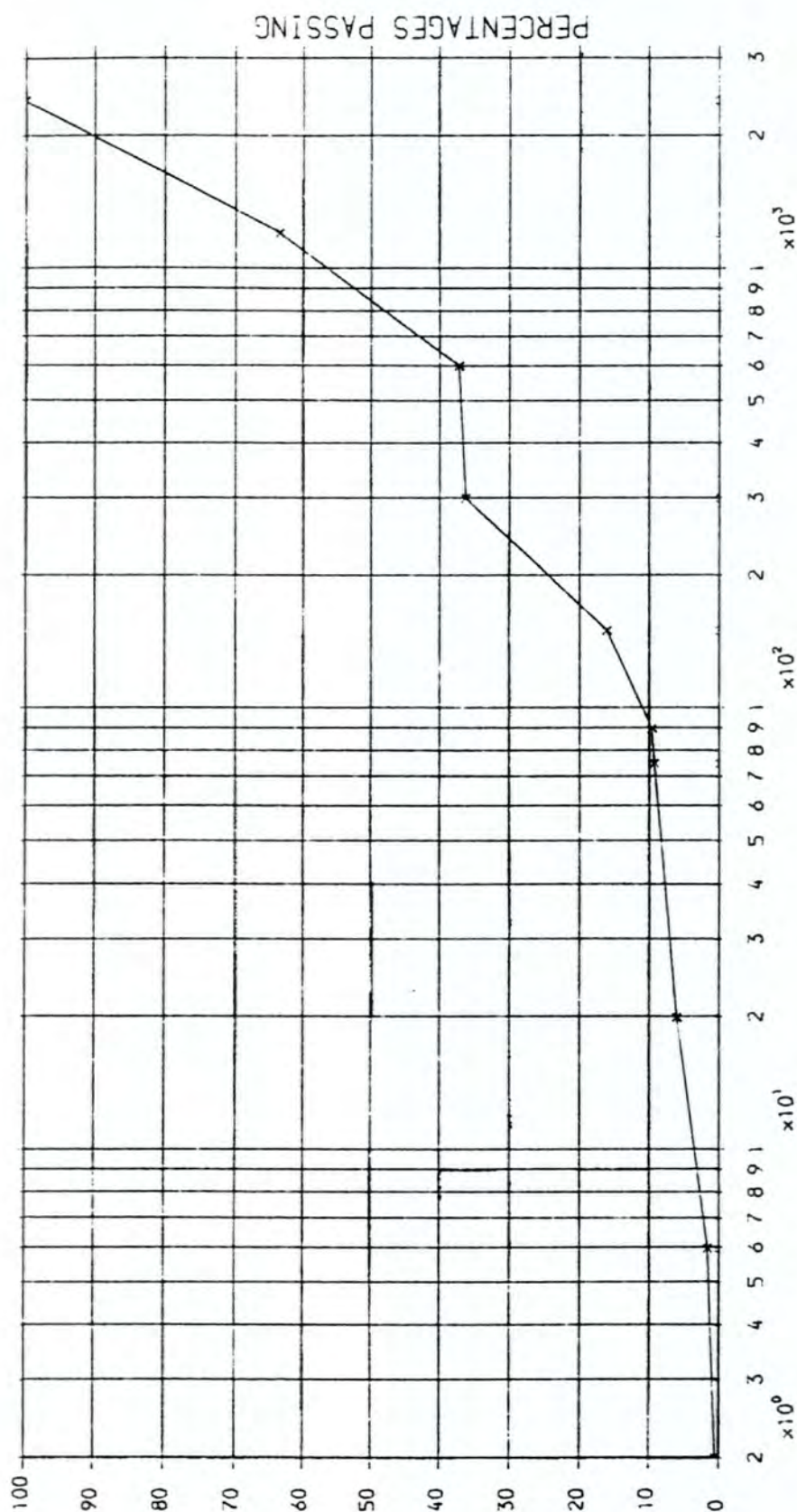
TARGET GRADING DOTTED

COMPUTED GRADING FULL

GRADING CURVES      MIX:(L);      FILLER:POZZOLAN



PARTICLE SIZES  
 TARGET GRADING DOTTED  
 COMPUTED GRADING FULL



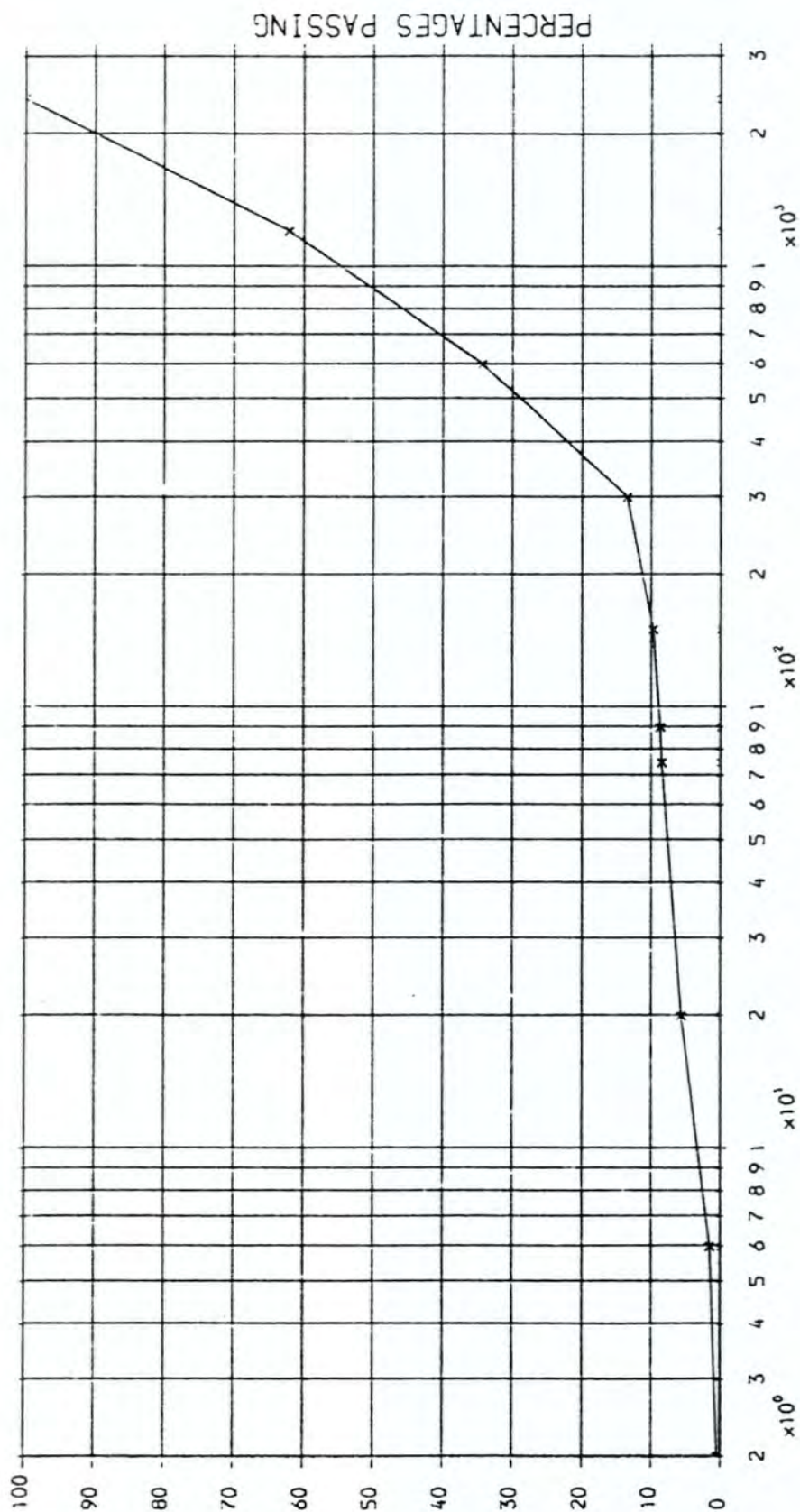
## PARTICLE SIZES

TARGET GRADING DOTTED

COMPUTED GRADING FULL

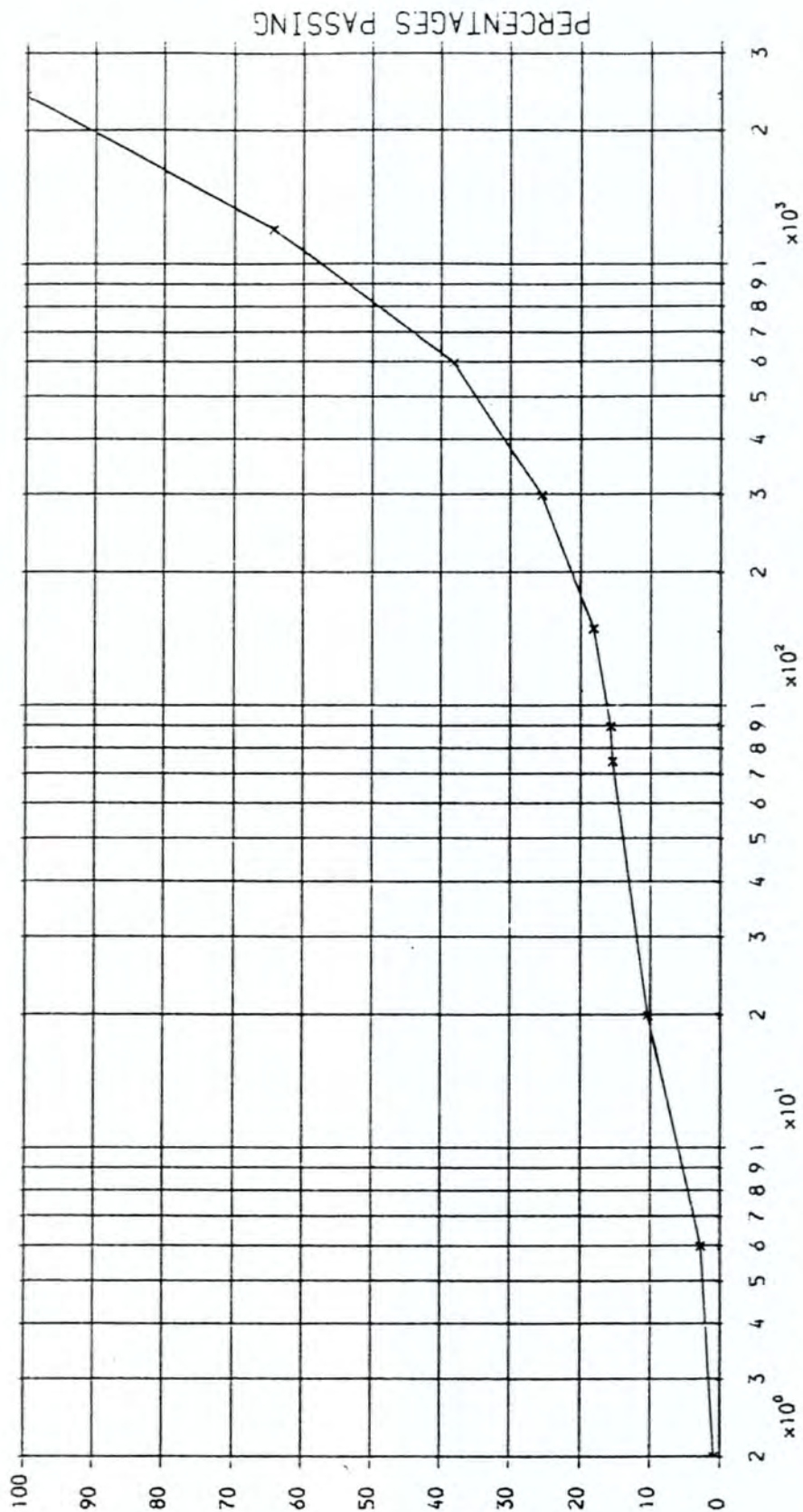
GRADING CURVES

MIX: (M): FILLER: POZZOLAN



# GRADING CURVES

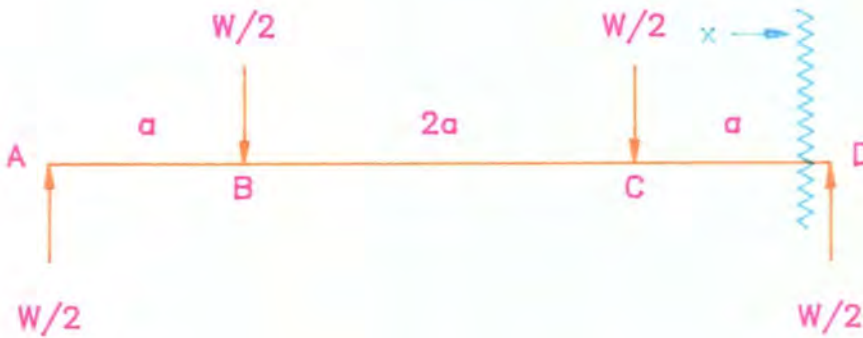
MIX: (S101); FILLER: POZZOLAN



# APPENDIX (2)

## Appendix 2

### Simply supported beams by Macaulay's method



The differential equation of bending can be written as;

$$EI \frac{d^2y}{dx^2} = M$$

The bending moment of the beam at the distance  $(x)$  from point  $(A)$  is;

$$M = -\left(\frac{W}{2}x\right) + \left[\frac{W}{2}(x-a)\right] + \left[\frac{W}{2}(x-3a)\right]$$

The square brackets means that the term only evaluated when positive. Therefore;

$$EI \frac{d^2y}{dx^2} = -\left(\frac{W}{2}x\right) + \left[\frac{W}{2}(x-a)\right] + \left[\frac{W}{2}(x-3a)\right]$$

Integrating, without expanding the bracket terms we have;

$$EI \frac{dy}{dx} = -\frac{Wx^2}{4} + \left[\frac{W}{4}(x-a)^2\right] + \left[\frac{W}{4}(x-3a)^2\right] + C$$

Integrating again gives;

$$E I y = -\frac{Wx^3}{12} + \left[ \frac{W}{12}(x-a)^3 \right] + \left[ \frac{W}{12}(x-3a)^3 \right] + Cx + D$$

The constants  $C$  and  $D$  can be determined from the end conditions. When  $x = 0$  ;  
 $y = 0$ , the square bracketed terms are omitted, and hence  $D = 0$ .

When  $x = 4a$  ;  $y = 0$ , the square bracketed terms are included, and hence;

$$C = \frac{3Wa^2}{4}$$

The deflection form is therefore;

$$EIy = -\frac{Wx^3}{12} + \left[ \frac{W}{12}(x-a)^3 \right] + \left[ \frac{W}{12}(x-3a)^3 \right] + \frac{3Wa^2}{4}x$$

at  $x = a$

$$EIy = -\frac{Wa^3}{12} + \frac{3Wa^3}{4}$$

Then

$$EI = +\frac{2a^3}{3} \left( \frac{W}{y} \right)$$

if  $a = 113mm$  Then

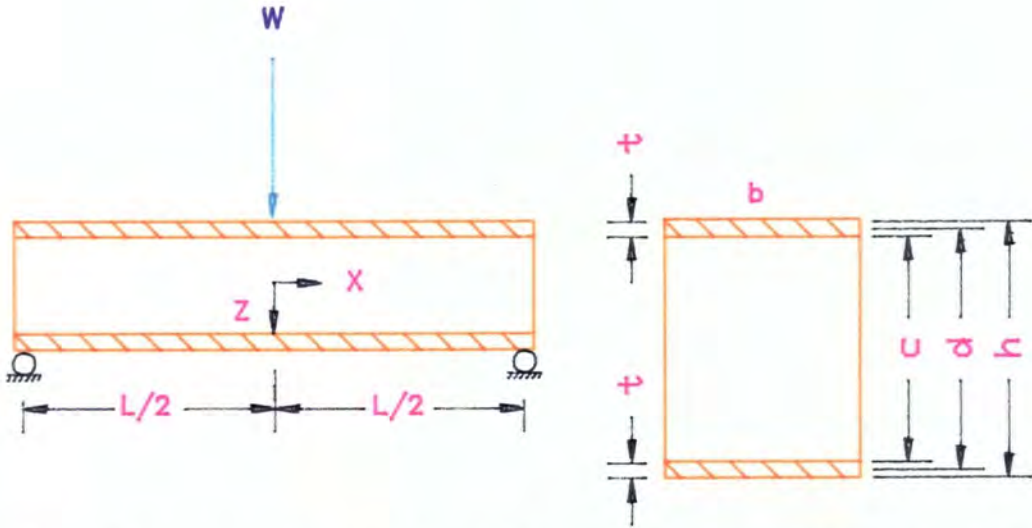
$$EI = 0.96 \times 10^6 \times \frac{W}{y} \quad 1.1$$

Where  $W/y$  is the slope of the graph.

# APPENDIX (3)

## Appendix 3

### Sandwich Beam



Assuming that cross-section are plane and perpendicular to the longitudinal axis when bending takes place.

This assumption leads to the well known relationship between bending moment ( $M$ ) and curvature ( $1/R$ );

$$\frac{M}{EI} = -\frac{1}{R}$$

Where  $EI$  = flexural rigidity =  $D$

In sandwich beam the flexural rigidity is the sum of the flexural rigidities of the two separate parts, faces and core, measured about the centroidal axis of the entire cross-section. Thus;

$$D = 2E_f \left[ \frac{bt^3}{12} + bt \left( \frac{d}{2} \right)^2 \right] + E_c \frac{bc^3}{12}$$

or

$$D = \frac{bt^3}{6}E_f + \frac{btd^2}{2}E_f + \frac{bc^3}{12}E_c \quad (1)$$

Where  $E_f$  and  $E_c$  are the moduli of elasticity of the faces and core respectively, and  $d$  is the distance between the center lines of the upper and lower faces;

$$d_1 = \frac{h + c}{2}$$

(Assuming the beam is narrow so that stresses in the  $y$  direction can be taken as zero).

The first term of the equation (1) in the right hand side represent the local stiffness of the faces, bending separately about their own centroidal axes. Its value is less than 1% of the second term when ;

$$E_f \frac{bt^3}{6} \times 100 < E_f \frac{btd^2}{2}$$

or

$$3\left(\frac{d}{t}\right)^2 > 100$$

or

$$\frac{d}{t} > 5.77 \quad (2)$$

The third term amounts to less than 1% of the second (and may consequently be neglected) when;

$$E_c \frac{bc^3}{12} \times 100 < E_f \frac{btd^2}{2}$$

Then

$$6 \times \frac{E_f}{E_c} \times \frac{t}{c} \times \left(\frac{d}{c}\right)^2 > 100$$

But  $d/c$  is approximately equal to 1 and  $t/c = 0.1$  (if  $t = 8mm$ , and  $c = 70$ ) Then;

$$\frac{E_f}{E_c} > 167 \quad (3)$$

Therefore if condition (2) and (3) are satisfied, the flexural rigidity (D) for the sandwich beam can be written as;

$$D = \frac{btd^2}{2} \times E_f \quad (4)$$

Because sections remain plane and perpendicular to the longitudinal axis (as assumed before). The strain at a point distance  $Z$  below the centroidal axis 'CC' is;

$$\epsilon = \frac{M.Z}{D}$$

This strain may be multiplied by the appropriate modulus of elasticity to give the bending stress at the level  $Z$ . For instance, the stresses in the faces and the core are respectively;

$$\sigma_f = \frac{M.Z}{D} \times E_f$$

$$\sigma_c = \frac{M.Z}{D} \times E_c$$

The maximum face and core stresses are obtained with  $Z = \pm h/2$  and  $Z = \pm c/2$  respectively;

$$(\sigma_f)_{max} = \pm \frac{M.E_f}{D} \times \frac{h}{2}$$

$$(\sigma_c)_{max} = \pm \frac{M.E_c}{D} \times \frac{c}{2}$$

Therefore;

$$\frac{(\sigma_f)_{max}}{(\sigma_c)_{max}} = \frac{E_f}{E_c} \times \frac{h}{c}$$

If the ultimate strengths of the face and core materials are exactly in proportion to their moduli, the faces will fail marginally before the core does so, since  $h/c$  is slightly greater than unity.

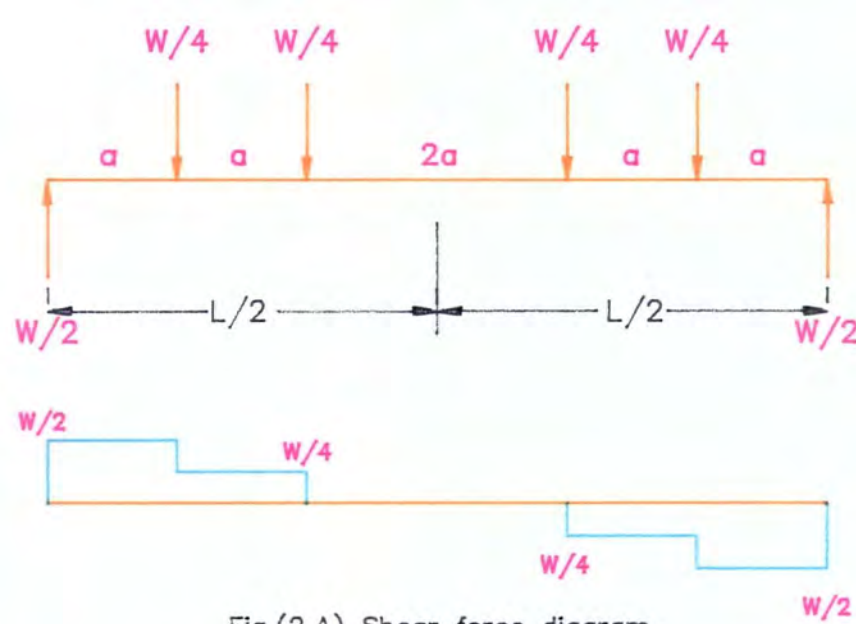


Fig.(2.A) Shear force diagram

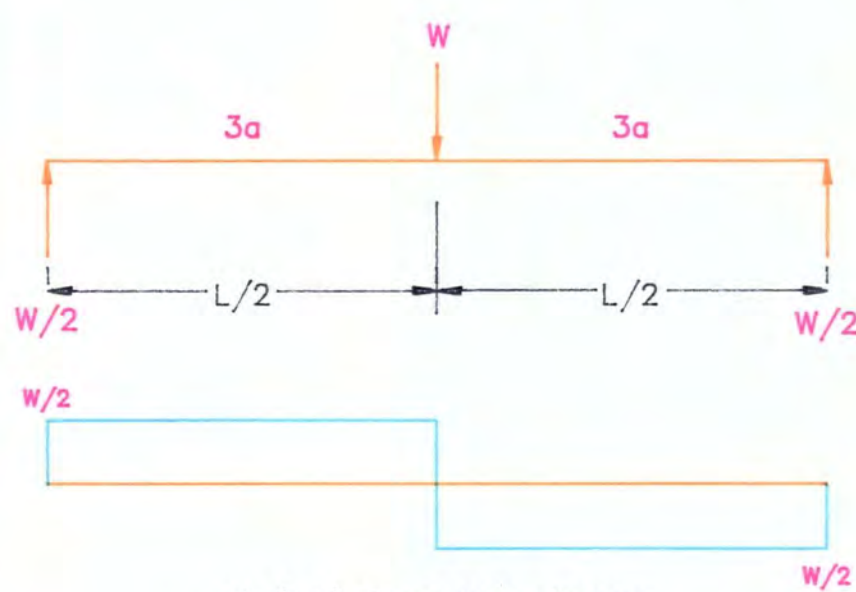


Fig.(2.B) Shear force diagram

The shear deformation of the core, may be obtained by integration of following equation in any particular situation;

$$\frac{dy_s}{dx} = \frac{Q}{AG} \quad (1)$$

Where **Q** is the shear force at the section under consideration , and **G** is the modulus of rigidity of the core, and  $A = bd^2/c$ .

In four point loading situation, the shear force diagram will be as shown in Fig(2.A).

At  $0 \leq x \leq a$ ,  $Q = W/2$

Therefore;

$$y_s = \frac{W}{2AG} \times x + constant$$

But at  $x = 0$ ,  $y=0$ , therefore constant = 0;

From there, the shear deformation at  $x = a$  will be

$$y_s = \frac{W}{2AG} \times a \quad (2)$$

At  $a \leq x \leq 2a$ ,  $Q = W/4$

Therefore;

$$y_s = \frac{W}{4AG} \times x + constant$$

But at  $x = a$ ,  $y = (\frac{W}{2AG}) \times a$

therefore, constant =  $Wa/4AG$

From there, the shear deformation at  $x = 2a$  will be;

$$y_s = \frac{3W}{4AG} \times a \quad (3)$$

At  $2a \leq x \leq 4a$ ,  $Q = 0$

Therefore,  $y_s = \text{constant}$

But at  $x = 2a$ ,  $y_s = (3W/4AG) \times a$

Therefore, the shear deformation at  $x = 3a$  will be;

$$y_s = \frac{3W}{4AG} \times a \quad (4)$$

In the case of a central point load, the shear force diagram will be as shown in

Fig.(2.B)

At  $0 \leq x \leq 3a$ ,  $Q = W/2$

Therefore;

$$y_s = \frac{W}{2AG} \times x + \text{constant}$$

But At  $x = 0$ ,  $y = 0$ , therefore,  $\text{constant} = 0$

From there;

$$y_s = \frac{W}{2AG} \times x$$

Therefore;

$$\text{at } x = a \quad y = \frac{W}{2AG} a \quad (5)$$

$$\text{at } x = 2a \quad y = \frac{W}{AG} a \quad (6)$$

$$\text{at } x = 3a \quad y = \frac{3W}{2AG} a \quad (7)$$

The bending deflection in different position of the beam were calculated according to the *Macauley's Method* as follow;

## 1. Four Points Loading

the differential equation of bending can be written as;

$$EI\left(\frac{d^2y}{dx^2}\right) = M$$

Therefore;

$$EI\left(\frac{d^2y}{dx^2}\right) = \frac{Wx}{2} - \frac{W}{4}[(x-a)] - \frac{W}{4}[(x-2a)] - \frac{W}{4}[(x-4a)] - W[(x-5a)]$$

Integrating twice, and applying the boundry condition of  $x = 0$ ,  $y = 0$ , and  $x = L$ ,  $y = 0$ , therefore;

$$EIy = \frac{Wx^2}{12} - \frac{W}{24}\{[(x-a)^3] + [(x-2a)^3] + [(x-4a)^3] + [(x-5a)^3]\} \\ + \frac{Wx}{24L}\{(L-a)^3 + (L-2a)^3 + (L-4a)^3 + (L-5a)^3\} - \left(\frac{WL^2}{12}\right)x$$

Putting the value of  $L = 1260mm$ , and  $a = 210mm$ , the bending deflection at different position on the beam will be as follow;

$$\text{at } x = a, \quad y_\beta = \left(\frac{1.43 \times 10^7}{D}\right) \times W \quad (8)$$

$$\text{at } x=2a, \quad y_\beta = \left(\frac{2.43 \times 10^7}{D}\right) \times W \quad (9)$$

$$\text{at } x=3a, \quad y_\beta = \left(\frac{2.78 \times 10^7}{D}\right) \times W \quad (10)$$

Where  $D = EI$

## 2. Central Point Loading

$$EI\frac{d^2y}{dx^2} = \frac{Wx}{2} - W[(x-3a)]$$

Integrating twice and applying the boundary condition of  $x = 0, y = 0$ , and  $x = L, y = 0$ , and putting their values ( $L = 1260\text{mm}, a = 210\text{mm}$ ). The bending deformation will be as follow;

$$\text{at } x=a, \quad y_{\beta} = \left(\frac{2.01 \times 10^7}{D}\right)W \quad (11)$$

$$\text{at } x=2a, \quad y_{\beta} = \left(\frac{3.55 \times 10^7}{D}\right)W \quad (12)$$

$$\text{at } x=3a, \quad y_{\beta} = \left(\frac{4.17 \times 10^7}{D}\right)W \quad (13)$$

The total deflection at any point on the beam can be written as;

$$y = y_{\beta} + y_s$$

As  $M/I = \sigma/\hat{y}$ , and  $\sigma = E \times \epsilon$ , (in the elastic reigen), therefore, the strain will be in form of;

$$\epsilon = \frac{M \times \hat{y}}{I \times E} \quad (14)$$

1. Point load at the centre.

the bending moment at the centre is  $M = (WL/4)$ . Then;

$$\epsilon \text{ /unit load} = \frac{L \times \hat{y}}{4 \times EI} \quad (15)$$

and

$$\sigma_y = \frac{W \times L \times \hat{y}}{4 I} \quad (16)$$

2. Four points loading

The bending moment of the centre is  $M = W L / 8$ . Therefore;

$$\epsilon \text{ /unit load} = \frac{L \times \hat{y}}{8 \times EI} \quad (17)$$

and

$$\sigma_y = \frac{W \times L \times \hat{y}}{8 \times I} \quad (18)$$

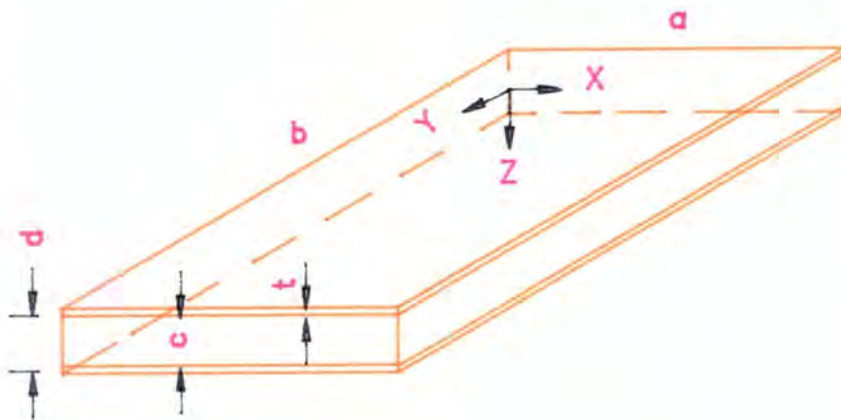
# APPENDIX (4)

## Appendix 4

### Behaviour of Sandwich Panel under Bending and Buckling

The following assumptions are made for the isotropic sandwich panels with very thin identical faces;

1. No longitude or edge ribs in the panel,
2. Perfect bounding between the core and faces,
3. Neglecting the stresses in Z-direction,
4. The core is much less stiff than the faces,
5. Deflection are small (ordinary theory of bending is valid). Also membrane forces not altered by displacements in the Z-direction.
6. Supported on four sides.



The total strain energy and potential energy ( $u + v$ ) at the equilibrium is given

by equation (5.27 of reference 20);

$$\frac{\partial}{\partial a_{mn}}(u + v)_{mn} = \left[ \frac{Gd\pi^2 a}{4} \frac{\rho Q^2}{b(1 + \rho Q)} + N_x \pi^2 \frac{ab m^2}{4 a^2} \right] a_{mn} - \frac{4q}{x^2} \frac{ab}{mn} = 0 \quad 2.1$$

Where

$N_x, q$  = applied load

$a_{mn}$  = unknown amplitude of the  $m, n$  the mode of deformation

$$Q = \frac{m^2 b^2}{a^2} + n^2$$

$$\rho = \frac{\pi^2}{2(1-\nu^2)} \frac{E t d}{Q b^2}$$

### 1. Assuming no transverse pressure (i.e $q = 0$ )

Equation (2.1) is satisfied when  $a_{mn} = 0$

Therefore;

$$-N_x = \frac{Gd}{m^2} \left( \frac{a}{b} \right)^2 \frac{\rho Q^2}{(1 + \rho Q)} = P_{cr}$$

For the lowest critical load ( $n$ ) must be equal to unity. The above equation can be rearranged as follow;

$$P_{cr} = \frac{\pi^2 D_2}{b^2} K \quad 2.2$$

Where

$$D_2 = \frac{E t d^2}{2(1 - \nu_f^2)}$$

and

$$K = \frac{[(mb/a) + (a/mb)]^2}{1 + \rho[(m^2 b^2/a^2) + 1]}$$

which is a dimension less coefficient and can be determined from fig.(5.4 of reference 20) in term of *length/width ratio* of the panel and the quantity of  $\rho$ .

## 2. Assuming no axial load(i.e $N_x = 0$ )

The displacement  $W$  for a simply supported rectangular plate is given by expression of (5.12 of reference 20).

$$W = \sum_{m=1}^{\infty} \sum_{n=1}^{\infty} a_{mn} \sin \frac{m\pi x}{a} \sin \frac{n\pi y}{b} \quad 2.3$$

If  $N_x = 0$ , equation (2.1) can be written as;

$$a_{mn} = \frac{16qb^4}{\pi^6 mn D} \times \frac{1 + \rho Q}{Q^2} \quad (m,n \text{ odd}) \quad 2.4$$

The maximum deflection occurs at the centre of the panel ( $x = a/2$ ,  $y = b/2$ ), in which case equation (2.3) can be written as;

$$W_{max} = \frac{16qb^4}{\pi^6 D} \sum \sum \left[ \frac{(-1)^{(m-1)/2} (-1)^{(n-1)/2}}{mn} \times \frac{1 + \rho Q}{Q^2} \right] \quad (m,n \text{ odd}) \quad 2.5$$

This can be simplified in the form of (equation 5.35 from reference 20)

$$W_{max} = \frac{qb^4}{D_2} (\beta_1 + \rho \beta_2) \quad 2.6$$

Where  $\beta_1$  and  $\beta_2$  can be obtained from fig. (5.5 of reference 20)

The stresses also can be evaluated by differentiation of equation (2.3) and the insertion of the value of  $a_{mn}$  from equation (2.4).

The peak stresses are given in equation (5.39 of reference 20).

1. Direct stresses in the faces ;

$$\sigma_{xx} = \frac{qb^2}{dt} [\beta_3 + \nu \beta_4] \quad (\text{at } x=a/2, y=b/2) \quad 2.7A$$

$$\sigma_{yy} = \frac{qb^2}{dt} [\beta_4 + \nu \beta_3] \quad (\text{at } x=a/2, y=b/2) \quad 2.7B$$

2. Shear stresses in the faces;

$$\tau_{xy} = \frac{qb^2}{dt} [1 - \nu] \beta_5 \quad (\text{at } x=0, y=0) \quad 2.8$$

3. Shear stresses in the core are;

$$\tau_{xz} = \frac{qb}{d} \beta_6 \quad (\text{at } x=0, y=b/2) \quad 2.9A$$

$$\tau_{yz} = \frac{qb}{d} \beta_7 \quad (\text{at } x=a/2, y=0) \quad 2.9B$$

The values of  $\beta_1$  to  $\beta_7$  can be found from fig.(5.5 of reference 20)

# APPENDIX (5)

## Appendix 5

### Design procedures of B-Deck programme

For any polymer concrete **BRIDGE-DECK** section the value of the following parameters are calculated, using the equivalent section method, and reducing the polymer concrete to the equivalent steel area.

$I_f$ ; the total equivalent second moment of area, in terms of the steel,

$Z_{st}$ ; the equivalent bending modulus of the section in terms of the tension steel,

$Z_{sc}$ ; the equivalent bending modulus of the section in terms of the compression steel,

$Z_{ft}$ ; the modulus of bending in terms of the tension polymer concrete.

#### Stress criterion:

For reinforced **BRIDGE-DECK** the failure moment of the section is calculated by using the equivalent steel bending modulus, tension or compression, which gives the lowest failure moment, ie;

either

$$M_u = Z_{st} \times f_y$$

or

$$M_u = Z_{sc} \times f_y$$

Whichever is the lowest.

From this the permissible working load is calculated using the appropriate expression for bending moment, ie;

for simple support;

$$M_u = (F \times W_w \times L^2)/8$$

for partially continuous, ie; simple support one end, continuous the other end;

$$M_u = (F \times W_w \times L^2)/10$$

for fully continuous;

$$M_u = (F \times W_w \times L^2)/12$$

where F is the load factor, and  $W_w$  is uniformly distributed maximum working load.

### **Deflection criterion**

The flexural stiffness of the section is calculated using the full equivalent section in terms of the steel stress. The central deflection of the uniformly loaded **BRIDGE-DECK** is calculated as:

for simple support

$$d_{max} = (5 \times W_w \times L^4)/(384 \times E_s \times I_f)$$

for partially continuous support

$$d_{max} = (W_w \times L^4)/(125 \times E_s \times I_f)$$

for fully continuous support

$$d_{max} = (W_w \times L^4)/(192 \times E_s \times I_f)$$

the permissible working load from the deflection criterion is calculated by using a specified value of the deflection/span ratio so that for example for the simple span;

$$d_{max}/L \leq 1/360$$

$$= (5 \times W_w \times L^3)/(384 \times E_s \times I_f)$$

In almost all practical cases the effective design criterion is that of deflection.

The design of the unreinforced roof sheet is slightly different. Here the deflection criterion is always operative, so that although bending modulus and thus the critical polymer concrete tensile stress in the unreinforced panel is obtained easily from the second moment of area of the polymer concrete alone, it is necessary only to consider the deflection caused by the two modes of design loading.

For the shortest spans a load of 200kg is considered to act at the centre of span, so that the permissible span is calculated from the expression;

$$d_{max}/L = (2000 \times L^2)/(384 \times E_f \times I_f)$$

Assuming fully continuous support.

For longer spans the effect of the specified uniformly distributed load becomes critical, and when this happens the span is calculated from the expression:

$$d_{max}/L = (0.75 \times 10^3 \times L^3)/(192 \times E_f \times I_f)$$

## Table key

For each set of sections there are the following tables;

Table 1. Section dimensions.

Table 2. Geometrical properties.

Table 3. Maximum purlin spacings, roof sheets.

Table 4. Maximum U.D.L. stress criterion, simply supported.

Table 5. Maximum concrete depth, formwork, simply supported.

Table 6. Maximum U.D.L. deflection criterion.

Table 7. Maximum concrete depth, formwork

Table 8. Maximum U.D.L deflection criterion, continuous.

Table 9. Maximum concrete depth, formwork.

## Section key

A set of tables is provided for each set of sections.

Section Nos:000    The original bridge panels.

Section Nos:100    Roof sheeting.

Section Nos:200    Bridge deck, 32mm ribs.

Section Nos:300    Bridge deck, 65mm ribs.

**Table contents**

**Table 1: Section dimensions**

(all dimensions in mm)

Column contents:

Column no:	Column heading	Column contents
Col 0	NUM	section number
Col 1	SHT THS	thickness of base sheet
Col 2	SHT WTH	width of panel or sheet
Col 3	RIBS	number of ribs per panel
Col 4	TOP THS	thickness of top of rib (10mm standard)
Col 5	BOT THS	thickness of bottom of rib (25mm standard)
Col 6	DEPTH	depth of rib above sheet.
Col 7	BARS	number of bars per rib
Col 8	TYPE	bar type 0 for round bar, 1 for flat strip
Col 9	THICKS	round bar diameter, flat strip, thickness
Col 10	DEPTH	round bar, 0 flat strip depth of strip
Col 11	LEV 1	distance from outside of sheet to C.L of top bar or single strip.
Col 12	LEV 2	distance from outside of the sheet to C.L of bottom bar.

**Table 2: Geometrical properties**

(all dimensions in mm)

Column contents:

Col.0	NUM	Section number
Col.1	AM	Modular ratio
Col.2	FYP AREA	Area of section, including steel
Col.3	STL AREA	Area of steel reinforcement in each sheet
Col.4	YBAR	Distance of centroid of section above base (ie from face of sheet)
Col.5	2ND MOI	2nd moment of area of total section.
Col.6	ZTS	Modulus of section top of steel, (in terms of steel stress)
COL.7	ZBS	Modulus of section bottom of steel, (in terms of steel stress)
Col.8	ZTF	Modulus of section, top of polymer concrete (in terms of polymer concrete stress)
Col.9	ZBF	Modulus of section, bottom of polymer concrete (in terms of polymer concrete stress)

**Table 3: Maximum Purlin Spacings**

Note: This table gives maximum purlin spacings for the section if it is used as roof sheeting. All values are based on the need to support a concentrated load of 200kg as a line load at the centre of any span.

The deflection criterion is always critical. Values are quoted for maximum permissible deflections of 1/360th of the span and 1/250th of the span.

Continuous support assumes that the sheet will be continuous over several purlins, and that the ends will cantilever beyond the outer supports for a distance of not less than 1/5th of the span.

**Table 4: Max U.D.L Stress criterion, single span**

Note: The table gives values of maximum permissible uniformly distributed load in  $\text{kN/m}^2$  on sheets of the listed spans in metres.

The critical stress is always the steel yield stress. A load factor is applied to the failure load to give the permissible load.

In all cases the simple support deflection criterion gives smaller loads than the stress criterion. For all values to the right of the dotted line on the table for deflection criterion for continuous spans again gives smaller loads than the stress criterion.

It follows from the above that, in most cases, the stress criterion loads may only be used to give guidance on the use of bridge panels for such functions as temporary decking, where the deflection criterion is not expected to apply.

**Table 5: Max. concrete depth, stress criterion, simple span**

Note: The table gives maximum permissible depths of concrete which may be placed on the panels when they are used as permanent formwork for in-situ reinforced concrete work.

Again, it will be found that the deflection criterion gives lower values than the

stress criterion except where a dotted line appears on the table.

All the reinforcement required by the in-situ concrete must be provided during the construction of the in-situ slab. The steel in the bridge panel cannot be used for this purpose, since the bond between the bridge panel and the in-situ concrete is not adequate for the transmission of the load between these two components.

**Table 6: Maximum U.D.L deflection criterion, simple support**

**Table 7: Maximum concrete depth**

Note: It will be seen from the previous notes that the values in these tables apply to all cases where the bridge panel is used as formwork for in-situ concrete or as permanent decking in any other context and where it cannot be continuous over supports. Typical cases are permanent formwork supported on either the bottom flange or on a shelf angle of the main beams.

**Table 8: Max U.D.L deflection criterion, continuous support**

**Table 9: Maximum concrete depth**

Note: It will be seen from the previous notes that all the values above and to the right of the dotted line in these tables apply where the bridge panel is to be used either as formwork for concrete or as permanent decking in any other context and where it may be continuous over supports. For cases below and to the left of the dotted line the relevant values should be extracted from the tables 4 and 5, modified for continuous support.

# APPENDIX (6)

Appendix 6

Wind loads

1. Loading due to the roof

The maximum roof load to the side wall units is given as:

a. Dead load

COMPONENT	PLAN		SUPPORT KN/m
	Kg/m <sup>2</sup>	KN/m <sup>2</sup>	
TILES	60		
BATTENS(38x25 @ 3 m/m <sup>2</sup> )	2.5		
TRUSSES	22		
CEILINGS	2.4		
FITTING etc.	1.0		
TOTAL	87.9	0.862	0.862x7.38/2=3.18

b. Super load

Super load=0.75 KN/m<sup>2</sup>

$$= 0.75 \times 3.69 = 2.77 \text{ KN/m}$$

## 2. Determination of wind pressures on the building (cp3,chapter V,part 2,1970).

The characteristic wind pressure is given by:

$$q = 0.613 V_s^2$$

where:

$V_s$  is the design wind speed= $V \times s_1 \times s_2 \times s_3$  (m/sec.)

$V$  is the basic wind speed=52 m/sec. (UK maximum)

$s_1, s_2, s_3$  are multiplying factor relating to topology,height above ground and life of structure respectively.

Assuming the location of building is in open country with no obstruction.Building size-class B.The greatest horizontal or vertical dimension does not exceed 50 m.

Height to the top of the roof , $H_1=4.33$  m

Height to the top of the wall , $H_2=2.80$  m

Taking the topography factor ( $s_1$ ) and statistical factor ( $s_3$ ) as unity.

From table 3(cp3:chap.V:part 2)

$$roof \quad : \quad s_2 = 0.83$$

$$walls \quad : \quad s_2 = 0.78$$

Design wind speed:

$$\text{roof : } V_s = 52 \times 1 \times 0.83 \times 1 = 43.16 \text{ m/s}$$

$$\text{walls : } V_s = 52 \times 1 \times 0.78 \times 1 = 40.56 \text{ m/s}$$

Dynamic pressure:

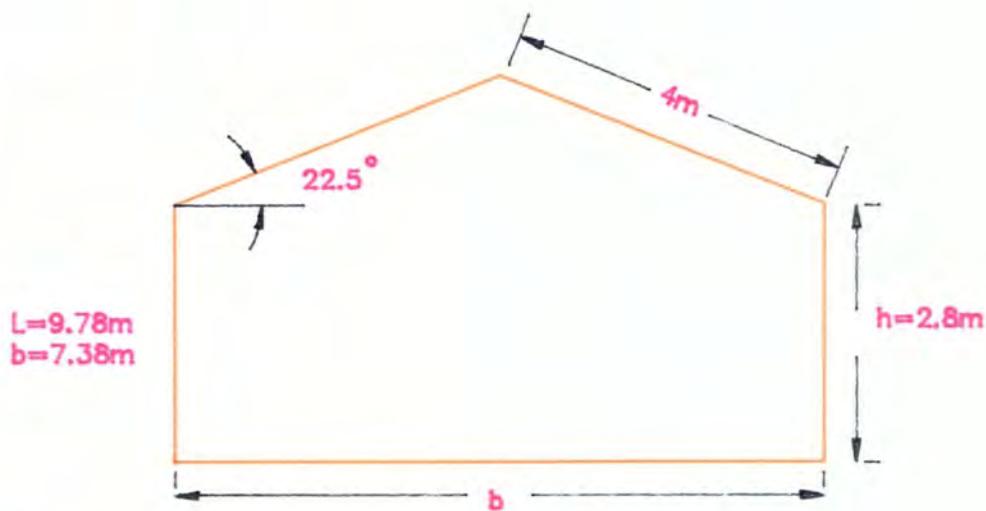
$$\text{roof : } q = 0.613 \times 43.16^2 = 1.14 \text{ KN}$$

$$\text{walls : } q = 0.613 \times 40.56^2 = 1.01 \text{ KN}$$

### 1. Roof

The external pressure coefficients  $c_{pe}$  are determined from table (8) of cp3:chapter

V:part 2:1970,and are as follow:



$$\frac{h}{b} = \frac{2.8}{7.38} = 0.379 < \frac{1}{2}$$

Roof angle	Wind at right angles to building (on pitch)		Wind parallel to building (on gable)	
	Wind ward slope	Lee ward slope	Wind ward half	Lee ward half
22.5°	-0.3	-0.4	-0.7	-0.6

The internal pressure coefficient are taken from Appendix E(cp3).The case will be considered where there is only a negligible probability of a dominant opening occurring during a severe storm.Here  $c_{pi}$  shall be taken as the more onerous of +0.2 and -0.3.

The wind loading normal to the roof slope =  $q \times A \times (c_{pe} - c_{pi})$

$$= 1.14 \times 4 \times 9.78(c_{pe} - c_{pi}) \tag{1}$$

$$\text{per meter run} = 1.14 \times 4(c_{pe} - c_{pi})$$

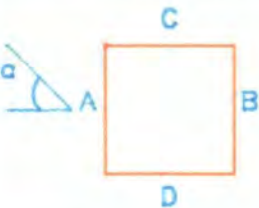
2. Walls

The external pressure coefficient are taken from table 7(cp3).These are shown below;

$$\frac{h}{b} = \frac{2.8}{7.38} = 0.379 < \frac{1}{2}$$

$$\frac{l}{b} = \frac{9.78}{7.38} = 1.32$$

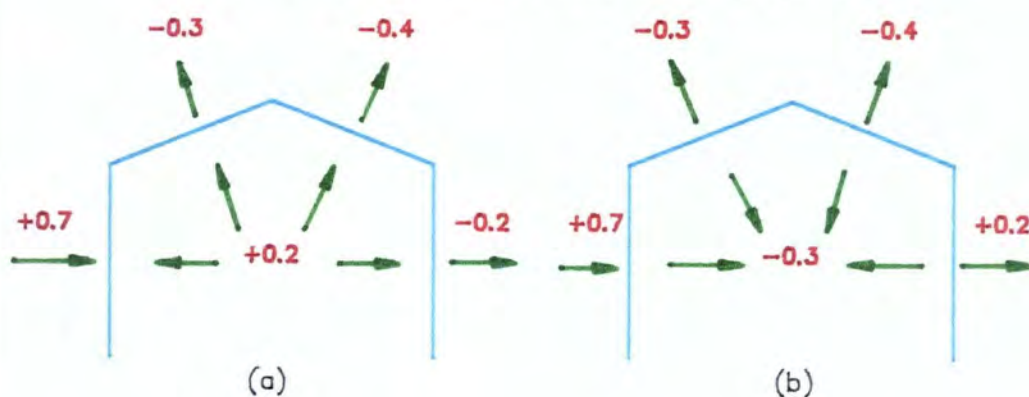
$$1 < \frac{l}{b} \leq 1.5$$

PLAN	WIND ANGLE $\alpha$	C <sub>pe</sub> FOR SURFACE			
		A	B	C	D
	0°	0.7	-0.2	-0.5	-0.5
	90°	-0.5	-0.5	0.7	-0.2

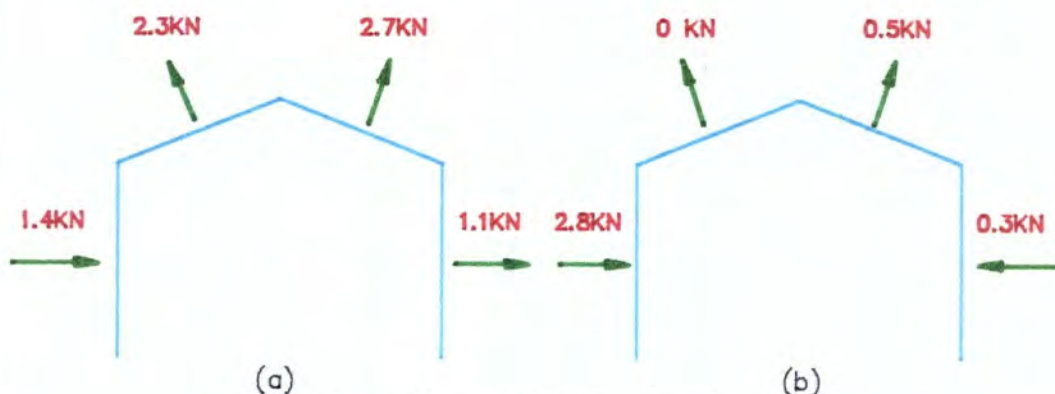
The wind loading normal to the wall =  $1.01 \times 2.8 \times 9.78(c_{pe} - c_{pi})$

The wind loading normal to the wall/m run =  $1.01 \times 2.8(c_{pe} - c_{pi})$

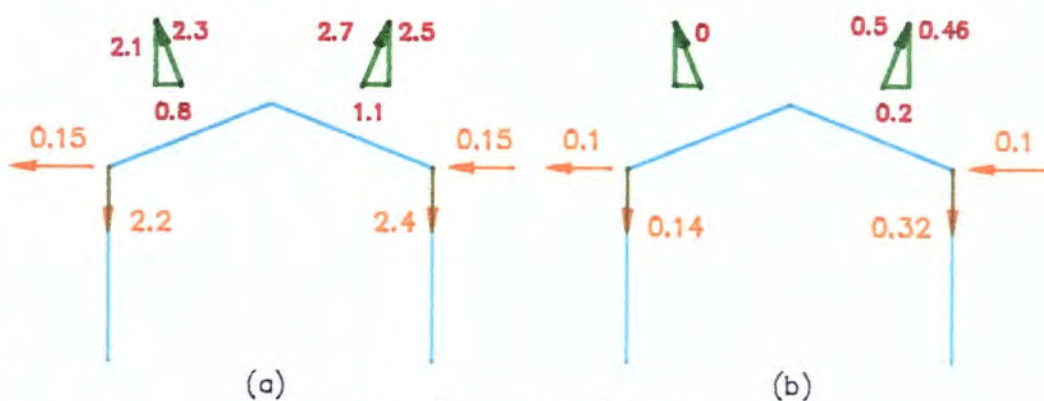
Wind normal to side of the building ( $\alpha=0^\circ$ )



Pressure Coefficients



Forces/m run due to the wind

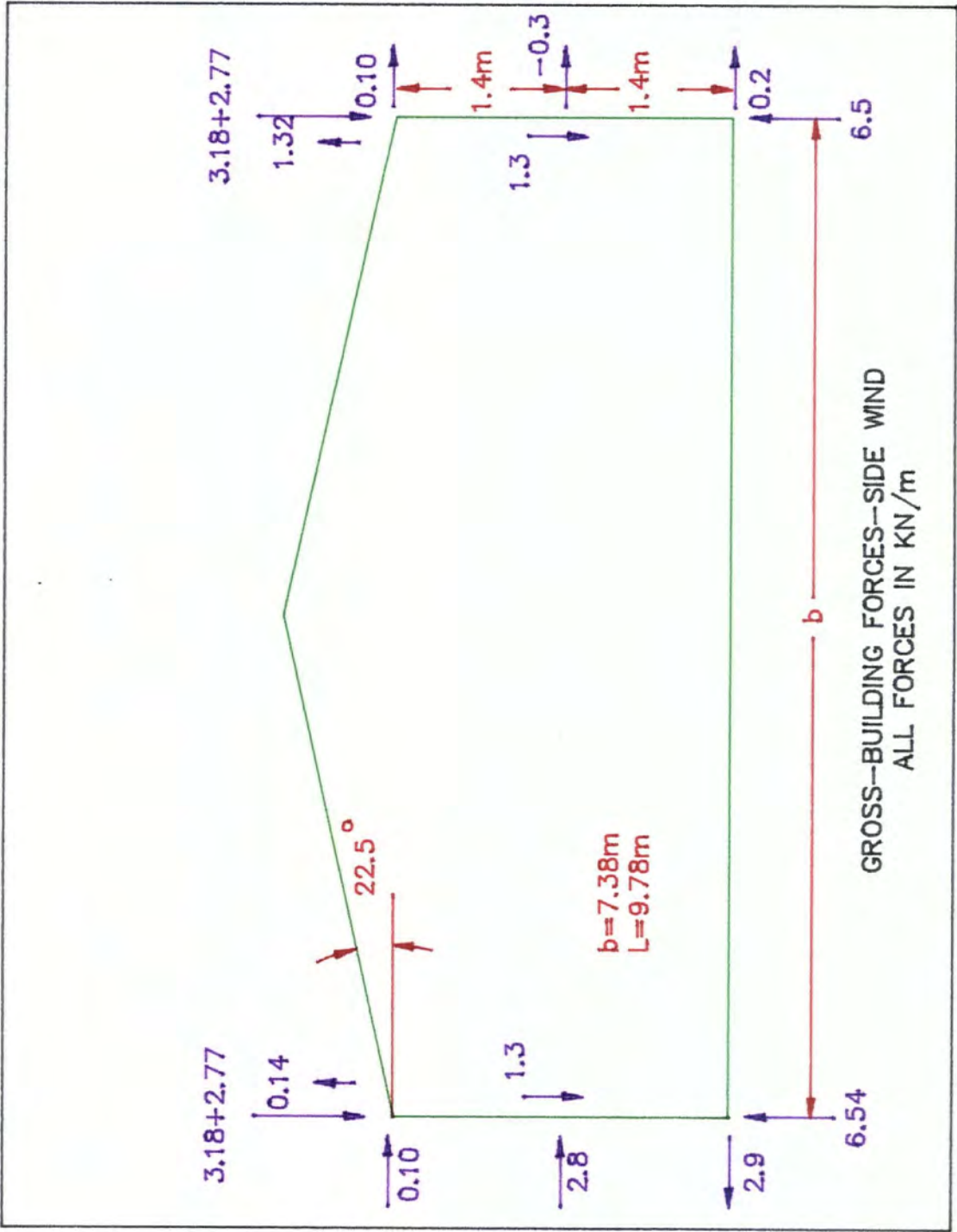


Reaction forces/m run

(a) Internal pressure

(b) Internal suction

LOADS (KN/m)	Dead + Imposed	Wind	Wind Wall weight
VERTICAL REACTION (KN/m)	<p>Dead: 4.48</p> <p>D+I: 7.25</p> <p>D+I+W: 5.05</p> <p>Moment: 2.38</p>	<p>Dead: 4.48</p> <p>D+I: 7.25</p> <p>D+I+W: 4.85</p> <p>Moment: 1.96</p>	<p>Dead: 4.48</p> <p>D+I: 7.25</p> <p>D+I+W: 5.93</p> <p>Moment: -0.14</p>
REMARK	<p>Maximum uplift load=2.4</p> <p>Then: Minimum down ward load=3.18-2.4=0.78</p> <p>Therefore: No net uplift load.</p>		



## 1. Wall loads

- a. Lateral loads on individual wall panels;

Worst case:

$$2.9 \times 1.2 = 3.48KN/panel$$

- b. Maximum axial load from base of the wall panel(dead load + supper load)=

$$(3.18 + 2.77 + 1.3) \times 1.2 = 8.7KN/panel$$

## 2. Building forces

- a. Wind on gable

$$Area = (7.38 \times 2.8) + (7.38 \times \frac{1.53}{2}) = 26.31m^2$$

$$\text{wind ward end, gable force} = 0.7 \times 1.01 \times 26.31 = 18.6KN$$

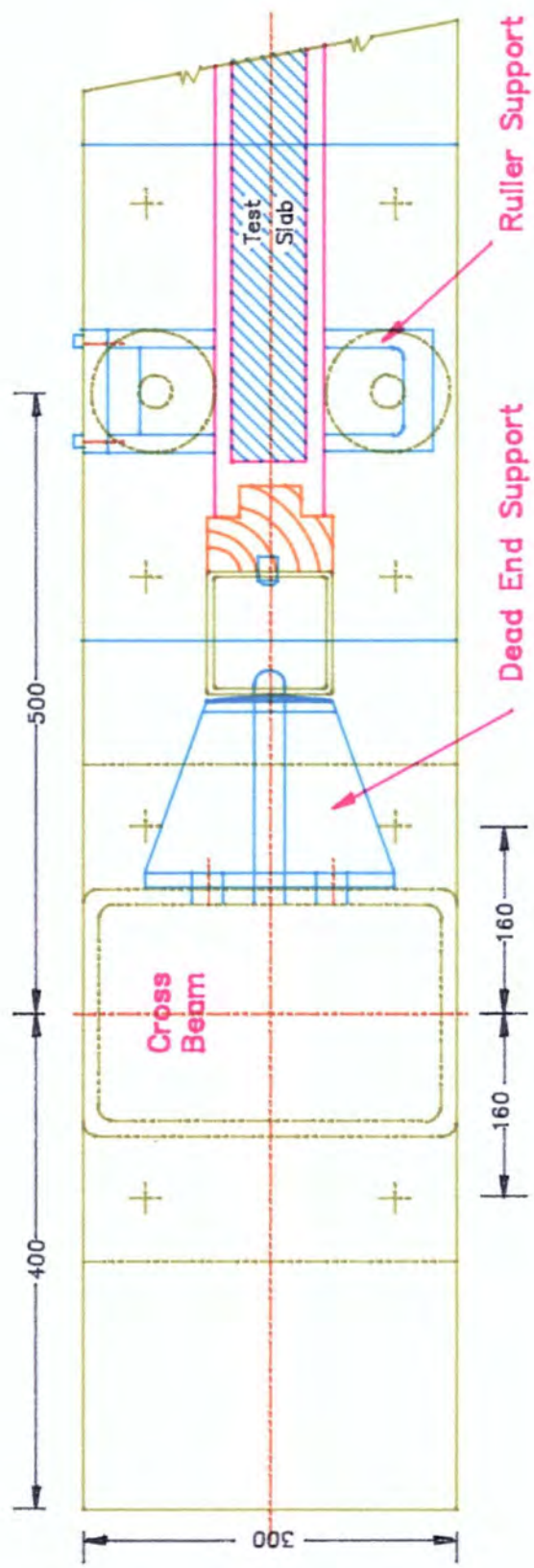
$$\text{lee ward end, gable force} = 0.2 \times 1.01 \times 26.31 = 5.31KN$$

- b. Wind on eaves

$$\text{maximum horizontal force from roof wind loading} = 0.1KN/m$$

$$\text{maximum horizontal force on a wall panel} = 2.8KN/m$$

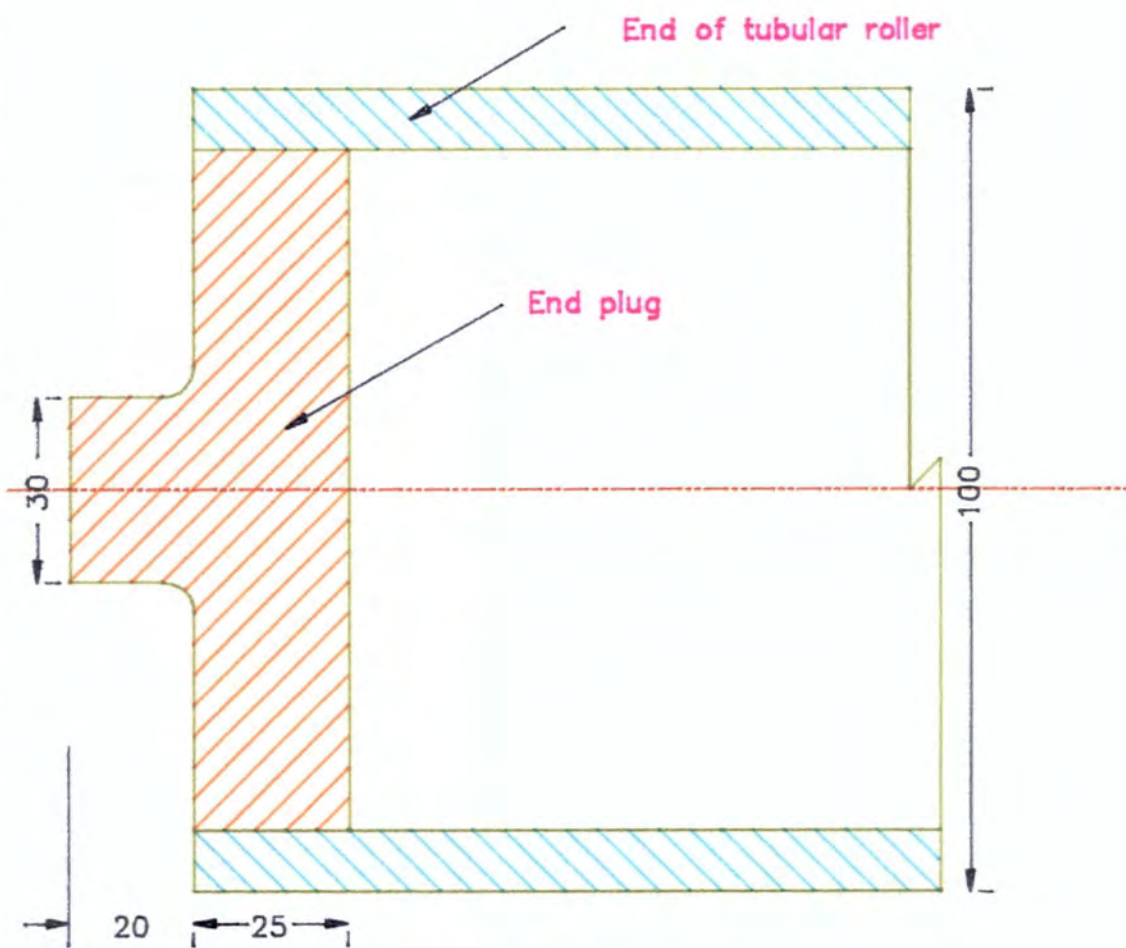
# APPENDIX (7)



General Arrangement of Dead End

Fig.(1)

SLAB LOADING ACCESSORIES

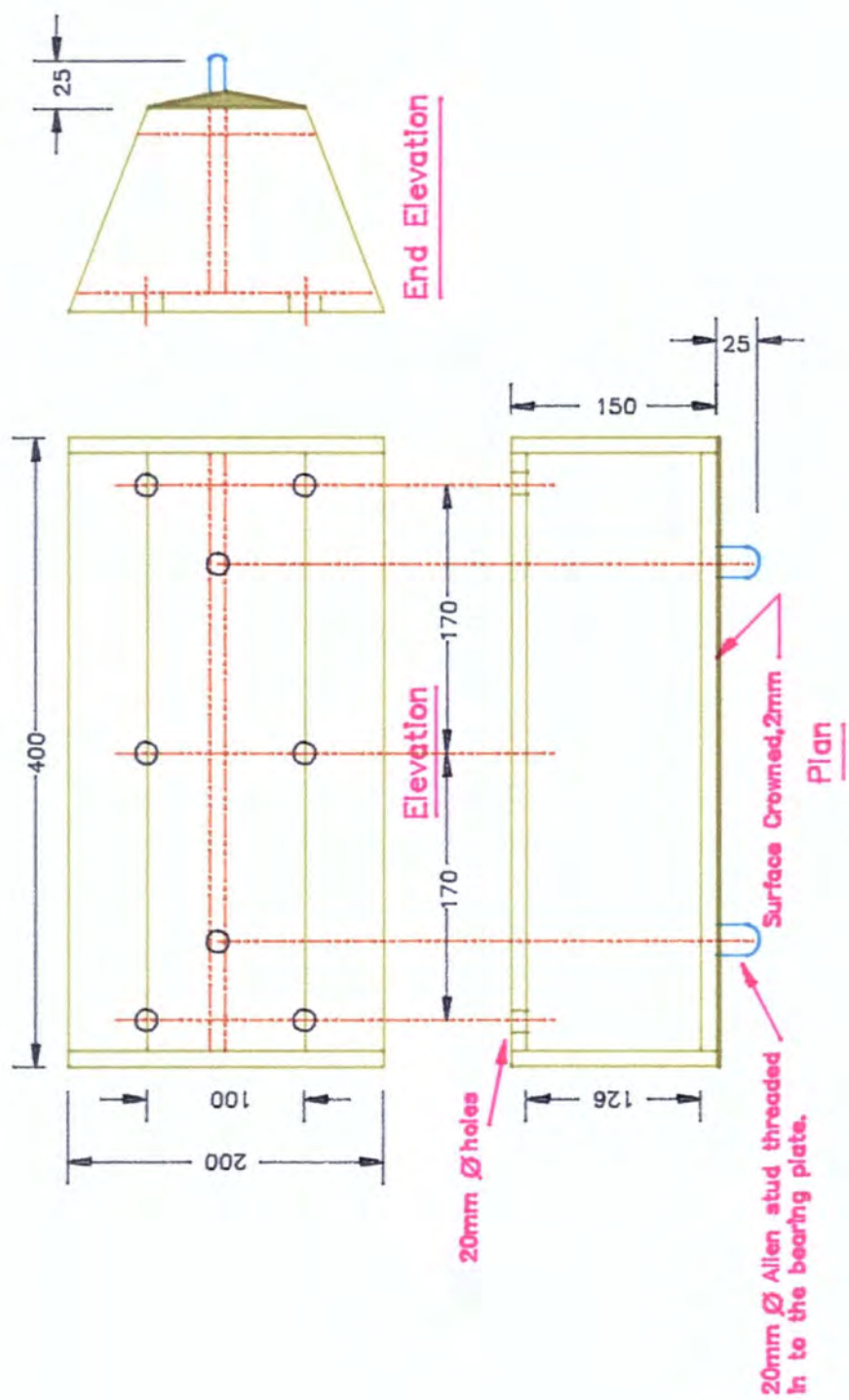


Section

Detail of end plug of support roller.

Fig.(2)

SLAB LOADING ACCESSORIES



Dead End Support Assembly

SLAB LOADING ACCESSORIES

Fig.(3)

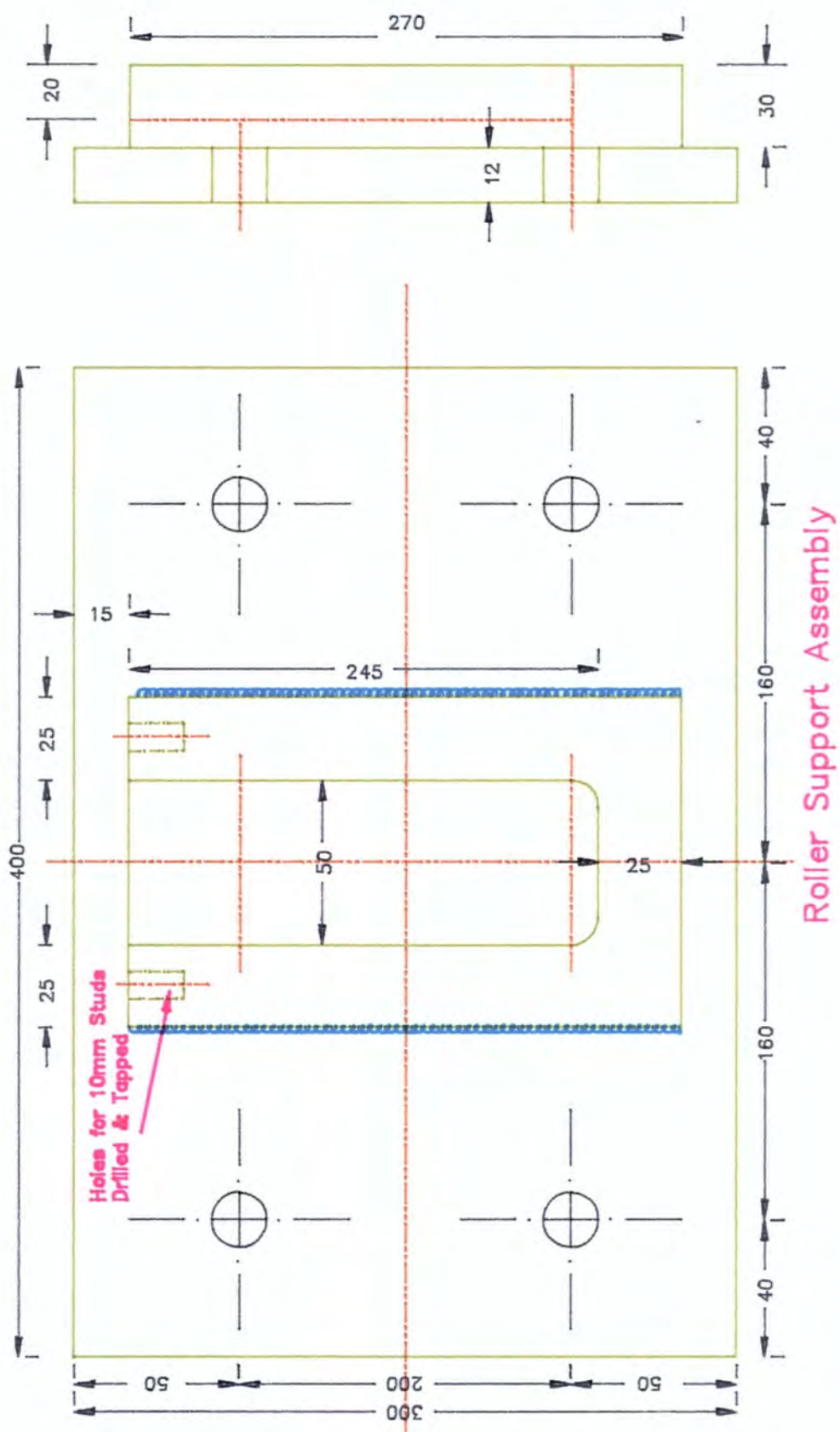
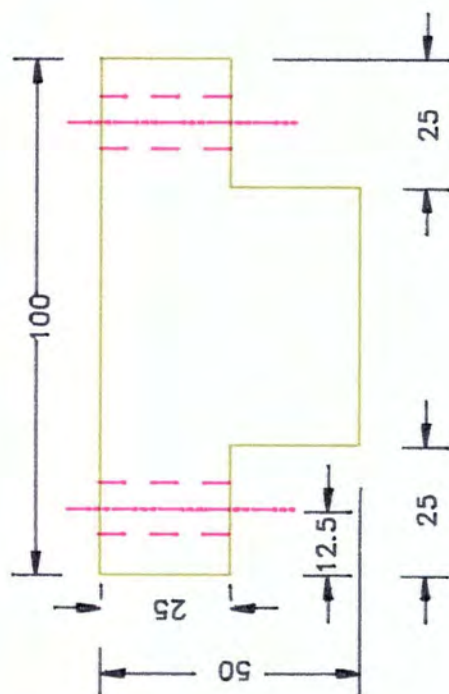
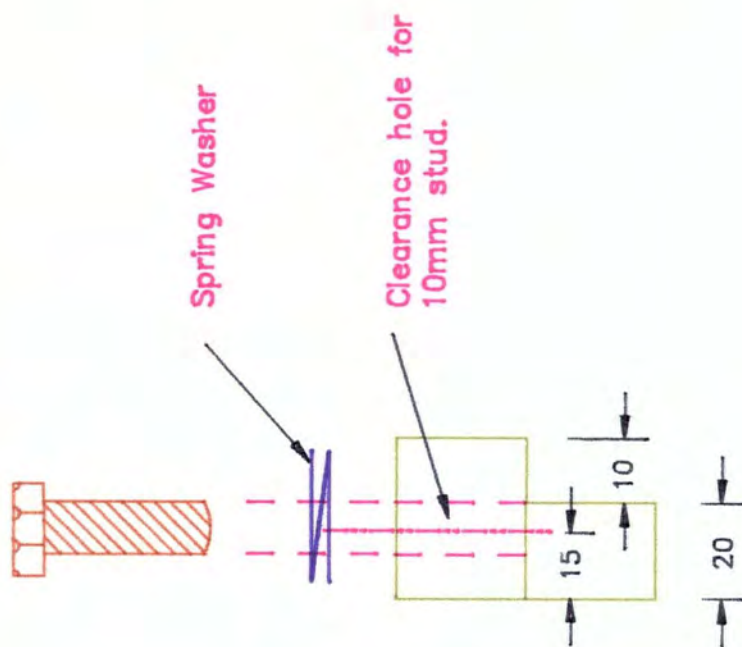


Fig. (4)



Elevation



End Elevation

Cap for Roller Support.

Fig.(5)

SLAB LOADING ACCESSORIES

# APPENDIX (8)

## Appendix 8

### Finite Element Analysis For The Corrugated Sheets

Finite element analysis is one of the methods which can be used to compare the experimental deflection or deformation of any components with theoretical study.

The finite element analysis was carried out by means of the available **PAFEC 75** computer programme. **PAFEC 75** is a **P**rogramme for **A**utomatic **F**inite **E**lement **C**alculations. The full system is capable of dealing with most finite element calculations found in engineering, including thermal shock, crack growth, orthotropic materials, plastic deformations, etc.

Using the structural property values of the polymer concrete which were obtained experimentally and recorded in the earlier parts of this thesis, a finite element analysis was carried out for the corrugated sheets, studied in this research and the results are reported in this appendix.

In order to carry out a finite element analysis on even the most simple of problems, a large amount of data is required. Therefore a programme was written to reduce the time and errors involved in preparing the data.

After defining the geometry of the corrugated sheet in terms of length, width, thickness and shape of the profile, and also the number of required elements, the programme automatically numbered all the nodes and elements.

This programme together with the data file can be seen at the end of this thesis.

A quarter of the corrugated sheets sample was considered in this analysis and was divided into 96 elements (16 x 6). Each element had dimensions of 13.25 x 140 mm in x and y dissection respectively, given a total length of the sample of ( 210 x 625 mm).

The load was applied so as to resemble the load position in the testing procedure and was distributed across the width, to act on nodes located at the mid-length of the element, at one side of the specimen along the x axis. The restraints ( $U_y, U_z, \theta_x, \theta_z$ ) were applied on the other side of the specimen (nodes no: 301-333) to resemble a simply supported situation, and also along the y axis at one edge of specimens with restraints of  $U_x, \theta_y, \theta_z$ . This is illustrated in fig.(1).

The out put of the computer analysis (displacement) for nodes located at the mid-length of the elements at both sides of the specimens are shown in table (2 & 3), and the cross-section of the sample, under the load is shown in fig. (4).

From the results the value of load/displacement along the Z direction was determined.

Putting this value in the expression of:

$$E = slope \times \frac{L^3}{48 \times I}$$

The value of I under this load was found to be:

$$I_a = \frac{48 \times 22000}{200 \times 1250^3} = 0.3699 \times 10^6$$

Where  $I_a$  =I value after loading.

Using the computer programme, the I value before loading was calculated to be

$0.6056 \times 10^6 \text{ mm}^4$  giving a ratio of:

$$\frac{I_a}{I_b} = \frac{0.3699 \times 10^6}{0.6056 \times 10^6} = 0.61$$

Where  $I_b$  = I value before loading.

NODES NO:  
ELEMENTS NO:

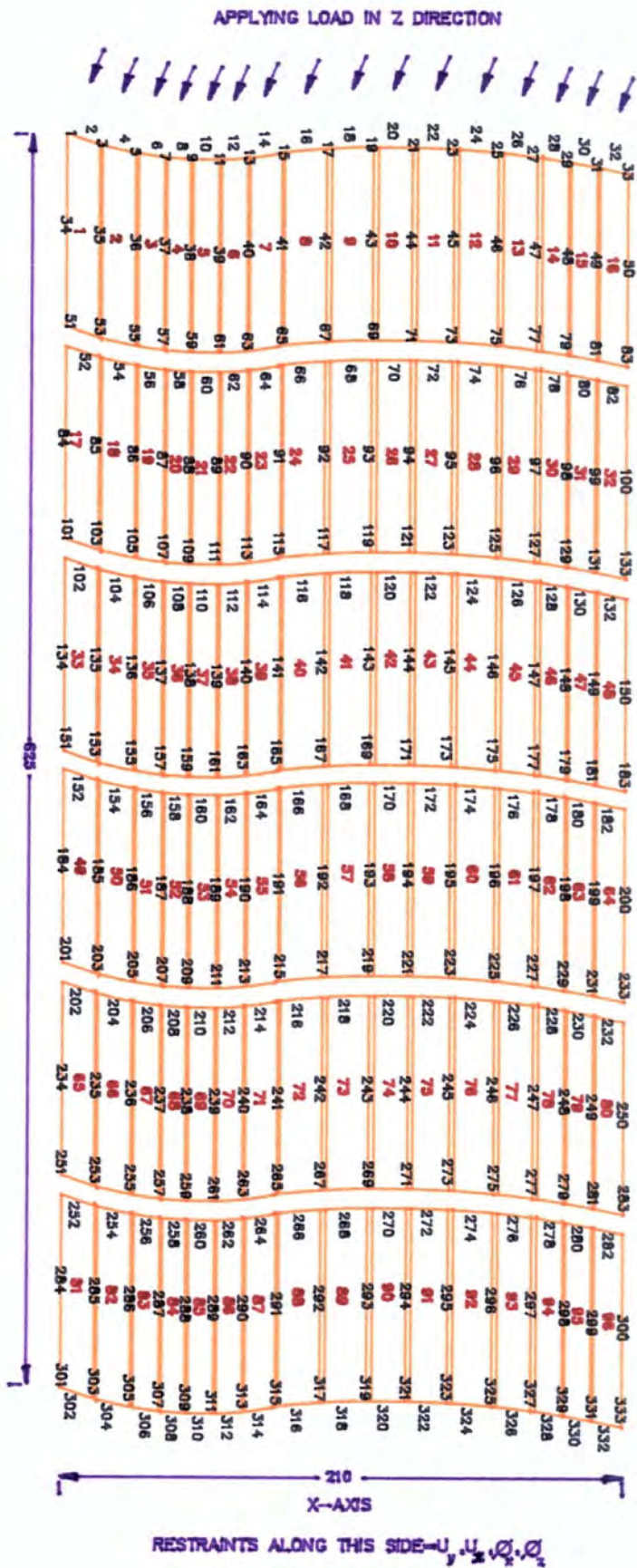


Fig.(1)

NODE NO:	CO-ORDINATES OF NODES BEFORE LOADING		CO-ORDINATES OF NODES AFTER LOADING		DISPLACEMENT (mm)	
	X (mm)	Z (mm)	X (mm)	Z (mm)	$\Delta X$	$\Delta Z$
1	0	13.89	-3.162	-2.141	3.162	16.031
3	13.125	25.254	8.818	13.986	4.307	14.068
5	26.250	35.903	20.507	20.080	5.743	15.823
7	39.375	43.07	32.430	27.860	6.945	15.210
9	52.50	44.892	45.217	30.005	7.283	14.887
11	65.625	40.896	59.729	26.856	5.896	14.040
13	78.750	32.12	75.507	18.346	3.243	13.774
15	91.875	20.845	91.728	7.582	0.147	13.563
17	105.00	10.00	105.436	-0.815	-0.436	10.815
19	118.125	2.50	119.84	-8.678	-1.715	11.178
21	131.25	0.027	133.178	-8.625	-1.928	8.652
23	144.375	3.491	144.501	-5.112	-0.126	8.603
25	157.50	11.894	154.527	-0.810	2.973	12.704
27	170.625	23.052	172.696	10.235	2.071	12.817
29	183.75	34.067	183.664	20.456	0.086	13.611
31	196.875	42.077	196.897	27.128	-0.022	14.949
33	210.00	45.00	210.00	31.259	*	13.741

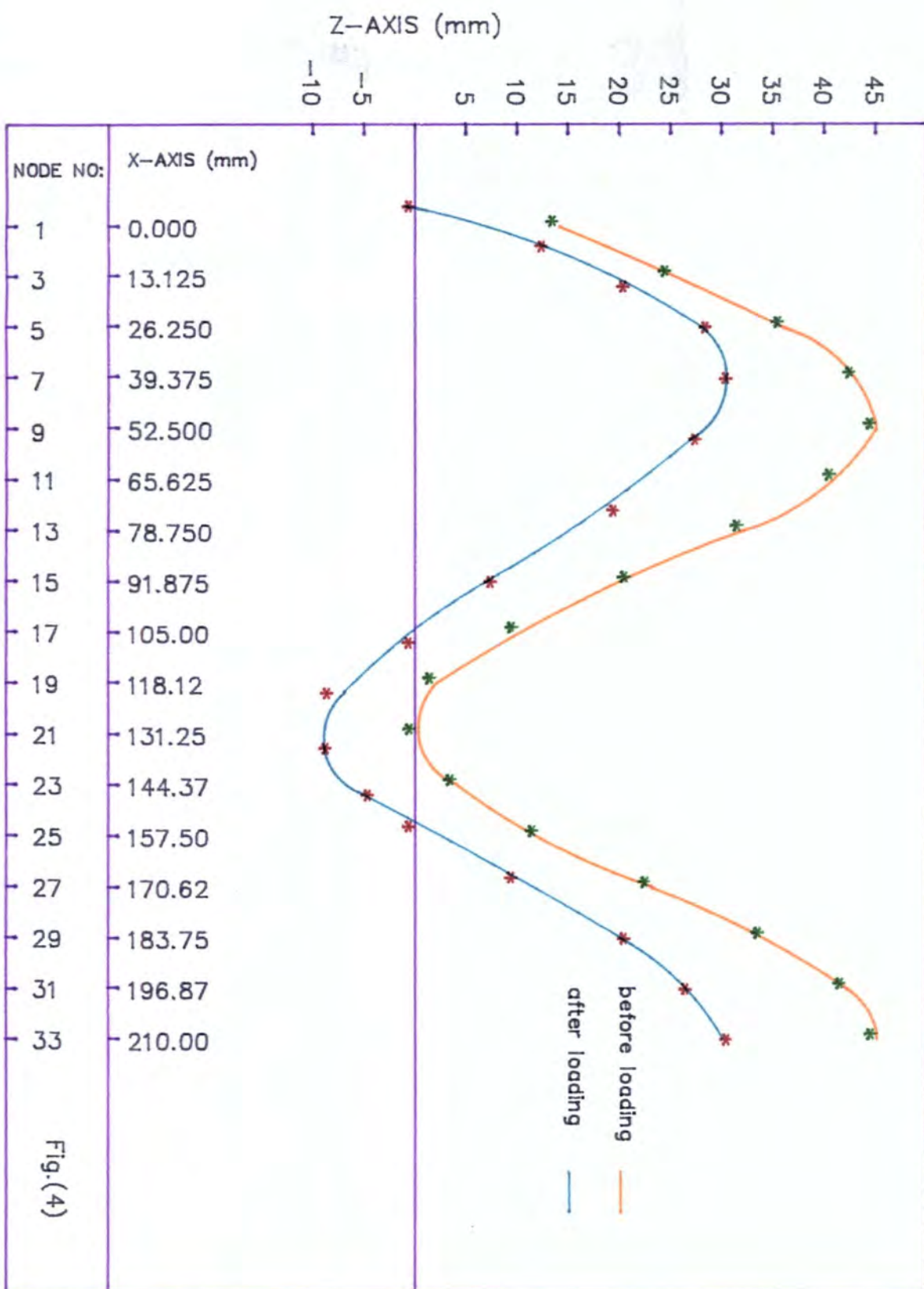
Restraints

Table (2)

NODE NO:	CO-ORDINATES OF NODES BEFORE LOADING		CO-ORDINATES OF NODES AFTER LOADING		DISPLACEMENT (mm)	
	X (mm)	Z (mm)	X (mm)	Z (mm)	$\Delta X$	$\Delta Z$
301	0	13.89	1.075	13.89	-1.075	*
303	13.125	25.254	14.275	25.254	-1.150	*
305	26.250	35.903	27.375	35.903	-1.125	*
307	39.375	43.07	40.450	43.07	-1.075	*
309	52.50	44.892	53.500	44.892	-1.000	*
311	65.625	40.896	66.550	40.896	-0.925	*
313	78.750	32.12	79.575	32.12	-0.825	*
315	91.875	20.845	92.600	20.845	-0.725	*
317	105.00	10.00	105.650	10.00	-0.650	*
319	118.125	2.50	118.775	2.50	-0.650	*
321	131.25	0.027	131.875	0.027	-0.625	*
323	144.375	3.491	144.975	3.491	-0.600	*
325	157.50	11.894	158.050	11.894	-0.550	*
327	170.625	23.052	171.075	23.052	-0.450	*
329	183.75	34.067	184.025	34.067	-0.275	*
331	196.875	42.077	197.150	42.077	-0.125	*
333	210.00	45.00	210.00	45.00	*	*

Restraints

Table (3)



# REFERENCES

## REFERENCES

1. ARNOLD, L.K. *Introduction To Plastics*, The Iowa State University Press.1968.
2. IWINSKI, T. *Theory Of Beams*, Pergamon Press Ltd. London 1967.
3. KINNEY, G.F. *Engineering Properties and Applications of Plastics*, John Wiley & Sons, Inc., U.S.A 1964.
4. DAVIES, J.D. *Structural Concrete*, Pergamon Press Ltd. 1964.
5. BIRTLEY, A.W. *Plastics Materials*, Leonard Hill, U.S.A,  
& SCOTT, M.J. NEW YORK 1982.
6. COOK, J.G. *Glass Fibre Reinforced Plastics*, George Newnes Ltd. London 1960.
7. JONES, L.L.& *Yield Line Analysis Of Slabs*, Butler & Tanner  
WOOD, R.H. Ltd. London 1967.
8. MILES, D.C.& *Polymer Technology*, Temple Press Books,  
BRISTON, J.H. London 1965.

9. CAGLE, C.V.            *Adhesive Bonding, Techniques And Applications*,  
  
Mc Graw-Hill inc., New York 1968.
10. TROITSKY, M.S.        *Stiffened Plates, Bending, Stability and Vibrations* ,  
  
Elsevier/ North Holland Inc., New York 1976.
11. MACGINTLEY, T.J.    *Structural Steelwork Calculations and Detailing*,  
  
Butterworth & Co., London 1973.
12. NEVILLE, A.M.        *Properties Of Concrete*, Pitman Publishing Ltd.  
  
London 1973.
13. SZILARD, R.            *Theory And Analysis Of Plates*, Prentice-Hall,  
  
Inc., New Jersey 1974.
14. BAER, E.                *Engineering Design For Plastics*, Reinhold  
  
Publishing Co., U.S.A 1964.
15. MACDERMOTT, C.P. *Selecting Thermoplastics For Engineering*  
  
*Applications*, Marcol Decker, Inc., New York 1984.
16. ULRICH, H.            *Introduction To Industrial Polymers*, Hanser-  
  
Publishers, Germany 1982.

17. BENJAMIN, B.S. *Structural Design With Plastics*, Polymer Technology Series 1969.
18. HOLLAWAY, L. *Glass Reinforced Plastics In Construction*  
Surrey University Press, Glasgow 1978.
19. JACKSON, N. *Civil Engineering Material*, Macmillan Press Ltd. London 1976.
20. ALLEN, H.G. *Analysis and Design of Structural Sandwich Panels*, Pergamon Press, Hungary 1969.
21. MARCH, H.W. *Effect Of Shear Deformation in The Core Of A Flat Rectangular Sandwich Panel.*(1) Buckling Under Compressive End Load. (2) Deflection Under Transverse Load, F.R.L Report 1583, May 1948.
22. HEMP, W.S. *Theory Of Sandwich Construction*, A.R.C, R & M, 2672, March 1948.
23. HOPKINS, H.G. *The Behaviour Of Flat Sandwich Panels Under*  
& PEARSON, S. *Uniform Transverse Load*, R.A.E, Report, 1942.

24. LEGGETT, D.M.A. *Sandwich Panels And Cylinders Under*  
& HOPKINS, H.G. *Compressive End Loads*, A.R.C, R & M, Aug 1942.
25. EVERARD, N.J. *Reinforced Concrete Design*, Schaum Pub Co.  
& TANNER, J.L. U.S.A, 1966.
26. PALIN, G.R. *Plastics For Engineers*, Pergamon Press  
Ltd. U.K, 1967.
27. REYNOLDS, C.E. *Reinforced Concrete Designers Hand book*,  
& STEEDMAN, J. Spottiswoode Ballantyne Ltd. London 1981.
28. MATTHAN, J.& *Ageing and Weathering Of Plastics, A*  
SCOTT K.A.& *Review Of Literature*, Rubber and Plastics.  
WIECHERS, M. Research Association Of Great Britain, 1970.
29. CYWINSKI, J. *The Role Of Peroxides In The Curing Of*  
*Polyester Resin*, Novadel Ltd.
30. MIDDLETON, K.G. *Using PAFEC 75 at NUMAC*, Engineering  
Science Department, Durham University 1977.
31. HENSHELL, R.D. *PAFEC 75 EASI DATA*, Pafec Ltd. 1976.

32. BRITISH STANDARD *Methods For Determination of the Viscosity*

188,1977. *Of Liquids.*

33. BRITISH STANDARD *Methods of Test For Soils For Civil*

1377, 1975. *Engineering Purposes.*

34. BRITISH STANDARD *Loading, Part 2, Wind Loads.*

CODE OF PRACTICE

cp3: Chapter v:

Part 2 1970.

35. FOLIE, G.M. *The Theory Of Sandwich Panels Subjected*

*To Transverse Loads Under Various Edge*

*Conditions, Dept. Of Civil Engineering,*

University Of Southampton.

36. SHENDY, M.E. *The Properties Of Concrete Sandwich Beams*

*With Polystyrene Concrete Cores, Dept.*

*Of Engineering Science, University Of*

*Durham, July 1981.*

37. SAGLAM, B. *The Properties Of Fibre Reinforced Cement*

*Based Sandwich Beams*, Dept Of

Engineering, University Of Durham, November 1976.



# OUTPUT OF THE COMPUTER

C  
C  
C  
Drawing for workability test

```
CALL PAPER(1)
CALL PSPACE(0.0,2.3622,0.0,2.3622)
CALL MAP(-30.0,30.0,-30.0,30.0)
CALL POSITN(0.0,-30.0)
CALL LINE(0.0,60.0)
CALL POSITN(-30.0,0.0)
CALL LINE(60.0,0.0)
CALL POSITN(0.0,0.0)
CALL ROTATE(ATAN(1.0))
CALL POSITN(0.0,-30.0)
CALL LINE(0.0,60.0)
CALL POSITN(-30.0,0.0)
CALL LINE(60.0,0.0)
DO 10 I=1,16
R=5.0+(I-1)
CALL POSITN(0.0,0.0)
IF(I.EQ.2.OR.I.EQ.5.OR.I.EQ.8.OR.I.EQ.11.OR.I.EQ.14)
&CALL BROKEN(5,5,5,5)
IF(I.EQ.3.OR.I.EQ.6.OR.I.EQ.9.OR.I.EQ.12.OR.I.EQ.15)
&CALL GRNPEN
CALL CIRCLE(R)
CALL REDPEN
CALL FULL
10 CONTINUE
DO 20 I=1,5
R=20.0+(2*I)
CALL POSITN(0.0,0.0)
IF(I.EQ.1.OR.I.EQ.4)CALL BROKEN(5,5,5,5)
IF(I.EQ.2.OR.I.EQ.5)CALL GRNPEN
CALL CIRCLE(R)
CALL REDPEN
CALL FULL
20 CONTINUE
CALL GREND
STOP
END
```

C  
C  
C

PROG TO CALCULATE SECOND MOMENT OF AREA OF THE SANDWICH PANEL.

```
REAL I,K
DO 10 J=1,2
WRITE(6,*)' THE TEST NO: '
READ(5,*)T
WRITE(3,*)' THE TEST NO:',T
WRITE(6,*)' THE THICKNESS OF THE EDGE OF THE PANEL ARE: '
READ(5,*)T1,T4
WRITE(6,*)' THE THICKNESS OF THE RIBS ARE: '
READ(5,*)T2,T3,T5
WRITE(6,*)' THE THICKNESS OF THE TOP AND BOTTOM PHASES ARE: '
READ(5,*)TF,BF
B=90.0*T1
TM=1160.0-T4-T1
C=TF*TM
D=BF*TM
TN=90.0-TF-BF
E=T2*TN
F=T3*TN
G=90.0*(35.0+T4)
K=T5*TN
H=100.0
A=B+C+D+E+F+G-H+K
Y=((B*45.0)+C*(90.0-TF/2.)+(D*BF/2.)+(E+F+K)*(TN/2.+BF)+(G-H)*45.)
Y=Y/A
I=(T1*(90.0**3)/12.)+B*ABS(45.0-Y)**2+TM*(TF**3)/12.+
&C*ABS(90.0-TF/2.-Y)**2+TM*(BF**3)/12.+D*ABS(BF/2.-Y)**2+T2*(TN**3)
&/12.+E*ABS(TN/2.+BF-Y)**2+T3*(TN**3)/12.+F*ABS(TN/2.+BF-Y)**2+
&(35.0+T4)*(90.0**3)/12.+G*ABS(45.-Y)**2-5.*(20.**3)/12.-
&H*ABS(45.-Y)**2+T5*(TN**3)/12.+K*ABS(TN/2.+BF-Y)**2
WRITE(3,20)A,Y,I
WRITE(6,20)A,Y,I
20 FORMAT(' A=',F15.2,' Y=',F15.2,' I=',F15.2)
10 CONTINUE
STOP
END
```

PANEL DIMENSIONS

NUM	SHT THS	SHT WTH	RIBS	TOP THS	BOT THS	DEPTH	BARS	TYPE	THICKS	DEPT
1	8.00	287.30	2	10.00	25.00	32.00	2	0	9.000	0.0
2	8.00	287.30	2	10.00	25.00	32.00	2	0	9.000	0.0
3	9.90	293.30	2	10.00	25.00	3.00	2	0	9.000	0.0
4	8.80	293.00	2	10.00	25.00	3.00	1	100	4.000	40.0

GEOMETRICAL PROPERTIES

NUM	AM	FYP AREA	STL AREA	YBAR	2ND MOI	ZTS	ZBS	ZTF	ZBI
1	30.	3418.40	254.47	16.85	32673.	49991.	5779.	42334.	-5818
2	30.	3418.40	254.47	15.98	28364.	27892.	6280.	35430.	-5323
3	30.	3008.67	254.47	17.24	32753.	11873.	4846.	-226321.	-5698
4	30.	2683.40	320.00	17.03	59405.	2531.	-3593.	-340662.	-10463

MAX. U.D.L., (KN/M2), DEFN. CRITERION

SIMPLE SUPPORT

SECTION	SPAN (M)							
	1.4	1.6	1.8	2.0	2.2	2.4	2.6	2.8
1	1.77	1.18	0.83	0.61	0.46	0.35	0.28	0.22
2	1.54	1.03	0.72	0.53	0.40	0.30	0.24	0.19
3	1.74	1.16	0.82	0.60	0.45	0.34	0.27	0.22
4	3.15	2.11	1.48	1.08	0.81	0.63	0.49	0.39

MAX. CONCRETE DEPTH (MM), STRESS CRITERION

SIMPLE SUPPORT

SECTION	SPAN (M)							
	1.4	1.6	1.8	2.0	2.2	2.4	2.6	2.8
1	7768.02	6797.02	6041.79	5437.61	4943.28	4531.34	4182.78	3884.01
2	4334.00	3792.25	3370.89	3033.80	2758.00	2528.17	2333.70	2167.00
3	1807.23	1581.33	1405.63	1265.06	1150.06	1054.22	973.13	903.62
4	385.67	337.46	299.97	269.97	245.43	224.98	207.67	192.84

FOR MEMBERS WITH CONTINUOUS SUPPORT

MULTIPLY THE FIGURES IN THIS TABLE BY 1.5

MAX. U.D.L., (KN/M2), DEFN. CRITERION

CONTINUOUS SUPPORT

SECTION	SPAN (M)							
	1.4	1.6	1.8	2.0	2.2	2.4	2.6	2.8
1	11.79	7.90	5.55	4.04	3.04	2.34	1.84	1.47
2	10.23	6.86	4.82	3.51	2.64	2.03	1.60	1.28
3	11.58	7.75	5.45	3.97	2.98	2.30	1.81	1.45
4	21.02	14.08	9.89	7.21	5.42	4.17	3.28	2.63

MAX. CONCRETE DEPTH (MM), DEFN. CRITERION

CONTINUOUS SUPPORT

SECTION	SPAN (M)							
	1.4	1.6	1.8	2.0	2.2	2.4	2.6	2.8
1	491.19	329.06	231.11	168.48	126.58	97.50	76.69	61.40
2	426.42	285.67	200.63	146.26	109.89	84.64	66.57	53.30
3	482.32	323.12	226.93	165.44	124.29	95.74	75.30	60.29
4	875.70	586.65	412.03	300.37	225.67	173.82	136.72	109.46

MAXIMUM PURLIN SPACINGS (M)MAXIMUM PURLIN SPACINGS (M)

SECTION NUMBER	SIMPLE SUPPORT,		CONTINUOUS	
	L/360	L/250	L/360	L/250
1	0.933	1.120	1.867	2.240
2	0.870	1.044	1.739	2.087
3	0.935	1.121	1.869	2.243
4	1.259	1.510	2.517	3.021

MAX. U.D.L., (KN/M2), STRESS CRITERION

SIMPLE SPAN

SECTION	SPAN (M)							
	1.4	1.6	1.8	2.0	2.2	2.4	2.6	2.8
1	186.43	163.13	145.00	130.50	118.64	108.75	100.39	93.22
2	104.02	91.01	80.90	72.81	66.19	60.68	56.01	52.01
3	43.37	37.95	33.74	30.36	27.60	25.30	23.36	21.69
4	9.26	8.10	7.20	6.48	5.89	5.40	4.98	4.63

FOR MEMBERS WITH CONTINUOUS SUPPORT

MULTIPLY THE FIGURES IN THIS TABLE BY 1.5

MAX. CONCRETE DEPTH (MM), DEFN CRITERION

SIMPLE SPAN

SECTION	SPAN (M)							
	1.4	1.6	1.8	2.0	2.2	2.4	2.6	2.8
1	73.68	49.36	34.67	25.27	18.99	14.62	11.50	9.2
2	63.96	42.85	30.10	21.94	16.48	12.70	9.99	8.0
3	72.35	48.47	34.04	24.82	18.64	14.36	11.30	9.0
4	131.36	88.00	61.80	45.05	33.85	26.07	20.51	16.4

C

```

REAL L
INTEGER A,A1,B1,C,A3,D1,E,F,G,H
DIMENSION Z(100)
WRITE(6,*)' WHAT IS THE TOTAL WIDTH OF THE SPECIMEN'
READ(5,*)X
WRITE(6,*)' WHAT IS THE TOTAL LENGTH OF THE SPECIMEN'
READ(5,*)L
WRITE(6,*)' HOW MANY DIVISIONS ARE ALONG THE WIDTH'
READ(5,*)N
WRITE(6,*)' HOW MANY DIVISIONS ARE ALONG THE LENGTH'
READ(5,*)M
WRITE(6,*)' WHAT IS THE MAX.HIGHT ALONG THE X DIRC.'
READ(5,*)A5
WRITE(6,*)' WHAT IS THE DISTANCE BETWEEN THE TWO PICK'
READ(5,*)L5
WRITE(6,*)' WHAT IS THE DISTANCE BETWEEN EACH CURVE'
READ(5,*)P5
WRITE(3,10)
10  FORMAT('  NODES'/'  AXIS.NO=1'/'  NODE.NO      X          Y          Z')
DO 90 I=1,100
Z(I)=0.0
90  CONTINUE
CALL CALCZ(X,A5,L5,P5,N,Z)
Y1=0
NN=2*N+1
AA=0
K5=0
DO 100 I=1,NN,2
D=AA*X/N
K5=K5+1
WRITE(3,20)I,D,Y1,Z(K5)
20  FORMAT(I6,3F8.2)
AA=AA+1
100  CONTINUE
I=I-2
A=I
150  Y1=Y1+L/M
B=I+(A+1)/2+1
NB=2*N+B
AA=0.0
K5=0
DO 200 I=B,NB,2
D=AA*X/N
K5=K5+1
NNB=(2*N+1)+(3*N+2)*M
IF(B.GE.NNB)GOTO 300
WRITE(3,20)I,D,Y1,Z(K5)
AA=AA+1
200  CONTINUE
I=I-2
GOTO 150
300  WRITE(3,30)
30  FORMAT('  ELEMENTS'/'  GROUP.NO=1'/'  ELEMENT.TYPE=44210'/'
&'  PROPERTIES=1'/'  NUMBER              TOPOLOGY')
IR=0
A1=1
A3=(A+1)/2+1
DO 500 I=1,M*N
400  B1=A1+2
C=A3+2*N+1

```

```

D1=C+2
E=(A1+B1)/2
F=2*N+2+IR
G=F+1
H=(C+D1)/2
WRITE(3,40)I,A1,B1,C,D1,E,F,G,H
40  FORMAT(I3,5X,8I6)
A3=A3+2
A1=A1+2
IR=IR+1
IF(MOD(I,N).EQ.0)THEN
    A1=A1+2+N
    A3=A3+2+N
    IR=IR+2*N+2
ENDIF
500 CONTINUE
STOP
END
SUBROUTINE CALCZ(X,A5,L5,P5,N,Z)
DIMENSION Z(100)
B4=0
N5=0
M5=L5
Q=0
I=0
30  D=N5*X/N
    I=I+1
    ZZ=2*4*ATAN(1.0)*(D-L5/4)/L5
    Z(I)=(A5/2)*(SIN(ZZ)+1)
    N5=N5+1
    IF(D.LT.M5)GOTO 30
    IF(P5.LE.Q)GOTO 50
    M5=D+P5
40  D=N5*X/N
    I=I+1
    Z(I)=0.0
    N5=N5+1
    IF(D.LT.M5)GOTO 40
50  B4=B4+D
    N5=1
    M5=L5
    IF(B4.LT.X)GOTO 30
RETURN
END

```

# TITLE FINIT ELEMENT TECHNIQUE FOR CORRUGATED SHEET

## NODES

AXIS.NUMBER=1

NODE.NUMBER

	X	Y	Z
1	0	0	13.89
3	13.125	0	25.254
5	26.25	0	35.903
7	39.375	0	43.07
9	52.5	0	44.892
11	65.625	0	40.896
13	78.75	0	32.12
15	91.875	0	20.845
17	105	0	10
19	118.125	0	2.5
21	131.25	0	.027
23	144.375	0	3.491
25	157.5	0	11.894
27	170.625	0	23.052
29	183.75	0	34.067
31	196.875	0	42.077
33	210	0	45
51	0	104.167	13.89
53	13.125	104.167	25.254
55	26.25	104.167	35.903
57	39.375	104.167	43.07
59	52.5	104.167	44.892
61	65.625	104.167	40.896
63	78.75	104.167	32.12
65	91.875	104.167	20.845
67	105	104.167	10
69	118.125	104.167	2.5
71	131.25	104.167	.027
73	144.375	104.167	3.491
75	157.5	104.167	11.894
77	170.625	104.167	23.052
79	183.75	104.167	34.067
81	196.875	104.167	42.077
83	210	104.167	45
101	0	208.333	13.89
103	13.125	208.333	25.254
105	26.25	208.333	35.903
107	39.375	208.333	43.07
109	52.5	208.333	44.892
111	65.625	208.333	40.896
113	78.75	208.333	32.12
115	91.875	208.333	20.845
117	105	208.333	10
119	118.125	208.333	2.5
121	131.25	208.333	.027
123	144.375	208.333	3.491
125	157.5	208.333	11.894
127	170.625	208.333	23.052
129	183.75	208.333	34.067
131	196.875	208.333	42.077
133	210	208.333	45
151	0	312.5	13.89
153	13.125	312.5	25.254
155	26.25	312.5	35.903
157	39.375	312.5	43.07
159	52.5	312.5	44.892

161	65.625	312.5	40.896
163	78.75	312.5	32.12
165	91.875	312.5	20.845
167	105	312.5	10
169	118.125	312.5	2.5
171	131.25	312.55	.027
173	144.375	312.5	3.491
175	157.5	312.5	11.894
177	170.625	312.5	23.052
179	183.75	312.5	34.067
181	196.875	312.5	42.077
183	210	312.5	45
201	0	416.667	13.89
203	13.125	416.667	25.254
205	26.25	416.667	35.903
207	39.375	416.667	43.07
209	52.5	416.667	44.892
211	65.625	416.667	40.896
213	78.75	416.667	32.12
215	91.875	416.667	20.845
217	105	416.667	10
219	118.125	416.667	2.5
221	131.25	416.667	.027
223	144.375	416.667	3.491
225	157.5	416.667	11.894
227	170.625	416.667	23.052
229	183.75	416.667	34.067
231	196.875	416.667	42.077
233	210	416.667	45
251	0	520.833	13.89
253	13.125	520.833	25.254
255	26.25	520.833	35.903
257	39.375	520.833	43.07
259	52.5	520.833	44.892
261	65.625	520.833	40.896
263	78.75	520.833	32.12
265	91.875	520.833	20.845
267	105	520.833	10
269	118.125	520.833	2.5
271	131.25	520.833	.027
273	144.375	520.833	3.491
275	157.5	520.833	11.894
277	170.625	520.833	23.052
279	183.75	520.833	34.067
281	196.875	520.833	42.077
283	210	520.833	45
301	0	625	13.89
303	13.125	625	25.254
305	26.25	625	35.903
307	39.375	625	43.07
309	52.5	625	44.892
311	65.625	625	40.896
313	78.75	625	32.12
315	91.875	625	20.845
317	105	625	10
319	118.125	625	2.5
321	131.25	625	.027
323	144.375	625	3.491
325	157.5	625	11.894
327	170.625	625	23.052

53	159	161	209	211	160	188	189	210
54	161	163	211	213	162	189	190	212
55	163	165	213	215	164	190	191	214
56	165	167	215	217	166	191	192	216
57	167	169	217	219	168	192	193	218
58	169	171	219	221	170	193	194	220
59	171	173	221	223	172	194	195	222
60	173	175	223	225	174	195	196	224
61	175	177	225	227	176	196	197	226
62	177	179	227	229	178	197	198	228
63	179	181	229	231	180	198	199	230
64	181	183	231	233	182	199	200	232
65	201	203	251	253	202	234	235	252
66	203	205	253	255	204	235	236	254
67	205	207	255	257	206	236	237	256
68	207	209	257	259	208	237	238	258
69	209	211	259	261	210	238	239	260
70	211	213	261	263	212	239	240	262
71	213	215	263	265	214	240	241	264
72	215	217	265	267	216	241	242	266
73	217	219	267	269	218	242	243	268
74	219	221	269	271	220	243	244	270
75	221	223	271	273	222	244	245	272
76	223	225	273	275	224	245	246	274
77	225	227	275	277	226	246	247	276
78	227	229	277	279	228	247	248	278
79	229	231	279	281	230	248	249	280
80	231	233	281	283	232	249	250	282
81	251	253	301	303	252	284	285	302
82	253	255	303	305	254	285	286	304
83	255	257	305	307	256	286	287	306
84	257	259	307	309	258	287	288	308
85	259	261	309	311	260	288	289	310
86	261	263	311	313	262	289	290	312
87	263	265	313	315	264	290	291	314
88	265	267	315	317	266	291	292	316
89	267	269	317	319	268	292	293	318
90	269	271	319	321	270	293	294	320
91	271	273	321	323	272	294	295	322
92	273	275	323	325	274	295	296	324
93	275	277	325	327	276	296	297	326
94	277	279	327	329	278	297	298	328
95	279	281	329	331	280	298	299	330
96	281	283	331	333	282	299	300	332

PLATES AND SHELLS

PLATE NUMBER MATERIAL NUMBER THICKNESS

1,11,8

MATERIAL

MATERIAL NO. E, NU

11,22E03,0.2

IN DRAW

DRAWING NO, TYPE NO, INFORMATION NO, ORIENTATION, SIZE NO.

1,1.23,0.10

LOADS

CASE OF LOAD, NODE NUMBER, DIRECTION OF LOAD, VALUE OF LOAD

1,2,3,10

1,4,3,10

1,6,3,10

1,8,3,10

1,10,3,10

1,12,3,10  
1,14,3,10  
1,16,3,10  
1,18,3,10  
1,20,3,10  
1,22,3,10  
1,24,3,10  
1,26,3,10  
1,28,3,10  
1,30,3,10  
1,32,3,10  
STRESS.ELEMENT  
START,FINISH,STEP  
1,96,1  
OUT.DRAW  
DRAWING.NUMBER,PLOT.TYPE,ORIENTATION,SIZE.NUMBER  
2,1,0,10  
3,20,0,10  
4,30,0,10  
RESTRAINTS  
NODE.NUMBER,PLANE,AXIS.NUMBER,DIRECTION  
333,2,1,2346  
33,1,1,156  
END.OF.DATA